

REPORT DOCUMENTATION PAGE

Public reporting burden for this collection of information is estimated to average 1 hour per response, including the time for reviewing the data needed, and completing and reviewing the collection of information. Send comments regarding this burden estimate or any other aspect of this collection of information, including suggestions for reducing this burden, to Washington Headquarters Services, Directorate for Information Operations and Reports, 1215 Jefferson Davis Highway, Suite 1204, Arlington, VA 22202-4302, and to the Office of Management and Budget, Paperwork Reduction Project (0704-0188).

AFRL-SR-BL-TR-98-

0806

ing
of
ite

1. AGENCY USE ONLY (Leave Blank)		2. REPORT DATE December, 1995	3. REPORT Final
4. TITLE AND SUBTITLE USAF Summer Research Program - 1995 High School Apprenticeship Program Final Reports, Volume 15A, Wright Laboratory			5. FUNDING NUMBERS
6. AUTHORS Gary Moore			
7. PERFORMING ORGANIZATION NAME(S) AND ADDRESS(ES) Research and Development Labs, Culver City, CA			8. PERFORMING ORGANIZATION REPORT NUMBER
9. SPONSORING/MONITORING AGENCY NAME(S) AND ADDRESS(ES) AFOSR/NI 4040 Fairfax Dr, Suite 500 Arlington, VA 22203-1613			10. SPONSORING/MONITORING AGENCY REPORT NUMBER
11. SUPPLEMENTARY NOTES Contract Number: F49620-93-C-0063			
12a. DISTRIBUTION AVAILABILITY STATEMENT Approved for Public Release			12b. DISTRIBUTION CODE
13. ABSTRACT (Maximum 200 words) The United States Air Force High School Apprenticeship Program's (USAF- HSAP) purpose is to place outstanding high school students whose interests are in the areas of mathematics, engineering, and science to work in a laboratory environment. The students selected to participate in the program work in an Air Force Laboratory for a duration of 8 weeks during their summer vacation.			
14. SUBJECT TERMS AIR FORCE HIGH SCHOOL APPRENTICESHIP PROGRAM, APPRENTICEDHIP, AIR FORCE RESEARCH, AIR FORCE, ENGINEERING, LABORATORIES, REPORTS, SCHOOL, STUDENT, SUMMER, UNIVERSITIES			15. NUMBER OF PAGES
			16. PRICE CODE
17. SECURITY CLASSIFICATION OF REPORT Unclassified	18. SECURITY CLASSIFICATION OF THIS PAGE Unclassified	19. SECURITY CLASSIFICATION OF ABSTRACT Unclassified	20. LIMITATION OF ABSTRACT UL

UNITED STATES AIR FORCE
SUMMER RESEARCH PROGRAM -- 1995
HIGH SCHOOL APPRENTICESHIP PROGRAM FINAL REPORTS

VOLUME 15A
WRIGHT LABORATORY

RESEARCH & DEVELOPMENT LABORATORIES

5800 Uplander Way
Culver City, CA 90230-6608

Program Director, RDL
Gary Moore

Program Manager, AFOSR
Major David Hart

Program Manager, RDL
Scott Licoscas

Program Administrator, RDL
Gwendolyn Smith

Submitted to:

AIR FORCE OFFICE OF SCIENTIFIC RESEARCH

Bolling Air Force Base

Washington, D.C.

DTIC QUALITY INSPECTED 3

December 1995

19981214 072

PREFACE

Reports in this volume are numbered consecutively beginning with number 1. Each report is paginated with the report number followed by consecutive page numbers, e.g., 1-1; 1-2, 1-3; 2-1, 2-2, 2-3.

Due to its length, Volume 15 is bound in two parts, 15A and 15B. Volume 15A contains #1-26. Volume 15B contains reports #28-52. The Table of Contents for Volume 15 is included in both parts.

This document is one of a set of 16 volumes describing the 1995 AFOSR Summer Research Program. The following volumes comprise the set:

<u>VOLUME</u>	<u>TITLE</u>
1	Program Management Report
	<i>Summer Faculty Research Program (SFRP) Reports</i>
2A & 2B	Armstrong Laboratory
3A & 3B	Phillips Laboratory
4	Rome Laboratory
5A, 5B, & 5C	Wright Laboratory
6A & 6B	Arnold Engineering Development Center, Wilford Hall Medical Center and Air Logistics Centers
	<i>Graduate Student Research Program (GSRP) Reports</i>
7A & 7B	Armstrong Laboratory
8	Phillips Laboratory
9	Rome Laboratory
10A & 10B	Wright Laboratory
11	Arnold Engineering Development Center, Wilford Hall Medical Center and Air Logistics Centers
	<i>High School Apprenticeship Program (HSAP) Reports</i>
12A & 12B	Armstrong Laboratory
13	Phillips Laboratory
14	Rome Laboratory
15A&15B	Wright Laboratory
16	Arnold Engineering Development Center

HSAP FINAL REPORT TABLE OF CONTENTS

i-xiv

1. INTRODUCTION	1
2. PARTICIPATION IN THE SUMMER RESEARCH PROGRAM	2
3. RECRUITING AND SELECTION	3
4. SITE VISITS	4
5. HBCU/MI PARTICIPATION	4
6. SRP FUNDING SOURCES	5
7. COMPENSATION FOR PARTICIPATIONS	5
8. CONTENTS OF THE 1995 REPORT	6

APPENDICIES:

A. PROGRAM STATISTICAL SUMMARY	A-1
B. SRP EVALUATION RESPONSES	B-1

HSAP FINAL REPORTS

A STUDY OF LITHIUM POLYMER BATTERIES

John D. Adkins

**Miamisburg High School
1860 Belvo
Miamisburg, OH 45342**

**Final Report for:
High School Apprentice Program
Wright Laboratory**

**Sponsored by:
Air Force Office of Scientific Research
Bolling Air Force Base, DC**

and

Wright Laboratory

August 1995

A STUDY OF LITHIUM POLYMER BATTERIES

John D. Adkins

Miamisburg High School

Abstract

Lithium polymer batteries were studied. By using a lithium polymer electrolyte a battery is able to maintain any shape and still give more power ounce for ounce than many other batteries. Because of this, it would seem the best way to make a battery, however, this battery is still in development.

Introduction

Over the last 25 years, technological progress has required lightweight, compact power sources capable of storing electrical energy. This source could be used anywhere from space and military applications to cellular phones and laptop computers in the commercial world. Because lithium is both lightweight and highly active, it and a polymer electrolyte could be combined to form a lightweight, compact rechargeable lithium-polymer battery. Since the electrolyte has polymer qualities, the battery can be molded to any shape or form necessary for the application, and because it is rechargeable, the battery is also cost effective. However, due to two technological challenges, poor interfacial stability and poor ionic conductivity the ideal battery is still under development, but we believe a simple ionic conductor will mitigate if not solve these problems.

Methodology

To investigate the properties of the single ionic conductor proposed, we performed molecular orbital calculations using both Gaussian 92 and HyperCube for various geometry optimizations. Since the principle mode of bonding for the lithium ion is through electrostatic interaction, we also utilized semi-empirical electrostatic potential calculations using HyperCube. The electrostatic potential calculations provided us with some qualitative measure of work necessary to move the lithium ion through the channel.

Results

Most polymer electrolytes are composed of a salt dissolved in a polymer. For a polymer electrolyte to conduct, the salt must dissociate in the polymer so the resulting anions and the cations can split into ions and induce conductivity. By this we mean the solid solute will then be surrounded by solvent molecules of opposite charges. The problem with this system is that eventually the anions and the cations split and migrate to different sides of the electrolyte which in turn causes a high concentration gradient that leads to poor interfacial stability. With a single-ionic conductor, this layer of resistance cannot build because the channel acts as the anion and is immobile, therefore unable to migrate to sides of the electrolyte. Interfacial stability is how long it can run before failure. The system in question provides a constant solvation sphere for the lithium ion to travel through. This implies that the energy of activation for the ionic conduction process will be minimal because the local solvation structure around the lithium ions does not vary significantly within the channel and, therefore,

the ion-channel interaction energy remains essentially constant within the channel as illustrated in Table 1 which uses semi-empirical electrostatic potential calculations.

Another problem with polymer electrolytes is poor ionic conductivity at ambient/subambient temperatures. This is important because the battery needs to run as well in the winter as in the summer. This problem arises because the polymer chains rely on molecular motion to facilitate movement of the ions from the anode to cathode. Because molecular motion is directly related to temperature, ionic conductivity drops off with the temperature. However, through the use of the constant solvation sphere, the ionically conducting channel should not rely as much on molecular motion to induce movement in the lithium ion which will allow operation at ambient and subambient temperature.

Conclusions

From our experiments we have learned that a single ionic conductor will help to improve poor interfacial stability. Also, because the channel does not rely on molecular motion to facilitate movement of the lithium ion, poor ionic conductivity at ambient and subambient temperatures is improved.

Table 1. Electrostatic Potentials as a function of distances within the channel.

-5*	-4	-3	-2	-1	0	1	2	3	4	5
-0.241**	-0.285	-0.289	-0.276	-0.258	-0.252	-0.254	-0.271	-0.284	-0.241	-0.248

* Distance in Å; "0" Angstroms corresponds to the Electrostatic Potential in the middle of the channel

** Electrostatic Potential in kcal/mole

LDV OPTICS EVALUATION FOR CRF FLOW MEASUREMENTS

Justin J. Bellante

**Dayton Christian High School
325 Homewood Ave.
Dayton, OH 45405**

**Final Report for:
High School Apprenticeship Program
Wright Laboratory**

**Sponsored by:
Air Force Office of Scientific Research
Bolling Air Force Base, DC**

and

Wright Laboratory

August 1995

LDV EVALUATION FOR CRF FLOW MEASUREMENTS

Justin J. Bellante
Dayton Christian High School

Abstract

Experiments were conducted in order to study the stability of laser anemometer optics. The effect of operating time and temperature on the power output of the laser anemometer was studied. The optical configurations tested consisted of: 1) 83mm probe with standard color separator optics 2) 83mm probe with ColorBurst system 3) 15mm probe with the ColorBurst system and 4) Projection optics. It was found that temperature had no effect on the power output of the 83mm fiber-optic probe; however, it did affect the crossing of the beams. Time had a major effect on the power output of all fiber-optics systems tested. The shifting of the laser alignment caused the beam to be misguided into the fibers; therefore, power was lost. The results display the temporal stability of the ColorBurst over the standard color separator optics when using the fiber-optic probe. The projection optics show the highest output power because it eliminates the use of fiber-optic couplers, which cause losses in power output from the system. Of the fiber-optics systems tested, the ColorBurst shows the most stability and gives the most output power; however, when possible, the projection optics should be used to provide the highest beam power in the measurement volume.

LDV OPTICS EVALUATION FOR CRF FLOW MEASUREMENTS.

Justin J. Bellante

Introduction

The Compressor Research Facility (CRF) Laser Anemometer (LA) measurement system tested is a two component system with on-axis backscatter light detection. Light is provided, in two beams, by a five Watt argon-ion laser. Each of these two beams, green at 514nm and blue at 488nm, are then split again resulting in two beams in each wavelength. One blue and one green beam then passes through a Bragg cell to provide optimum signal processing and flow direction detection. These beams will be referred to as shifted and the other corresponding beams will be referred to as unshifted. Next, all four beams pass through the couplers where they are aligned and launched into 50m of fiber-optic cable. Finally, the beams go through the fiber-optic probe and are aligned into a focal point.

During a recent test, it was observed that the Compressor Research Facility (CRF) Laser Anemometer (LA) fiber-optic probe lost power. Since the probe was operated at a higher ambient temperature than normal in this test, it was theorized that the power loss resulted from this elevated temperature. This loss in power is devastating to compressor tests because low beam power results in longer (unproductive) test time. It was also noticed that power output was decreasing over the last two test dates. The first test to use the CRF LA system was the ADLARF test conducted in July of 1993. The ACF testing powers in March of 1995 were very similar to those in the ADLARF test. However, by the end of the ACF test the power was consistently lower in the blue and green beams. Testing of the LA system gave an understanding of what was effecting the power through-put and will help provide more effective testing for future compressor tests.

The original CRF LA optical configuration was tested in order to see what affected its capability to make quick, timely measurements during the ACF test. The power of the beam plays a major role in the measuring capabilities of the probe; thus, the initial experiments were designed to see what affected beam power. Among

these experiments, power was tested as a function of time and temperature. The effect of the Bragg cells on output power was also investigated. In order to test the power output of the probe as a function of temperature, a box of styrofoam was designed and built to heat the probe. An iron/constantan thermocouple was placed on the skin of the probe to give precise temperature measurements. Beam geometry also plays a major role in the ability of the probe to take accurate measurements; therefore, a test was designed to measure the deviation of beam crossing as a function of temperature.

Once the original optical configuration, shown in Figure 1, was evaluated, other optical arrangements were studied to determine the appropriate optical configuration to be used for future LA tests in the CRF. In order to test the stability of the optics train, a comparison of the new TSI ColorBurst system, as seen in Figure 2, to the original optical system was performed. The 83mm probe was then compared to a 15mm probe that had not yet been used. Finally, a test was designed to analyze beam power using projection optics seen in Figure 3. All of these configurations would then be compared and the optimum setup would then be proposed for the next CRF LA application.

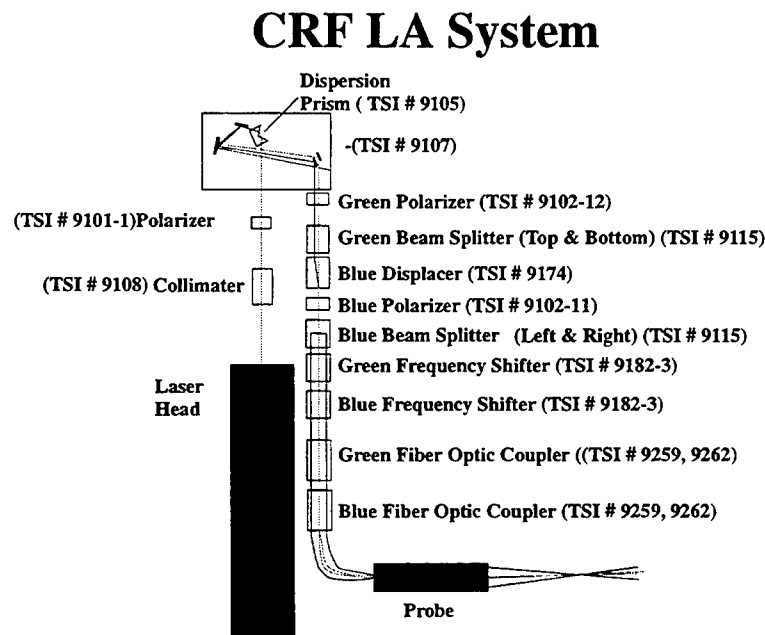


Figure 1. Original Optics Configuration

ColorBurst & Fiber-Optics

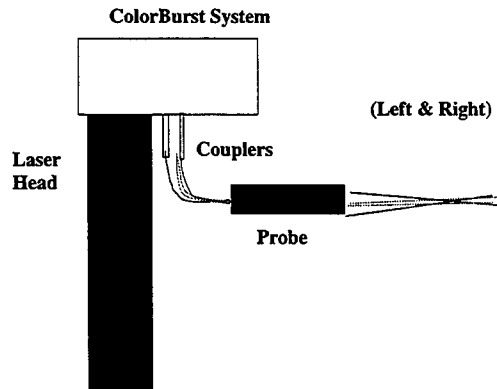


Figure 2. ColorBurst System with Fiber-Optics.

Projection Optics

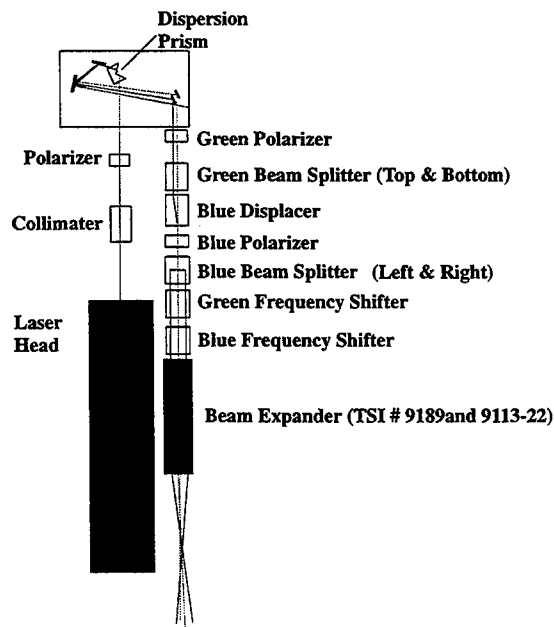


Figure 3. Projection Optics Configuration.

Methodology

Tests were conducted to study the stability of the LA system. Several system configurations were examined and compared in order that the best system could be used in the future CRF application. Test were run to analyze

power output as a function of time and temperature. Beam focal point alignment was also tested as a function of temperature. A summary of the tests performed is represented in Table 1.

Table 1. Test Descriptions

Test #	Probe	Optics System	Temp °F	Laser Power	Intent* of Exp
Test 1	83mm	Original	70-130	4.0 W	$P=f(T)$
Test 2	83mm	Original	70-140	----	$Fp=f(T)$
Test 3	83mm	Original	Room	3.5 W	$P=f(t)$
Test 4	83mm	Orig w/o Braggs	Room	3.5 W	$P=f(t)$
Test 5	83mm	ColBur	Room	3.5 W	$P=f(t)$
Test 6	15mm	ColBur	Room	3.5 W	$P=f(t)$
Test 7	-----	Project. Optics	Room	3.5 W	$P=f(t)$
Test 8	-----	-----	Room	3.5 W	$P=f(t)$

*T= Temperature *t= Time *Fp= Focal Point *P= Power

The effect of heat on the probe was investigated in Test 1. First, the 83mm probe was placed in a styrofoam box. Then a thermocouple was attached to the skin of the probe to measure the probe case temperature and a piece of styrofoam was then put over the thermocouple in order that the air temperature in the box would not affect the measurements. Next, the temperature of the probe was raised by a heater tape located at the bottom of the box. The power of the four beams (shifted blue, unshifted blue, shifted green, and unshifted green) was measured as the probe temperature was elevated in ten degree increments, between 80 and 120° F. In order to eliminate the variability in the launching of the beams into the fibers, the couplers were realigned to get maximum power before each measurement was taken. The data received from this test is seen in Table 2.

Table 2. Temperature Evaluation of the 83mm Probe (Test 1).

Time (Min.)	Temp (°F)	U Blue	S Blue	U Green	S Green	Laser Power
0	71.2	110	87	230	210	4.0W
36	72.6	115	85	255	230	4.0W
109	80.2	115	83	250	220	4.0W
187	90.0	115	80	260	230	4.0W
255	100.0	115	75	245	225	4.0W
323	110.0	110	70	255	220	4.0W
402	120.0	115	75	255	230	4.0W
463	130.0	110	75	260	235	4.0W

A constant power output was observed in Test 1. As seen in Figure 4, as the temperature was increased, the power of each beam was relatively constant throughout the experiment.

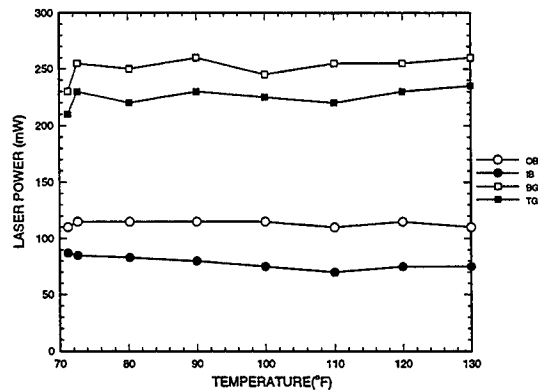


Figure 4. Temperature Evaluation of the 83mm Probe.

Measuring the differences in the location of the focal points of the two sets of crossing beams (blue and green) at temperatures from 70 to 140 °F was performed in Test 2. The beams were projected through a microscope objective lens onto a beam stop. Then, the lens was adjusted until it magnified the crossing of one set of beams. The procedure was then repeated for the second set of beams and the distance between the focal points of the two sets of beams was measured. This was repeated as the probe temperature was elevated. These results are presented in Table 3.

Table 3. Temperature Effect on Focal Point, 83mm Probe (Test 2).

Temp (°F)	Beam Cross Deviation(in.)	% Probe Vol. Length
70.6	.001	1.5%
80.0	.007	10.5%
90.0	.012	17.9%
100.0	.003	4.5%
110.0	.010	14.9%
120.0	.015	22.3%
130.0	.011	16.4%
140.0	.014	20.9%

Test 2 showed an unsteady fluctuation of the distances between the blue and green beam crossing locations using the 83mm probe. This fluctuation can easily be seen in Figure 5. The difference in distance between the blue and green crossing points varies from 0.001 to 0.015 in. or 1.5 to 22 percent of the probe volume length.

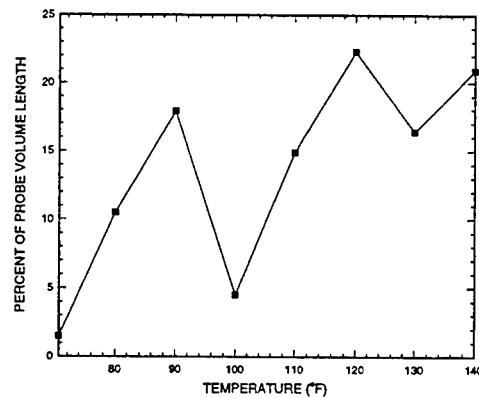


Figure 5. Temperature Effect on Focal Point, 83mm Probe.

Since temperature was found to have little impact on beam power, the remaining tests were performed at room temperature and the temporal stability of the optics was investigated. Test 3 was conducted at a constant laser head power of 3.5 Watts. The laser head power is measured before the beam exits the laser casing and enters the collimator (see Figure 1). Beam power readings were taken throughout the test at a constant temperature without adjusting the fiber-optic couplers or the laser head mirrors. To get more precise results, measurements were taken at frequent intervals over a long period of time. During this time, the laser operated continuously. These power measurements are displayed in Table 4.

A steady reduction of power was observed in Test 3. Figure 6 shows a steady drop in each beam's power reading over a period of 460 minutes with measurements taken roughly every thirty minutes at room temperature. In all the figures, the hollow squares (labeled BG) represent the unshifted green beam, the solid squares (labeled TG) represent the shifted green beam, the hollow circles (labeled OB) represent the unshifted blue beam, and the solid circles (labeled IB) represent the shifted blue beam. All figures where power was tested as a function of time are charted on the same scale to aid in the comparisons of results.

Table 4. Power Evaluation with Bragg Cells and 83mm Probe (Test 3).

Time (Min.)	Temp (°F)	U Blue	S Blue	S Green	U Green	Laser Power
0	Room	95	75	225	205	3.5W
21	Room	85	70	225	200	3.5W
62	Room	80	70	220	190	3.5W
93	Room	75	60	208	180	3.5W
120	Room	72	60	200	170	3.5W
155	Room	65	55	187	155	3.5W
180	Room	64	52	186	160	3.5W
210	Room	55	45	168	145	3.5W
240	Room	50	45	165	145	3.5W
270	Room	50	45	155	135	3.5W
300	Room	50	35	135	110	3.5W
330	Room	35	25	125	90	3.5W
360	Room	35	25	125	90	3.5W
390	Room	35	25	125	90	3.5W
420	Room	35	30	115	95	3.5W
460	Room	30	25	105	90	3.5W

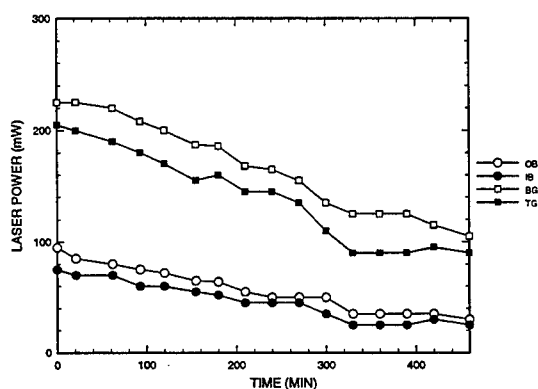


Figure 6. Power Evaluation with Bragg Cells and 83mm Probe.

The effect of the Bragg cells on the power of the beam at room temperature over a period of time was conducted in Test 4. The laser head power was again set at 3.5 Watts. Before the experiment, the Bragg cells were removed and the shifted beams were realigned into the fiber-optics. The power of the beams was then initially optimized and measurements were taken at thirty minute intervals, see Table 5.

Table 5. Power Evaluation Without Bragg Cells, 83mm Probe (Test 4).

Time (Min)	Temp (°F)	Outer Blue	Inner Blue	Bottm Green	Top Green	Laser Power
0	Room	95	130	245	275	3.5 W
36	Room	90	125	235	265	3.5 W
66	Room	80	115	235	245	3.5 W
98	Room	75	110	230	250	3.5 W
146	Room	80	110	240	260	3.5 W
173	Room	80	105	235	255	3.5W

The results of Test 4 are very similar to those of Test 2 as seen in Figure 7 and 5. Even with the Bragg cells removed, the power of each beam continued to drop in time. The initial powers in the test differed from those of Test 2. When beams go through the Bragg cells, two of the beams (inner blue and top green) are shifted in Test 2, but unshifted in Test 4.

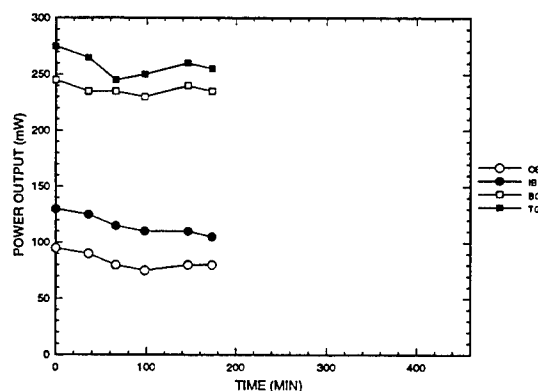


Figure 7. Power Evaluation Without Bragg Cells, 83mm Probe.

Test 5 investigated the stability of the power output of the 83mm probe using the TSI ColorBurst system. Power was initially optimized with the laser head power set at 3.5 Watts. The power output through the probe was then measured over a period of time without any further adjustments or alignments being made. The power measurements taken are presented in Table 6.

Table 6. Stability Evaluation of ColorBurst System, 83mm Probe (Test 5).

Time (Min)	Temp (°F)	U Blue	S Blue	U Green	S Green	Laser Power
0	Room	108	160	225	225	3.5 W
38	Room	118	165	225	220	3.5 W
120	Room	120	165	212	225	3.5 W
149	Room	120	168	207	225	3.5 W
181	Room	120	175	205	225	3.5 W
248	Room	120	176	190	217	3.5 W
286	Room	117	175	185	210	3.5 W
325	Room	108	175	175	205	3.5 W
346	Room	105	175	172	205	3.5 W

The results of Test 5 show that the ColorBurst system is more stable than the original color separator optics over time. Figure 8 shows steady power readings of all four beams leaving the 83mm probe throughout the test period. In the figure, the bottom green beam drops slightly; however, the drop is relatively insignificant compared to the results of Test 3 shown in Figure 6.

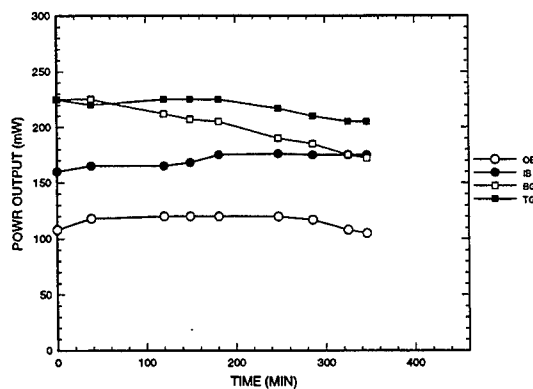


Figure 8. Stability Evaluation of the ColorBurst System, 83mm Probe.

Test 6 involved the 15mm probe with the ColorBurst system. Similar to Test 5, the beam power was initially optimized with the laser head power set at 3.5 Watts. Measurements of the beam power, shown in Table 7, were then taken at room temperature without making any additional alignments or adjustments.

Table 7. Stability Evaluation of ColorBurst System, 15mm Probe (Test 6).

Time (Min)	Temp (°F)	U Blue	S Blue	U Green	S Green	Laser Power
0	Room	135	160	265	255	3.5 W
25	Room	135	145	265	255	3.5 W
50	Room	115	130	265	260	3.5 W
90	Room	140	150	260	260	3.5 W
115	Room	130	140	250	255	3.5 W
135	Room	130	140	250	255	3.5 W

The Test 5 and Test 6 results were similar. Figure 9 shows the fairly steady power output over time, similar to Test 5 and in Figure 8. Test 6 was performed over a shorter time period, yet the basic trend in the data is the same. However, the 15mm probe consistently had a higher power output compared to the 83mm probe when using the ColorBurst system. From this it is believed that the input ends of the 83mm probe fibers need to be polished.

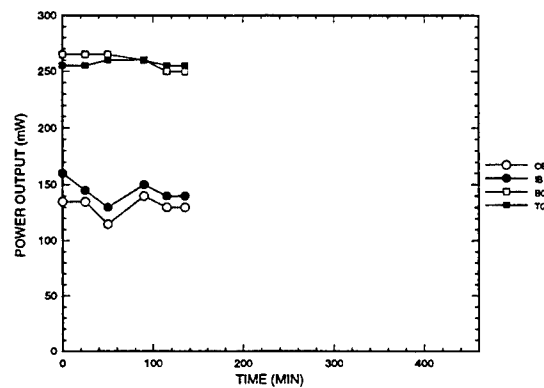


Figure 9. Stability Evaluation of the ColorBurst System, 15mm Probe.

Instead of using fiber-optics, Test 7 used the projection optics, see Figure 3. The experiment was performed at room temperature and with the laser head power set at 3.5 Watts. This experiment tested the power of the beams as a function of time. Table 8 shows the power output of the projection optics.

This test shows the advantages of the projection optics over fiber-optics. The beam powers in the projection optics are substantially higher than any of the previous tests. It is also noticeable that the beam powers are very steady at room temperature over a period of time (see Figure 10).

Table 8. Stability Evaluation of Projection Optics (Test 7).

Time (Min)	Temp (°F)	U Blue	S Blue	U Green	S Green	Laser Power
0	Room	200	240	470	380	3.5 W
40	Room	200	250	460	370	3.5 W
80	Room	200	260	470	380	3.5 W
120	Room	200	260	470	380	3.5 W
160	Room	200	260	470	370	3.5 W
190	Room	200	260	460	370	3.5 W

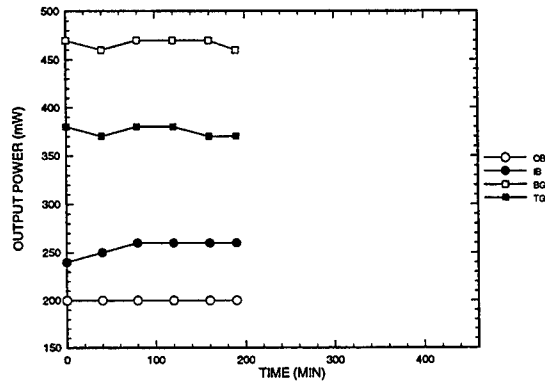


Figure 10. Stability Evaluation of Projection Optics.

Since the power output of the fiber-optics probes showed a loss over time while the projection optics did not, a variation in laser alignment was suspected as the cause. Therefore, the stability of the laser itself was examined in Test 8. The laser beam was passed through an alignment block hole. Power measurements were taken of the beam before the block and after the block. The measurements were then compared to see if shifting of the laser was taking place. The data of Test 8 is located in Table 9.

Table 9. Stability Evaluation of Laser (Test 8).

Time	Before Block	After Block
0	3.0 W	3.0 W
30	3.0 W	2.95 W
65	3.0 W	3.0 W
95	3.0 W	2.9 W
125	3.0 W	2.9 W
155	3.0 W	2.85 W
185	3.0 W	2.85 W

The Test 8 results show instability in the laser head. Figure 11 displays a drop in power over time. This drop is due to the shifting of the laser alignment. As the laser shifted, it did not completely go through the alignment block; thus, power was lost. This change in alignment can significantly reduce the power entering the fibers at the couplers. These components require the beam position to remain constant to within 5 micrometers over the run. Therefore, the laser itself may have contributed to the observed loss of probe output power in the ACF test.

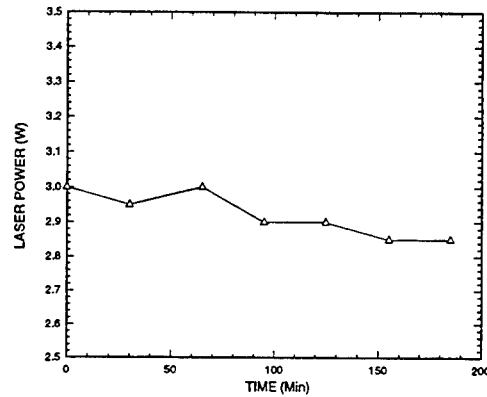


Figure 11. Stability Evaluation of Laser.

Finally, using the 15mm probe and the ColorBurst system, tests were performed to determine power transmission through the fiber-optics. Laser head power was set at 4.0 Watts and power readings were taken as the beams exited the Bragg cells and the 15mm probe. The same procedures were then repeated with the laser head power set at 3.5 Watts.

Measurements taken of the beams exiting the Bragg cells before they entered the couplers were significantly higher than those taken of the beams after leaving the head of the 15mm probe are shown in Tables 10 and 11. In the table, U and S represent the shifted and unshifted beams.

Table 10. Percent of Power Transmission Through the 15mm Probe at 4.0W.

Beam	Bragg Cells mW	Probe mW	% Output	Laser Power
U Blue	300	125	41.6	4.0 W
S Blue	380	170	44.7	4.0 W
U Green	560	260	46.4	4.0 W
S Green	620	400	64.5	4.0 W

Table 11. Percent of Power Transmission Through the 15mm Probe at 3.5W.

Beam	Bragg Cells mW	Probe mW	% Output	Laser Power
U Blue	280	125	44.6	3.5 W
S Blue	340	155	45.6	3.5 W
U Green	510	250	49.0	3.5 W
S Green	570	340	59.7	3.5 W

Next, a test was run to measure the focal point movement of the 15mm probe. First, the laser head power was set at 4.0 Watts and the beam power output through the probe was optimized. The distance between the focal point of the two sets of beams was then measured. The testing showed that the beams were not crossing at the same distance from the probe. In addition, the crossings were not aligned with the optical center of the probe. Therefore, the results show that the probe was faulty in its beam alignment.

A comparison summary of power measurements taken in several tests with various system combinations are shown in Tables 12 and 13. Power levels are represented in milliwatts, unless otherwise noted. Table 12 presents the power output for ADLARF, ACF, and this investigation when using the ColorBurst and projection optics. Table 13 shows the decrease of the measurement system power output of the LA system from ADLARF to the post ACF testing dates.

Table 12. Comparison of Power Out of Bragg Cells in Different Tests.

	U Blue	S Blue	U Green	S Green	Laser Power
ADLARF	225	185	640	500	4.2 W
Pre ACF	420	360	730	590	4.75 W
Post ACF	280	320	660	500	4.0 W
ColorBurst	300	380	560	620	4.0 W
Proj.Optics	280	340	660	500	4.0 W

Table 13. Comparison of Probe Output Powers in Different Tests.

	U Blue	S Blue	U Green	S Green	Laser Power
ADLARF	134	134	285	306	4.2W
Pre ACF	160	160	300	350	4.0W
Post ACF: 83mmProbe OrigOptics	115	90	260	235	4.0W
83mmProbe ColorBurst	130	190	230	220	4.0W
15mmProbe ColorBurst	135	160	265	255	3.5W
Projection Optics	220	300	520	400	4.0W

Table 14 shows the efficiency of the fiber-optic cables and couplers by comparing the measurements from the two tables above. The data in the table represents the percentage of power that exits the probe based on the power of the beam entering the couplers. The results show that power is lost through the couplers and fibers and that the coupling efficiency of the LA system dropped from the ADLARF testing dates to the post ACF testing dates.

Table 14. Coupling Efficiency: % Power Transmission Through the Couplers and Fibers.

	U Blue	S Blue	UGreen	SGreen
ADLARF	59.6%	72.4%	44.5%	61.2%
Pre ACF	41.1%	28.1%	39.4%	47.0%
Post ACF: 83mm Probe/ ColorBurst	43.3%	50.0%	41.1%	35.5%
15mmProbe/ ColorBurst	45.0%	42.1%	47.3%	41.1%
Projection Optics	78.6%	88.2%	78.9%	80.0%

Conclusions

This investigation clearly shows that the CRF LA system power is affected by time. It is concluded that the probe power output of each beam drops over time because of a shifting of the laser beam alignment. The power output is not affected by the probe temperature over the range of 70 to 130°F; however, temperature does affect the probe alignment. As the beam alignment changes in the couplers, power is lost. The alignment at the fiber-optics

input must be constant to within 5 microns. This shifting in alignment does not affect the Bragg Cell or projection optics power output.

Along with a lack of stability in power output, there is also a concern with beam quality of the laser. During testing it was noticed that with the laser head power set at 4.0 Watts, the output beam power was lower than those with the laser head power set at 3.5 Watts. Consequently, the laser should be examined by a representative from Coherent and the above stability problems should be investigated.

The longer and more inefficient measurements experienced in the ACF test may have been caused by the fluctuation in the laser alignment or reduced fiber-optic coupling efficiency. The sensitivity of probe alignment with temperature was eliminated near the end of ACF testing when the fiber-optics probe was maintained at a constant temperature.

Test results with the ColorBurst system combined with either the 83 or 15mm probe substantiate that the ColorBurst system improves the launching stability of the beams into the fibers. This new system is less sensitive to laser alignment and results in improved stability relative to the original CRF LA system optics. When using fiber-optics, the ColorBurst system has many advantages over the optics that are currently being used. The ColorBurst saves time during alignment because of its simplicity. Experiments would have to be conducted to determine the compatibility of the ColorBurst system with the projection optics if such a configuration was desired.

The 15mm probe provided a higher power output than the 83mm probe when using the ColorBurst system. Since these two systems use the same fiber-optics, this indicates possible degradation of the 83mm probe optical system. One possible source of degradation is the entry port to the fiber; therefore, the 83mm probe should be sent to TSI and it should be cleaned and checked for damages in the fiber-optics. In addition, it was discovered that there were major problems with the beam crossing of the 15mm probe. Because of these problems, the 15mm probe should also be sent back to TSI and repaired under warranty.

During tests, questions were raised about the reliability of the power meter that is currently being used to measure the power of the beams. A more accurate and consistent power meter with a digital display would save a significant amount of time in aligning and testing the system.

The recommendations and conclusions in this report concern only the light producing portion of the CRF LA system (laser, color separation, beam coupling, fiber-optics, and transmission optics); they exclude the effects of the actual test environment, receiving optics, and electronics for data acquisition. For the upcoming GESFAR test, the best option may be to use the projection optics in order to get the most power output, approximately twice the output power of the fiber-optic configuration. Tests should be run to analyze environmental and receiving optics concerns. One possible way to investigate the effects of the test chamber environment on the projection optics system would be to mount the system and use it in a calibration jet while other GESFAR compressor testing is being accomplished. If the projection optics retain alignment and output power during the test, it would provide the highest power in the measurement volume and, possibly, the highest data rate. Therefore, the shortest run time may be achieved with this configuration. If the projection optics are more efficient, the fiber-optics systems should only be used when the test configuration prevents the use of the projection optics, as was the case in the ACF test.

A STUDY OF THE THERMAL BREAKDOWN
OF TRICRESYL PHOSPHATE

Matthew L. Blanton

Wayne High School
5400 Chambersburg Rd.
Huber Hts, OH 45424

Final Report for:
High School Apprentice Program
Wright Laboratory

Sponsored by:
Air Force Office of Scientific Research
Bolling Air Force Base, DC

and

Wright Laboratory

August 1995

A STUDY OF THE THERMAL BREAKDOWN
OF TRICRESYL PHOSPHATE

Matthew L. Blanton

Abstract

The gas phase thermal decomposition of tricresyl phosphate was studied. To measure the chemical breakdown of tricresyl phosphate, amounts of up to 0.2 microliters of tricresyl phosphate were injected into a high temperature thermal reaction compartment (TRC) for thermal stressing. From there, the reaction products were focused onto a gas chromatograph - mass spectrometer (GC-MS) for separation and identification of thermal decomposition products. The results of the experiment reveal that tricresyl phosphate is highly stable in air at temperatures up to 500 degrees Celsius.

A STUDY OF THE THERMAL BREAKDOWN
OF TRICRESYL PHOSPHATE

Matthew L. Blanton

Introduction

Over the past few years, phosphate esters have been increasingly synthesized as a result of a constantly growing need for better, more efficient plastics, polymers and lubricants. One of the most widely used phosphate esters is tricresyl phosphate (TCP). There are many advantages with the use of this product. TCP is fire-resistant and non-corrosive, as well as an excellent anti-wear additive in lubricants. On the other hand, TCP does have its disadvantages. Studies have proven that when TCP is in the 'ortho' isomer state, it becomes a potent neurotoxin, which, even in single doses, leads to severe flaccid paralysis associated with demyelination in the peripheral nerves and in the white matter of the spinal cord. Though extensive research has already been done, a great deal of information about TCP is still left unknown. One bit of information important to the Air Force is that of the safety of TCP. Because TCP is used in lubricants at high temperatures, a chemical reaction may occur, and the chemicals released may be harmful to the personnel exposed to them. To take necessary precautions, the chemicals released by TCP during thermal stress must be known. One study geared for finding this information is the thermal breakdown of tricresyl phosphate.

Methodology

To begin the gas phase thermal decomposition of tricresyl phosphate, 0.02 microliters to 0.2 microliters of tricresyl phosphate were injected into the high temperature thermal reaction compartment (TRC) for thermal stressing. The

tricresyl phosphate was first injected, as a liquid, into an injector tube containing silanized glass wool, located within the TRC. The tricresyl phosphate, while resting within this wool, was subjected to an injector temperature of 185 degrees Celsius. As the tricresyl phosphate vaporized, air then swept it into the reactor, where it was subjected to temperatures ranging, depending on the run, from 250 degrees Celsius to 750 degrees Celsius. This exposure time lasted for a well controlled two seconds, give or take 0.02 seconds. It is important to note that, during this two second exposure time, the tricresyl phosphate vapors have decomposed and that no further decomposition should take place. From the TRC, the reaction products were then carried into the gas chromatograph (GC) for separation. After the reaction products entered the GC, the air was immediately shut off, with helium substituting it to insure that no further oxidation could take place. While transitting through the GC, all the reaction products were separated according to molecular weight. The products with the lighter molecular weights moved ahead of the products with heavier molecular weights, and continued in this pattern throughout the GC. After separation, the products were introduced to the mass spectrometer (MS) where they were finally detected. As each separated product entered the MS, the exact GC retention time and molecular weight, as well as many other important parameters, were determined. These data were then processed on the GC-MS Chemstation for data analysis and editing. A mass spectrum was formed of each of the reaction products and a computerized mass spectral data base library search was done. When a library search takes place, one of two results may be encountered. {1} Possible matches may be found of the spectrum being searched, in which case probabilities, as well as the matching spectra, are provided to aid the experimenter. Or {2} no matches may be found, in which case the experimenter must resort to his or her own knowledge and experience to come up with the

reaction product's identity. In either case, knowledge of the starting materials, stressing conditions, and common sense must be applied before reporting the identity of any detected compound.

Results

Many products were formed during the decomposition of tricresyl phosphate. The most abundant of the products formed were Methyl phenol, Methyl benzene, Phenol, and Benzene. Other, less abundant products formed consisted of acetic acid, Benzofurans, Naphthalenes, and dozens more. Of these products, Methyl phenol was, in many of the spectra, the first to appear. It was not until temperatures reached 500 degrees Celsius that many of the other products began to appear. This is due to the assumption that at 500 degrees Celsius and above, the Methyl phenol decomposes to give other products. The Methyl phenol then can react with itself and its progeny to form many varied organic compounds. Generally, temperatures below 500 degrees Celsius did not form many different decomposition products, other than Methyl phenol. At 500 degrees Celsius to 600 degrees Celsius, the decomposition and reactions proceeded relatively slowly. Above 600 degrees Celsius, however, there was an obvious acceleration in the decomposition of tricresyl phosphate, until temperatures above 725 degrees Celsius to 750 degrees Celsius were reached, at which time the decomposition moved toward more complete combustion. These results prove the fact that tricresyl phosphate is highly stable at temperatures reaching 500 degrees Celsius.

Conclusion

The future looks bright for the use of tricresyl phosphate as an additive in lubricants. Because tricresyl phosphate is highly stable, even at high temperatures, it will be used in a new lubrication technique pioneered at Wright

Patterson Air Force Base, known as vapor lubrication. Vapor lubrication will enable high temperature machinery, such as turbine engines and high speed tool producing spindles, to operate at much higher temperatures than has ever been possible before.

References

- Gunderson, Reigh C. and Andrew W. Hart. Synthetic Lubricants.
New York: Reinhold Publishing Corporation, 1962.
- O'brien, Richard D. Toxic Phosphorous Esters - Chemistry, Metabolism, and
Biological Effects. New York: Academic Press, 1960.
- Shubkin, Ronald C. Synthetic Lubricants and High-Performance Functional
Fluids. New york: Marcel Dekker, Inc., 1993.

**Calibrating Transducers for Dynamic
Data Acquisition**

Robert D. Boyer

**Dayton Christian High School
325 Homewood Avenue
Dayton, Ohio 45405**

**Final Report for:
High School Apprenticeship Program
Wright Laboratory**

**Sponsored by:
Air Force Office of Scientific Research
Bolling Air Force Base, DC**

and

Wright Laboratory

August 1995

Calibrating Transducers for Dynamic Data Acquisition

Robert D. Boyer
Dayton Christian High School

Abstract

Accelerometers and pressure transducers were calibrated. Several tests were performed, but in all cases a calibration device that emitted a given amount of stimulus. The transducer sent its response to various output devices such as data analyzers and voltmeters which quantified the data into a more useable form. These calibrations determine whether the transducer is functioning correctly as well as it's sensitivity to the given stimulus. This information allows the transducer to be accurately used for data acquisition.

The various transducers used in stress testing must first be tested to ensure that they are functioning properly, and then their sensitivity must be determined. This process is called calibration and it is vital for accurate data acquisition. A transducer is a device that converts energy from one form into another usually more quantitative or usable form. Many transducers convert their output onto electrical energy, which is readily readable as volts. These devices allow data to be easily gathered and used, but it is first necessary to know the ratio between the amount of stimulus that the transducer receives and the amount of electrical energy that is given as output. This is accomplished with the use of devices that emit a known quantity of the stimulus to the transducer. This method of calibration is used not only to determine a transducer's sensitivity, but it is also used to ensure that the transducer is working correctly.

The two types of transducers being dealt with are accelerometers, and pressure transducers, which are commonly called microphones. These types of transducers are used to determine the amount of stress a structure can safely endure or to locate the source of structural integrity problems. Centrifugal force, gravitational force, and other related forces are measured with an accelerometer. Vibration is one motion to which an accelerometer will respond. Pressure transducers are sensitive to changes in pressure and are used to determine acoustical stress or aerodynamic problems. Many structures, such as automobiles and especially airplanes, benefit from this type of testing because of the high levels of noise and vibration that are produced during their operation and the consequently high levels of stress they must withstand. The demands placed on these structures make transducers and,

therefore, their calibration important to the industries that produce them.

A calibration exciter, a power supply, and two output devices are necessary to calibrate an accelerometer. A piece of double-sided tape is used to attach the accelerometer to the calibration exciter. A wire lead connects the accelerometer to the power supply, which is attached to an oscilloscope and a multimeter. Activating the calibration exciter causes it to vibrate the accelerometer at one gravity. The accelerometer then draws fifteen volts from the power supply and sends a signal to both the oscilloscope and the multimeter through the power supply. This signal is presented as a sine wave by the oscilloscope and a reading in millivolts by the multimeter. The reading and the sine wave should be stable, but if one or both of them are not stable then the accelerometer is damaged or defective and cannot be used. Whether the accelerometer is defective or not, the information must be logged. The log contains the accelerometer's model and serial numbers as well as a sensitivity in millivolts per gravity obtained from the multimeter if the accelerometer functioned correctly or a reason for the negative rating if it was defective. This completes the process of calibrating an accelerometer.

Calibrating a pressure transducer is a very involved process because a piston phone calibration, static calibration, and a random noise calibration as well as a test of its input and output impedance must be done. A piston phone calibration is performed by connecting the pressure transducer to a signal conditioner that sends the signal to a data analyzer. The piston phone is placed over the pressure transducer so that its signal, which in this case is a constant 124 decibels, will be gathered by the transducer. The data analyzer plots the data it is

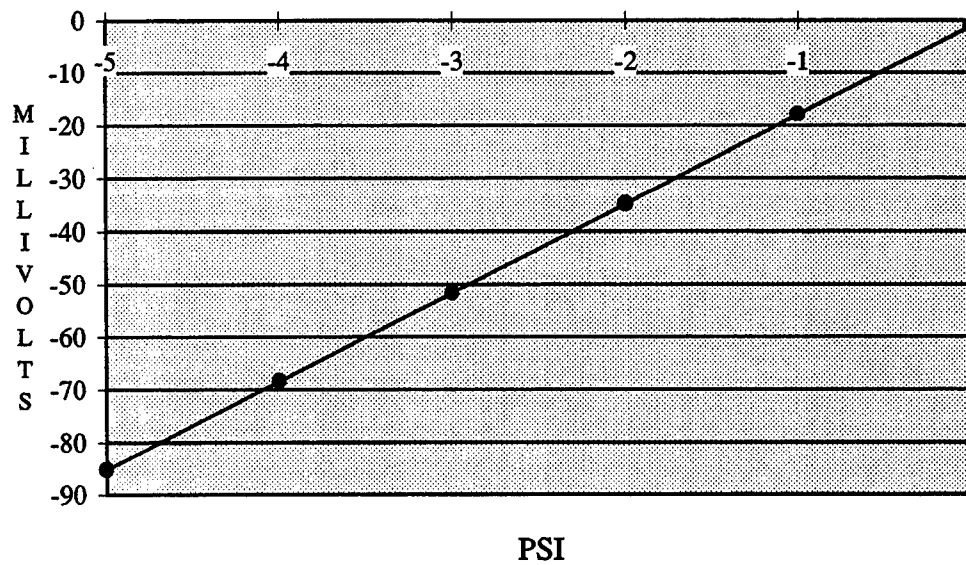
receiving and determines the transducer's sensitivity in millivolts per PSI, pounds per square inch. Another test done to determine a pressure transducer's sensitivity is a static calibration. In this test the transducer is placed in a vacuum, and the pressure is increased in one PSI increments. The data is sent from the pressure transducer to a computer where it is recorded and used to create a chart of the calibration. A random noise calibration ensures that the pressure transducer is functioning correctly over its entire range of frequencies. The pressure transducer is attached to both a signal conditioner and a random noise generator. When the generator is activated, it produces noise in a wide band of frequencies. The transducer takes those frequencies and sends them to a signal conditioner which then sends a signal to a data analyzer. If the pressure transducer is functioning correctly, the data analyzer will show that all the frequencies are getting through at about the same level and that the coherence, or integrity, of the data is a consistent line at one. The last step in calibrating a pressure transducer is a test of its input and output impedance. A solid electrical connection is made with an ohmmeter on the transducer's two input wires until the meter's reading is stable. This is done three times to ensure that the reading is accurate. The same procedure is followed on a pressure transducer's output wires to determine the output impedance. All of these tests ensure that the pressure transducer is ready to be used for accurate data acquisition.

When a calibration is completed, a graph is often made as a visual record of the data. The data analyzer used to calibrate pressure transducers created a graph of the calibration as the data was collected. Computer programs exist that create a graph from a body of data. Graphs for the static calibration were created using this type of program. Both types of graph

were stored in computer files for future reference. Graphs from samples of the static, random noise, and piston phone calibrations are on the next two pages.

These graphs are very useful calibration tools. A straight line on a static calibration's graph shows that the pressure transducer's sensitivity remains consistent over a range of pressures. In a random noise calibration, a graph clearly shows whether all frequencies are being received by the pressure transducer. A coherence graph shows which frequencies are getting through the transducer accurately. Sensitivity at a given frequency is determined by a piston phone calibration. The largest peak is the one caused by the sound emitted by the piston phone. There is also a peak at sixty hertz the graph because of external noise that is always present. Obtaining this type of data is the purpose of calibrating a transducer.

Pressure Transducer-Static Calibration



<u>volts</u>	<u>PSI</u>	<u>mV</u>
-.001049	0	-1.049
-.017916	-1	-17.916
-.034775	-2	-34.775
-.051609	-3	-51.609
-.068390	-4	-68.390
-.085135	-5	-85.135
-.068423	-4	-68.423
-.051641	-3	-51.641
-.034804	-2	-34.804
-.017940	-1	-17.940
-.001061	0	-1.061

SLOPE= 59.432

INTERCEPT= 0.0653585

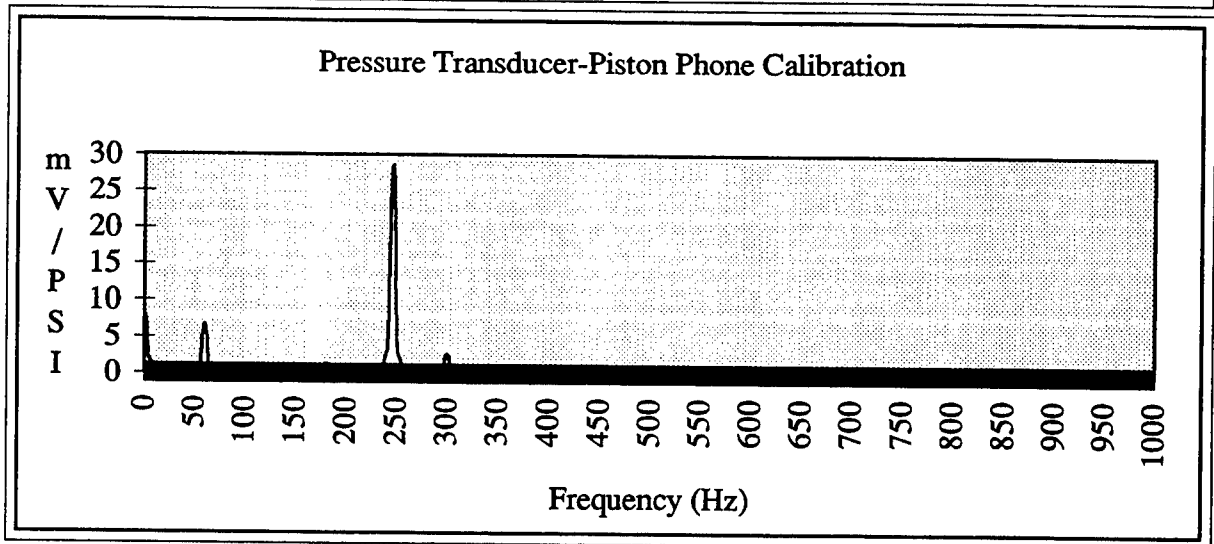
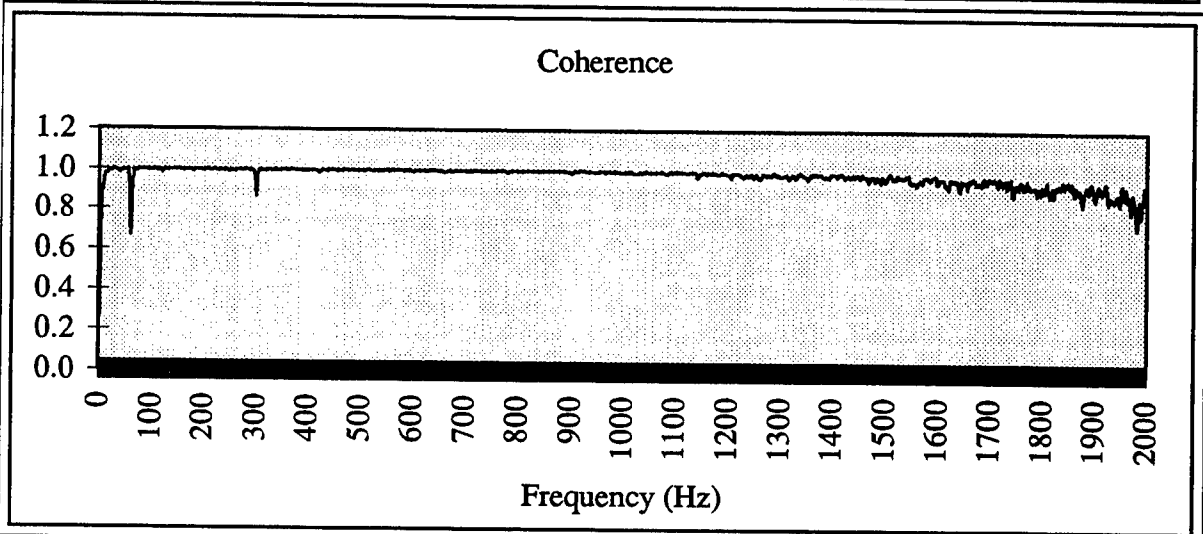
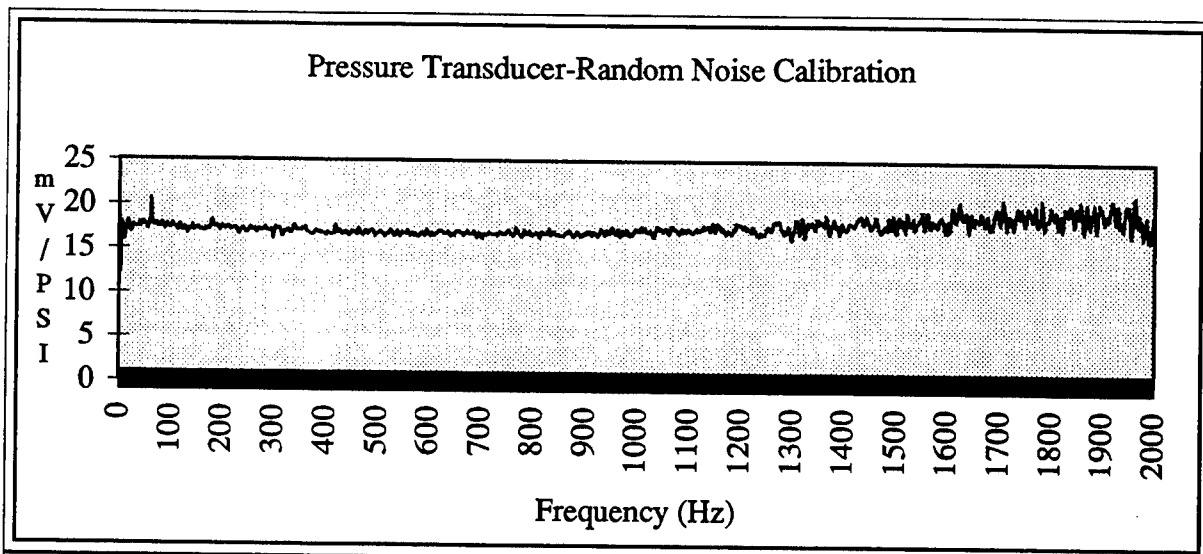
XD ID=KULITE MOD LQ-125-5D; S/N 5248-1B-113; EX=10VDC; T=23C

DATE=04-21-1995

TIME=08:27:44

XD No. 10

CONST FILE SEQ No. 11



References

Data Acquisition Systems 1994-1995 Catalog. Strawberry Tree Incorporated. 1994.

Wright Laboratory Structural Dynamics Branch-Solving Dynamic Problems. U.S.

Government Printing Office. 1992

David Banaszak- Electrical Engineer & Mentor.

A MICROANALYSIS OF EVERDAY HOUSEHOLD ITEMS

Laura K. Braydich

**Miamisburg High School
1860 Belvo Road
Miamisburg, Ohio 45342**

**Final Report for:
High School Apprentice Program
Wright Laboratory**

**Sponsored by:
Air Force Office of Scientific Research
Bolling Air Force Base, DC**

and

Wright Laboratory

October 1995

A MICROANALYSIS OF EVERDAY HOUSEHOLD ITEMS

A scanning electron microscope (SEM) is made up of four basic elements. These elements are an electron gun, magnetic lenses, a vacuum system, and a device that displays the image the microscope produces. To begin with, the electron gun emits electrons which strike the specimen and create an image. Next, the magnetic lenses are used to direct the path of the electrons emitted from the electron gun. Moreover, it is very important to have a vacuum system to remove air molecules because they scatter electrons easily. Finally, an SEM must have a device that displays the image produced from the electrons.

An SEM is used to create a detailed and realistic picture of the surface of an object. The image is produced when a tight beam of electrons moves over the sample. These electrons might scatter off the sample or emit secondary electrons from the specimen's surface. The scattered or secondary electrons are collected by an electronic device located next to the sample. These are the electrons that created the image that appears on the monitor.

This summer we created a catalog of various samples to be used in briefings and presentations. Aside from learning how to operate an SEM, we had to learn how to prepare and load the specimens. Before a sample can be placed into an SEM it must first be prepared. To begin with, if the sample is alive it must be killed. Most of the insects were killed either by drowning them in alcohol or starvation. Next, the sample must be mounted on a silver stub with either super glue or silver paint. After being mounted the sample must be placed in a desiccator to draw out any moisture. This is very important because if there is moisture in the sample the electrons striking the specimen will cause the moisture to boil and the specimen will move in the microscope. Once removed from the desiccator, the sample must be placed in a gold-palladium sputter coater, so the specimen is able to conduct electrons. Finally, once the specimen is coated it is now ready to be placed in the microscope.

In order to place the sample in the microscope, it had to be picked up with tweezers to avoid contamination. Once the sample has been placed in the chamber, a vacuum must be created. This was very easy since all we had to do was press the *VAC* button. After waiting a couple minutes the vacuum was stable and we could turn the screens on. Once the image appeared, the zoom, magnification, and focus buttons were used to create a good picture. The zoom button increased the magnification in a series

of ten (10, 20, 30, etc.). Likewise, the magnification button increases by an order of magnitude. Next, the coarse, medium, and fine focus buttons were used to create a clear picture. The coarse button was generally used for magnifications lower than 500. Where as, the medium focus was generally used for magnifications between 500-1000. Finally, the fine focus was used for magnifications over 1000. Once a clear image of the specimen has been created a picture is ready to be taken. Pictures were taken on instamatic film. The negatives were processed and sent to a graphics shop to be made into slides.

We began the project collecting various samples. First, in the woods by the lab different insects and plants were collected. Next, household items, like sugar and salt, were collected from the cafeteria. Other samples, like hair from pets and fabrics, were collected from our homes. We collected and prepared over 60 samples. However, we were only able to look at and photograph about half. Those that were photographed have been placed into an album, and those that have not are still at the lab.

SCANNING ELECTRON MICROSCOPES

Johnna Brough

Miamisburg High School
1860 Belvo Rd.
Miamisburg, OH 45342

Final Report for:
High School Apprentice Program
Wright Laboratory

Sponsored by:
Air Force Office of Scientific Research
Wright Patterson Air Force Base, OH

and

Wright Laboratory

October 1995

SCANNING ELECTRON MICROSCOPES

Johnna Brough
Miamisburg High School

Abstract

Scanning electron microscopes are used for various subjects and in various fields. My designated project was to catalog various specimens using an E-TEC microscope dating from around the mid-seventies. This catalog was to be used in various briefings and conferences by the lab who provided my sponsorship. I was given a partner to work with and we completed what we hope will be a useful resource for our sponsors and other educators. My partner and I have both had previous experience with scanning electron microscopes, but this program helped us to define our skills as well as giving us experience in a business environment.

SCANNING ELECTRON MICROSCOPES

Johnna Brough

Introduction

I began working with scanning electron microscopes approximately four years ago with a group from my high school. This group is known as SEMEDS, which stands for Scanning Electron Microscope Educators. SEMEDS is sponsored by Wright Patterson Air Force Base and is used mainly in training students of high school age. It consists of two visits to the base: one to learn about the microscope and one to learn how to use it. On account of our enthusiasm our group was able to return more than our allotted amount of times. This led to several interviews and eventually a job opportunity for myself and another classmate with the HSAP. We were assigned the project of creating a catalog of acceptable scanning electron microscope (SEM) photographs to be used by the base as they see fit.

Methodology

We began with the collection of substances. Specimens ranging from various insects to sugar and paper were obtained. We then set about the preparation of the specimens for the E-TEC, the microscope we were using. The specimens were first put in a desiccator to dehydrate them of all moisture. After twenty-four to thirty-six hours in a desiccator the specimens were then loaded into a gold-palladium sputter coater.

In this coater they are covered with a gold-palladium mixture to ensure the specimen's conductivity. Once the specimens were coated we placed them in the E-TEC. By adjusting the focus and the magnification gradually we were able to obtain suitable specimens. We used base magnifications of 70x, 130x, 220x, 350x, 500x, 700x, and 1000x. On some specimens we were able to obtain higher magnifications. In obtaining higher magnifications the astigmatism of the picture had to be adjusted as well as the focus to maintain a clear and precise picture. After taking the pictures of the specimens we then had to prepare the negatives ourselves in order for them to be used again. These negatives were made into transparencies and slides, some of which my partner and I were able to use in our own briefings.

Conclusion

Although we did not learn new and different chemical equations or more specialized chemistry, we did learn more about a medium that is considerably important to the scientific and medical world. We took rudimentary skills at a sophisticated machine and honed them after months of practice. We even became familiar enough with the machine to give demonstrations on it in our last month of residency. My only hope is that the pictures we took will interest others to participate in programs to become more familiar with SEM's and learn that they too can operate a sophisticated piece of machinery.

**SUPPORT OF LASER RADAR (LADAR)
AUTOMATIC TARGET ACQUISITION (ATA)
ALGORITHM DEVELOPMENT AND EVALUATION**

Kimberly N. Cabral

**Choctawhatchee High School
110 Racetrack Road
Fort Walton Beach, FL 32548**

**Final Report for:
High School Apprenticeship Program
Wright Laboratory**

**Sponsored by:
Air Force Office of Scientific Research
Bolling Air Force Base, DC**

and

Wright Laboratory

August 1995

SUPPORT OF LASER RADAR (LADAR)
AUTOMATIC TARGET ACQUISITION (ATA)
ALGORITHM DEVELOPMENT AND EVALUATION

Kimberly N. Cabral
Choctawhatchee High School

Abstract

The creation of an automatic target acquisition algorithm for detection, identification, and aimpoint selection of fixed high-value and critical mobile targets was studied. Three-dimensional, wire frame models were generated to aid in the identification process. Targets were extracted from real ladar range imagery also to aid in the process. For future use, the synthetic images would be compared to the actual (unidentified) targets. Through an organized process, the actual target could then be identified.

SUPPORT OF LASER RADAR (LADAR) AUTOMATIC TARGET ACQUISITION (ATA) ALGORITHM DEVELOPMENT AND EVALUATION

Kimberly N. Cabral

INTRODUCTION

A direct relationship exists between technology and the degree of needed sensor capability: as technology improves, the need increases. The importance of laser radar, or ladar, has been established, as it can do much for the Air Force. In example, it can be used in such programs as Tactical Ladar Seeker, Advanced Tactical Ladar System, and Low-Cost Anti-Armor Submunition.

To attain a system for effective development of ladar seekers, Wright Laboratory created LRTAG (Laser Radar Technical Analysis Group), a team of government and civilian workers with the goal of creating an automatic target acquisition algorithm suite which could accurately detect and identify fixed high-value and critical mobile targets. Fixed high-value targets include petroleum tanks and bridges. APC's (armored personnel carriers), trucks, SCUDs are critical mobile targets. The LRTAG classifier, then, would be designed for low-cost imaging ladar seekers, government-owned, and capable of modification with future technological advance.

PROBLEM

The development of an effective and relatively cheap ATA algorithm has already been established as a problem. Yet a significant problem is creating an algorithm which has high performance- successful distinguishment between a BRDM and an M60, for example. This is highly important, since it would not be favorable to destroy a friendly vehicle on the

battlefield. The synthetic images need be as real and the identification process as accurate as possible.

METHODOLOGY

Before reviewing the procedure, the LRTAG classifier itself must be understood. It is designed to compare unknown targets to a set of templates of known targets. Templates of each potential target type are generated and then compared with the unknown target. Since both objects are three-dimensional, only those relatively similar may be compared. (For example, a cargo truck would not be compared with a main battle tank.) The process will be discussed more closely shortly.

The classifier consists of four main modules: the sequencer module, pose measurement module, model projection module, and pyramid correlator module.

Classifier results are displayed in the Sequencer, as it is the controlling module. It is responsible for the actions in the other three modules and compiles the information from them to give a final output.

Each segmented object goes through the Pose Measurement module so its orientation can be established. This module measures the azimuth angle of the longest axis of the target. The type of target is independent of this measurement.

The Model Projection module, based on orientation and sensor position of target model as sent by the Sequencer, correlation matches the object. Then a list of the reference pixels intersecting the three-dimensional wire-frame models at a specified position is created to

form a ladar, or synthetic, image. (A program dubbed IRMA does this.) Indeed, synthetic images save the government money as well as time.

Actual three-dimensional correlation matching occurs in the Pyramid Correlator module. The x , y , and z coordinate points from the templates of known objects are compared with those coordinates of the unknown targets. Correlation match quality (how well the pixels agree) is then determined, the values ranging from zero to one, one being the most desirable. If, in example, an unknown target is compared with three known targets (synthetic images) and the correlation values for the unknown with each are .02, .98, .50 (respectively), then the unknown target will assume the name of the known target it had a .98 correlation value with (the second one).

Two personal tasks this summer were the generation of three-dimensional wire-frame models and the extraction of real laser radar imagery. The wire models were a part of the wire projection module, or the identification algorithm suite. The range of the target, then, is based on its orientation and position as well as the sensor's position. The real ladar imagery was used in the pyramid correlation process, as the synthetic imagery was compared to the models already created.

In the generation of models, the desired vehicles were first researched in a military vehicle reference book to find length, width, height, etc. The information was used to transfer the picture from the book to the computer. Several polygons were created to make a model of the actual target. To distinguish between visible and non-visible polygons, the right-hand rule for the order of the vertices was used. The number of vertices in a three-dimensional polygon could range from 3 to 30, and the possible number of polygons in a model is virtually unlimited.

Axes were x horizontal, y from front to back, and z vertical.

A few examples of models built in UNIX follow.

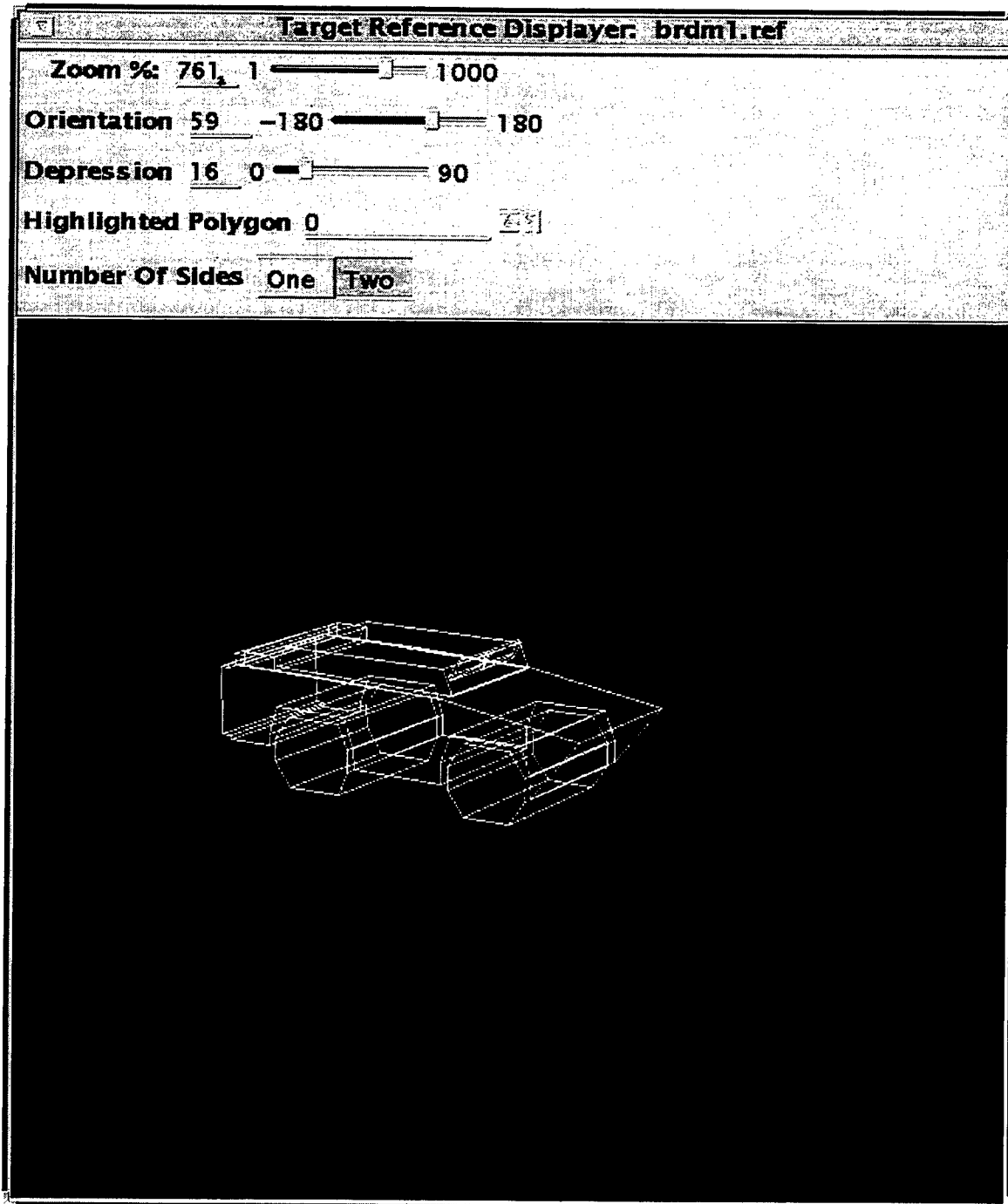


Figure 1 shows a BRDM1, an amphibious scout car. It has been upgraded by the BRDM2, seen in figure 2.

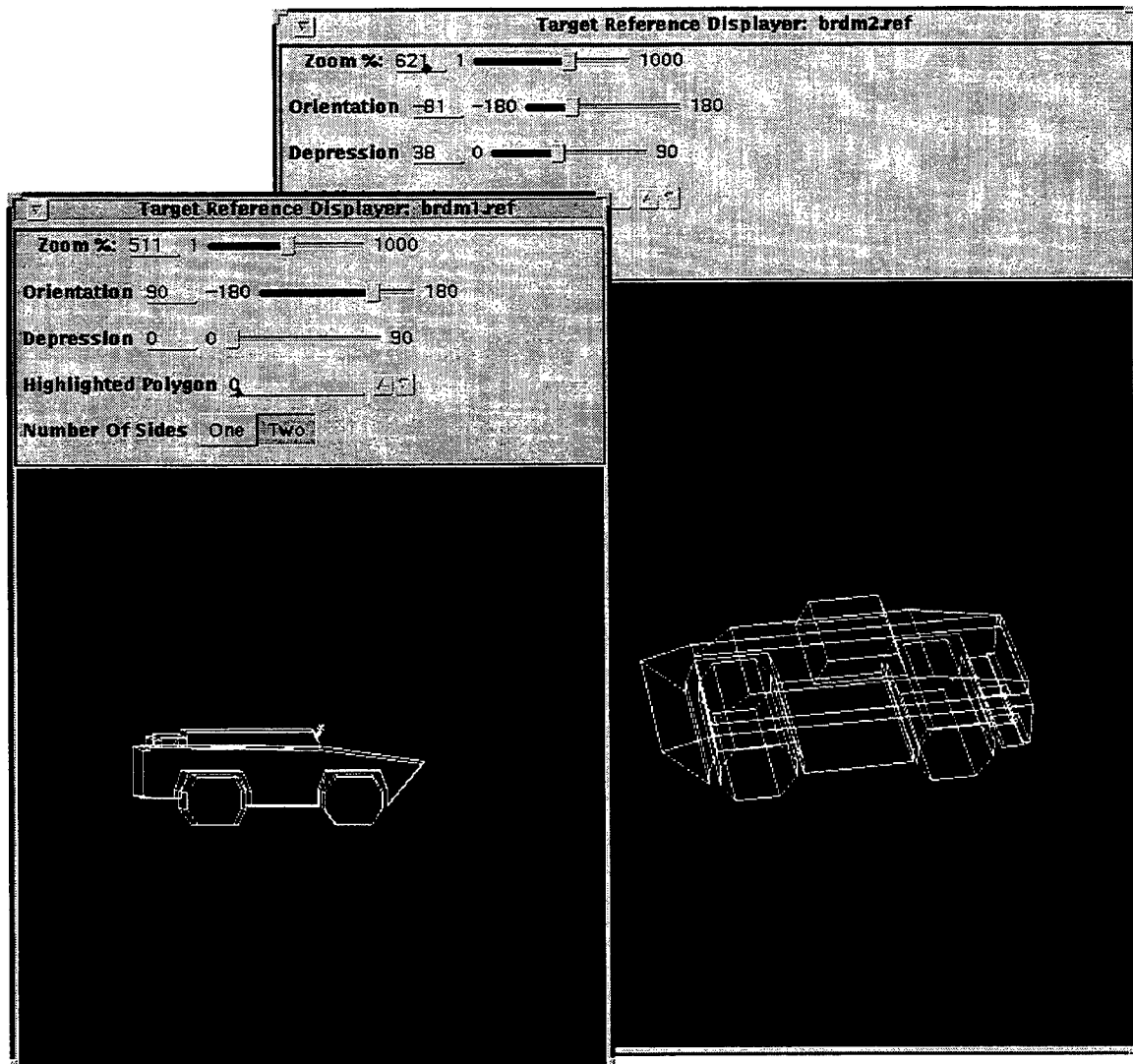


Figure 2

In Figure 2 one can see the difference between the BRDM1 and BRDM2.

In the display models, "zoom," of course, makes the model larger or smaller. The "orientation" moves the model in and out of the y axis, so the viewer can see the left and right sides of the figure. "Depression" moves the model up and down, with the center point grounded. The "highlighted polygon," of which there is none in this figure, makes it easier for the viewer to see in which polygon there has been a creation error. One can see the sides which are supposed to be seen by the human eye in a straight-on look if the "number of sides" is one. This selection also helps the builder to see if the polygon vertices were put in the correct order.

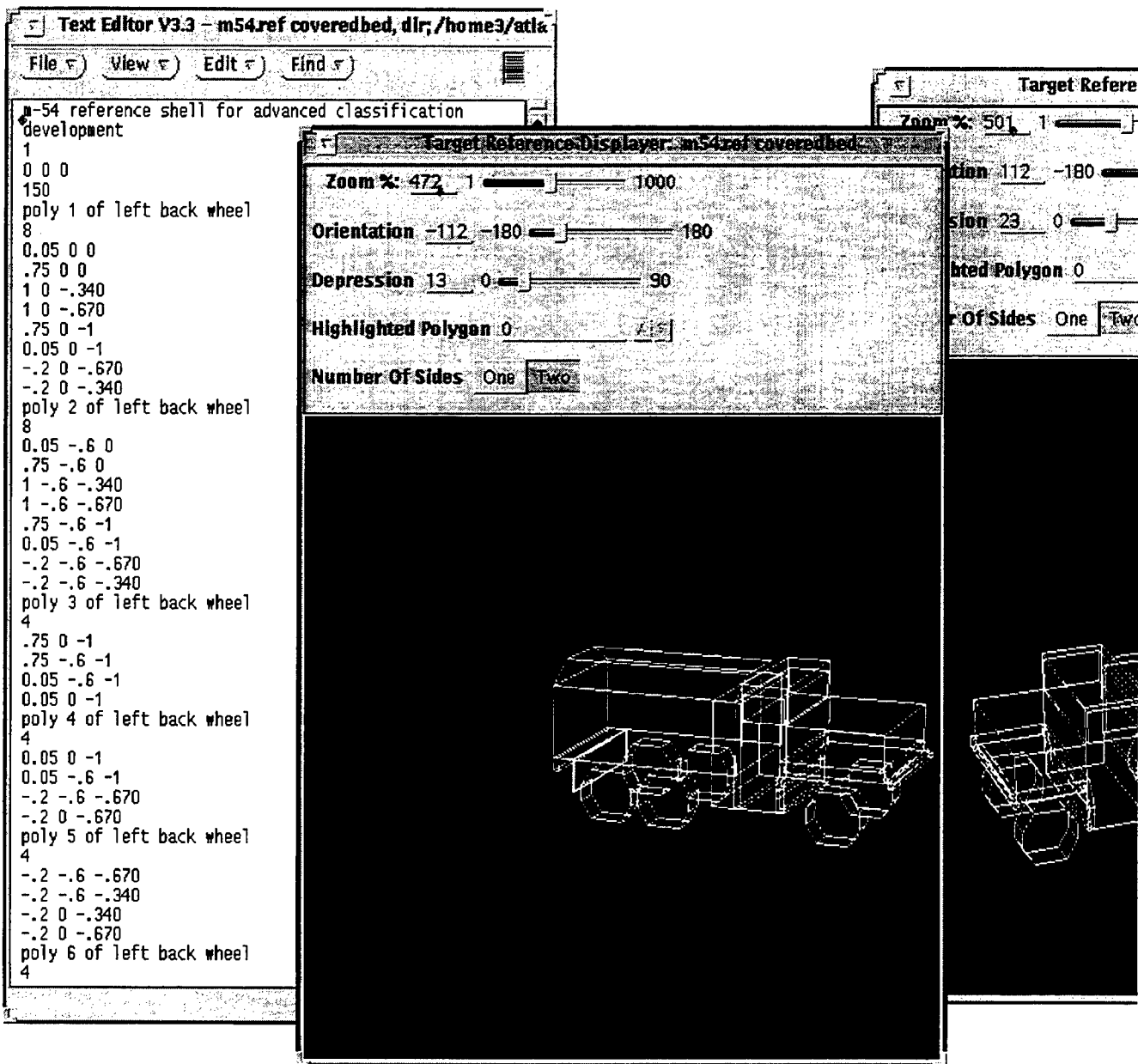


Figure 3

An M54 and M35 are seen above in Figure 3. The top four lines seen under the screen entitled "Text Editor" introduce the model. The first line normally tells what the model is, the second the number of aimpoints, and the third the coordinates of the aimpoint. The

fourth line, the total number of polygons in the model. Naturally, as more polygons are added to the model, this number has to be upgraded or newer polygons will not show in the display. The series of numbers under each comment line are the x, y, z coordinates for that particular polygon. This series must go in the particular order as mentioned before to make the graph correct in its display of visible polygons (counterclockwise).

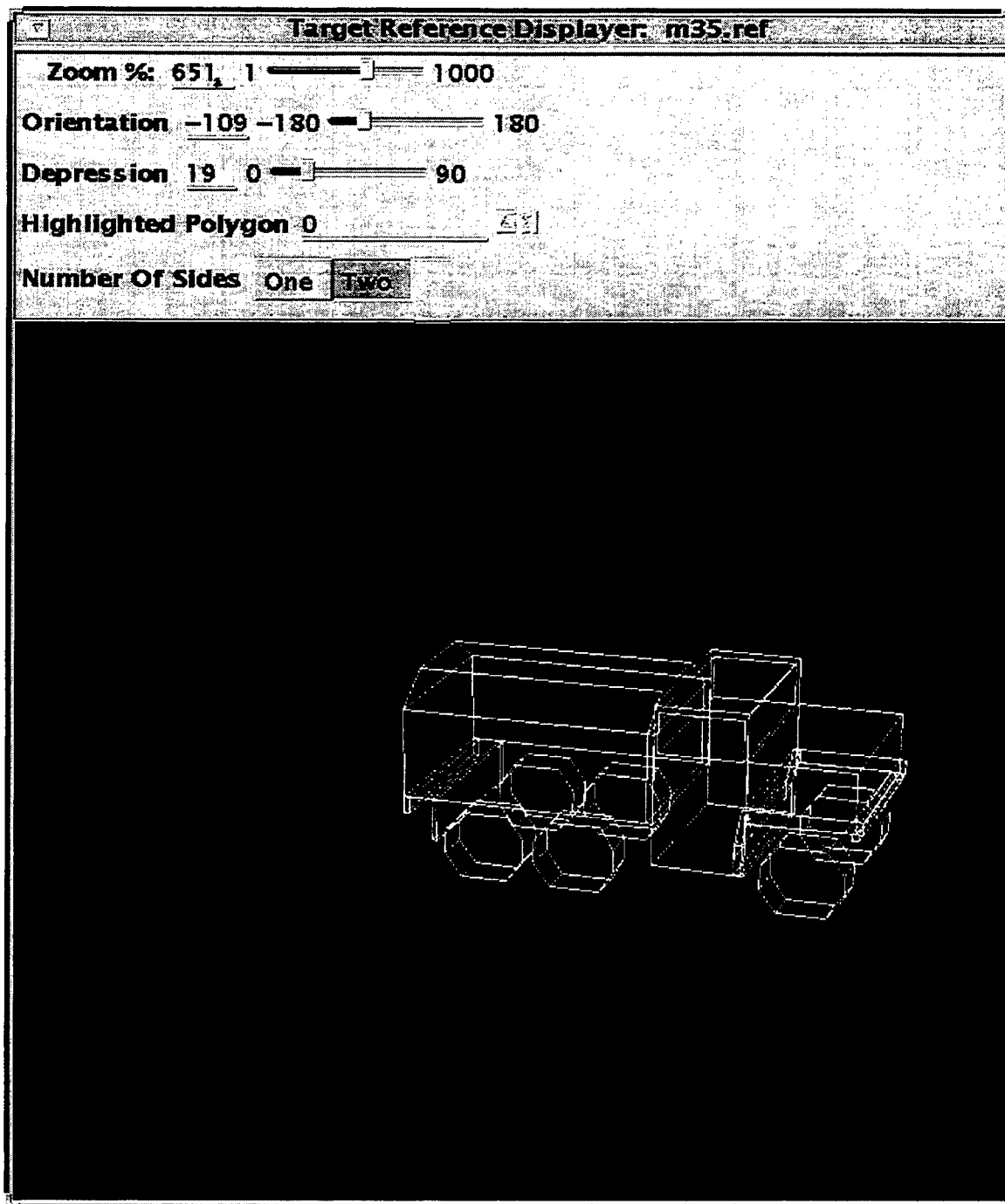


Figure 4

The M35, can again be seen in Figure 4. Its similarity to the M54 is apparent.

Real laser radar imagery was extracted through the Scoretool program. Several “flights” (7001 to 7020) were taken. Each flight had several flights within it with various targets to

extract. In corresponding header files, the names of the targets in reference to their range on the image were listed. The images were manually extracted from the synthetic image using this information, and each image was saved separately with its appropriate name. The header files were listings of the existing targets as recorded by one knowledgeable of the flight's contents. (The purpose of the header file is to aid in identification of the targets.) An example of a Scoretool image may be seen in Figure 5. The image could be manipulated using the "file," "view," "point select," etc. on the right side of the picture to center on the targets without the excess pixels.

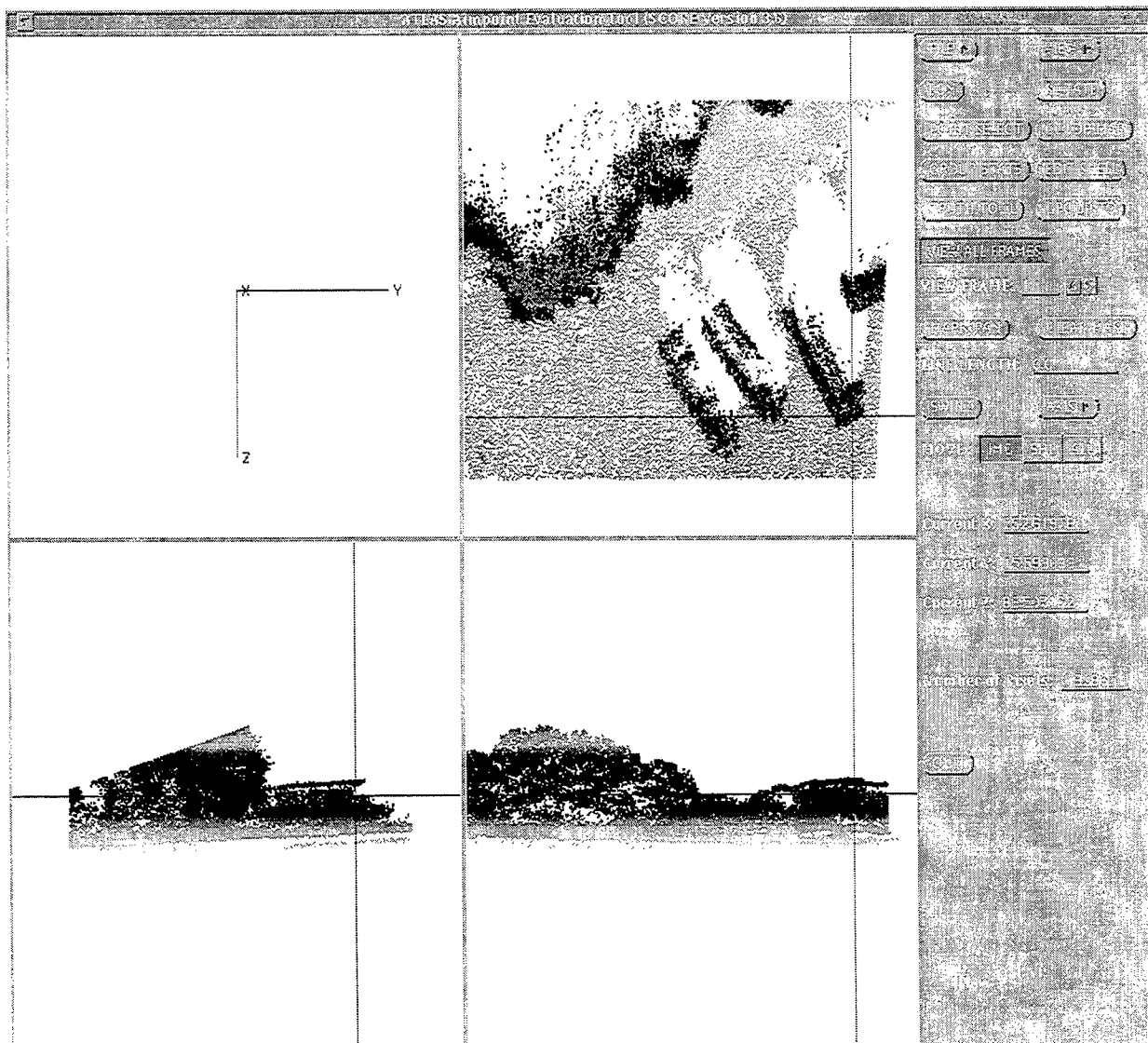


Figure 5

The three rectangular figures seen in the top right screen will be the targets looked for. To find out the names of the targets, one would look up that particular flight in the corresponding header file and find the names listed according to range.

CONCLUSION

The LRTAG classifier is successful but subject to several inconsistencies due to outside factors. A future goal is to improve the algorithm suite to its maximum performance.

ACKNOWLEDGMENTS

Heartfelt thanks to

KAREN NORRIS-ZACHARY for being an excellent mentor.

TODD HOLMES for the tremendous help with the models and Scoretool.

DUANE GECI for all of the computer help.

HERLINE for being so friendly.

SCOTT, DAVE, and everyone else at the IPL for their hospitality.

DON HARRISON and MIKE DEILER for making HSAP 1995 what it was.

DR. KLAUSIDUS for his support.

STEVE WHYTE and GINNY WOLFE for their help.

CLARENCE GOODEN for all of the advice.

LYNN DEIBLER and AL for their help , and others in MNGA who provided assistance.

OTTO for being so friendly.

JOHN VEST for everything.

All other HSAPers: Robin Carley, Nancy Deibler, Mike Dooley, David Hernandez,

Vanessa Hurst, Neill Perry, Trey Reyher, Douglas Ritchie, Ryan

Sheffield, Albert Tu, Elizabeth Walker, Josh Weaver, Gabrielle White

Wolf, Tuan Yang

PROGRAMS TO CONVERT FORMAT OF POLYGON IMAGE MODELS INTO CHAMP
"PLY" FOR USE BY SCENE GENERATION SPECIALISTS IN REAL TIME SEQUENCE
PRODUCTION

Robyn Marie Carley

Fort Walton Beach High School
Hollywood Boulevard
Fort Walton Beach, Florida 32548

Final Report for:
High School Apprenticeship Program
Wright Laboratories

Sponsored by:
Air Force Office of Scientific Research
Eglin Air Force Base

and

Wright Laboratories

August 1995

PROGRAMS TO CONVERT FORMAT OF POLYGON IMAGE MODELS INTO CHAMP
"PLY" FOR USE BY SCENE GENERATION SPECIALISTS IN REAL TIME SEQUENCE
PRODUCTION

Robyn M. Carley
Fort Walton Beach High School

Abstract

File formats of polygon model imaging programs were studied. The objective was to find models with 500 or less polygons and convert them to CHAMP format. The files were to be used in real-time scene generation by contractors for KHILS. Files were taken from a compiled database in an ONYX Reality Engine. Programs were written to convert from both IRMA and Wavefront. Emphasis was on Wavefront due to the high numbers of polygons in IRMA files.

PROGRAMS TO CONVERT FORMAT OF POLYGON IMAGE MODELS INTO CHAMP
"PLY" FOR USE BY SCENE GENERATION SPECIALISTS IN REAL TIME SEQUENCE
PRODUCTION

Robyn M. Carley

Introduction

The Kinetic Kill Vehicle Hardware in the Loop Specialists at Wright Labs create sequences that run at actual speeds and test the reactions of the programming for missile seekers and detectors. In order to correctly analyze this software, military targets have to be created for the systems to detect. Because of the high number of calculations involved in real-time scene generation, the best targets are low resolution. To simplify the calculations during sequences, few to no calculations are made during real-time to take actual infra-red data into consideration - data is created and assumed to be sufficient. Therefore polygon models from multiple programs could be used in scene generation. A recent test called for the use of tanks as targets, and rather than create models of tanks from scratch, the decision was made to find low resolution model files left from other testing and to simply convert the formats to a format compatible with the software currently in use. Gail Mitchell, a contractor from SAIC in Shalimar, compiled a database of models that were in the hard drive on the KHILS ONYX Reality Engine as a starting point.

The engineers in KHILS frequently use the Composite High Altitude Maneuvering PBV software (CHAMP) to perform temperature and infra-red data testing for hypothetical missiles, and they have adopted the CHAMP polygon file format for most of the scenes they generate.

The CHAMP polygon file format is as follows:

12 4	number of vertices / number of polygons
1.2 1.3 2.3 3.2 2.1 1.3 300 0	first three numbers: x,y,z coordinates of vertices
1.2 1.3 2.3 3.2 2.1 1.3 300 0	fourth through sixth numbers: x,y,z coordinates of normals
1.2 1.3 2.3 3.2 2.1 1.3 300 0	seventh number: temperature (degrees Kelvin)

1.2 1.3 2.3 3.2 2.1 1.3 300 0 eighth number: transference

1 2 3 4 vertex order for formation of polygons

Temperature and transference are aspects used by CHAMP for infra-red data in projectile modeling. Since they were irrelevant to the scenes made with the polygon models during the summer, throughout the programming the constant values 300 and 0 were used.

Methodology

The first program written converted from IRMA files to CHAMP files. The format was simple, and easily changed. In any file, the first two lines were composed of junk information, such as the date the file was created, the length of the file, and the source of the data. The third line held a number equal to the number of objects in the file. The next line was a short name, then a blank line occurred. Next was a line with the number of vertices, and a second number for which no purpose could be found by the programmers. Lines of x, y, z vertex coordinates came next in the file. The vertex definitions were followed by 2 more "junk" lines, a line with a number equal to the number of polygons in the file, and a blank line. Then there were lines of vertex ordering data, and another blank line. The IRMA files that were worked with were composed of triangles. Therefore, each vertex ordering line had four numbers, but the fourth was a copy of the third. Then the next name would occur, and the pattern was repeated as many times as there were objects (the number on line 3).

The program (convert.c) read in the object name and used it as a label to name the CHAMP output file for the object. Each object had a separate polygon file so that parts of the object could be moved independently of the whole (i.e. a tank turret rotating with the tank stationary). The vertices were read in to three arrays (x, y, and z) of floating point integers and the polygon order numbers were read in to three arrays (xn, yn, and zn) of integers. The program used the numbers representing the numbers of polygons and vertices and wrote them to

the CHAMP file. The vertex lines were written using a loop (performed for each vertex) that printed element i of x, y, and z and then printed "1.00 0.00 0.00 300 0" and a carriage return. Since the IRMA format did not include normals, 1 0 0 was used until a program could be run which calculated the normals using the right-hand rule and wrote them over the existing numbers. The program then wrote element j of the arrays xn, yn, and zn to a line with a carriage return. It printed zn twice to conform to the CHAMP polygon file format which requires four vertices in a polygon definition line. Then the program closed the file and repeated the loop, opening a new file with the new object name.

After writing the program to convert from IRMA to CHAMP, compiling it, debugging it, and running it, use of IRMA was vetoed. IRMA polygon files of vehicles include not just external faces of a vehicle, but also the modeling of all internal objects in the vehicle, such as engine, axles, and oil pans. The smallest of the IRMA files was comprised of 627 objects. Without more information on the polygon files describing which objects were the outside of the vehicles, the output of convert.c on a small IRMA file was too massive to be of any use for real-time scene generation.

The second program written this summer was Wavescan. Wavescan reads in a Wavefront polygon file with the label "name.obj", ciphers the data, and outputs one CHAMP "name.ply.asc" file. While Wavescan does make provisions for multiple objects in one file, the naming process for the objects was obscure. Different objects also shared vertices, which made it difficult to output more than one CHAMP file without complex sorting algorithms. (The ".asc" is a naming preference of the engineers in MNGA as it identifies the files as ASCII rather than the binary files which CHAMP outputs after it runs calculations.)

The Wavescan file format is based on first-character line parsing, and the significant characters are as follows:

#	comment lines
g	object or section name
v	x, y, z coordinate vertex definition
vn	x, y, z coordinate normal definition
vt	x, y, z coordinate texture definition
f or fo	vertex order for polygon definition

The significant difference between Wavefront and CHAMP is that Wavefront does not have a structured order for line definitions. Any of the above lines could be entered in a polygon file in any order, while CHAMP files must follow the order described earlier. Wavefront also utilizes different normals with the same vertex, whereas CHAMP's normals are defined as part of each vertex. This element simply meant that most converted CHAMP files would have more vertices than the original Wavefront files.

Wavescan was originally very similar to convert, in that it read in the vertices and normals into arrays of floating point numbers. By using an if-else structure in the program, all of the pertinent lines could be parsed and read in while all other lines could be ignored. By reading in the name of the file to be converted, taking off the ".obj" suffix, and appending ".ply.asc" to the name, a label was created for the CHAMP output file, and the program began. Minor problems occurred with the separate line definitions of normals and vertices, but that was solved by deciding to recreate each vertex as it was defined in the "f" or "fo" lines, instead of following the numbering scheme used in Wavefront. That is, where Wavefront created two polygons which both used vertices 2 and 3, but different normals, Wavescan used 2 and 3 in the first polygon, but renamed them to 4 and 5 for the second polygon. A counter kept track of how many vertices had been used until the next vertex was encountered. This not only made it easier to write the CHAMP polygon file, but also optimized the file for real-time usage.

The main problem with Wavescan was the ordering format. An "f" or "fo" line could be in four different formats:

1. v/vt/vn 3 numbers, separated by slashes, representing vertex, texture, and normal
2. v//vn 2 numbers, separated by 2 slashes, representing vertex and normal
3. v/vt 2 numbers, separated by 1 slash, representing vertex and texture
4. v 1 number, representing a vertex

While this parsing made Wavefront a flexible code, it was difficult to design a program that could determine between the four types and decide which numbers to save and which to ignore. The solution to this problem was to write a subfunction which read in the characters as a string, replaced the slashes with spaces, and returned a case number (1-4) and the values (1-3 numbers) to the main function. The function then used a case-switch routine to determine which action to use, and read in the correct numbers to the array.

Next, the function used the values in the array to determine which vertex and normal array values to print to the CHAMP file (and increment a counter for every vertex definition in the output file). In order to not have to go to the end of a file, write the vertex order line, and rewind the file pointer, a junk file was opened, the vertex order was written to it, and at the end of the program the junk file data was appended on the output file and the junk file was erased. (A subroutine was written to guarantee that the junk file did not already exist, preventing the program from writing over existing files.)

Another minor obstacle occurred when I discovered the Wavefront can have up to (and maybe more than) 20 sided polygons, while CHAMP is limited to 4. Another engineer in the office had encountered this program before, and he helped to design an algorithm for the numbering system to make it compatible with CHAMP.

When Wavescan reached the end of the Wavefront file, the number of vertices and

polygons had each been counted, and the file pointer was set to the beginning of the file to write out the two necessary values. The program then wrote the name of the output file to the screen, and ended.

Results

In the end (after minor and major problems and syntax mistakes) Wavescan works. It has not yet been commented, so anyone trying to adapt the code might be confused by all of the subroutines and counters, but it is an efficient program that accurately converts Wavefront files into CHAMP format. Three different files have been run through it, and all of the subsequent CHAMP images correspond to the Wavefront images, which means there are no errors in the program. One complication did occur because most Wavefront files do not include normals (Wavefront has the capability to calculate normals, making them unnecessary). When this occurred, the normal 1 0 0 was used as a default. After Wavescan ran, another program written by a KHILS engineer which calculates normals for CHAMP files was linked to Wavescan and was run to replace the default value with the correct normal throughout the file.

This program should simplify the work of scene-generators by removing the time usually taken by creating polygon models by hand for each test.

Acknowledgements

I would like to thank my mentor, Charles Coker, for sponsoring my apprenticeship for the past two years. Eric Olson, Walt Krawczyk, and Dennis Garbo for helping with programming bugs and having supreme patience with my questions. Major Bert Schneider, the section chief of MNGI, and Lynn Deibler, the section chief of MNGA, who helped make me feel welcome this summer and were there for any problems with hardware and lack of computers. All the other apprentices for helping to make this summer a little bit more fun and less grueling labor. Jeanette Williams, the secretary for the HSAP program at Wright Labs, and Don Harrison and Mike Deiler for organizing the HSAP program at WL and making it possible for me to work this summer. And I would like to thank AFOSR, DOD, and RDL for sponsoring the HSAP program across the country.

Diverse Electronic Warfare Applications

Allyn J. Crowe

**Bellbrook High School
3491 Upper Bellbrook Rd.
Bellbrook, OH 45305**

**Final Report for:
High School Apprentice Program
Wright Laboratories**

**Sponsored By:
Air Force Office of Scientific Research
Bolling Air Force Base, DC**

and

Wright Laboratories

August 1995

Diverse Electronic Warfare Applications

Allyn J. Crowe
Bellbrook High School

Abstract

Various Electronic Warfare software applications were studied. GW Basic, Visual Basic, HT Basic, Microsoft Excel, DaDisp, Matlab, and Design-Cad were some of the programs used. Building circuits, troubleshooting and repairing electronics, IEEE-488 interfacing, writing computer programs, drawing block diagrams, and performing a link analysis were some of the activities performed. One side project is discussed briefly: The linking of two computers so that all of the drives on both computers can be used on one. One of the main programs written is also included.

Diverse Electronic Warfare Applications

Allyn J. Crowe

There are many engineering tools that are constantly used in electronic warfare research and development. One of the main tools is the computer. An engineer working in electrical warfare must know how to use a computer. Without a computer that can do more than one thing at a time, the engineer would have to do each step and work out the equations. This might take more time and most likely more effort than using a computer to work it out. The computer can also be used to plot a graph of a waveform or other item that might be needed to be plotted. The computer also has the versatility that it can do many different types of plots where a spectrum analyzer can not plot what an oscilloscope would display. A computer can also make other parts of the engineer's job easier. It can be used to do block diagrams of a system set-up or can be used to do the layout of one single circuit. If there is not software already written for the task they want to use it for then the engineer can write his own program. There are many different programming tools that are available for low cost. The computer can also be used to "talk" to most of the common equipment used by the engineer. This is useful because that way the engineer can use many pieces of equipment and only have to use one control program.

To start off my tour at the Avionics Laboratory I learned how to use some of the basic tools that an electrical engineer would use. We started simple and then worked into some of the more difficult pieces of equipment. They were all relatively easy to use. As one of my projects I used a function generator to output a Sine wave and examined it through the different pieces of equipment. The feature about the digital Spectrum Analyzer that stood out was the different types of plots that it could display. It had many different plots it could display. This made the relating of information from one piece of equipment easier.

After I had learned the basic uses of the equipment I moved on to the computer. I have used computers quite a bit in the past so I felt at home on them. To me using the computer to run all of the equipment was easier than running each piece by itself. After I had used the program MatLab to produce some Amplitude Modulation plots, and had worked with AM for a little while, I moved on to programming. I had not done much programming in the past, but I had done a little. This made it a little easier for me to understand how to write the program and

what it was going to do. The completed program was named "Sequences: a program to generate Maximal Length Sequences," and that is exactly what it does. This is a copy of the program that we wrote.

"Sequences"

A program to generate maximal length sequences

Written by: Allyn Crowe and Jason Leopold

Sponsored by:

Wright Lab, Wright Patterson Air Force Base, OH

and

Air Force Office of Scientific Research, Bolling Air Force Base, DC

Written: June, 1995

```
5 CLS
6 PRINT;PRINT;PRINT
7 PRINT " ***** "
8 PRINT " * * "
9 PRINT " * * "
10 PRINT " * This program will generate * "
11 PRINT " * maximal length sequences * "
12 PRINT " * And will be really cool * "
13 PRINT " * Because it was written by * "
14 PRINT " * Allyn Crowe * "
15 PRINT " * and * "
16 PRINT " * Jason Leopold * "
17 PRINT " * We hope you enjoy it! * "
18 PRINT " * "
19 PRINT " * "
20 PRINT " * "
21 PRINT " * "
22 PRINT " ***** "
23 INPUT " Press enter to continue";A$
```

```

24 CLS

70 REM *****
75 REM ** This is the part of the program where the initial conditions **
80 REM ** are entered. It also defines the array and calculates the **
85 REM ** number of bits it will display on the screen **
90 REM *****
100 INPUT "Enter Register Length - ";N
110 DIM R(N+1),X(N+1),T(N+1),F(N+1)
120 L=2^N-1
130 M=0
300 FOR I=1 TO N
310 PRINT "Enter initial fill value in register ";I;:INPUT " - ";R(I)
320 NEXT I
350 FOR I=1 TO N
360 F(I)=R(I)
370 NEXT I
400 FOR I=1 TO N
410 PRINT "Enter tap condition for register ";I;:INPUT " - ";T(I)
420 NEXT I
450 REM *****
460 REM ** This is the part of the program that identifies the number **
470 REM ** of taps **
480 REM *****
500 J=0
510 FOR I=1 TO N
520 IF T(I)=1 THEN GOSUB 2000
530 NEXT I
540 REM *****
550 REM ** This is the part of the program that does the calculations **
560 REM ** using the "exclusive or" function **
565 REM *****

```

```

600 X(0)=0
610 FOR K=1 TO J
620 X(0)=X(K) XOR X(0)
630 NEXT K
640 R(0)=X(0)
650 PRINT R(N);" ";
660 M=M+1
691 REM *****
692 REM **   This is the shift part of the program. It shifts all of   **
693 REM **                                     the bits over.          **
694 REM *****
700 FOR I=N TO 1 STEP-1
720 R(I)=R(I-1)
730 NEXT I
735 REM *****
736 REM **   This is the part of the program that checks each new   **
737 REM **   sequence to see if it's the same as the initial register **
738 REM *****
740 FOR I=1 TO N
750 IF R(I)<>F(I) THEN GOTO 500
760 NEXT I
770 IF M=L THEN GOTO 800
780 PRINT " Sequence is NOT an m-sequence"
790 PRINT: PRINT "Sequence is ";M;"bits long"
795 END
800 PRINT " Sequence is an m-sequence"
810 GOTO 790
1010 REM *****
1020 REM **   This is the subroutine that takes the taps and places the **
1030 REM **   values in a slot that will be worked with later          **
1040 REM *****

```

```
2000 J=J+1
2010 X(J)=R(I)
2020 RETURN
```

At the start of the program you input the number of digits that will be used to generate the sequence. This is the length of your register. Then you input an initial fill of ones and zeros into this register. After that you input the location of the register taps that define what sequence will be generated. After you have done this the program will display the last number in the register each time it is clocked. As the program runs it checks the register to see if the register matches the initial fill state. If it does match then the program checks to see if it cycled the right number of clock pulses. If the register meets both of those requirements then the program will tell you that it is a maximal length sequence. If it does not meet both of those requirements, at the same time, then it will check only so many sequences before it tells that the sequence you entered is not a maximal length sequence. The equation used to tell the program the right number of clock pulses is a relatively easy one:

$$L = 2^N - 1$$

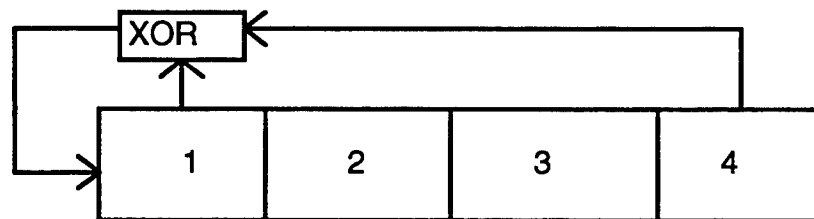
The variable (L) is the number of clock pulses, and the variable (N) is the length of the register. If the number of register states that are checked before the program finds the initial sequence is not equal to the formula's result then the program will tell you that the sequence is not a maximal length sequence. This is done to insure that the program does not attempt to go on forever by trying to calculate a sequence that will never repeat back to its initial values. The other check that is done is the individual check of each sequence to see if it is the same as the initial fill. This is done so that the program does not calculate a sequence that ends early, and mistakenly declare that it is a Maximal Length Sequence. Together these two checks should prevent any non-maximal length sequences from being mistaken for maximal length sequences.

The function that the program uses to determine the new bit of information is the “Exclusive Or” function.

The “Exclusive Or” Function

X	Y	N
1	1	0
1	0	1
0	1	1
0	0	0

This function basically states that if you have one one and one zero the result will be a one. If you have two ones or two zeros the result will be a zero. The following diagram is what the program does.



This is an example of a sequence that will be generated from a register that will be four bits long. The taps are on bits one and four. As the program starts, all of the slots are filled, say with all ones. To start the process you would XOR bits four and one, this would give you a zero. That zero is put in slot one. All of the other numbers are shifted over one slot to the right during a clock pulse. The readout that would be give on the screen after 15 clock pulses would be as follows:

1 1 1 0 1 0 1 1 0 0 1 0 0 0 1

Sequence is an m-sequence

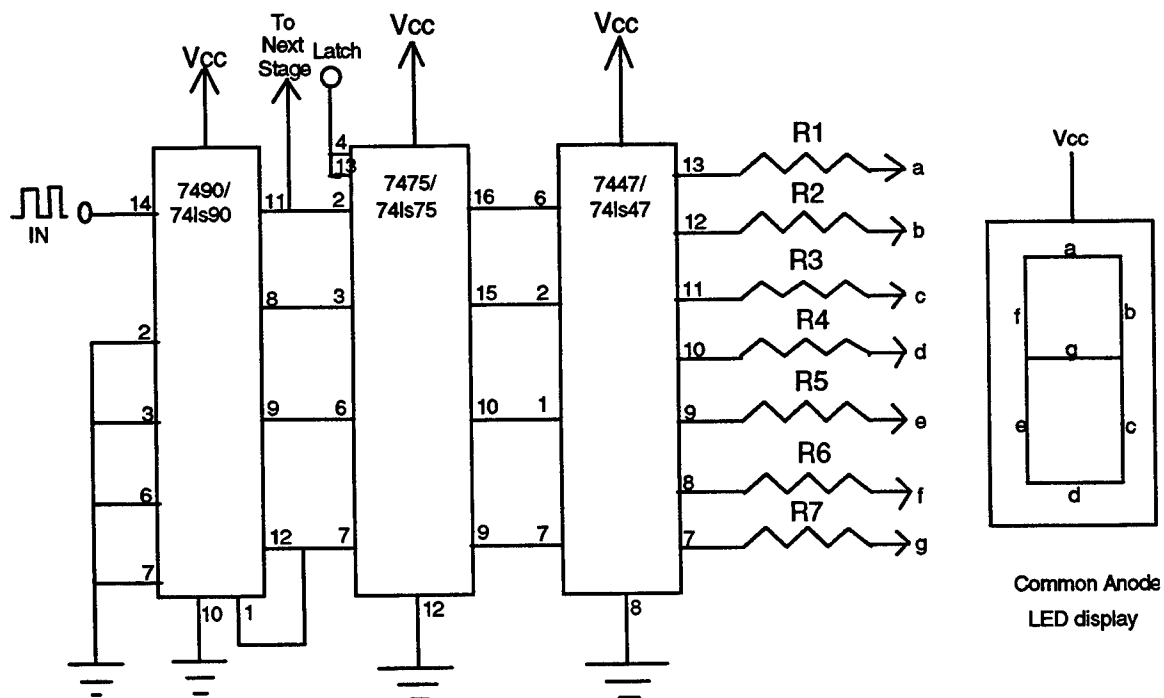
Sequence is 15 bits long

This gives you the last digit of all of the registers it tested. Then it tells you that the sequence is a maximal length sequence and that it took 15 clock pulses before it repeated itself. You can use this program to test sequences that are extremely long, but the larger the register the longer the sequence and the longer the program takes to run.

Writing the program I learned many things. I learned about the OR functions and the AND functions. I learned more about the BASIC programming language. And I learned about the difficulty and time it takes to write a program. It also taught me how much easier a computer makes some calculations.

After I had finished writing my program we moved on to circuits. There are two main types of circuits we designed and built. The first was digital, and the second was linear. We used the Radio Shack Engineer's Notebook II as our reference. We built these simple circuits on breadboards. Breadboards are a solderless circuit-boards that are used for low power circuits. They are not supposed to have more than five volts put into them. The breadboard is generally used as a learning tool, but it might be used for some low power application circuits. The nice thing about the breadboards is that they are solderless so a circuit can be easily disassembled and a new one reassembled without the mess of soldering.

The area of circuitry that I concentrated the most on was the digital circuitry. I built an "Exclusive Or" gate to relate the program that I had made and the breadboarding. It was just the function, so all that it did was put out low or high according to the function table. Then we moved away from the "Exclusive Or" function and moved into other sections of the digital realm of circuits. One circuit I built was a decimal counting unit. The following diagram is the layout for it.



The outputs would be connected to the pins on the display corresponding to the letters on the diagram. This is a common circuit. The breadboarding gave me some experience in circuit building. We didn't have enough time to go into circuit design though.

While we were breadboarding we started on some troubleshooting. If a circuit we had built would not work we had to figure out why and fix it. After we were done breadboarding we used these techniques we had developed to fix some electrical objects. We would get the schematic, if we could do so in a quick time, and follow what the problem was and attempt to fix it. It did not always work. We worked on a couple of the computers a lot also. We were having some problems with one of them and we found out what it was, and fixed it.

One of the small side projects that we did was we linked two of the computers in the lab. We tried using three different software packages to do this. The first one was called "Brooklyn Bridge." It came with it's own link cable and had a choice of running it in a windows-like environment or from a DOS-like environment. The only problem that I had with it was that I could not get it to connect to the other computer. This made it a little difficult to link the computers together. The next package I used was a DOS based program. It came included in the DOS package. There was actually two different programs that were needed to link the two computers. One was for the server computer, Interserver, and the other was for the client computer, Interlink. The problem that I had with this program was that you could only use one computer when this was running. So two people could not be working on both computers but still have the link active. The third package that we tried was called "Comm Works." Of the three I think that it was the best one. It was easy to run, and was able to be ran in the background. Another good thing about it was that both computers could be used at the same time. And yet another nice thing about it was that it could be used not only for linking of two computers but could also be used for network connections, E-Mail, and other remote connections. It was based in windows so everything was easy to get to.

Another one of the projects that I did was performing a link analysis. I used Microsoft's Exel spreadsheet program to do this. A link analysis is used to analyze the uplink and downlink sections of a single radio-frequency carrier satellite system. The equation only considers the ideal gains, losses, and effects of thermal noise associated with the earth station transmitter, earth station receiver, and satellite transponder. This is a copy of what I did:

Data(variables)		Units	variable
Uplink			
Earth station transmitter power at saturation	33.00	dBW	Pt
Earth station back-off loss	3.00	dB	Lbo
Earth station branching and feeder losses	4.00	dB	Lbf
Earth station transmit antenna gain	64.00	dB	At
Additional uplink atmospheric losses	0.60	dB	Lu
Free-space path loss	206.50	db	Lp
Satellite reciever G/Te ratio	-5.30	dBK ⁻¹	G/Te
Satellite branching and feeder losses	0.00	dB	
Bit rate	120.00	Mbps	Fb
Modulation scheme	8.00	PSK	
Downlink			
Satellite transmitter output power at saturation	10.00	dBW	
Satellite back-off loss	0.10	dB	
Satellite branching and feeder losses	0.50	dB	
Satellite transmit antenna gain	30.80	dB	
Additional downlink atmospheric losses	0.40	dB	
Free-space path loss	205.60	dB	
Earth station recieve antenna gain	62.00	dB	
Earth station branching and feeder losses	0.00	dB	
Earth station equivalent noise temperature	270.00	K	
Earth station G/Te ratio	37.70	dBK ⁻¹	
Bit rate	1.2E+08	Mbps	
Modulation scheme	8.00	PSK	
Calculations			
<i>Uplink budget:</i>			
EIRP(Earth Station)	90.00	dBW	
Carrier power density at the satellite antenna	-117.10	dBW	
C/No at the satellite	106.20	dB	
Eb/No	25.41	dB	
<i>Downlink Budget:</i>			
EIRP(satellite transponder)	40.20	dBW	
Carrier power density at earth station antenna	-165.80	dBW	
C/No at the earth station reciever	100.50	dB	
Eb/No	19.71	dB	

This is one of the harder and more in depth link analysis's. Not all link analyses have a satellite in between two ground stations. This was a nice way to become familiar with Exel. It is a nice program with good user interface.

One of the last things that I did was that I drew some block diagrams. I used a program called Design-Cad. The diagrams that I did were the layout of a system that was made up of various pieces of equipment. After I

had done the overall system I did the individual parts. It was an O.K. program, but at first I thought that it did not have very much power. It was hard to learn all of the commands, and where everything was that I needed in the menu system. After I became used to it though, I found that it had lots of capabilities.

As is evident there are many different things that go into research and development in the electronic warfare area. The computer plays a large part in this. I think that in the future it will play an even larger part. The engineer uses the computer to help him do many things that would take a lot longer if he/she had to do it by hand. The software that they use is what helps them even more. And if there is not any software written for the task they need it for, they can write their own.

I enjoyed my tour at the laboratory. I learned a lot that I think that I will use in the future. I have gained some insight into what an electrical engineer does. I would, and will, recommend this program to many others. I cannot wait until next summer, I hope that I get to return to this lab and learn more.

References

Engineer's Notebook II "Integrated Circuit Applications", 1982, Radio Shack a division of Tandy Corporation.

**WATER QUALITY ANALYSIS OF SURFACE WATERS
ON TEST AREAS C-64 AND C-74**

**Nancy Deibler
High School Apprentice
Environmental Assessment Branch**

**Wright Laboratory Armament Directorate
WL/MNSE
Eglin AFB, Florida 32542-5434**

**Final Report for:
High School Apprenticeship Program
Wright Laboratory Armament Directorate**

**Sponsored by:
Air Force Office of Scientific Research
Bolling Air Force Base, Washington D.C.**

August 1995

**WATER QUALITY ANALYSIS OF SURFACE WATERS
ON TEST AREAS C-64 AND C-74**

Nancy Deibler
High School Apprentice
Environmental Assessment Branch
Wright Laboratory Armament Directorate

ABSTRACT

A water quality analysis was conducted in 1976 in the area of Test Area C-64 and C-74 in 1995 a similar analysis was conducted. Results of this analysis will update the database and create a dataline for future analysis to be compared to determine test areatesting effects. Stream samples were collected from Bull Creek and Ramer Creek in the area of Test Area C-64, and three samples were collected from Rocky Creek tributaries in the area of Test Area C-74. A control sample was collected from Turkey Creek, which does not transverse or drain any ranges. Temperature, dissolved oxygen levels, conductivity, and velocity, were measured in the field with portable sensors. pH, hardness, turbidity, alkalinity, and concentrations of nitrate, nitrite, and phosphate were measured in the laboratory with various instruments. Comparing results of the control stream and the test areastreams shows no signs of unnatural disturbances to the streams from testing on the ranges. Water quality analysis should be conducted periodically to monitor the effects of test areatesting on the streams.

CONTENTS

INTRODUCTION.	4
PROCEDURES.	5
RESULTS.	6
CONCLUSION.	11
MISCELLANEOUS.	12
ACKNOWLEDGMENTS.	13
BIBLIOGRAPHY.	14

**WATER QUALITY ANALYSIS OF SURFACE WATERS
ON TEST AREAS C-64 AND C-74**

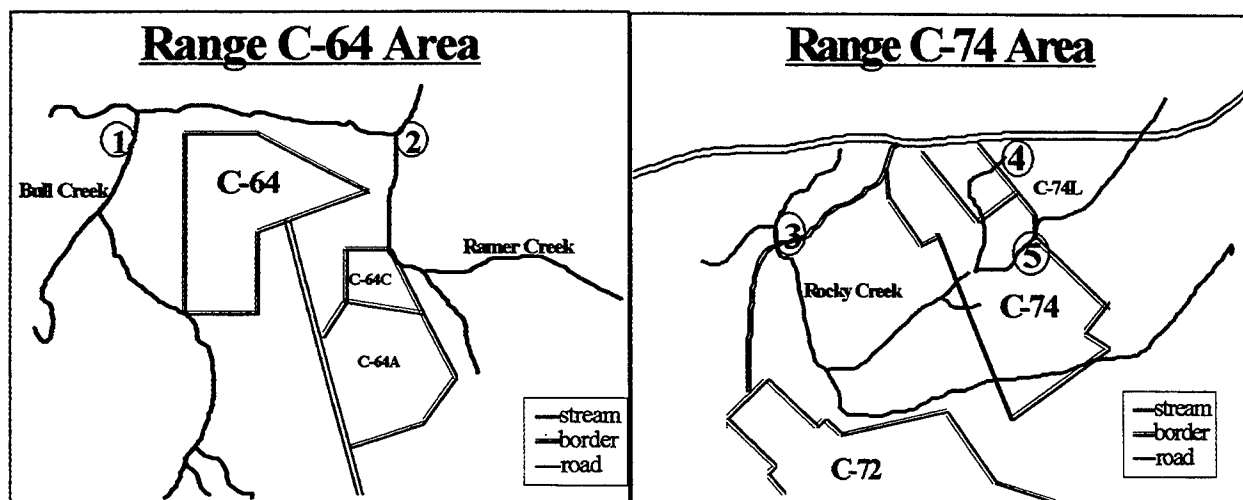
Nancy Deibler

INTRODUCTION

A water quality analysis of streams was conducted in the area of Test Areas C-64 and C-74. There has been testings on these test areas with various munitions. Water quality analysis can help determine if the testing on the test areas is harmful to various species in the streams. Some of the species in these waters are endangered species like the Okaloosa Darter which is only found in this area. A similar analysis of the streams on the test areas was conducted 1976. Conducting this 1995 analysis will update the baseline found 20 years ago. These results will create a database to which future analysis can be compared to determine testings effects.

PROCEDURES

Locations of water sampling was determined by accessibility and areas of possible contamination. Tests with various munitions have been conducted on Test Area C-64. Two samples were taken in the area of Test Area C-64. Sample one was collected along the west border of the test area from Bull Creek. Sample two was taken from Ramer Creek along the east side of the range. On Test Area C-74 there is a sled track and other test areas where various tests have been conducted. Three samples were collected in the area of Test Area C-74. Sample three was taken from a Rocky Creek tributary that leads into Test Area C-74. The other two were taken in the northeastern part of the range. Sample four was collected in the area of Test Area C-74L. Sample five was collected south of Test Area C-74L further into the range. The last sample was taken from Turkey Creek as a control. Turkey Creek does not flow through or drain a range; therefore the results from this sample will show the normal water quality parameters for the area.



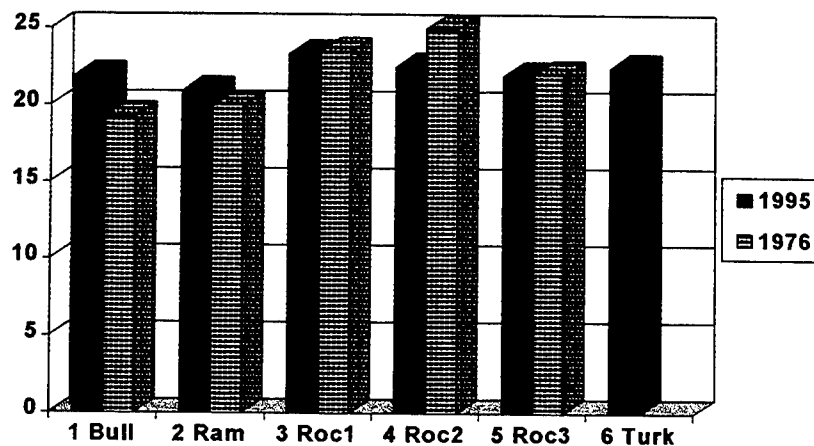
Temperature, dissolved oxygen, conductivity, and velocity of the streams had to be measured in the field. Chest-waders were worn to measure these parameters in the streams and to collect the water samples. Approximately 250 milliliters of the sample water was collected in clean plastic bottles for further analysis in the laboratory. Samples were collected underwater to be kept airtight. Immediately after collection the samples were transferred to a cooler with ice to prevent degradation of the water. In the laboratory pH, turbidity, alkalinity, hardness, and concentrations of nitrate, nitrite, and phosphate were measured with various instruments. Samples were kept cool overnight and brought to room temperature before testing was conducted.

RESULTS

Average velocity was measured with a Global Flow Probe. The instrument is placed in the water and slowly moved up and down and side to side. This gives the average velocity of the stream in the area from which the water sample is taken. The velocity of a stream shows the rate at which sediment, floating debris, and contamination, if there is any, travels down the stream.

The temperature, which is defined as the intensity of heat, is important because it determines the type and amount of life in an aquatic community. Change in the temperature of the water greater than the normal degree changes can have many effects on the water community, including causing an increase in biological rate and a decrease in oxygen, magnifying toxicity of most poisons, and changing the biological clock for some animal behaviors. A Corning portable Sensor was used to measure the temperature of the streams. The chart below shows the data from 1976 and 1995. Most surface waters in the United States have a temperature ranging from 0 to 40 degrees Celsius. Temperature is affected by latitude, altitude, season, time of day, flow, depth, and many other factors. The temperatures of the samples are all normal for the factors in this area.

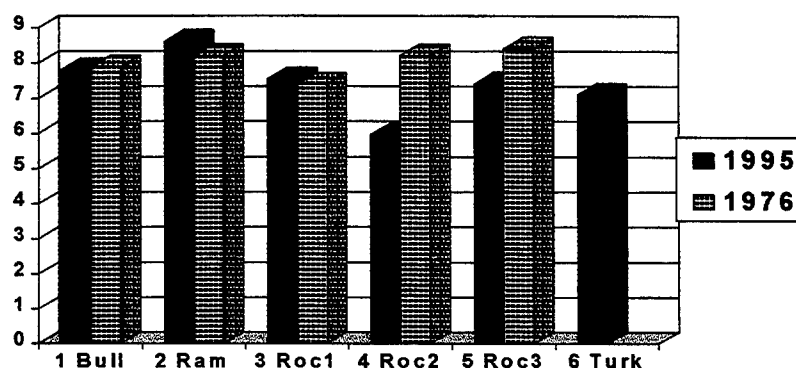
Temperature (Celsius)



Oxygen is necessary for almost all life in a stream to function. Plants and animals use oxygen to breathe and bacteria uses oxygen to decompose organic matter. The minimum dissolved oxygen concentration may be even lower than 4 milligrams per a liter for some adult fish and some plants to survive, but any reduction in the dissolved oxygen levels will reduce plant and animal activity. Dissolved oxygen was measured with a Corning Portable Sensor. The normal dissolved oxygen level of a stream is determined by the species of life that lives in it, and the temperature directly affects the dissolved oxygen levels. The dissolved oxygen levels for these streams are normal for this area. There are no significant reductions in oxygen levels compared to the control and 1976

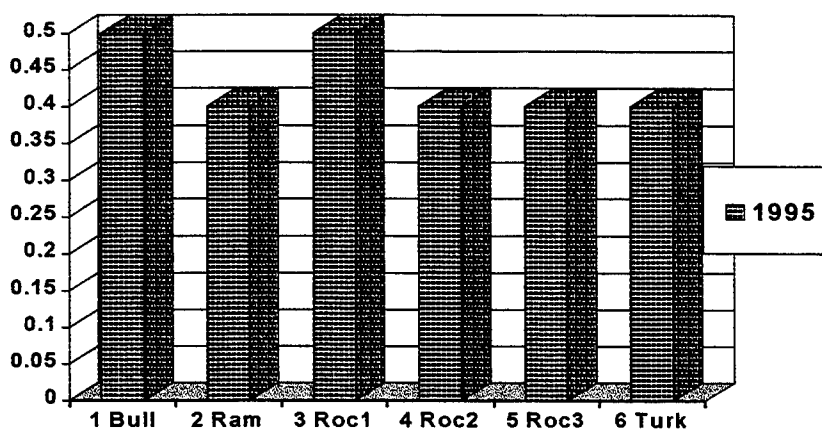
results. Sample 4 has a slightly lower dissolved oxygen level. This could be due to fluctuations that occur daily due to photosynthesis activity and the activity of the plants and animals. Sample 4 may have been taken earlier in the day or may have had more plant and animal activity in the area of collection. The level is not low enough to cause significant change to the community.

Dissolved Oxygen (mg/l)



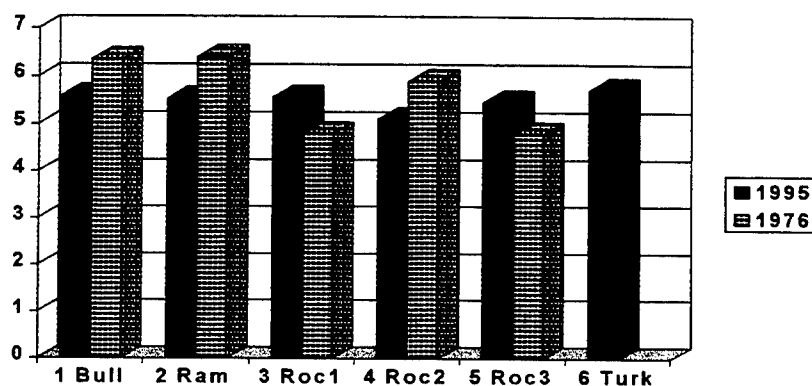
Turbidity is a measure of suspended sediment, such as, clay, sand, and small organic and inorganic matter. Turbidity is common in streams due to the flow of the water. Turbidity of the samples was measured with the HACH Ratio Turbidimeter. The instrument shines a beam of light through the sample. Then detectors measure the light scatter in all directions. The amount of turbidity is determined by the size, shape, and amount of particles in the sample. There is little turbidity in these samples due to the streams gentle flow and smooth sandy bottoms.

Turbidity (NTU)



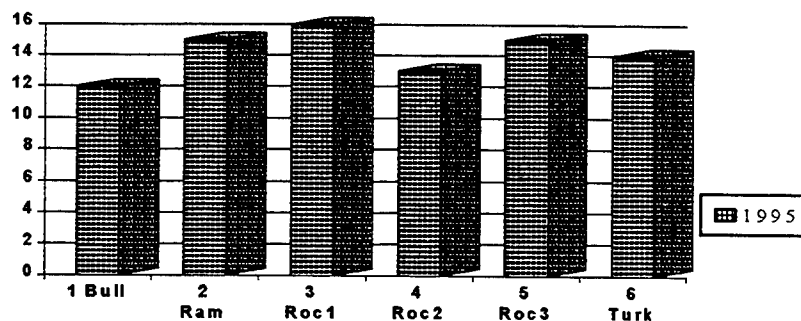
The measurement of pH is the tendency to accept or donate hydrogen ions. The pH indicates, but does not measure, the degree of acidity or alkalinity of the water. Changes in the pH of water may cause increases in the toxicity of the water. Lowering of the pH may cause a release of carbon dioxide or may allow some trace metals to become soluble. With the Fisher Scientific Accumet pH meter, the pH of each sample was measured three times. The pH levels of these streams are normal for this area. The sandy bottoms of these streams create a acidic pH level. Carbon dioxide and natural organic acids may also be natural causes of the acidic waters.

p H



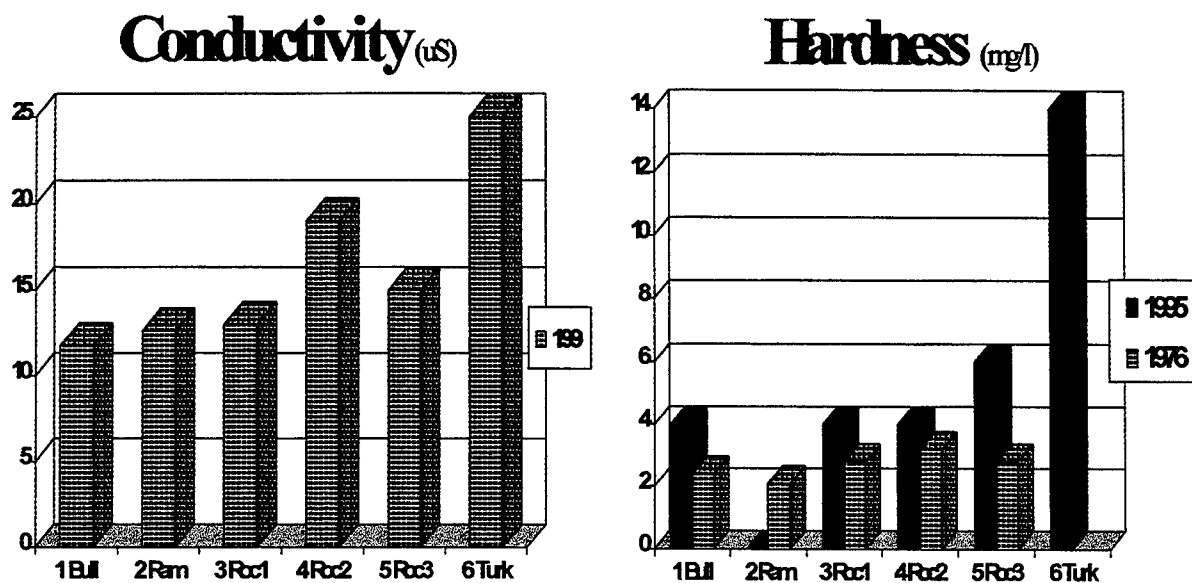
Alkalinity determines the capability of the water to buffer against a pH change. Alkalinity is mostly a measure of the presence of carbonates, bicarbonates, and hydroxides. With higher concentration of these chemicals the water can withstand greater changes in the pH. The alkalinity was measured with the LaMotte Fresh Water Chemical Test Kit by titration. These results show that the streams have normal buffering ability. This parameter is not compared to the analysis of 1976, because it and some others were not measured in 1976.

A l k a l i n i t y (m g / l)



Conductivity is a measurement of the water's capacity to convey electrical current. Conductivity can show the concentration of ionized substances in the water. It can be used to determine the purity of the water. Conductivity was measured with a Corning Portable Sensor.

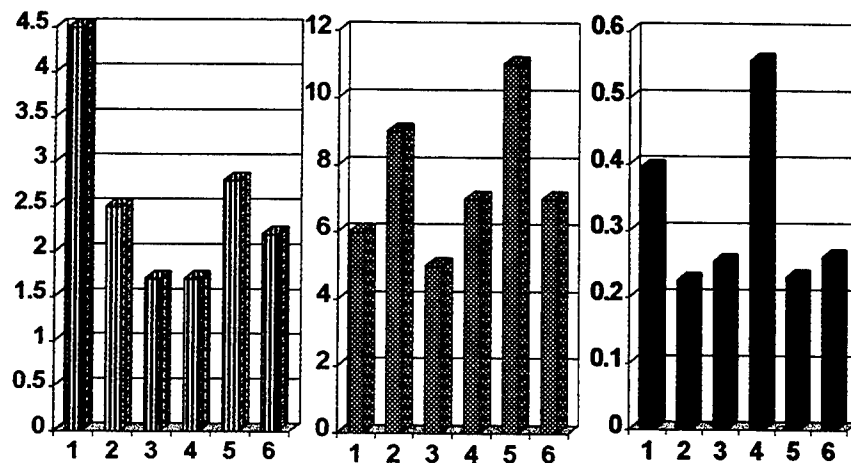
Hardness is a measure of total concentration of calcium and magnesium in the water. If other polyvalent ions are present in large amounts, they are also included considered part of the hardness of the water. Too much hardness is undesirable for aesthetic and economic reasons, and some must be removed before the water can be used. Hardness was measured with the LaMotte Fresh Water Chemical Test Kit. Results from the conductivity and hardness testing show that the streams are very pure, even somewhat purer than the control stream. Turkey Creek, the control stream, has higher levels of conductivity and hardness.



Nitrate is the most completely oxidized state of nitrogen and is found in the last stage in the nitrogen cycle. It is converted from nitrite by nitrate-forming bacteria under aerobic conditions. Large amounts of nitrate indicate biological wastes finishing stabilization. Nitrite is an intermediate stage in the breaking down of compounds containing organic nitrogen. Nitrite-forming bacteria convert ammonia to nitrite under aerobic conditions. Large amounts of nitrite indicate partially broken down organic wastes. Phosphate is an important nutrient for the plants and animals in the water. It is often an essential nutrient for algae growth. Large amounts

of phosphate can cause overgrowth of algae especially if there are large amounts of nitrate present also. This could lead to a decrease in dissolved oxygen in the water. Nitrate, nitrite, and phosphate levels were measured with the HACH Spectrophotometer. The levels of nitrate, nitrite and phosphate present is normal for the streams as can be seen by comparison to the control, sample 6. Sample 1 from Bull Creek has a higher level of nitrate present which could be due to increased animal activity in the area at the time of collection. There is not a significant increase in the nitrate level. Sample 4 from Rocky Creek had higher levels of phosphate present. The sample is located off of a heavily traveled road and is in a rain runoff pattern. The day the sample was taken it was raining. Waste from the road and bank may have been washed into the stream. This could have increased the phosphate concentration in the stream. Again the increase is not significant.

Nitrate[■], Nitrite[▨], Phosphate[■] (mg/l)



CONCLUSION

As the results from water quality analysis show the streams in the areas of Test Areas C-64 and C-74 do not show any significant signs of disturbance from testing on the ranges. Now these results cannot be used to determine if any future testing causes disturbances to the streams. Analysis periodically can keep the database up to date and help monitor the natural changes in the water, as well as, the unnatural disturbances.

MISCELLANEOUS

I was involved in another project related to streams on the Eglin Test Areas. I was given the scenario of an explosion at a site and a chemical cloud released as a side effect. I was to determine the change of the pH of a stream if the cloud passed over the stream. I worked with Luis Santana and Don Harrison to develop a methodology to solve this problem. I used many equations from chemical engineering books and other water related references . A methodology was developed but the accuracy of the equation has not been tested. For the methodology to be accepted, it must be tested further.

ACKNOWLEDGMENTS

I could not have accomplished any of this without the help of many other individuals. I would like to thank Luis Santana for all his understanding help. Ric Crews was a key helper in my project this summer. I truly appreciate all the time he spent helping me with my project. Captain Brad Noland helped collect the stream samples and was ready to help me whenever I needed anything. I am very grateful to all the members of the Environmental Assessment Branch for all their support this summer. I would like to thank Don Harrison and Mike Deiler for coordinating the apprenticeship program. Their hard work made the program successful. Last I would like thank all the other apprentices for great laughs and encouraging support.

BIBLIOGRAPHY

Environics Branch, "Water Quality: Streams and Ponds on Selected Test Areas on Eglin Air Force Base, Florida," Air Force Armament Laboratory, United States Air Force, Eglin Air Force Base, Florida, 1977.

Environmental Studies Board, "Water Quality Criteria 1972," National Academy of Sciences and National Academy of Engineering, Washington, D.C., 1972.

Hammer, Mark J., and Kenneth A. Mac Kichan, "Hydrology and Quality of Water Resources," John Wiley & Sons, New York, Chichester, Brisbane, and Toronto, 1981.

Montgomery, James M., "Water Treatment Principles and Design," John Wiley & Sons, New York, Chichester, Brisbane, Toronto, and Singapore, 1985.

Perry, John H., "Chemical Engineers' Handbook," Third Edition, McGraw-Hill Book Company, Inc., New York, Toronto, and London, 1950.

Welch, Paul S., "Limnological Methods," McGraw-Hill Book Company, Inc., New York, Toronto, and London, 1948.

**MULTIMEDIA PRESENTATIONS
AND
USER'S MANUAL**

Cindi L. Dennis

**Beavercreek High School
2660 Dayton-Xenia Rd.
Beavercreek, OH 45434**

**Final Report for:
High School Apprenticeship Program
Wright Laboratory**

**Sponsored by:
Air Force Office of Scientific Research
Bolling Air Force Base, DC**

and

Wright Laboratory

August 1995

MULTIMEDIA PRESENTATIONS AND USER'S MANUAL

Cindi L. Dennis
Beavercreek High School

Introduction:

The use of digitized video, pictures, graphs, and spreadsheets in presentations has increased dramatically in the past several years. Now, in order to be able to sell an idea or product, the presentation itself must be of excellent quality. Therefore, many businesses, including laboratories, are moving towards multimedia presentations that include video, sound, photographs, drawings, charts, graphs, and more. Thus, it was my job to find software and hardware capable of not only meeting these future needs, but also compatible with the installed software and hardware.

Methodology:

First, I familiarized myself with the available CPU and software and their limitations. Then, I examined the various products that were available in the marketplace. After doing so, I examined the prices of the various items; compatibility with current software and hardware; ability, as in does it do the job; and were the items advanced enough to do the job for several years. After asking these questions, I recommended the Intel Smart Video Recorder Pro because it accepted AVI - Video for Windows - format and had the ability to compress the files to a more reasonable size. It also included software that performed basic editing functions and accepted raw video from such sources as the digital camera (Canon's RC-250), VCRs, and camcorders. While it does not work with MPEG format video (the most advanced form of digital video that is closest to movie quality), neither did the local applications accept MPEG. The Smart Video Recorder Pro produced a good, clear image and the video playback dropped few or no frames compared to other products.

Recommendations:

After surveying the resources on the system and the resources available commercially, these are my recommendations for improvement or to meet current needs:

1) An excellent digital camera produces digital images at conventional film quality. The best digital camera is Kodak DCS 420 which costs about \$10,000. However, since the quality of digital cameras continues to improve and the price continues to fall, I recommend waiting several years for the price to catch up with the quality before purchasing a digital camera. Currently, the scanner produces excellent images at near conventional quality so it is cheaper right now to simply use a 35mm camera, process the film, and then scan it into the computer. Furthermore, the Multimedia Center (BBCG/SCCV) in Building 20, Room 102, Area B, has the Kodak Camera available for use and so does Bruce Cox in the PhotoMechanics Facility in Building 45.

2) The best graphics printer currently is the Kodak XLS 8600. It is a dye-sublimation printer that prints photograph quality on special paper (at \$2.09 per sheet) or on special transparencies (at \$2.60 per transparency). It costs \$10,000 and only the specific paper/transparency can be used. Also, a new scanner that produces even better quality images than the current HP ScanJet IIC is necessary because the printer will not accept the color format of the IIC and the images have imperfections that will show up conspicuously on the Kodak printer. Two of the best flatbed scanners are the Microtek ScanMaker IIHR for about \$1,049 or the Epson ES-1200C Professional for \$1,209. The Microtek is a triple-pass scanner that uses 24-bit color. It is 600x1200 dpi and 2400x2400 dpi with software enhancement. The Epson is a single-pass scanner that uses 30-bit color. It has a resolution of 2400x2400 dpi and both a SCSI port and a bi-directional parallel port, so it can be connected to more than one CPU. I recommend the Epson over the Microtek because the base resolution is higher. It is better to go with the higher resolution than the enhancement since the enhancement can only do so much. Furthermore, the 30-bit color is better since it will prolong the use of the scanner as the amount of color increases.

3) For mobility, a CD-ROM Writable is needed (CD-R). The CD-Rs can be multisessional even though once you have written to the disc, it is permanent. Also, the discs hold 640-650 Megabytes and are only about \$7. Most multimedia applications appear to be going towards the CD-ROM, not its rival, the magneto-optical.

Another option, if the immediate need for large amounts of portable space that can be accessed quickly is not too great, is waiting until 1996 when Phillips will introduce its CD-Erasable (CD-E). It will allow rewriting on CDs and should come in, the manufacturers claim, at about \$1,500.

The specific CD-R that is recommended is the Yamaha Quad-speed CDE-100 from CD-ROM Direct for \$3095. (The best that is available is a quad-speed CD-R and since this technology must last for several years, I recommend that you go with no lower than a quad-speed.) The specific portables are the Quad-speed CD-ROMs by Toshiba from Sound Electro Flight for \$330. (On the portable CD-ROM, nothing less than a Quad-Speed is acceptable.)

4) For the system itself, in order to write to a CD-R, a second at least 640M hard drive is required. Otherwise, the data flow rate will not be constant and causing the disc to have breaks between information, thereby making it difficult to read. This hard drive must be dedicated solely to writing CDs. The RAM memory must also be increased to the maximum amount and more VRAM (Video RAM) obtained. Another hard drive devoted solely for digital images and video storage is also needed.

5) In order to upgrade your video editing capability, I recommend Adobe's Premier 4.0 for \$324.98 from PC Zone. It goes well beyond the current editing capabilities and is user friendly like Adobe Premier 1.1.

6) In several years, the developments in multimedia will force you to upgrade again. In that case, I suggest that you take a look at the MPEG format. Since it is not yet fully mainstream and some manufacturers have doubts about it, the capture technology was not purchased. Also, the capture and edit technology is in the higher price range. (The lowest price being around \$5,000 and many over \$40,000.) Since this format is only just out of its infancy, it is better to wait than to have to deal with the numerous bugs and the various "standards". However, in the future, there will be one standard.

In conclusion, with the products purchased and the hardware and software that was available from local branches, WL/FIVE now has the ability to create multimedia presentations. The ability exists for loading images or movies from the Internet in any format, playing all of them, and editing the images and many videos. Most of the image and video formats can also be added to PowerPoint as part of a presentation or onto the coming home-page. Thus, this technology will enable the Flight Dynamics Lab to increase their presentation capability.

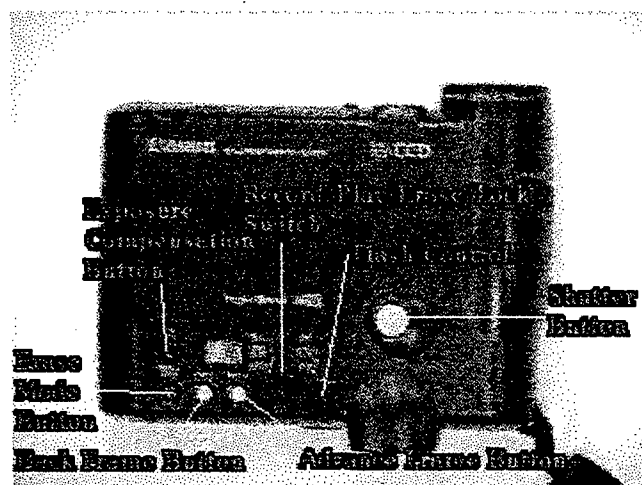
USER'S MANUAL

RC-250 Still Video Camera by Canon:

Taking Pictures:

- (1) Insert Video Floppy Disk
- (2) Insert battery or connect to outlet
 - (a) Connecting to outlet:
 - (b) Insert the power pack with the connectors pointing up.
 - (c) Pull out the slider, push in, and release the slider.
 - (d) Insert the video cord into the video out port on the camera.
 - (e) Connect adapter to the battery charger and tighten screw.
 - (f) Plug in battery charger.
- (3) Push switch to record
- (4) Camera should travel to the first available frame
- (5) Point at object - Make sure that it is well lighted and if within 3.3 feet (1 meter) use the Macro function.
- (6) Press down on shutter button to take picture. Film will automatically advance to next available frame.

Top View of Digital Camera



Front View of Digital Camera

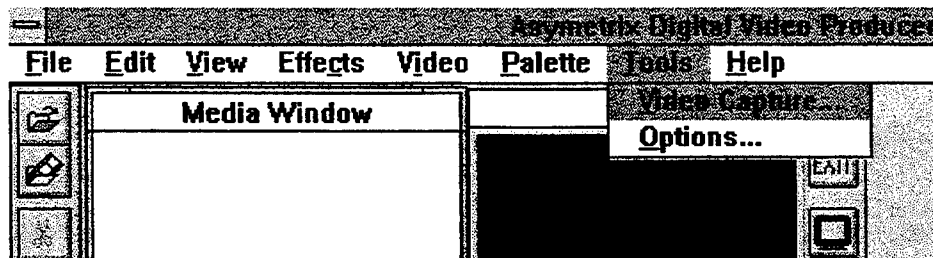


Erasing Pictures:

- (1) Connect camera to the computer or TV monitor.
 - (a) Insert the video floppy disk into the drive on the camera.
 - (b) Remove the battery and insert the power pack with the connectors pointing up.
 - (c) Pull out the slider, push in, and release the slider.
 - (d) Insert the video cord into the video out port on the camera.
 - (e) Connect adapter to the battery charger and tighten screw.
 - (f) Plug in battery charger.
 - (g) Connect RCA-composite cable to the video out port on the adapter and the other end to the RCA-composite port on the CPU or video-in port on the TV monitor. If the TV only has an antenna connection, use the cord provided with the battery pack.
 - (h) Turn on the camera by moving the switch up to the ERASE /PLAY mode. An image should now appear on the screen.
 - (i) Advance the photos until you arrive at the one you want to erase by clicking on the yellow FORWARD or REVERSE buttons on the top of the camera.
- (2) Press down on the shutter button while holding down on the MODE button. The display number should blink twice, then the image is erased.

Digital Video Producer:

There are two methods of capture. One is by double clicking on the Digital Video Producer Capture or by going into Digital Video Producer (DVP) and choosing **Video Capture** from the Tools menu. The only difference is that when you go through DVP, the clip just captured appears in the *Media Window*.



Note: If you are using the digital camera, the instructions differ from that of a video, whether live or taped.

CAMERA:

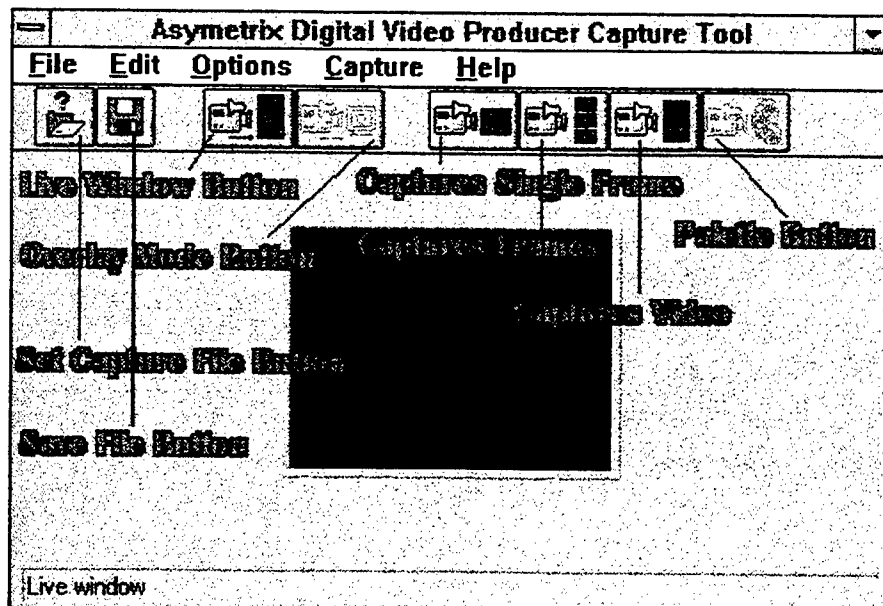
- (1) Insert the video floppy disk into the drive on the camera.
- (2) Remove the battery and insert the power pack with the connectors pointing up.
- (3) Pull out the slider, push in, and release the slider.
- (4) Insert the video cord into the video out port on the camera.
- (5) Connect adapter to the battery charger and tighten screw.
- (6) Plug in battery charger.
- (7) Connect RCA-composite cable to the video out port on the adapter and the other end to the RCA-composite port on the CPU.
- (8) Turn on the camera by moving the switch up to the ERASE /PLAY mode. An image should now appear on the screen.
- (9) Advance the photos until you arrive at the one you want to save by clicking on the yellow FORWARD or REVERSE buttons on the top of the camera.
- (10) On the Capture menu, choose **Single Frame**. (You can also use **Frames** to capture them all together.)
- (11) Finally, in the File menu, choose **Save Single Frame As** and choose the file path and the filename

Video:

- (1) Connect the CPU with the VCR or camcorder via the RCA-composite cable.
- (2) Enter the Digital Video Producer Capture by either method.
- (3) If it a live feed from a camcorder then a picture should appear immediately.

If it is from a tape, then as soon as you press play an image should appear.
- (4) Set the tape to where you want the capturing to begin.
- (5) Go to Capture and choose **Frames** or **Video** --- **Frames** allows you to capture a frame at a time while **Video** captures continuously.
- (6) Whatever is playing in the window is what is being captured. If the picture isn't moving, make sure that you have a *Live Window*. (Press the button to obtain the *Live Window*)
- (7) When finished capturing a video, press ESCAPE or the right mouse button to stop capturing.
- (8) Go to File and **Save** the file with the correct filename and path. Do not, **DO NOT** set the file size to anything, the CPU will do that on its own. If you do, nothing will be saved to the file or, it will be in an incorrect format.

DIGITAL VIDEO CAPTURE DISPLAY



DIGITAL VIDEO CAPTURE MENU BARS

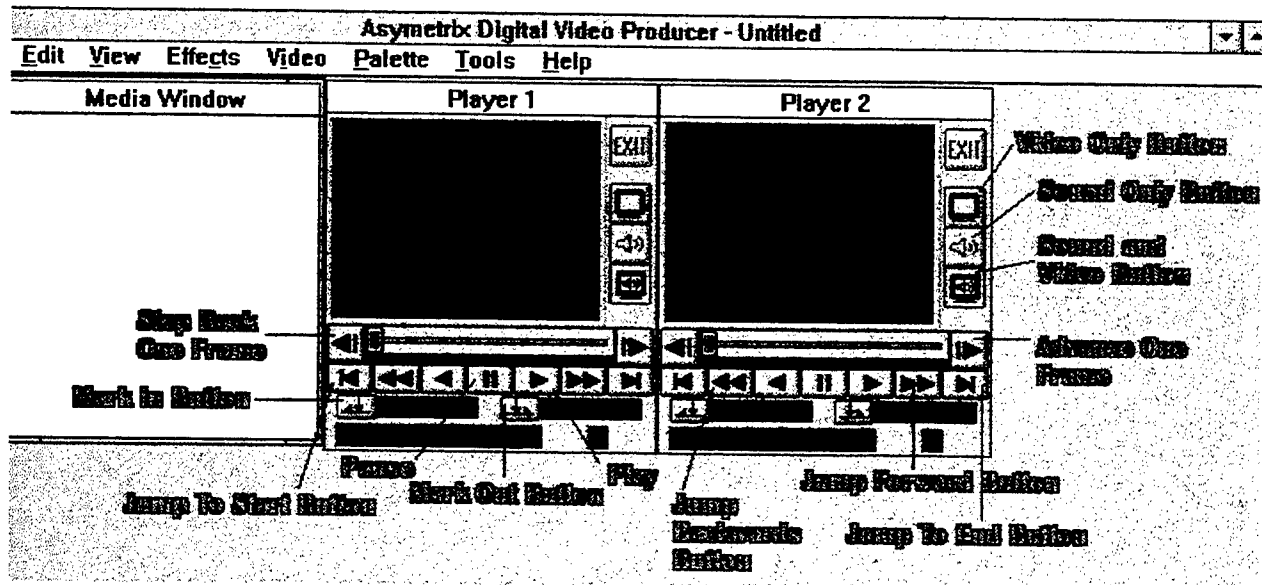
<u>F</u> ile	<u>E</u> dit	<u>O</u> ptions	<u>C</u> apture	<u>H</u> elp
Load <u>P</u> alette				
<u>S</u> et Capture File				
<u>A</u> llocate File Space				
Save Captured Video <u>A</u> s				
Save <u>P</u> alette				
Save Single <u>F</u> rame				
<u>E</u> xit				

<u>F</u> ile	<u>E</u> dit	<u>O</u> ptions	<u>C</u> apture	<u>H</u> elp
Audio <u>F</u> ormat				
Video <u>F</u> ormat				
Video <u>S</u> ource				
Video <u>D</u> isplay				
<u>C</u> ompression				
✓ <u>P</u> review Mode				
<u>O</u> verlay Mode				

<u>F</u> ile	<u>E</u> dit	<u>O</u> ptions	<u>C</u> apture	<u>H</u> elp
Single <u>F</u> rame				
<u>F</u> rames				
<u>V</u> ideo				
<u>P</u> alette				
<u>S</u> ettings				

Digital Video Producer:

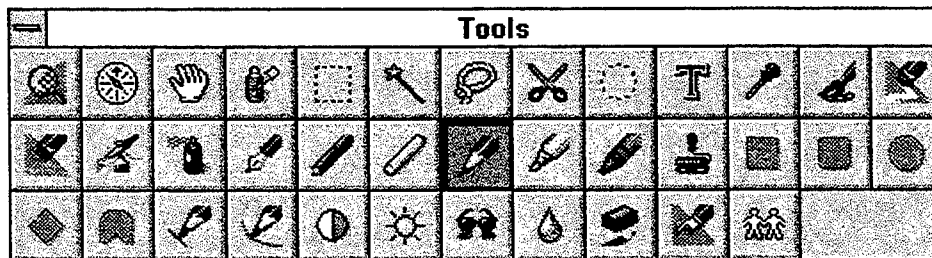
To start a new project, you must **Import Media** from the File menu. The clip will appear in the box called *Media Window*. In order to view the clip, you press the left mouse button down on a slide of the clip and drag it to the screen of *Player 1* or 2. The clip will then appear on the screen as it does when you play it via Media Player. You can make a selection from the clip by advancing to the frame you want and pressing the **Mark In** button, then, advancing to the final frame and pressing the **Mark Out** button. A yellow bar should outline the selection. Pressing the left mouse button and dragging to the *Timeline* allows you to add it to the *Timeline*. (To select all, just **Mark In** on the first frame and **Mark Out** on the last and then drag the clip to the *Timeline*.)



Building is what actually creates the video clip after editing. Before building, however, make sure that you have set the **Output Format** under the Video menu to the values that you want. Also, check the **Compression** format which is under the Video menu also. Indeo R3.2 is the best compression codec. The best *Key Frame* number is 4 and make sure that the *Data Flow Rate* is at least 600 Kbps (Kilobytes per second). When building, it is a good idea to have the CPU warn you on *data failure rate*. (Just check the box under **Build** which is under the Video menu.) Furthermore, if you want audio in the clip, you must have the audio positioned on the *Audio Track A* underneath the clip where it should be played. Otherwise, no audio will be built with the graphics.

If you want to apply a transition then you must have a clip on *Timeline A* and *B*. The transition will appear between the two and applies to every frame in both clips. If you want them to clip back to back, then you must put them on the same *Timeline*. No way exists for limiting the number of frames that the transition lasts. In order to do that you must select the portion of the clip that you want to have the beginning of the transition applied to and place it on *Timeline A*. Then, you take the number of frames from the clip that you want to have the ending of the transition and place it on *Timeline B*. Apply the desired transition and then **Build**. **Open a New Project** and place the beginning portion of the video clip, then the clip you just built, then snap the rest of the video clip that you want onto the end of the video you just built. Other than that, all the manipulations that will be done are very straightforward and intuitively obvious to the casual user.

PhotoFinish:



In order from left to right, the tools are as follows:

Zoom: Allows you to zoom in on various aspects of the current image. To zoom out, simply click the right mouse button instead of the left.

Locator: Allows you to determine exactly where you are in the image.

Hand: Allows you to move areas of a picture that is too big for the monitor into view.

Local Undo: Allows you to erase only what you did with the last tool.

Box Selection: Allows you to select an area for cutting, copying, or cropping into a new picture.

Magic Wand: Allows you to define areas of similar hues.

Lasso: Allows you to outline an object for cutting, copying, or cropping that is not precisely a quadrilateral.

Scissors: Allows you to define polygonal areas in the image.

Elliptical Selection: Allows you to outline and object in the shape of a circle for cutting, copying or cropping.

Text: Allows you to add Text to the image.

Eyedropper: Allows you to select a color from the background. Left mouse button makes it the outline and writing color; Right mouse button makes it the background color.

Paintbrush: Allows you to draw with the stroking style of the paintbrush. The more times you brush over, the darker the color.

Eraser: Allows you to erase whatever is under this one tint at a time to white.

Color Replacer: Allows you to replace the primary color with the secondary color.

Airbrush: Allows you to control the tint of what you are making.

Spray Can: Allows you to make random spraying of the color - like a spray can, it does not all go to one spot.

Pen: Allows you to write to an area with a color.

Charcoal: Colors an area the color of charcoal - darkness varies according to the number of passes.

Chalk: Allows you to draw in color with a chalk like tool.

Colored Pencil: Allows you to draw with the characteristics of a pencil.

Marker: Allows you to draw with the characteristics of a marker.

Crayon: Allows you to draw with the characteristics of a crayon.

Paint Roller: Allows you to fill in an enclosed area with the chosen color.

Box: Allows you to make boxes that can be filled in the secondary color and have a border in the primary color.

Rounded Box: Allows you to make rounded boxes that can be filled in the secondary color and have a border in the primary color.

Ellipse/Circle: Allows you to make ovals that can be filled in the secondary color and have a border in the primary color.

Regular Polygon: Allows you to make equal-sided polygons that can be filled in the secondary color and have a border in the primary color.

Polygon: Allows you to make polygons that can be filled in the secondary color and have a border in the primary color.

Line: Allows you to draw a straight line in any color.

Curve: Allows you to draw a curved line in any color.

Contrast Paintbrush: Allows you to increase the contrast in a given area.

Brighten Paintbrush: Allows you to lighten a given area.

Tint Paintbrush: Allows you to darken a given area.

Blend Paintbrush: Allows you to blend together a given area.

Sharpen Paintbrush: Allows you to sharpen in a given area.

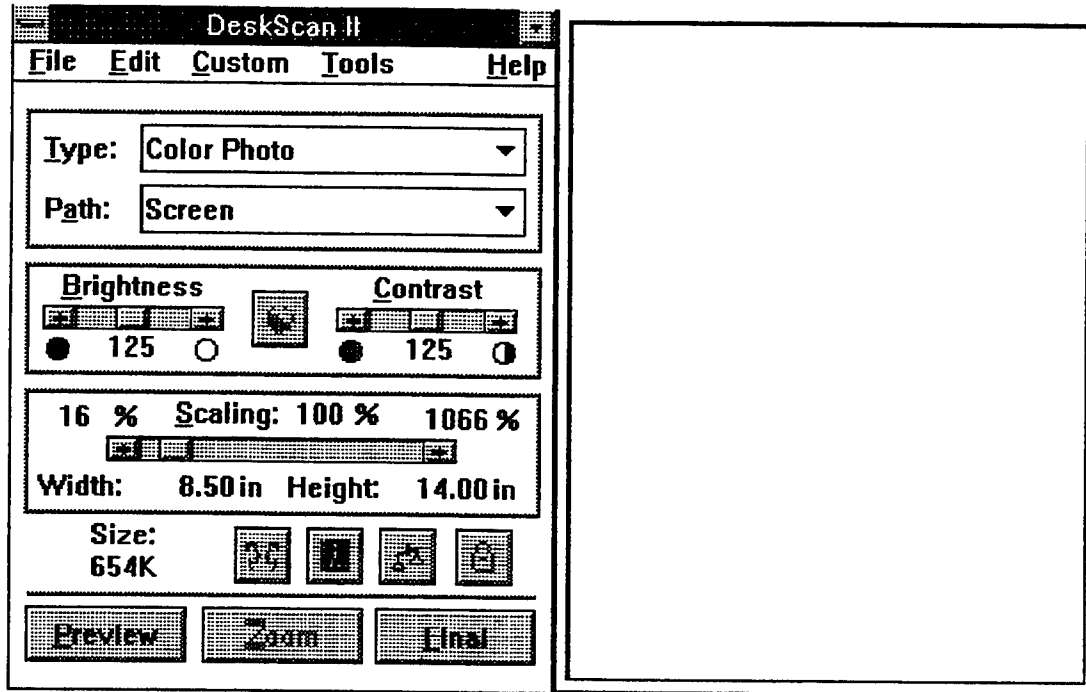
Smudge Paintbrush: Allows you to smudge in a given area.

Clone: Allows you to clone in a given area. To reset the “source pixels”, just press the right mouse button on top of the area that you want to begin at, and then place the cursor over the corresponding spot where you want to begin cloning and press the left mouse button.

Notes: 1) If you press down the Shift key while you are moving the cursor, you will be constrained to the horizontal plain.

2) There is no trick to editing images except practice and an extensive use of the clone tool.

DeskScan:



After placing the photograph or drawing in the upper right hand corner of the scanner where the two red triangles are, open up the Deskscan II icon and this screen will appear. Press the **Preview** button in order to see the image. Press **Zoom** in order to zoom in on the image by cutting off the bottom blank portion of the image and **Preview** again to zoom out. You can scan it in as a *Color Photo*, *Color Drawing* or *Black And White Drawing*, and others. Make sure that you set the resolution that you want via Custom, **Print Path** or choose *Resolution-300* or *-150*. (Don't go higher than about 300 on this scanner because all you get is pixelation and high memory requirements.) The buttons next to *Size 654K* are: Make a mirror image of the current image, make a negative of the current image, increase/decrease the length and width individually, and a lock to keep the width and height constant. You can select a part of the image by constraining the thin black box to surrounding only the amount desired. Press **Final** when you are ready to save the image that is outlined by the black box. From the selection given, TIFF is the best format to save under and BMP is the worst. TIFF is better because it is vectored and thus

enlarges with less pixelation. BMP is not vectored so it will often become pixelated when you attempt to increase the size. (It becomes more pronounced the greater the increase in size.) Include the drive and path if you want to save in a different directory than the one indicated. In order to rotate the image, you must go to PhotoFinish and choose Image, **Transform**, **Rotate**. In MS Imager you must go to Image and choose **Rotate**.

Note: In PhotoFinish, a positive number always rotates clockwise - to the right - while a negative number rotates counter-clockwise - to the left.

OmniPage Professional:

OmniPage Professional works almost the same way as DeskScan II. You go to Process and choose **Scan**, then set everything up the way you want it. Make sure that the first page of the document is in the upper right hand corner of the scanner before scanning. If you are scanning more than one page from the same document, make sure that you mark the box for *Multiple Pages*. Otherwise, just follow the messages on the screen. When you are finished with any editing, remember to **Save** the text. You can save it in many different formats including Word 5.0.

Notes: 1) If the page is printed long ways and it is not interpreted correctly, change the orientation of the page and scan it again.

2) Do not use the spell checker in here because it questions you about every word. Use the one in Word instead.

Sound:

Sound'LE or WAVE Studio are the best programs to use to record sound. However, the sound must be very loud and the microphone has to be right in front of the speakers or mouth. Otherwise, no sound will be picked up. In order to capture sound while capturing video, just enable audio capture under Settings in Capture and it will automatically capture sound from the microphone or line in. Make sure that the microphone is connected to the CPU and in front of the speakers!

Monologue:

To activate Monologue, minimize the icon once you have the settings you want, then go to the document and copy out the portion of the document you want spoken. After closing the document, click on the minimized icon of the monologue program with the right mouse button. Once it starts speaking, you cannot interrupt it.

Adding Multimedia to PowerPoint:

Power Point is not able to transfer different size and types of fonts, but they can be changed inside PowerPoint. You can add graphs or spreadsheets through Microsoft Excel. Adding photos from PhotoFinish or MS Imager is best done by entering the application and **Copying** the photo or section of the photo and then entering PowerPoint and **Pasting** the photo. A Media Clip is embedded the same way as a picture. To link a picture or video clip, go to Insert, choose **Object**, choose **Create From File**, choose **Link**, and then select the file. Embedding makes a picture/video clip a permanent part of the file so that even if the file is deleted from the hard drive or changed, it does not affect the embedded image (it still exists in the presentation even if the image does not exist anywhere else) unless you update the image. (Clicking on the right mouse button on the image allows you to edit the image. However, be sure to update the image before exiting the editing application.) Linking does not add the file, only a pointer to its location so that if the file changes, so does the object in PowerPoint.

In order to enlarge a media clip you go to **Draw** and choose **Scale** and then increase or decrease the percentage to the desired amount. Then, you can recenter the clip, etc. All resizing is easier to do if done immediately. However, you can adjust later provided that you first delete the text box or whatever is behind the clip and then click once on the media clip with the left mouse button. Now you are free to make corrections. However, be forewarned, this technique, rather than **Building** it to the appropriate size or Capturing it at the preferred size, causes some unexpected problems. The clip will have some difficulty in enlarging itself before playing and stopping itself. In order to stop the clip, you must click the mouse **OFF** the image, otherwise it assumes that you want to continue the media clip, not go on to the next slide. Furthermore, the image does not stop where it is at, but goes back to the beginning and will restart at the beginning. You can pause it in the middle by clicking on the far left button which is now the **PAUSE** button, restart by clicking on it again, or set it on a

particular screen by hitting the left or right arrows to advance or retreat. (That latter message is specific for linked objects. If it is embedded, then you can advance or retreat by dragging the slider on the bottom of the image.) Furthermore, when you enlarge an image, the image appears in the original size and then, moments after the clip begins, it enlarges itself and begins again. Also, at the end, the screen goes black, but if you interrupt the procession, the image returns to normal size before going on to the next slide. Therefore, it is best to set the size to the appropriate dimensions before you capture the video and then all these problems are avoided.

If you type some information in behind a media clip, it will show up before you actually run the clip, but not during. If you want decent information you must type around the clip for it shows through initially, but the information is hid as soon as the clip begins. Another idiosyncrasy of this program is that the background on the slide must be solid white otherwise strips of discoloration occur.

Interruptions are horrible under media player. It is better to let the clip play all the way through than to interrupt it, and move on. If you must interrupt, press PAUSE first. It is best to edit and then **Build** the clip to the desired length to begin with or Capture it that way before embedding or linking it into PowerPoint.

You can make an video clip almost like a single frame by using **Selection**. If you want a very small portion then you have to choose Edit and then **Selection** and set the numbers. Otherwise, setting the slider in the starting position and pressing the **Mark In** button, then moving the slider to the final frame and pressing the **Mark Out** button works just as well. A simpler method is just to Capture it as a **Single Frame** or use the editing software to **Build** an image.

In regards to sound in a video clip, even if you put the clip on *Mute*, when you embed it in an application, it automatically adds the sound to the clip. (The video graphics and sound are interwoven in this AVI format.) If you want to delete sound from a slide, it must be done in the video editing section or not captured at all. (Just disable the **Audio Capture** under **Settings** under Capture in Digital Video Producer Capture.) Otherwise, one way to handle this is to put all sound on mute via the Control Panel. Another way is to link the object and then make the media player into an icon after you choose to make the clip *Mute*. However, *Mute* must be rechosen before each slide show and the link updated. Unfortunately, linking doesn't work out very well when you have a

media clip, because the position of the image changes each time and it does not look very professional to have to adjust the media clip during the presentation. Also, you have to minimize the media player board, but the icon shows up. Thus, embedding is the best method.

Slides will automatically play their sound when displayed. In order to properly add sound to a slide, you must go through media player object. Otherwise, if you go through Sound*LE or just Sound, the object will not play. You must **Copy** the media clip and then **Paste Special** it into PowerPoint, otherwise the screen can show up anywhere if you simply **Insert** the **Object**. Sound can also be linked by following the exact same directions as for linking media clips and pictures.

That is the basically how to incorporate multimedia into PowerPoint 4.0. As a rule, everything is straight forward and easy to use. Therefore, enjoy creating videos and images and editing them. These multimedia presentations will make Wright Laboratories' Flight Dynamics Lab more competitive in selling their services.

**PERL And AWK Based Post Processor
For EPIC FEM Computation**

Michael J. Dooley
Niceville High School

Final Report for:
High School Apprenticeship Program
Mentor: Mike Nixon
WL/MNMW
Wright Labs
Eglin AFB

Sponsored by:
Air Force Office of Scientific Research
Bolling A.F.B.
Washington DC

and

Wright Laboratory
Eglin A.F.B.

August 1995

**PERL And AWK Based Post Processor
For EPIC FEM Computation**

Michael Dooley
Niceville High School

Abstract

This paper documents the development of a PERL and AWK based post-processor for the EPIC Finite Element or FEM hydrocode. The post-processor, called POSTER, gives three levels of summary reports from EPIC textual output files. The reports give the user a method of quickly evaluating the major run parameters for a completed simulation with EPIC.

Introduction

This as well as last summer I worked in the Computational Mechanics section of the Warheads Branch at Wright Laboratories located at Eglin, A.F.B. Florida. Under the guidance of Mr. Michael E Nixon, my project was to design a post-processor for EPIC FEM runs. To design this software, several UNIX utilities were researched including AWK, PERL, SED, and UNIX C. Each of these languages has both benefits and drawbacks, so each language had to be properly researched. EPIC also had to be researched to find out what output is produced as well as what output is to be post-processed.

After the initial research was completed, the next step was to thoroughly study EPIC. EPIC is a FORTRAN program that simulates dynamic events such as impact, penetration, and blast. EPIC code is derived from Lagrangian finite element formation, where the equation of motion is directly integrated rather than traditional stiffness matrix approach. For all practical purposes, the equations involved are well beyond the scope of high school calculus, so the goal of the EPIC post-processor would be limited strictly to the processing of output data, rather than the calculations themselves. EPIC outputs data in two formats, graphical and textual. Figure A.1 is an example of graphical EPIC of two penetrators impacting a concrete cylinder and the various stress and temperature effects the impact has on the cylinder.

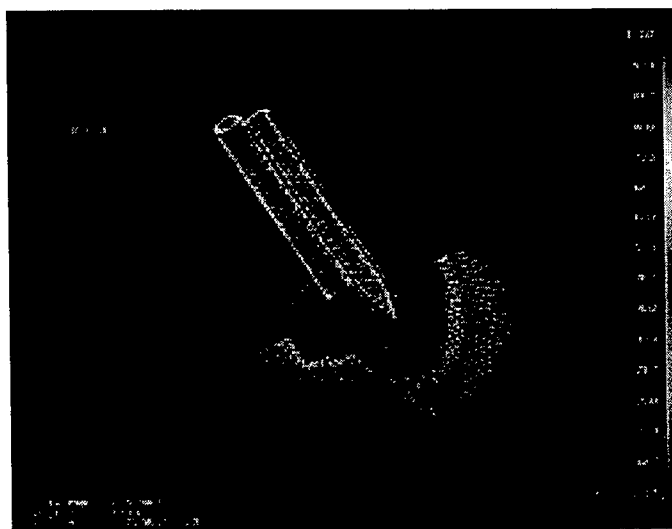


FIGURE A.1

The purpose of my post-processor however, was to manipulate textual output. The EPIC output file includes the input data, preprocessing data, main processing data, and postprocessing results. This is often very large (ranging from 50 kilobytes to over one megabyte in size) and difficult to read as shown in Figure A.2.

```

$TYPE CASE...DESCRIPTION OF PROBLEM..... LINE 1
  2 44 OAL Test LINE 2
$GEOM PRNT SAVE NSLD NMAS NRST NRG NCHK NOCH SCATpcXYZ SPLT DP3 UNIT CDCT
PER LINE 3
  6 0 0 2 0 0 0 0 0.000044000 0 0 0 0 0 LINE 4
$##### MATERIAL DATA LINE 5
$MATL 0 DAM FAIL FRAC EFAL...DESCRIPTION OF SOLID LIBRARY MATERIAL.....
LINE 6
  9 0 1 0 1.0999.04340 STEEL (RHA) RC-30 LINE 7
$MATL 0 DAM FAIL FRAC EFAL...DESCRIPTION OF SOLID LIBRARY MATERIAL.....
LINE 8
 11 0 1 0 1.0999.0TUNGSTEN (.07NI,.03FE) RC-47, APPROX FRACTURE LINE 9
$MATL 0 DAM FAIL FRAC EFAL...DESCRIPTION OF CRUSHABLE LIBRARY MATERIAL.....
LINE 10
 71 0 1 0 1.0 2.0*SAC-5 CONCRETE (PRELIMINARY) (HJC MODEL) LINE 11

```

FIGURE A.2

There are also many references to computations and data not easily accessible in the output file that can baffle even experienced EPIC users. The purpose of the post-processor will be to read in the output files, make sense of what processing the EPIC code underwent and create software that allows the user to select what information concerning the EPIC run he/she desires available for immediate or future study. After the exploration of EPIC was concluded, it was then necessary to choose a programming language most suited to postprocessing the EPIC output. After some investigation, PERL was chosen for this role.

Equipment Used

Silicon Graphics Indy 150 MHz RISC Based UNIX Workstation

Gateway 2000 DX-2 66 MHz Personal Computer with DOS 6.22 and Windows For Workgroups

IRIX UNIX AWK Interpreter

IRIX UNIX PERL 4.036 Interpreter

Unisys 386 SX-20 MHz Personal Computer with DOS 6.22 and Windows for Workgroups

Silicon Graphics Indigo 33 MHz RISC Based UNIX Workstation

Methodology

PERL is the acronym for Practical Extraction and Report Language and was developed by Larry Wall. PERL is a UNIX based, C similar script language, more powerful than previous UNIX data processing script languages, such as SED and AWK, which were reliant on repeating data patterns for proper code execution. PERL has no such limitations. This language seemed to combine the benefits of script language convenience and the power of a language like C. Another advantage of PERL is the large library of built in functions that make the language even more powerful and easier to use. One advantage is PERL's major uses is data processing, more specifically data processing computation, extraction, and manipulation. Other PERL uses include directory and UNIX system manipulation. After concluding that PERL would be the best way to design the post-processor, the programming of the software could begin. After a few weeks, an efficient PERL program that would perform its task with little to no complications was developed. The PERL program had to take data from the EPIC output file, be able to make determinations from numbers and statements in the EPIC output file, process that information and present an eye pleasing correct summary of the information processed. The PERL program designed seemed to accomplish all of the tasks it had been assigned. (Although the actual program with subroutines is over 500 lines, an example of the code is in Appendix A). For easier references, the official title of the post-processor Perl Output Summary of Textual EPIC Results was designated POSTER. However, a problem with a certain section of the EPIC output file arose, and it seemed that a limitation of PERL had been identified.

Last summer, it was concluded that AWK was difficult to use and could not perform the tasks assigned. AWK is UNIX based C like script language, and with its limitations I was sure it could not be used in the development of the post processor. However, upon further reflection, it seemed that AWK could easily solve the problem with the PERL program. The problem was PERL required much more time than should be necessary to process node information from the EPIC output files. After identifying the

problem, I quickly concluded the AWK could quickly process the data and output it the exact same manner as the PERL program. So it was decided that instead of having one program in the postprocessing software, I would link a PERL and an AWK program together using a shell script. AWK is a UNIX script language designed to quickly process patterned files. As long as the file remained in the same patterned or altered becoming a different although stabilized pattern, AWK would have no problem. Although the PERL program would have completed this assignment in the post-processor, AWK it seemed would be a much better choice for obvious reasons, and would be faster and more efficient than PERL. An example of the AWK code is in Appendix B.

Results

Once all of the parts of the post-processor were working properly, and the various bugs were eliminated, the software was then refined and a user option that would allow the user to control the amount of output he/she wanted was created. Three levels of output, one that produced a short summary of the post-processor's result, a detailed summary, and a very detailed summary was added. Appendix D is an example of the PERL and AWK outputs, with highlights indicating various levels of indepthness available to the user.

Once everything was compiled and completed, reports were generated from actual EPIC runs. After several runs were completed, and the results compared with the actual EPIC output files, the postprocessor seemed to perform well in all cases. Some minor refinements were necessary to account for some EPIC output irregularities, but once those were identified, the programs executed without any problems. The program was also documented to allow future users to modify the overall function of the postprocessor and allow for new options as the EPIC code evolves over the next few years. Both AWK and PERL, once their strengths and weaknesses were identified, were very well suited to the tasks that each language had been assigned. Although either AWK or PERL could have performed both parts, I felt that I found the best possible combination of the two, that allowed for the best possible efficiency, precision, speed and accuracy in code execution. The addition of a UNIX based C-shell script for overall management also added to the overall usability of the postprocessor.

ADDITIONAL PROJECTS

In addition to the EPIC postprocessor, several other projects and assignments to accomplish were assigned during my internship. The first was an AWK program to reorganize data files from terminal programs in UNIX. However, the phone entries in one terminal program contained many deviations from its basic format, turning one AWK program to three AWK program, Appendix C.

Another project assigned this summer, was to view declassified movies and catalogue them according to age and subject. Also this summer I designed and constructed World Wide Web home pages for the Warheads Branch and the various sections that make up the Branch.

ACKNOWLEDGMENTS

Michael E Nixon

Mike Deiler and Don Harrison

Major Howard Gans

Capt. Gus Martinez

Josh Weaver and Gabrielle White Wolf

The Members of the Computational Mechanics Section

APPENDIX A SECTION OF PERL CODE

```
do {
    do {
        $line = <FILE1>;
        $flagger = $array1[$count];
    } until ($line =~ /$flagger/);
    @nextarr = split(/ +/, $line);
    $NSTUF = $nextarr[3];
    $NSTUF = $NSTUF * 1;
    $OSTUF = $text[$count];
    print("There are $NSTUF $OSTUF \n");
    $count++;
    if ($line =~ /NSLID/) {
        $NSLID = $NSTUF;
    }
} until ($count == 5);
do {
    do {
        $line = <FILE1>;
        $flagger = $array1[$count];
    } until ($line =~ /$flagger/);
    @array_two = split(/=/, $line);
    $ASTUF = $array_two[1];
    $BSTUF = $text[$count];
    print($BSTUF, " Number is:", $ASTUF);
    $count++;
} until ($count == 6);
$line = <FILE1>;
@unit = split(/=/, $line);
$VALUE = $unit[0];
if ($VALUE == 0) {
    print("English Units were used.\n");
}
if ($VALUE == 1) {
    print("SI units were used.");
}
if ($VALUE == 2) {
    print("CGS Units were used.");
}
do {
    $line = <FILE1>;
} until ($line =~ /CDUCT/);
@cduct = split(/=/, $line);
$CDUCT = $cduct[1];
if ($CDUCT == 1) {
    print("This simulation accounts for heat induction.\n");
}
elseif ($CDUCT == 0) {
    print("This simulation does NOT account for heat induction.\n");
}
}
```

```

do {
    $line = <FILE1>;
} until ($line =~ /PER/);
@per = split(/=/, $line);
$PER = $per[1];
if ($PER == 0) {
    print("This simulation will not use the PER option for shaped charge warheads.\n"); }
elseif ($PER == 1) {
    print("This simulation will use the PER option.\n"); }
elseif ($PER == 2) {
    print("This simulation will use the PER option reported as 2.\n"); }
elseif ($PER == 3) {
    print("This simulation uses a combination of the PER=1 and PER=2 options.\n"); }
elseif ($PER == 4) {
    print("This simulation uses a slightly different collapse criteria that");
    print("was used with the EPIC Mass-Point Algorithm.\n");
}
print "\n";
$count = 1;
&matl_counter; #Calls subroutine matl_counter
print("THE LIST OF MATERIALS ARE: \n");
print "\n";
while ($count <= $final_count) {
    do {
        $line = <FILE1>;
    } until ($line =~ /INPUT DATA/);
    @matl = split(/ +/, $line);
    $MATL = $matl[4];
    $MATL2 = $matl[5];
    do {
        $line = <FILE1>;
    } until ($line =~ /MATERIAL NUMBER/);
    @solid = split(/ +/, $line);
    $SOLID = $solid[3] * 1;
    $count = 1;
    do {
        $line = <FILE1>;
        $count++;
    } until ($count > 2);
    @number = split(/ +/, $line);
    $NUMBER = $number[1];
    $NUMBER2 = $number[2];
    print($MATL, " ", $MATL2, " ", "Number: $SOLID : $NUMBER $NUMBER2\n");
    print "\n";
    $count++;
}
&node_inp_cnt;

print "\n";
do {
    $line = <FILE1>;
} until ($line =~ /PROJECTILE NODE INPUT DATA/);

```

APPENDIX B AN EXAMPLE OF THE AWK PROGRAM

```
((flag == 2) && ($4 != VALUE) && ($0 != "") && ($4 !~ /ECRIT/) && (NF == 10) && ($2 !~ /DATA/))
{
    print("The ECRIT value has changed: " $4 " \n")
    print("The CYCLE is: " $1 "   " "The TIME is: " $3 " \n")
    print(" \n");
    VALUE = $4
}
((flag == 2) && ($1 ~ /CYCLE/) && ($2 ~ /\=/) && (NF == 3)) { print ("The core was dumped
at:\n");print ($0 " \n") }
((flag == 2) && ($1 ~ /TIME/) && ($2 ~ /\=/) && (NF == 3)) { print ($0 " \n")}
(($1 ~ /CYCLE/) && ($4 ~ /ECRIT/)) { flag = 1}
((flag == 1) && ($1 != "")) {
flag = 2
VALUE = $4 }
```

APPENDIX C EXAMPLE OF ONE OF THE AWK TERMINAL SCRIPTS

```
($3 ~ /ZZ_/) {
    if (NF == 9) {
        n = split($9,array,"");
        printf($1 " " $2 " " $3 " " $4 " " $5 " " $6 " " $7 " " $8 " " array[1] array[2] "\n");
    }
    if (NF == 8) {
        n = split($8,array,"");
        printf($1 " " $2 " " $3 " " $4 " " $5 " " $6 " " $7 " " array[1] array[2] "\n");
    }
    if (NF == 7) {
        n = split($7,array,"");
        printf($1 " " $2 " " $3 " " $4 " " $5 " " $6 " " array[1] array[2] "\n");
    }
    if (NF == 6) {
        n = split($6,array,"");
        printf($1 " " $2 " " $3 " " $4 " " $5 " " array[1] array[2] "\n");
    }
    if (NF == 5) {
        n = split($5,array,"");
        printf($1 " " $2 " " $3 " " $4 " " array[1] array[2] "\n");
    }
    if (NF == 4) {
        n = split($4,array,"");
        printf($1 " " $2 " " $3 " " array[1] array[2] "\n");
    }
}
($3 !~ /ZZ_/) {
    if (NF == 6) {
        n = split($5,array,"");
        printf($1 " " $2 " " $3 " " $4 " " array[1] array[2] " " $6 "\n"); }
    else if (NF == 5) {
        n = split($4,array,"");
        printf($1 " " $2 " " $3 " " array[1] array[2] " " $5 "\n"); }
```

APPENDIX D POSTER OUTPUT

This is a summary of EPIC Output from OUT.TXT

This EPIC simulation is described as: OAL Test
with simulation number 44

This is a two dimensional axisymmetric geometrical simulation without spin.

There are 2 Slidelines.

There are 0 Concentrated Masses.

There are 0 Restrained Nodes.

There are 0 Rigid Surfaces.

There are 0 Chunks.

PATRAN Case Number is: 44

English Units were used.

This simulation does NOT account for heat induction.

This simulation will not use the PER option for shaped charge warheads.

THE LIST OF MATERIALS ARE:

SOLID MATERIAL

Number: 9 : 4340 STEEL

SOLID MATERIAL

Number: 11 : TUNGSTEN (.07NI,.03FE)

CONCRETE MATERIAL Number: 71 : *SAC-5 CONCRETE

GEOMETRY SUMMARY

TOTAL NUMBER OF NODES = 14740

NUMBER OF PROJECTILE NODES = 1595

NUMBER OF TARGET NODES = 13145

TOTAL NUMBER OF ELEMENTS = 28228

NUMBER OF SLIDING SURFACES = 2

***END OF SHORT SUMMARY**

PROJECTILE NODE INPUT DATA

NODE INPUT DATA FOR A ROD

FIRST ROD NODE	(N1)	=	1
LAST ROD NODE		=	968
TOTAL NUMBER OF ROD NODES		=	968

NODE INPUT DATA FOR A ROD

FIRST ROD NODE	(N1)	=	1001
LAST ROD NODE		=	1018
TOTAL NUMBER OF ROD NODES		=	18

NODE INPUT DATA FOR A ROD

FIRST ROD NODE	(N1)	=	1017
LAST ROD NODE		=	1594
TOTAL NUMBER OF ROD NODES		=	576

APPENIDX D cont.

NODE INPUT DATA FOR A ROD

FIRST ROD NODE (N1) = 1596
LAST ROD NODE = 1606
TOTAL NUMBER OF ROD NODES = 11

NODE INPUT DATA FOR A NOSE SHAPE

NOSE SHAPE IS OGIVAL
SPH/NABOR MATERIAL (NMAT) = 0
FIRST NOSE NODE (N1) = 1607
LAST NOSE NODE = 1627
TOTAL NUMBER OF NOSE NODES = 21

NODE INPUT DATA FOR A FLAT PLATE

JOIN OPTION (JOIN) = 0
FIRST PLATE NODE (N1) = 2001
SPH/NABOR MATERIAL (MATL) = 0
LAST PLATE NODE = 15145
TOTAL NUMBER OF PLATE NODES = 13145

ELEMENT INPUT DATA FOR A ROD

MATERIAL (MATL) = 11
NUMBER OF INNERMOST, CLOCKWISE, TOP NODE (N1) = 1
UNIFORM MATERIAL NUMBER THROUGHOUT = 11
FIRST ROD ELEMENT = 1
LAST ROD ELEMENT = 1544
TOTAL NUMBER OF ROD ELEMENTS = 1544

ELEMENT INPUT DATA FOR A ROD

MATERIAL (MATL) = 9
NUMBER OF INNERMOST, CLOCKWISE, TOP NODE (N1) = 1001
UNIFORM MATERIAL NUMBER THROUGHOUT = 9
FIRST ROD ELEMENT = 1545
LAST ROD ELEMENT = 1568
TOTAL NUMBER OF ROD ELEMENTS = 24

ELEMENT INPUT DATA FOR A ROD

MATERIAL (MATL) = 9
NUMBER OF INNERMOST, CLOCKWISE, TOP NODE (N1) = 1017
UNIFORM MATERIAL NUMBER THROUGHOUT = 9
FIRST ROD ELEMENT = 1569
LAST ROD ELEMENT = 2336
TOTAL NUMBER OF ROD ELEMENTS = 768

ELEMENT INPUT DATA FOR A ROD

MATERIAL (MATL) = 9
NUMBER OF INNERMOST, CLOCKWISE, TOP NODE (N1) = 1596
UNIFORM MATERIAL NUMBER THROUGHOUT = 9
FIRST ROD ELEMENT = 2341
LAST ROD ELEMENT = 2352
TOTAL NUMBER OF ROD ELEMENTS = 12

ELEMENT INPUT DATA FOR A NOSE

APPENDIX D cont.

MATERIAL NUMBER (MATL) = 9
NUMBER OF FIRST NOSE NODE (N1) = 1607
UNIFORM MATERIAL NUMBER THROUGHOUT = 9
FIRST NOSE ELEMENT = 2353
LAST NOSE ELEMENT = 2388
TOTAL NUMBER OF NOSE ELEMENTS = 36

ELEMENT INPUT DATA FOR A FLAT PLATE

MATERIAL (MATL) = 71
FIRST NODE (N1) = 2001
FIRST PLATE ELEMENT = 2389
FIRST PLATE ELEMENT = 2389
LAST PLATE ELEMENT = 28228
TOTAL NUMBER OF PLATE ELEMENTS = 25840

* END OF MEDIUM SUMMARY

RTZ PROJECTILE VELOCITIES

X VELOCITIES Y VELOCITIES Z VELOCITIES

0.000000E+00 0.000000E+00 -0.132000E+05

RTZ TARGET VELOCITIES

X VELOCITIES Y VELOCITIES Z VELOCITIES

0.000000E+00 0.000000E+00 0.000000E+00

NUMBER OF NODES WHOSE DATA ARE SAVED (NPLOT) = 11

NODES 963 964 965 966 967
968 1600 1601 1602 1595
1599

NUMBER OF ELEMENTS WHOSE DATA ARE SAVED (LPLOT) = 15

ELEMENTS 1537 1538 1539 1540 1541
1542 1543 1544 2341 2345
2349 2337 2338 2339 2340

Dumps were made at:

CYCLE TIME (in Microseconds)

15438 2000.01

30933 4000.03

46302 6000.03

55722 7271.67

ECRIT CYCLE TIME (in Microseconds)

2362 10 0.16807

2362 510 0.167952

2362 1010 0.167985

2390 1500 0.166394

* END OF DETAILED SUMMARY

FLOW ANGLE MEASUREMENT FOR THE TURBINE RESEARCH FACILITY

Mark Fecke

Chaminade-Julinne High School

Final Report for High School Apprenticeship Program
Wright Laboratory

Sponsored by
Air Force Of Scientific Research
Bolling Air Force Base, DC

And
Wright Laboratory

August 1995

FLOW ANGLE MEASUREMENT FOR THE TURBINE RESEARCH FACILITY

Mark Fecke

Abstract

In order to evaluate turbine performance, pressure and temperature measurements must be made at the inlet and exit of the turbine blade row. Since the turbine is rotating, the flow direction relating to the measurements location may vary. The objective of this work was to measure this flow angle at the exit of the test turbine. Because of the transient nature of the flow a hot-film anemometer was used to measure the flow angle. This paper documents the calibration of the hot-film at two different total temperatures and presents a theory for using the hot film to determine flow angle at elevated temperature. Finally the flow angle measured during a turbine test is presented.

Introduction

The Turbine Research Facility (TRF) is an experimental test facility designed to evaluate the performance of full scale axial flow turbines for the Air Force. To reduce costs, the facility operates in a blow down cycle. A high pressure reservoir is filled with a mixture of gasses to obtain the proper aerothermodynamics in the turbine during the test period. This high pressure chamber is isolated from the initial evacuated environment of the turbine and the receiving tanks by a quick acting valve. Once the high pressure chamber is pressurized with the proper mixture of gases and heated to the desired temperature, the turbine is accelerated to the desired operating speed by an electric motor. The quick acting valve is then opened to start the test. The turbine is maintained at a constant operating speed by using a electromagnetic brake. However, because of the finite volume of the high pressure reservoir combined with the required mass flow of the turbine, the test duration is only 2-3 second long. This short run time demands the use of high response instrumentation.

The specific task to be accomplished in this effort was to measure the flow angle at the facility's downstream measurement location. This flow angle is critical to the positioning of the facility's instrumentation to accurately measure the total pressure and total temperature of the turbine discharge flow. For this purpose a hot-film anemometer was used.

The hot-film anemometer is the most commonly used tool to measure fluid velocity and turbulence. Simply stated, a hot-film probe is a thermal transducer. An electric current is passed through a fine filament and maintained at an elevated temperature.. As the flow rate varies, the heat transfer from the filament varies. Thus the electric power dissipated in the sensor is a measure of cooling effect resulting from the fluid flowing over the heated sensor. This cooling effect largely depends on the mass flow passing over the sensor and the temperature difference between the sensor and the fluid. If the temperature difference is relatively large, the cooling effect will primarily depend on the mass flow cooling rather than changes in fluid temperature. The filament is made from a material which possesses a high temperature coefficient of resistance. When the temperature of the filament varies the

resistance varies . The variation of resistance is then measured by the change in voltage to maintain a constant temperature related to the variation in flow velocity.

A differential feedback amplifier senses that the bridge is unbalanced and adds current to keep the temperature of a probe constant. Before turning the power on, the adjustable register is set to a larger value that would be required to balance the bridge. When the power is turned on, the feedback amplifier increases the current, causing the temperature of the sensor to rise above the ambient air temperature and balance the bridge. Increasing the velocity will cool the sensor and unbalance the bridge. This makes the feedback amplifier raise the voltage and rebalance the bridge. The heat transfer from the wire, if all other factor stay constant (humidity, temperature, concentration, density ect.), will be proportional to the electric power (iv) provided by the bridge. For a constant current this power is proportional to the voltage. Therefore the velocity is proportional to the voltage because of the electronics and the size of the film. The voltage can quickly change in relation to the transient heat transfer from the wire; thus the temperature remains almost constant as the velocity changes and thus remains transient of the use of the TRF test which last only 2 or 3 seconds.

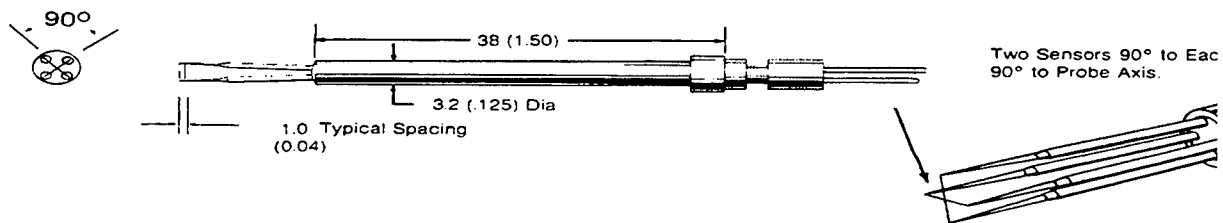


Figure 1. A standard TSI 1240-60 dual sensor hot-film probe, as used in the study.

The probe sensor is typically made out of tungsten or platinum deposited on a backing material and connected to the electronic package by leads attached to the ends of the film. A thin protective coating is put over the film to prevent damage by abrasion or chemical reaction. The hot-film probe is about 1 mm long and varies in diameter. The film used in the study was .06 mm in diameter. The body of the probe encompasses the wires that

connect the film to the connector at the other end of the probe. This connector allows the probe to be mounted in a probe holder which is used to position the probe in the flow field.

Design of the Mounting Fixture

The design of the mounting fixture was the initial step in preparing the test. This included making a fixture that would fit the TRF flow path that would allow the probe to be set up at the proper orientation angle and depth. In order to make the fixture, measurements had to be made of the existing opening in the TRF flow path hardware. A rough sketch was then made to get a general idea of how the fixture would be made. The next step was to devise a way to seal the fixture to the casing so the flow path would be sealed. This design was complicated by the TRF hardware which had a inner and outer wall. The design process concluded with the final configuration shown in **Figure 2**. Fabrication of the probe holder was done in-house to expedite fabrication for installation and testing.

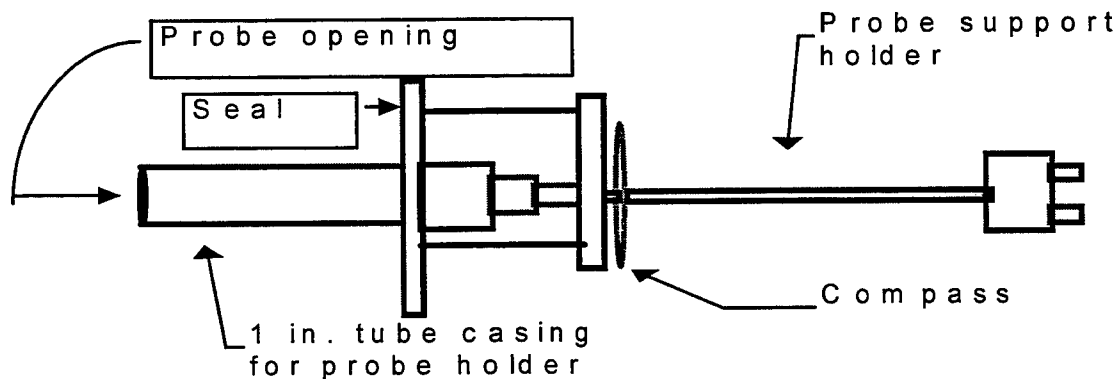


Figure 2. Sketch of mounting fixture and probe installation (mechanical drawing located in Appendix A **Figure 7** and 8-A)

Procedure for Balancing IFA 100

The TSI IFA 100 was used to measure the voltage of the probe. It can accommodate up to four channels, but only two of these channels were required by the TSI 1240-60 standard "X" probe used for the flow angle measurement. During the test the IFA 100 output voltage was recorded on the TRF transient data acquisition

system. This system was then used to provide the voltage vs. time history of each of the hot films of the 1240-60 probe for post processing. Balancing of the probe was performed in accordance with the procedures presented in **APPENDIX B Table 1-B**. The resistance's measured for the probes used in this test are presented in **Table 3-B** which is also in **APPENDIX B**.

Calibration

Once the electric current was balanced, the probe was calibrated. The calibration of the probe was performed at the Air Force Institution of Technology calibration facility. To calibrate the probe other information was needed. The total pressure (Pt), static pressure (Ps), and total temperature (Tt), were obtained from the calibration facility data acquisition system. The velocity of the flow was then calculated from these parameters. The IFA 100 provided the output voltage for each of the two channels of the TSI 1240-60 hot film. The calibration was retained with the probe oriented such that the flow bisected the probe at the reference angle of zero degrees.

(See **Figure 3**)

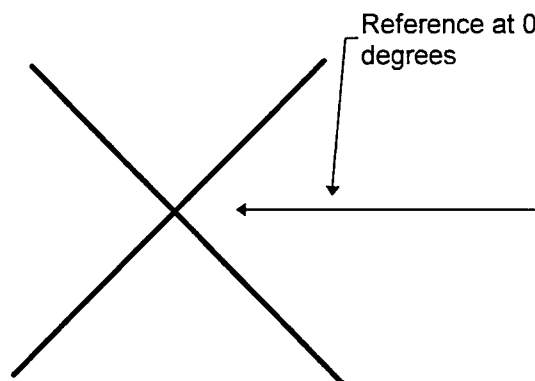


Figure 3. Flow bisecting to probe

Three flow calibration were performed. The calibration runs were made at 150 m/sec at 45 degrees C, 200 m/sec at 45 degrees C, and 200 m/sec at 55 degrees C. The data from the calibration are presented in tables below.

Once acquired, a correlation of the calibration data was developed. It was found that the orientation of the flow velocity could be related to the hot-film sensor voltage squared such that: $\cos(45+\alpha)/\cos(45-\alpha)$; $\alpha f(V_1^2/V_2^2)$ This is shown schematically in Figure 4-A.

TEST

The probe was then mounted in the TRF. The orientation of the probe is shown in Figure 3. The test that was run was done in the Turbine Research Facility. The Test lasted about two and one half to three seconds. The test was done to find the flow angle. The hot wire probe was inserted into the flow at 55 degrees. The test results from the two sensors are shown in Figure 6-A. By applying the calibration correlation, the flow angle was calculated over the run period. From the start to the end of the test period (relatively constant condition) the flow varied from 51-62 degrees.

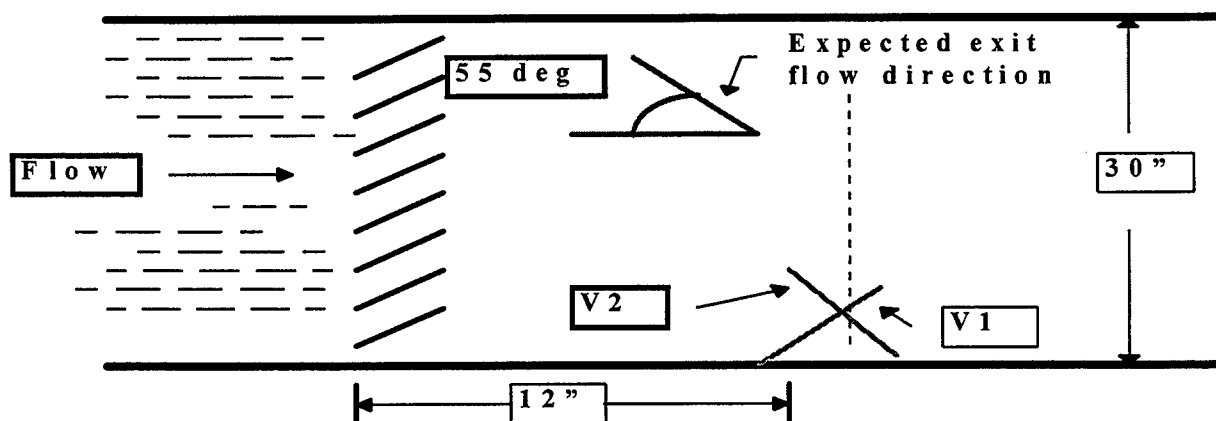


Figure 4. In side of the test chamber

Conclusion

The test was successful in measuring the flow angle at the facility's downstream measurement station. It was found that the flow varied from 51 to 62 degrees over the test period. These results are similar to what we had predicted so that the existing probe orientations were confirmed. In addition, a correlation between the flow angle and the square of the ratio of the sensor voltages was developed. This correlation can be used in future TRF tests to measure the flow angle. One recommendation would be to repeat the test and probe calibration to provide greater confidence in the calibration and test results.

APPENDIX A

V1 (Volts)	V2 (Volts)	Angle (deg)	Pt (Psi)	Ps (Psi)	Temp in (deg) C	Velocity (m/sec)
5.397	4.901	14.9	16.27	14.9	45.71	152.5
5.365	5.017	18.9	16.24	14.9	45.59	151.4
5.326	5.078	22.8	16.24	14.9	45.61	151.6
5.282	5.173	27.9	16.25	14.9	45.58	151.9
5.266	5.259	32.3	16.25	14.9	45.6	151.8
5.266	5.351	37	16.22	14.9	45.48	151.1
5.268	5.403	40.6	16.22	14.9	45.41	150.7
5.291	5.439	44.8	16.22	14.9	45.83	150.8
5.287	5.448	45	16.22	14.9	45.63	151
5.291	5.451	45.1	16.22	14.9	45.38	150.6
5.277	5.473	49.1	16.21	14.9	45.77	150.7
5.242	5.498	52.6	16.21	14.9	45.75	150.4
5.185	5.524	57.1	16.23	14.9	45.76	151.4
5.146	5.528	59.2	16.22	14.9	45.82	150.9

Table 1-A. Calibration. 150 m/sec at 45 degrees C

V1 (Volts)	V2 (Volts)	Angle (deg)	Pt (Psi)	Ps (Psi)	Temp in (deg) C	Velocity (m/sec)y
5.855	5.176	-0.4	17.92	14.29	45.55	200.3
5.821	5.178	0	17.91	14.29	46.11	200.3
5.687	5.484	25.2	17.97	14.29	45.77	201.4
5.637	5.554	29.3	17.91	14.29	45.76	200.1
5.623	5.654	33.6	17.9	14.29	45.76	199.9
5.623	5.743	38.1	17.91	14.29	45.61	200.1
5.655	5.813	42.3	17.92	14.29	45.65	200.4
5.647	5.823	44.7	17.86	14.29	46.14	199
5.661	5.827	44.8	17.86	14.29	45.5	198.9
5.658	5.824	44.8	17.87	14.29	45.83	199.2
5.656	5.839	48.9	17.86	14.29	45.97	199
5.618	5.879	52.7	17.91	14.29	45.95	200.6
5.555	5.874	56.5	17.9	14.29	46.06	199.8
5.501	5.882	59	17.87	14.29	45.99	199

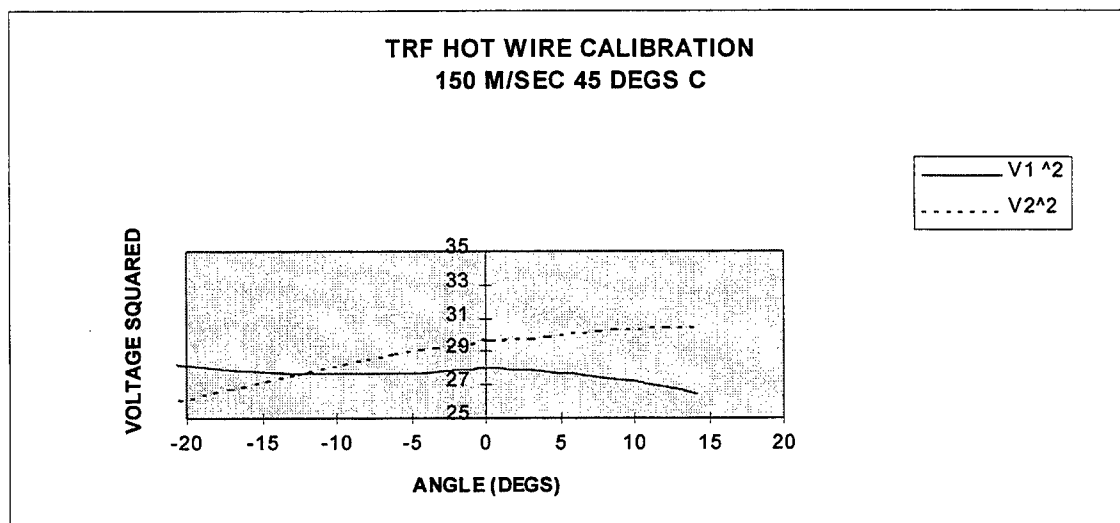
Table 2-A. Calibration. 200 m/sec at 45 degrees C

V1 (Volts)	V2 (Volts)	Angle (deg)	Pt (Psi)	Ps (Psi)	Temp. in (deg) C	Velocity (m/sec)
5.774	5.147	0	18.08	14.29	54.46	208.4
5.75	5.097	0.1	18.08	14.29	56.74	207.6
5.6	5.39	24.7	18.07	14.29	56.28	207.2
5.558	5.463	29	18.07	14.29	55.98	207.2
5.546	5.565	33.6	18.08	14.29	55.85	207.3
5.564	5.643	36.5	18.11	14.29	55.57	208.1
5.585	5.701	40.7	18.03	14.29	55.35	206
5.578	5.746	44.8	18.08	14.29	56.33	207.4
5.618	5.756	45.1	18.05	14.29	54.9	206.1
5.588	5.733	45.1	18.04	14.29	56.66	206.5
5.567	5.759	48.3	18.04	14.29	56.47	206.6
5.51	5.771	52.6	18.01	14.29	56.61	206
5.461	5.776	55.8	18.01	14.29	56.71	205.8
5.415	5.795	58.7	18.07	14.29	56.74	207.5

Table 3-A. Calibration. 200 m/sec at 55 degrees C

(Angle)- 45	V1 ^2	V2^2	(Angle)- 45	V1 ^2	V2 ^2
-30.1	29.12761	24.0198	-0.2	27.99468	29.58272
-26.1	28.78323	25.17029	0	27.95237	29.6807
-22.2	28.36628	25.78608	0.1	27.99468	29.7134
-17.1	27.89952	26.75993	4.1	27.84673	29.95373
-12.7	27.73076	27.65708	7.6	27.47856	30.228
-8	27.73076	28.6332	12.1	26.88423	30.51458
-4.4	27.75182	29.19241	14.2	26.48132	30.55878

Table 4-A. Data for figure 1 at 150 m/sec at 45 degrees



(Angle)- 45	V1 ^2	V2 ^2	(Angle)-45	V1 ^2	V2 ^2
-45.4	34.28103	26.79098	-0.3	31.88861	33.90733
-45	33.88404	26.81168	-0.2	32.04692	33.95393
-19.8	32.34197	30.07426	-0.2	32.01296	33.91898
-15.7	31.77577	30.84692	3.9	31.99034	34.09392
-11.4	31.61813	31.96772	7.7	31.56192	34.56264
-6.9	31.61813	32.98205	11.5	30.85803	34.50388
-2.7	31.97903	33.79097	14	30.261	34.59792

Table 5-A. Data for figure, 200 m/sec at 45 degrees C

TRF HOT WIRE CALIBRATION
200 M/SEC 45 DEGS C

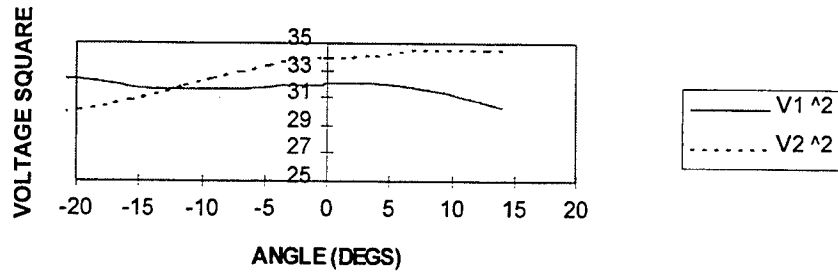


Figure 2-A. Calibration at 200 m/sec at 45 degrees C

(Angle)-45	V1 ^2	V2 ^2	(Angle)-45	V1 ^2	V2 ^2
-45	33.33908	26.49161	-0.2	31.11408	33.01652
-44.9	33.0625	25.97941	0.1	31.56192	33.13154
-20.3	31.36	29.0521	0.1	31.22574	32.86729
-16	30.89136	29.84437	3.3	30.99149	33.16608
-11.4	30.75812	30.96923	7.6	30.3601	33.30444
-8.5	30.9581	31.84345	10.8	29.82252	33.36218
-4.3	31.19223	32.5014	13.7	29.32223	33.58203

Table 6-A Calibration data for 200 m/sec at 55 degrees C

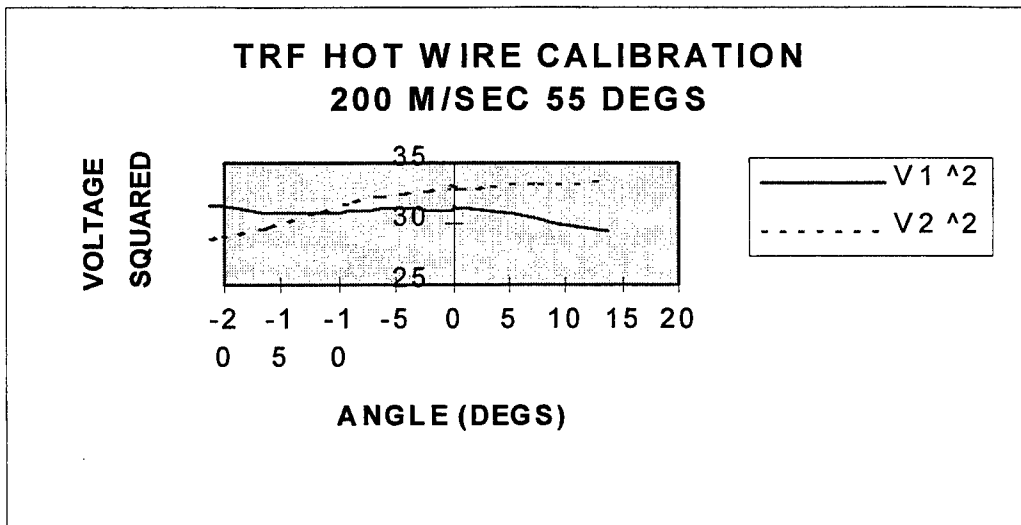


Figure 3-A. Calibration at 200 m/sec and 55 degrees

In the second plot that was done, was dealing with the proportion V_1^2 / V_2^2 and $\cos(45+H) / \cos(45-H)$ -

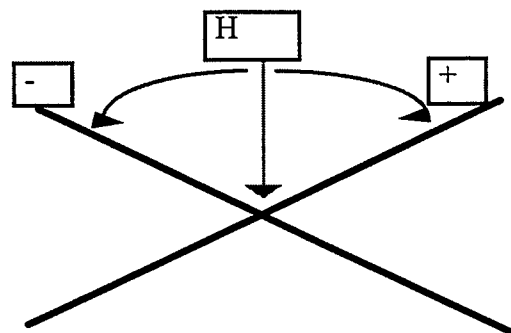


Figure 4-A. Shows the circulation is independent of the total temperature and velocity.

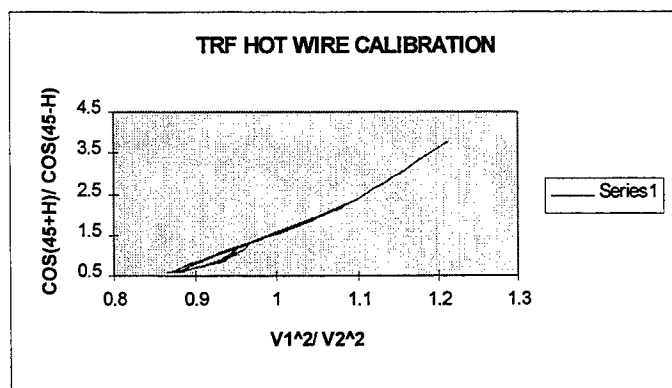


Figure 5-A Plot of $V1^2/V2^2$ vs. $\cos(45+H)/\cos(45-H)$

All three of the calibration curves collapse to a single correlation of the flow angle vs. the square of the hot film voltage.

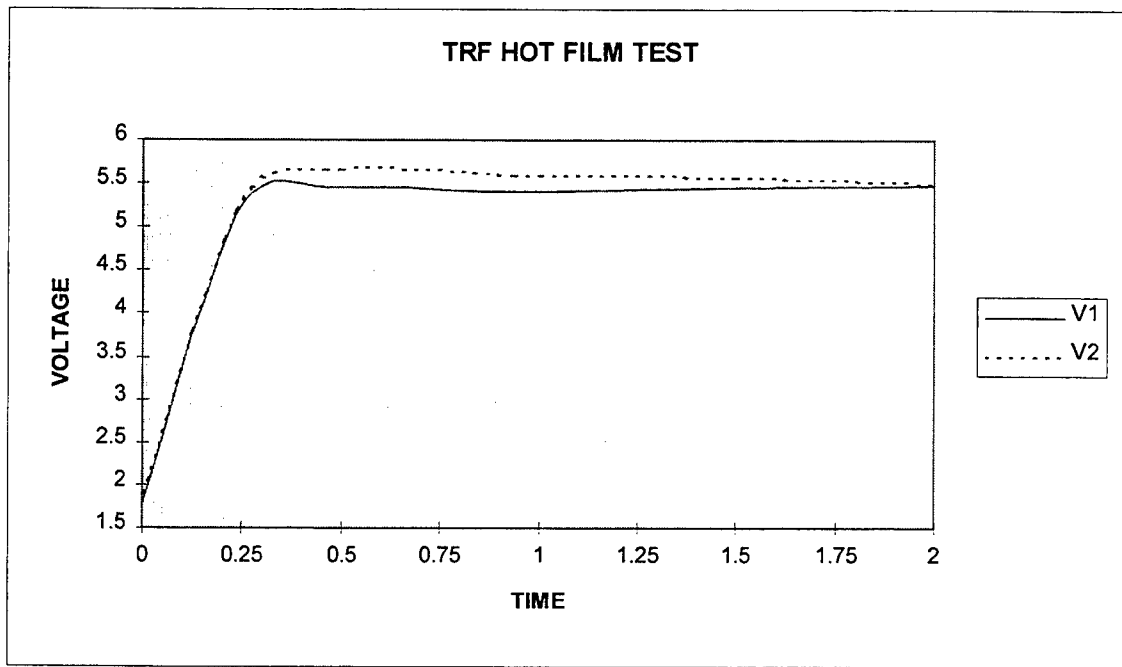
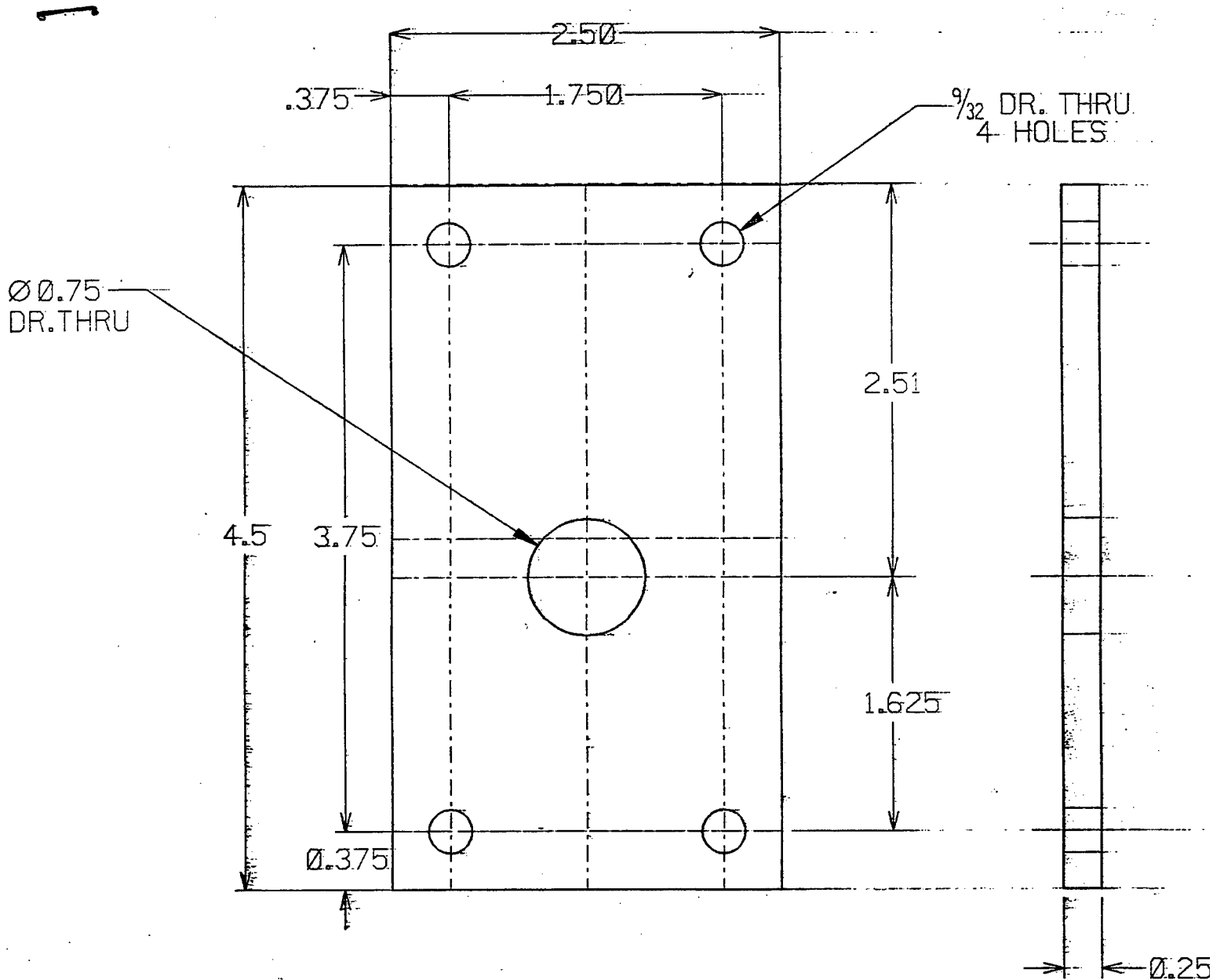


Figure 6-A. Time vs. Voltage of test data



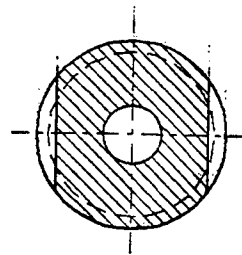
DESIGN #2

N.T.S.

13-15

Figure 7

NOTE:
PLEASE SEE SKETCH
FOR DISCREPANCIES.
DRAWING *NOT* FINISHED.
INCLUDED FOR CLARITY.



#1 DESIGNED

1
2
3
4

13-16.

APPENDIX B

Table 1-B. Probe Balancing Procedures

Rear panel:

- I. Select bridge, "std." for this application
- II. Set time constant switch to "OFF"
- III. Set signal conditioner input to "NIT" and coupling switch to "DC"
- IV. Connect output cable to "Bridge Voltage"
- V. Connect input cable to probe support holder

Front Panel

- I. Connect probe holder with shorting probe
- II. Select channel number
 - A. Touch "CHANNEL"
 - B. Touch channel holder
- III. Measure cable plus holder resistance
 - A. Press "RES MES"
 - B. Null the meter reading with the "OPERATE RES" control
 1. If display is (-), turn clockwise
 2. If display is (+), turn counter-clockwise
 - C. Press "RES MES" and display cable plus holder resistance
 - D. Enter cable plus holder resistance into memory for automatic compensation to subsequent measurements
 1. Press "CABLE RES"
 2. Press "CLEAR"
 3. Touch number panel for value of cable plus holder resistance just measured

4. Press "ENTER"

IV. Set designated probe resistance

A. Replace shorting probe with hot wire

B. Press "OPERATE RES" touch panel

C. Adjust value on display with "OPERATE RES" control knob to the desired operating resistance supplied by the manufactures

VI. Set system to run

VII. Tune frequency response

A. press "BRIDGE COMP" touch panel

B. Adjust "BRIDGE COMP" control knob until display reads 250 since the probe that is being used is a film that is 1240-60 (If the probe was not a -60 film then the setting would be obtained from **Table 1**.

<u>Wire:</u>	<u>Setting:</u>	<u>Film</u>	<u>Setting:</u>
-T1.5	35	-A10	70
-P2	83	-10	70
-P12.5	115	-20	115
-P15	120	-60	250

Table 2-B. Settings for hot wire and films

C. Press "RUN"

	V1	V2
Cable Plus Holder Resistance	.418	.414
Probe Resistance	5.21	5.25
Operating Resistance	7.71	7.86

Table 3-B. Data form balancing the probe.

**TOXICITY OF AQUEOUS FILM FORMING
FOAM REPLACEMENTS
TO MICROORGANISMS AND
FRESHWATER FISH**

Zackary W. Fordham

**Rutherford High School
1000 School Avenue
Lynn Haven, FL 32404**

**Final Report for:
High School Apprentice Program
Wright Laboratory**

**Sponsored by:
Air Force Office of Scientific Research
Bolling Air Force Base, DC**

and

**Wright Laboratory
FIVCF
Tyndall AFB, FL**

August 1995

TOXICITY OF AQUEOUS FILM FORMING
FOAM REPLACEMENTS
TO MICROORGANISMS AND
FRESHWATER FISH

Zackary W. Fordham
Rutherford High School

Abstract

The toxicity of Aqueous Film Forming Foam (AFFF) replacement agents were tested on both bacteria and freshwater fish. AFFF and many of its substitutes contain chemicals and surfactants which mainly threaten Waste Water Treatment Plants (WWTP) and the environment. The first test employed Polytox, a brand of commercial bacteria which strongly emulate those found in WWTP. Ten agents were subjected to the PolyTox test and their toxicity was measured by recording the biological oxygen demand. The second test involved exposing freshwater fish to various concentrations of different agents. The mortality rate in each test chamber indicated the toxicity of each agent.

TOXICITY OF AFFF REPLACEMENTS TO MICROORGANISMS AND FRESHWATER FISH

Zackary W. Fordham

Introduction

Due to today's rising awareness of the environment and its fragile balance there has been a considerable shift toward safe, responsible action in the use of any chemical. One of the most effective tools in firefighting is Aqueous Film-Forming Foam (AFFF). Though this is an accepted and successful product there is still room for improvement in regards to toxicity and biodegradability. There have been numerous attempts by both government and private industries to manufacture an AFFF replacement agent with safer environmental impact characteristics. The effectiveness of these newly developed products range from insignificant to highly promising. However, very few products can surpass both the firefighting efficiency and safety standards of AFFF. By analyzing newly developed foams it is possible to separate the high potential solutions from those which are less favorable. This research project investigated the toxicological effects of alternate foaming agents on both bacteria and freshwater fish in order to discover a promising AFFF replacement.

Methodology

A. WWTP Bacterial Inhibition The first test utilized a commercial brand of bacteria, called PolyTox, to determine the toxicity of ten agents to WWTP bacteria. An agent was first diluted to a 3% concentration and then mixed with the PolyTox in a Biological Oxygen Demand bottle. Over a period of 21 minutes a Dissolved Oxygen (DO) reading was recorded every two minutes and also at 19 & 21 minutes. After all readings had been taken, calculations were performed which defined the toxicity of the agent.

B. Aquatic Toxicity The second test is a short-term, acute, static, range-finding toxicity test using the common Goldfish, *Carassius auratus*, to ascertain a concentration range which is fatal to aquatic vertebrates. Due to time constraints of establishing a healthy population source only two agents were tested. The standard lab setup consisted of 48 fish divided into 12 test chambers. Eight tanks contained concentrations of an agent

at .3%, .03%, .003%, and .0003%. Two tanks were set aside as controls, and the last two tanks held regular AFFF at .3% and .03% concentrations. DO and pH readings were recorded and adjusted at 2 hrs, 4 hrs, 24 hrs, and 48 hrs after the initiation of the test.

Result

Of the Freshwater toxicity test the most difficult aspect was stabilizing the holding tanks in order to obtain a health testing population. Because of this delay there was only enough time to do two tests. Agent I and Agent G were chosen to be analyzed because of the vast differences in their elemental makeup. Agent I is a very biodegradable foam which uses many hydro-carbons. Agent G is also a biodegradable foam which uses more fluoro-carbons and proteins. By analyzing these two we hoped to find the safest combination. In this investigation Agent I proved to be 100% fatal at a .4% or .04% concentration. At .004% and .0004% there was a slight toxic effect. Agent G had a mild toxicity with a 50% mortality at .3% concentration. Concentrations of .03%, .003%, and .0003% had no noticeable effects on the fish population.

See Table 1

PolyTox Bacterial Toxicity Test Results:

See Figures 1-10

LEVEL OF MINIMUM TOXICITY

Table 1

AGENT CONCENTRATION

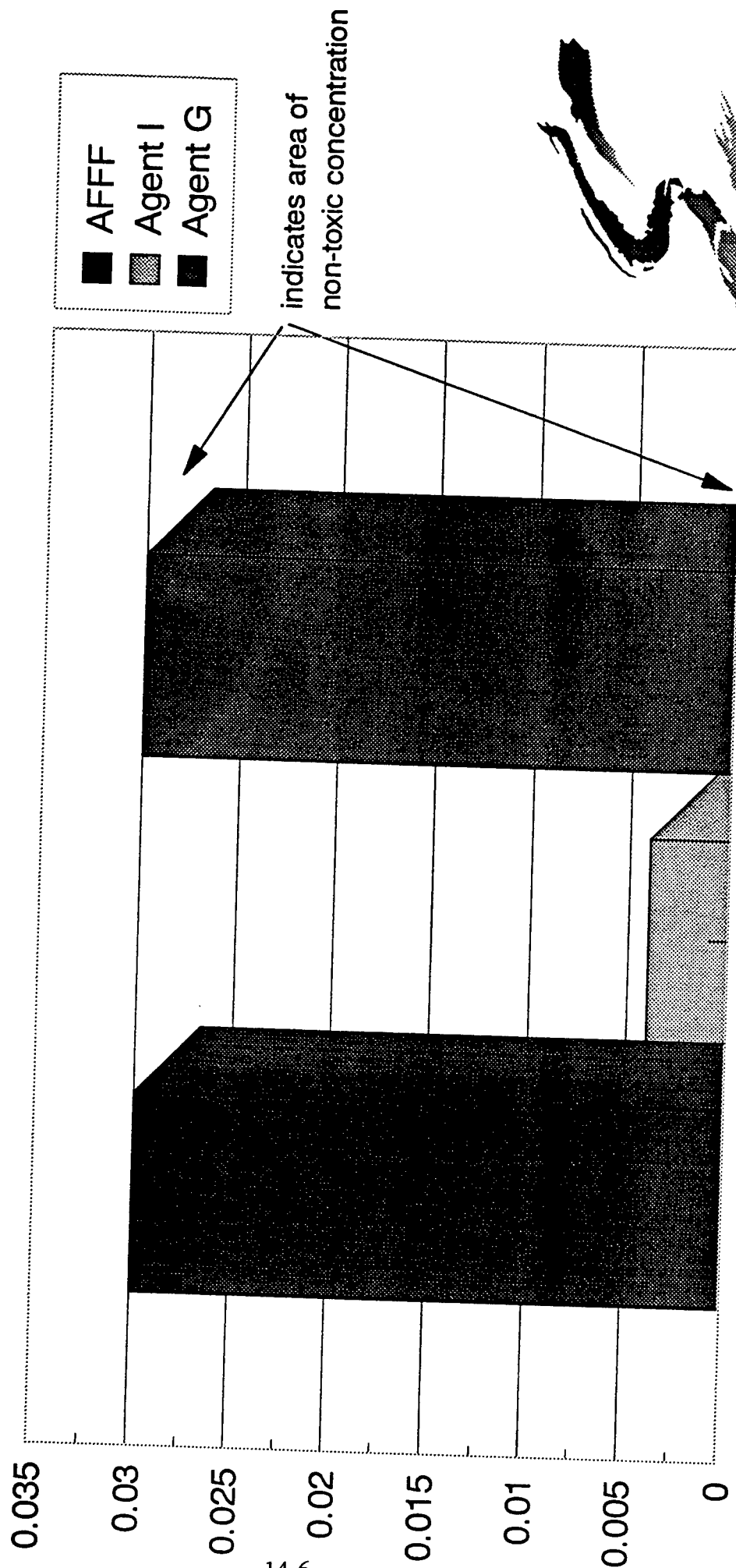


Fig.1: PolyTox 7-10-95 AFFF 1&2

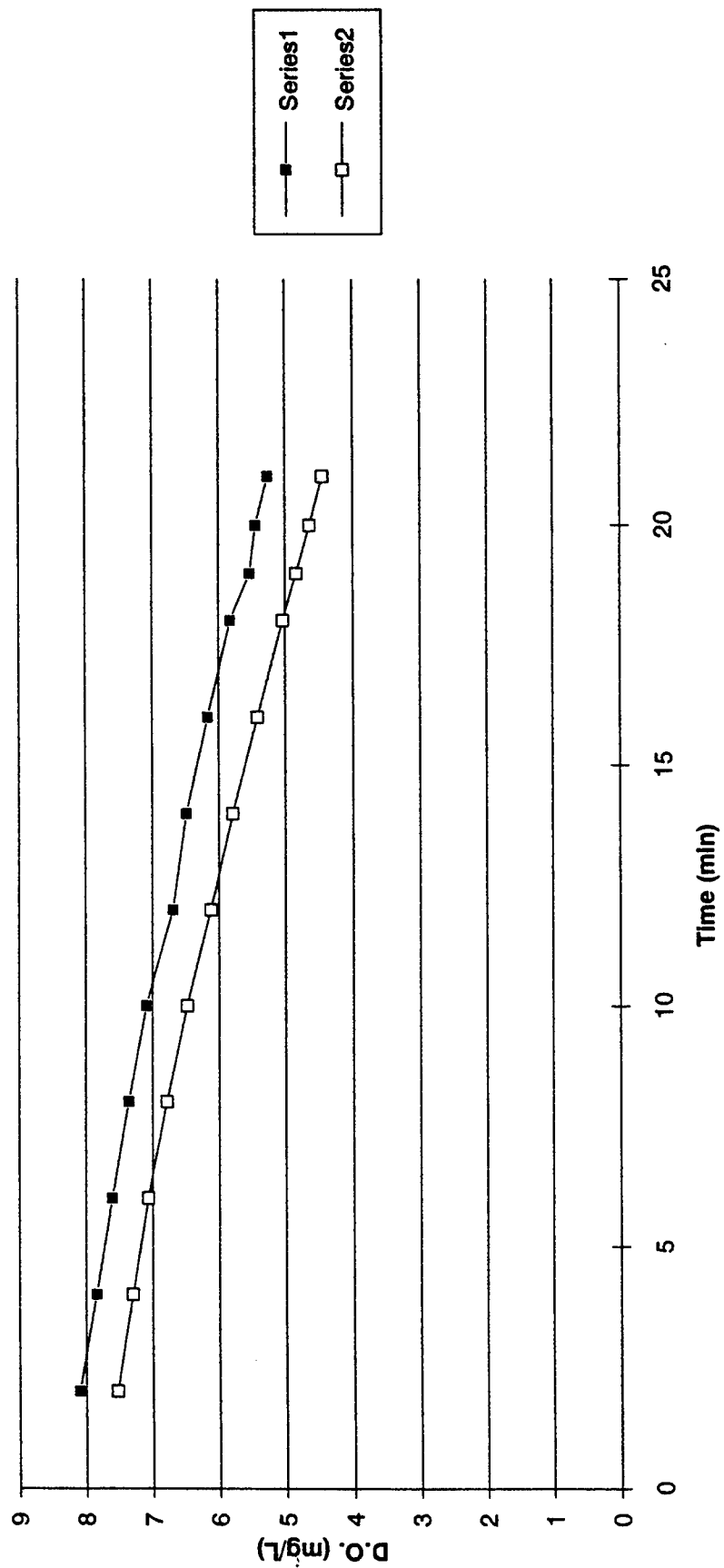


Fig.2: PolyTox 7-12-95 Agent A

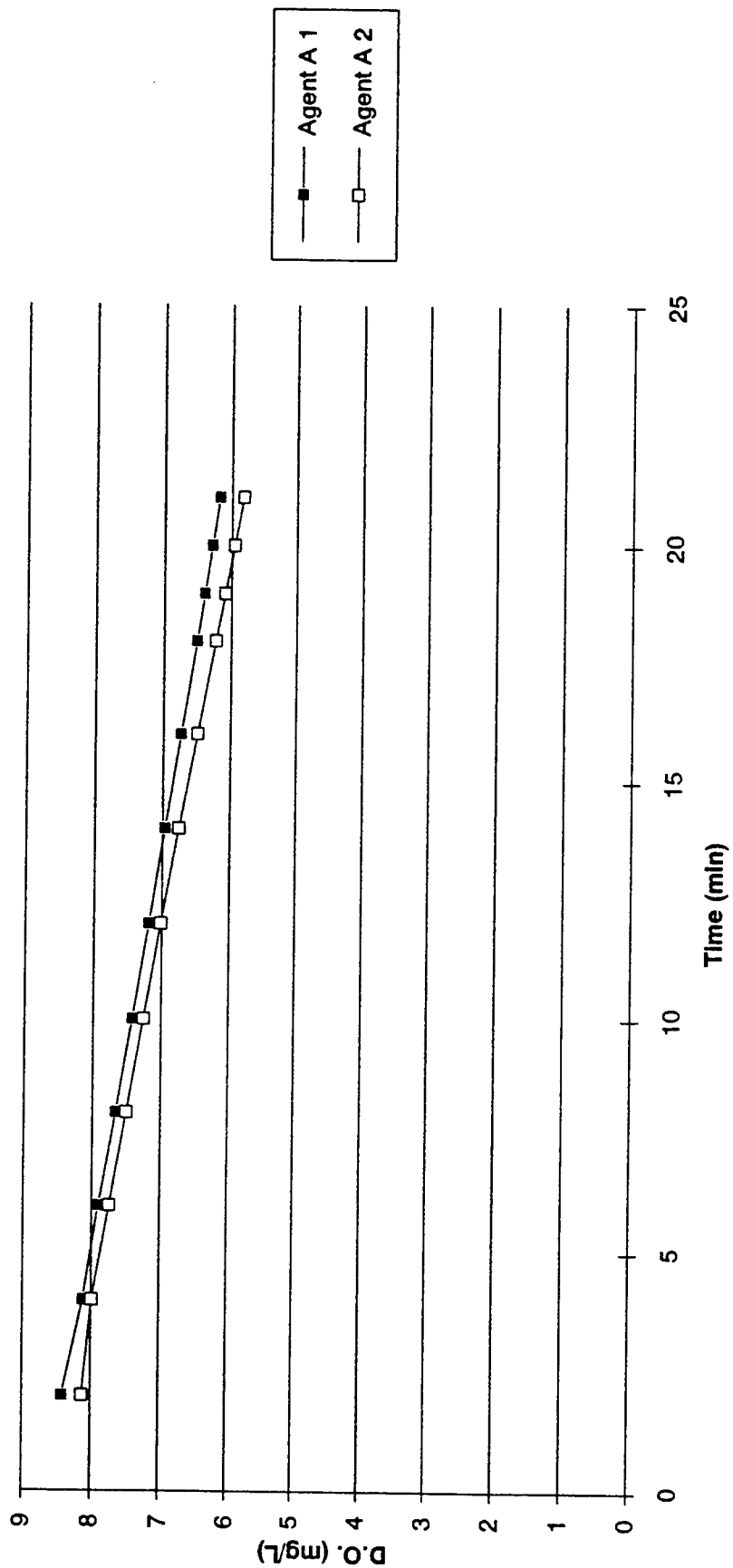


Fig.3: PolyTox 7-12-95 Agent B

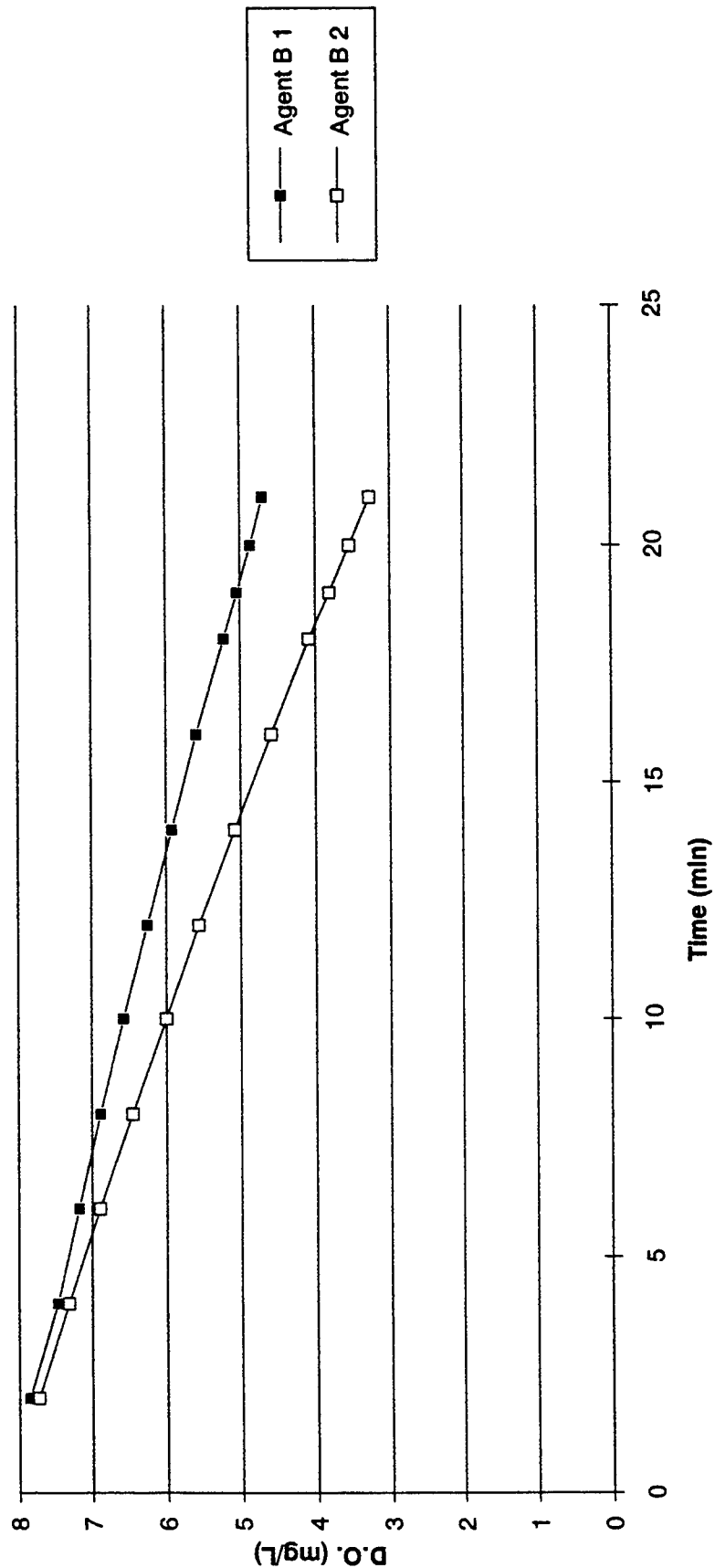


Fig.4: PolyTox 7-29-95 Agent C

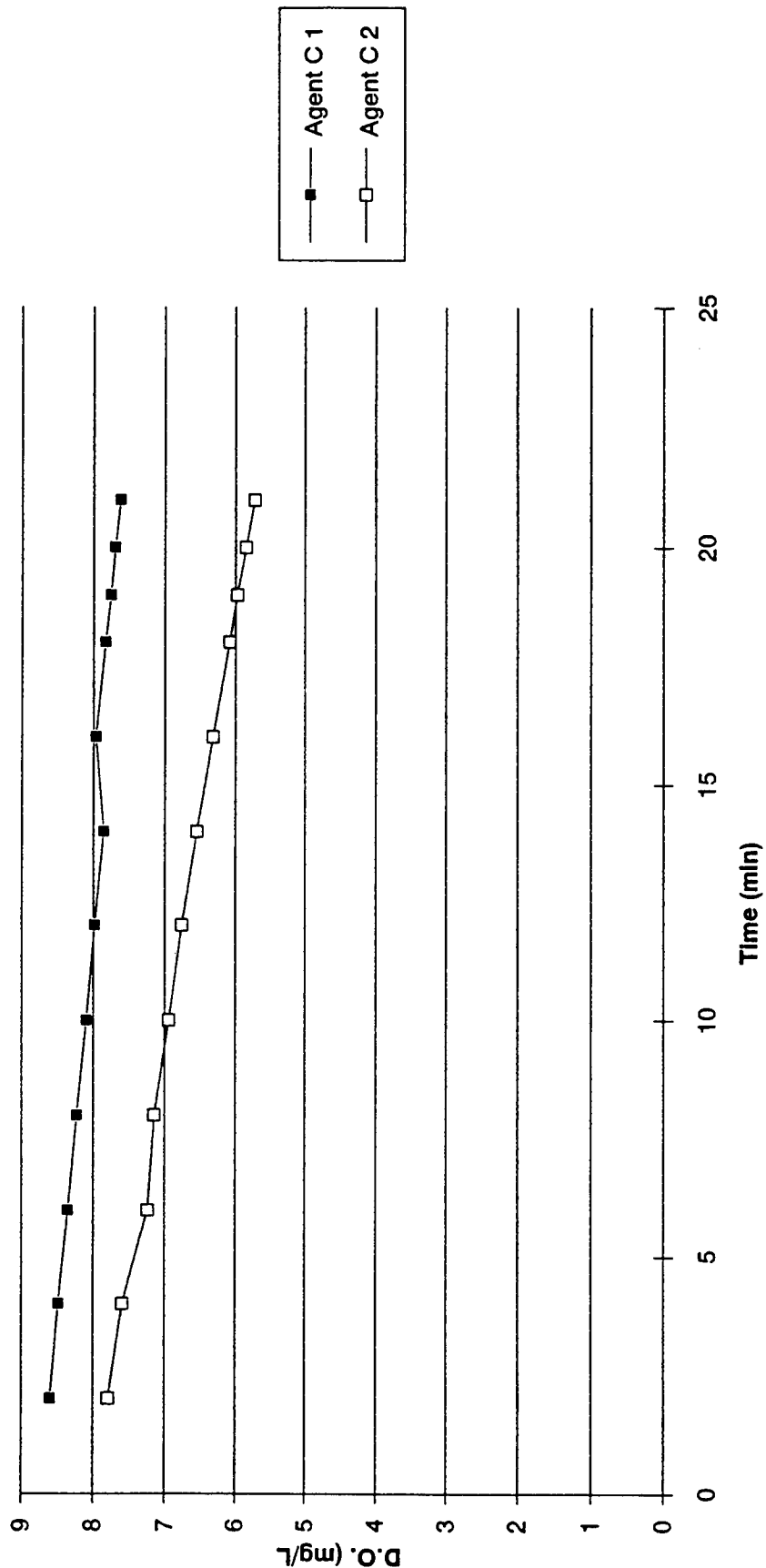


Fig.5: PolyTox 7-29-95 Agent D

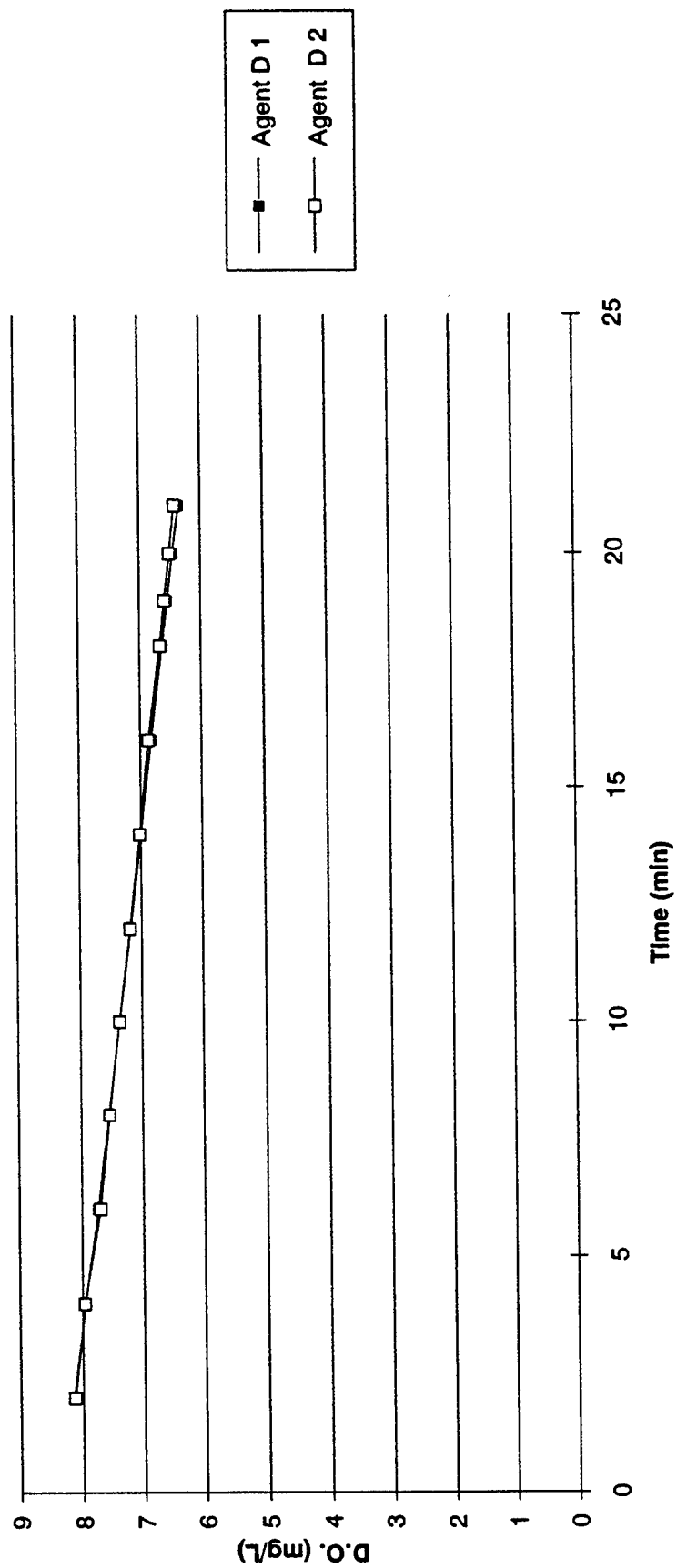


Fig.6: PolyTox 7-31-95 Agent E

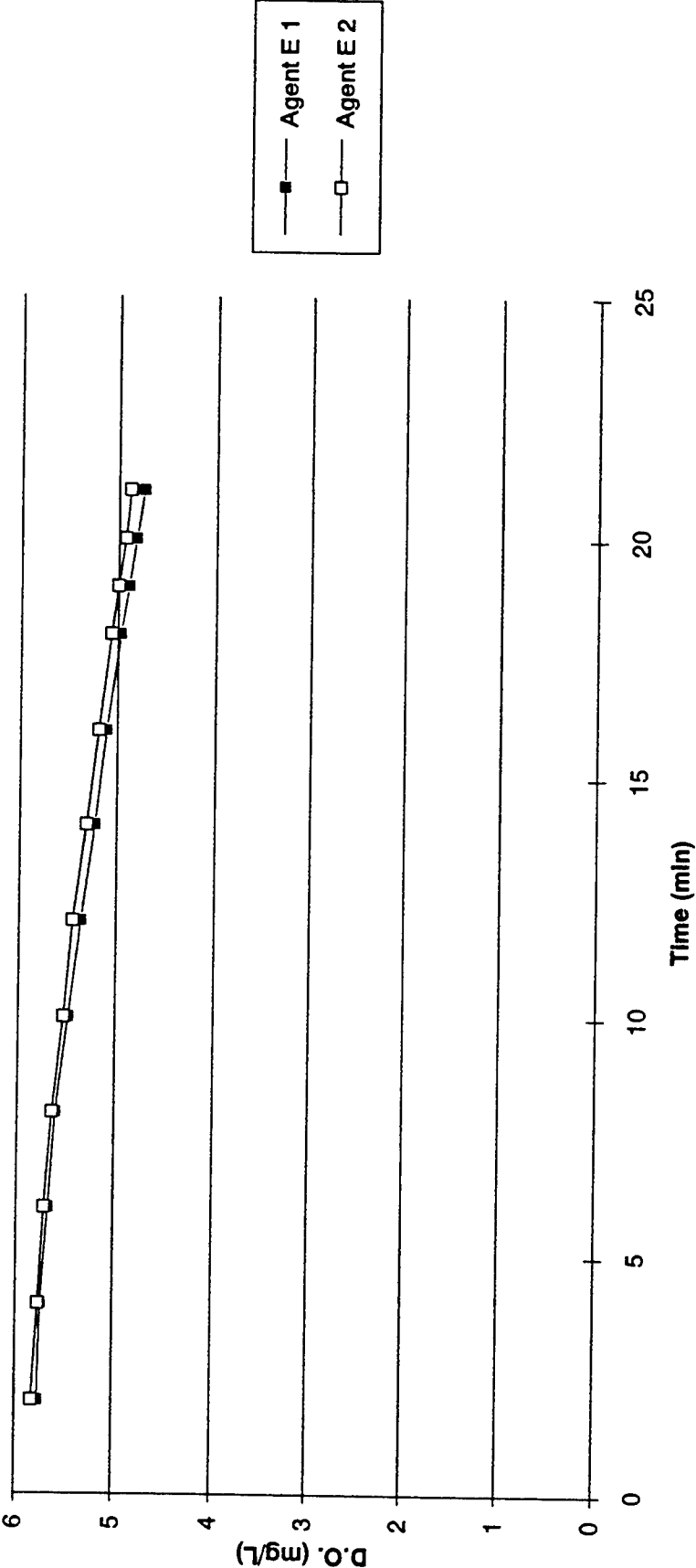


Fig.7: PolyTox 7-31-95 Agent F

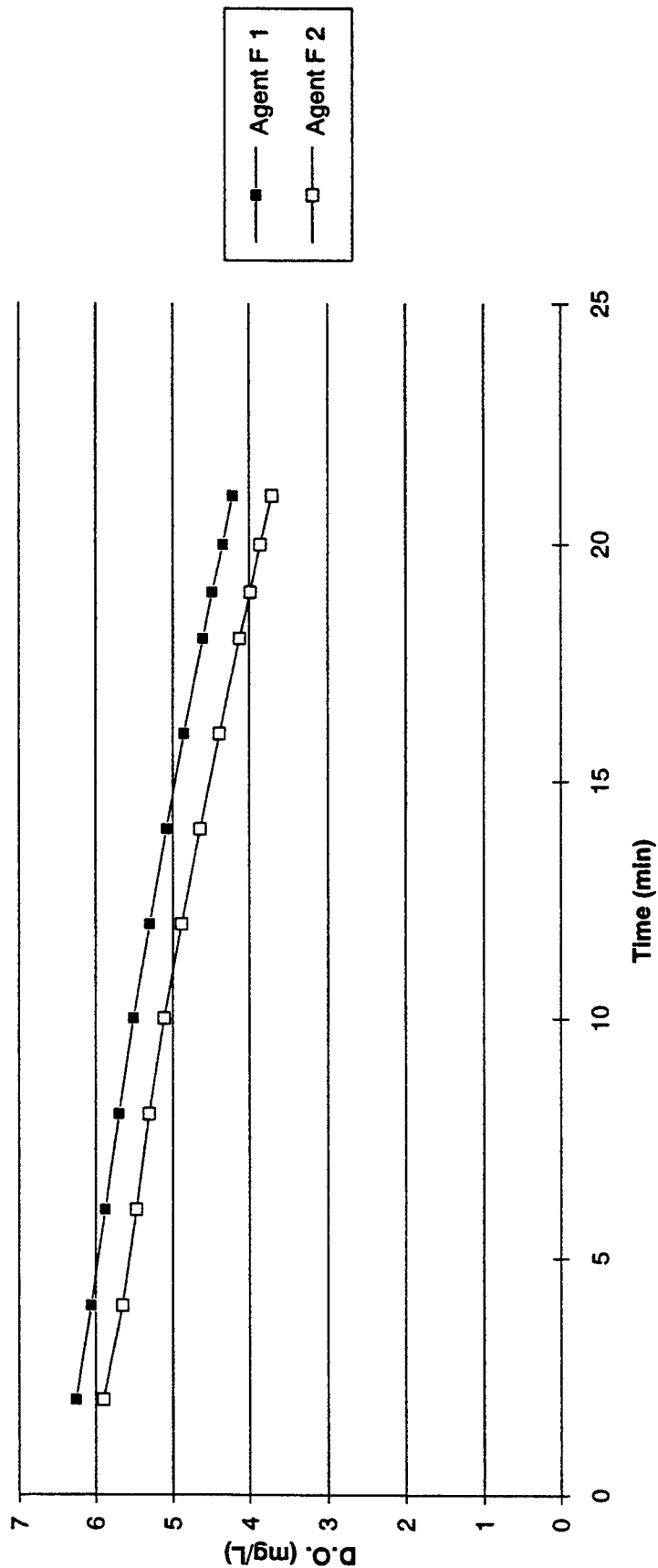


Fig.8: PolyTox 7-31-95 Agent G

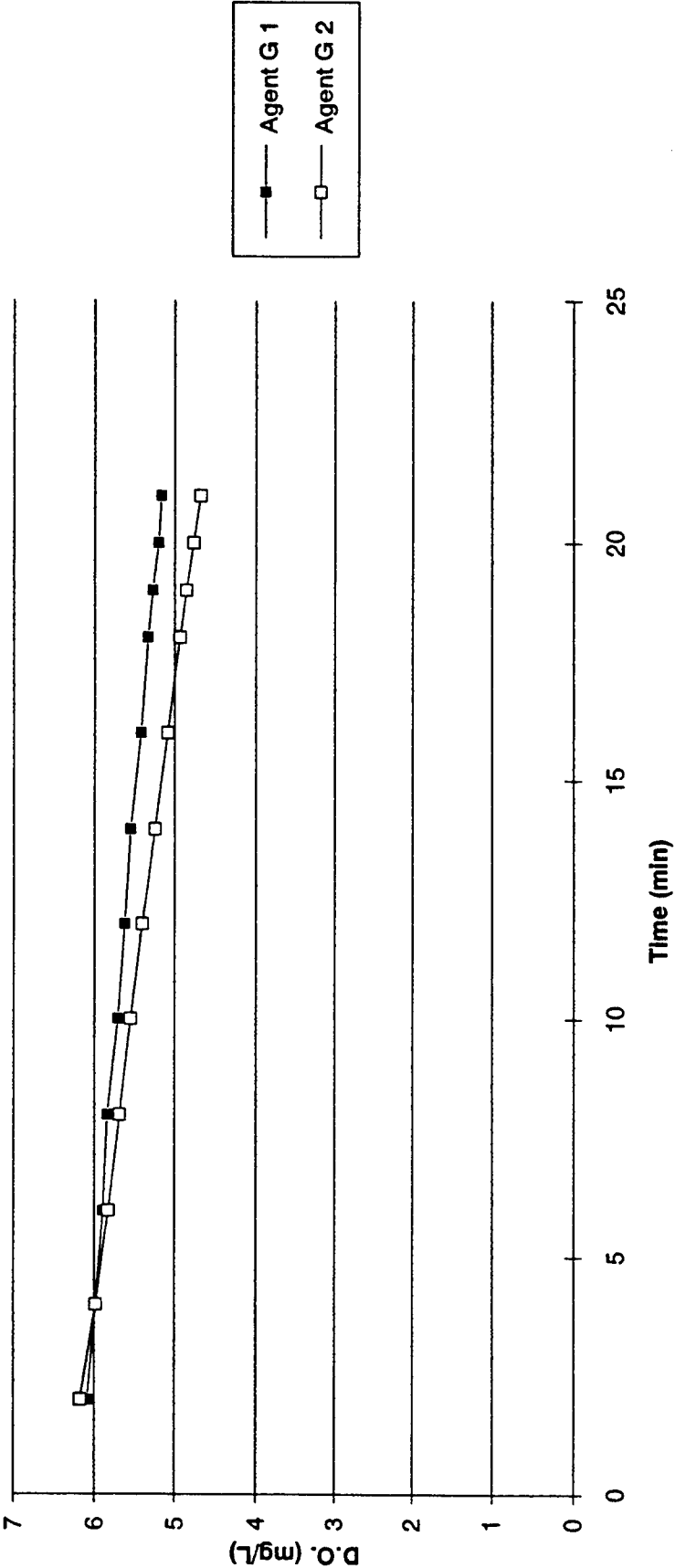


Fig.9: PolyTox 7-31-95 Agent H

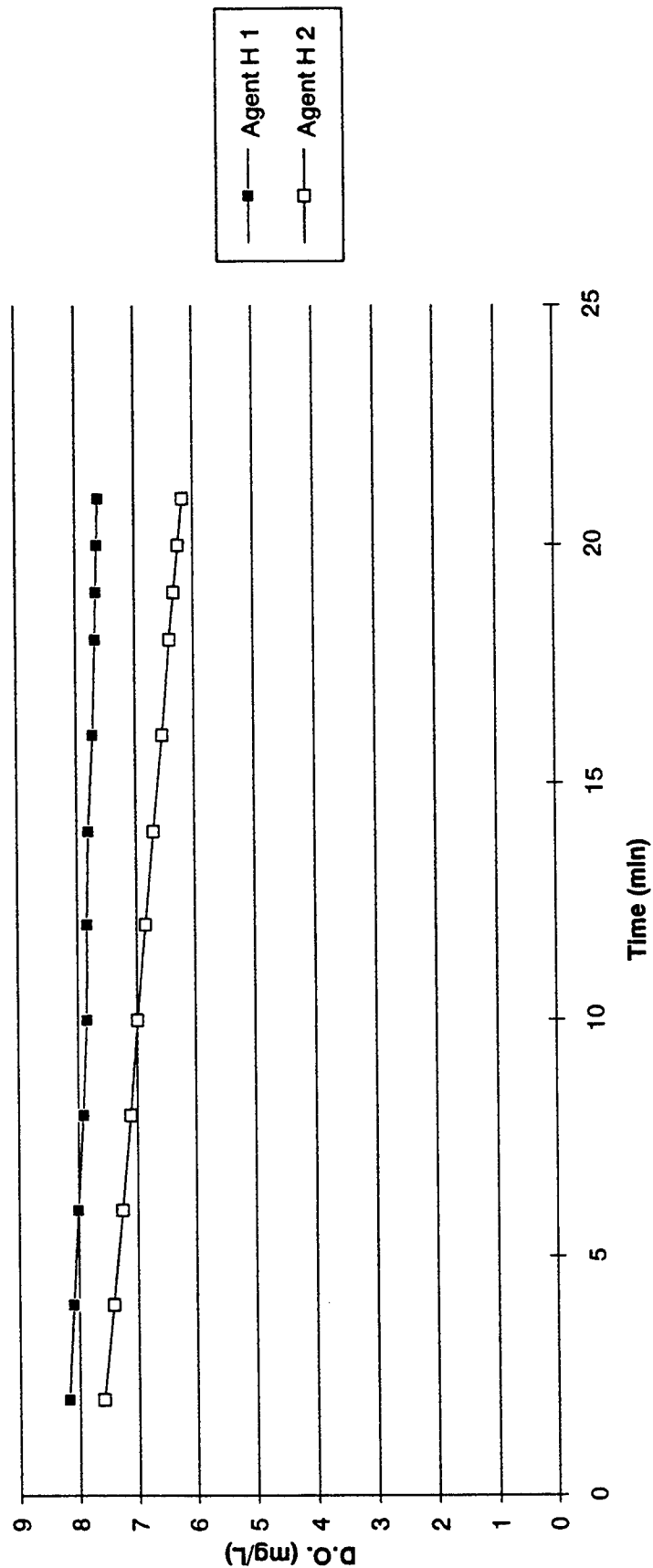
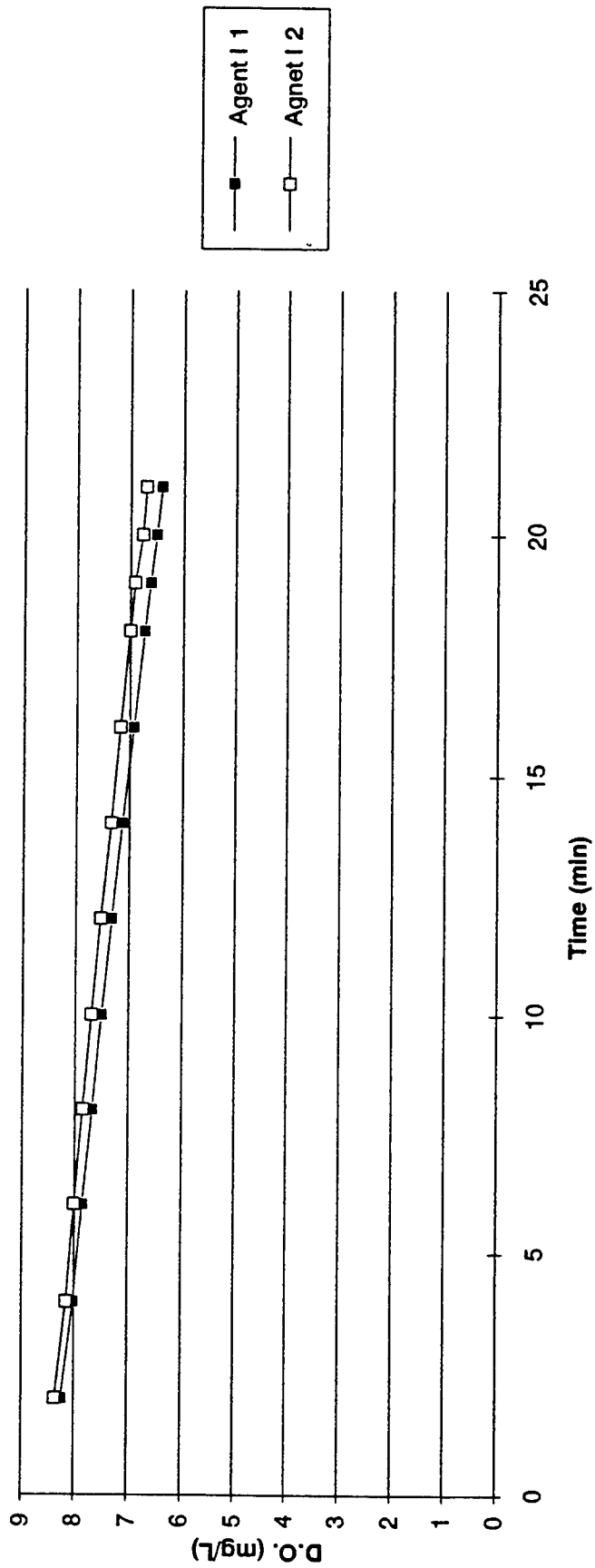


Fig.10: PolyTox 8-1-95 Agent I



Conclusion

Of the ten agents tested by PolyTox, Agent's B and G, the fluoro-protein foams, proved to be the least toxic. The hypothesis that hydrocarbon foams are more toxic than fluoro-protein foams was proved correct. Agent B and G were also much less toxic to WWTP bacteria than any of the other foams which used hydrocarbons in their solutions. Surprisingly, AFFF, whose main component are fluoro-carbons surfactants was found to have a low toxicity that surpassed the hydrocarbon foams. These results were also analogous with the freshwater toxicity test results. Agent I (a hydrocarbon foam) proved to be much more lethal than Agent G (a fluoro-carbon foam) or AFFF. However, Agent G was very similar to AFFF's toxicity level.

References

- Andrews, RC. 92. *The Environmental Impact of Firefighting Foam*. Industrial Fire Safety 1(1):26-31
- Andrews, RC. 92. *The Environmental Impact of Firefighting Foam Concentrations; Contemporary Management Considerations for the Chief Fire Executive; Strategic Analysis of Fire Prevention Programs*. ADF617 941.
- Ansul Co. 77. *Final Report: Environmentally Improved AFFF*. ADA 050 508
- Ansul. *Technical Bulletin: Environmental Impact of Ansulite AFFF Products*. fish toxicity, biodegradability, sewage treatment plant treatability, nutrient loading
- DiMaio, LR, RF Lange. 84. *Effect of Water Quality on Fire Fighting Foam*. Plant/Operations Progress 3(1):42-46
- Peterson, HB. 79. *Improved Environmental Properties of AFFF*. ADF 610 001. Rpt Number ESL-TR-79-12
- Office of Research and Development, U.S. Environmental Protection Agency. *Methods for Measuring the acute Toxicity of Effluents and Receiving Waters to Freshwater and Marine Organisms Fourth Edition*. August 1993. EPA/600/4-90/027
- Astm, *Standard Guide for Conducting Acute Toxicity Tests with Fishes, Macroinvertebrates, and Amphibians*. May 1989. E 729-88a
- PolyBac, PolyTox: *Toxicity Testing*. Courtney Place, 3894 Courtney Street, Bethlehem, PA 18017-89999.

SUMMER RESEARCH AT WRIGHT-PATTERSON
AIR FORCE BASE:
DELAMINATION IN GRAPHITE/EPOXY PLATES
CAUSED BY LOW-VELOCITY IMPACT

Craig M. Fortner

Thomas Worthington High School
300 W. Granville Road
Worthington, OH 43085

Final Report for:
High School Apprenticeship Program
Wright Laboratory

Sponsored by:
Air Force Office of Scientific Research
Bolling Air Force Base
and
Wright Laboratory

September 1995

DELAMINATION IN GRAPHITE/EPOXY PLATES
CAUSED BY LOW-VELOCITY IMPACT

Table of Contents

	Page
Title Page	
Abstract	i
Table of Contents	ii
I. Introduction	1
II. Cataloging References	2
A. Introduction	2
B. Discussion and Methodology	2
III. Scanning Graphite/Epoxy Plates	2
A. Introduction	3
B. Discussion	3
C. Methodology	3
IV. Bonding of Thermoplastics	
A. Introduction	4
B. Discussion	4
C. Methodology	4
V. Creating a Homepage	
A. Introduction	5
B. Discussion and Methodology	5
VI. Conclusions	6

DELAMINATION IN GRAPHITE/EPOXY PLATES
CAUSED BY LOW-VELOCITY IMPACT

Craig M. Fortner
Thomas Worthington High School

Abstract

The research program sponsored by the Air Force Office of Scientific research included several projects and activities instead of the normal singular project. The goals this summer included assisting Bryan Foos with research for both his Ph.D. from the Ohio State University and his work for the Nondestructive Evaluation Branch of the Materials Laboratory at Wright-Patterson Air Force Base. One of the main projects was ultrasonic scanning of graphite/epoxy plate for delamination at each layer. An instruction manual was later written for the ultrasonic scanning tank. Other projects included mounting and testing strain gages, bonding thermoplastics, cataloging references for Mr. Foos' dissertation, and creating a homepage on the Internet.

DELAMINATION IN GRAPHITE/EPOXY PLATES CAUSED BY LOW-VELOCITY IMPACT

Craig M. Fortner

I. Introduction

Bryan Foos introduced the various projects he hoped to accomplish over the summer on the first day. The first assignment was to catalog all of the references used by Mr. Foos in dissertation. These references included journal articles, book sections, and technical reports to name a few. The references were entered into a database which could automatically search the entries for keywords. By cataloging all of the references, Mr. Foos now has a functional list of all of the sources he currently has in his possession.

Another project involved scanning graphite/epoxy plates for delamination caused by low-velocity impact. Mr. Foos impacted seven inch by seven inch graphite/epoxy plates using a drop tower apparatus prior to my arrival this summer. By scanning the plates with pulse wave ultrasonic technology, Mr. Foos' conclusion that damage in the plates increases in plies farther away from the point of impact was verified. The scans generated color readouts which were manipulated to show several layers of delamination at one time. The concluding aspect of the project was the co-writing of an instruction manual for the large ultrasonic tank. The manual provided detailed instructions for scanning Mr. Foos' samples as well as a starting point for scanning other materials.

A third project called for the bonding of three different types of thermoplastics. Bonding methods with methylene chloride for Lexan, Ultem, and Cycloc were explored. The purpose of the experiments was to draw a conclusion on which method of bonding produced a bond suitable for testing. After a suitable bond was created, strain gages were mounted on the samples to gather data from future testing.

The final project was to create a homepage for the Internet. With the assistance of two other students, a homepage was created for Mr. Foos describing his work on his dissertation and at the lab.

Completing the page required learning Hypertext Markup Language (HTML) and getting information on various Internet servers and browsers.

Nearly all of this summer's work involved work on computers. The experience will certainly be invaluable in the coming years, as Macintosh, IBM, and UNIX-based workstations were used extensively. The experience of working in a chemistry lab and mounting strain gages will also certainly be valuable as well.

II. Cataloging References

A. Introduction

Mr. Foos' dissertation references were organized but not documented upon arrival this summer. By cataloging all 1400+ references, Mr. Foos now has an accurate record of all those sources in his possession.

B. Discussion and Methodology

In order to manage Mr. Foos' large quantity of references, End Note Plus was used on the Macintosh. The application is set up perfectly for Mr. Foos' purpose. Each source was entered along with the other required information for a reference. The application created a master list by author, and by clicking on the source, the remaining vital information opened in a new window. Perhaps the most valuable aspect of the database is its search capabilities. Keyword searches can be initiated in specific fields or all fields at once. The data entered for Mr. Foos will certainly be a great help when sources need to be located or referred to in official documents.

III. Scanning Graphite/Epoxy Plates

A. Introduction

Seven inch by seven inch graphite/epoxy plates were scanned from the top and the bottom to show the progression of damage in each ply caused by low velocity impact. Mr. Foos use the data and color printouts at a conference in San Francisco this November.

B. Discussion

The scanning tank setup included a main scanning body and data collection system from California Data Systems and a LeCroy digitizer. The tank was operated automatically by a UNIX-based workstation. When the sample is set up to be scanned, the workstation tells the scanner what to scan, the area to be scanned, resolution, etc. The scanner uses pulse wave ultrasonics to detect delamination at each level. This is an invaluable testing method for Mr. Foos. His studies involve delamination through the thickness of the plate, and any other testing method would either destroy the sample or give readouts only from the surface. By scanning both the front and back surfaces, Mr. Foos can get a clear picture of how the damage spreads through the plate. Consistent with his theory, the area of delamination increases as the plies get farther away from the point of impact. Another interesting observation is that the area of delamination in each ply resembles a peanut in shape. Surrounding plies have "peanut" delaminations with opposite orientation.

C. Methodology

Setting up the scan properly is a long and technical process. The plate must first be submerged in the ultrasonic tank, then the signal emitted from the sample must be located on the oscilloscope. The signal from the sample shows the front and back surface in an area where no delamination is present. In an area where there is delamination, the front surface and the delamination show up on the oscilloscope. Next, the parameters for the scan must be set. The final step is setting up the software. This is a step-by-step system run by the workstation. When all of the sections of the tank are set up properly, the scan can be started.

An interactive color map appears as the scan progresses. A much more detailed walkthrough was written for Mr. Foos and the rest of the Nondestructive Evaluation Branch.

IV. Bonding of Thermoplastics

A. Introduction

Experiments were conducted to study bonding methods of Lexan, Ultem, and Cyclic. The samples were to be studied by other members of the branch in the future. Three different methods of bonding were tried.

B. Discussion

The three types of thermoplastics were all dissolved by methylene chloride. Since methylene chloride evaporates extremely rapidly, it serves as a suitable bonding agent for the plastics. Completed samples were to have strain gages mounted on them for data collection purposes. Unfortunately, none of the bonding processes proved conclusive enough to begin bonding the samples at the required volume. Each method had one major flaw.

C. Methodology

The first method tried was to simply pour methylene chloride into a metal pan under a fume hood. Both samples were pressed into the chemical and then clamped together under even pressure. The resulting bond was very strong and even. This method produced the best bonds, but it was extremely wasteful. The methylene chloride evaporated almost instantly. Enough of the chemical had to be poured onto the pan to afford the time required to dip the samples. Usually the amount of chemical used for each bonded sample was around 20 mL of solvent.

The next method involved replacing the metal pan with a sponge. Methylene chloride was poured onto the sponge, and the process of pressing and clamping was repeated. The results of this method were uneven coating of the sample and very weak bonds. As a result, this method was ruled out for any further tests.

The third and final method of bonding tested involved using a piece of felt in the place of the metal pan. When the samples were pressed onto the methylene chloride soaked felt, they stuck just enough to leave felt fibers imbedded in the plastic. This, combined with an uneven coating and a relatively weak bond, caused the method to be disposed of as well.

V. Creating a Homepage

A. Introduction

Mr. Foos mentioned at the beginning of the summer that he would like to have his own homepage on the Internet describing his work at school and at the lab. The page was to be a model for other members of the branch if they wanted to create a page of their own.

B. Discussion and Methodology

Files put on the Internet are all created in Hypertext Markup Language (HTML). HTML is a non-case specific language, meaning that all computers understand the format. Numerous help files and walkthroughs were downloaded from the Internet for reference. Since HTML was new to everybody in the branch, much time was spent learning the language and appropriate "tags." Creating a homepage also required working knowledge of Internet browsers such as Netscape, Mosaic, and Fetch. By collaborating with two other students, a very impressive page was created for Mr. Foos. Others in the branch were nothing short of amazed by what we had accomplished.

VI. Conclusions

As a summer apprentice under Mr. Foos, I had quite a wonderful experience. I absorbed such a broad spectrum of knowledge, that I actually felt like I belonged in the branch. I learned what it is like to have a normal work week and what kind of stress it involves. I quickly learned to adjust to the work load and operation of the base which will certainly be valuable in the future. As a whole, the experience this summer was wonderful. I encountered a whole new world of independence and responsibility which I otherwise may have not experienced for years to come. In conclusion, my experiences will certainly aid me in my growth as a person and as a student.

**INPUT/OUTPUT CONTROL
OF THE
IEEE 488 BUS PERIPHERALS**

Laura E. Fouts

**Dayton Christian High School
505 Homewood Avenue
Dayton, Ohio 45405**

**Final Report for:
High School Apprenticeship Program
Wright Laboratory**

Sponsored by:

**Air Force Office of Scientific Research
Bolling Air Force Base, DC**

and

Wright Laboratory

August 1995

INPUT/OUTPUT CONTROL OF THE IEEE 488 BUS PERIPHERALS

Laura E. Fouts
Dayton Christian High School

Abstract

An IEEE 488 interface program was written to control a High Temperature Device Measurement System and a dual channel signal analyzer. The program was developed using Turbo Pascal. Data measurements were obtained from these two devices using the IEEE 488 bus interface. These data measurements involved a micro-electro-mechanical (MEMS) differential accelerometer, and SiC devices.

Equipment and Instrumentation

The IEEE 488 bus is a card that sends commands to devices connected to it. When it acts as a file, it receives a commands and interprets them. Similarly, it can receive data and interpret it to send to the computer as a text file. Two types of measurement systems were controlled by the IEEE 488, the High Temperature device Measurement System, and the Dual Channel Signal Analyzer.

The High Temperature Device Measurement System (HTDMS) uses an external program to control it. This particular program is written in Turbo Pascal. The HTDMS measures two to three terminal devices up to 475 degrees Celsius. Currently, it can measure bipolar, FET, and TLM measurements. Other measurement capabilities can be added if desired.

The Dual Channel Signal Analyzer displays input from two accelerometers. The accelerometer picks up accelerations along one axis(i.e., horizontal or vertical). It then sends the analog signals to the analyzer.

Operation

With the installment of the IEEE 488 bus, several devices were able to be controlled by the computer, thanks to a program written in Turbo Pascal. The program was adapted from the standard Pascal premises listed in the IEEE 488 bus card user manual. It was used specifically for the dual channel signal analyzer. It allowed for the computer to display results after testing on the analyzer. The set-up was a menu screen where the user could choose which function to use and or view. The program is easy to expand upon. New interface controls can easily be constructed to control new procedures. These procedures could be easily converted pre-windows Turbo Pascal programs; such as, the HTDMS program.

On the next page, four windows from the control program for the IEEE 488 bus are shown. The first window is the main menu and offers all the necessary basic options for operating the IEEE 488 bus. Next, a secondary window provides options for controlling the analyzer. The next two windows are: the main menu (again)and a help menu. The help menu box provides a brief description for each command. This assists the user in choosing the correct command. Finally, there is a little window box stating that Todd Stockert developed the program and the help system.

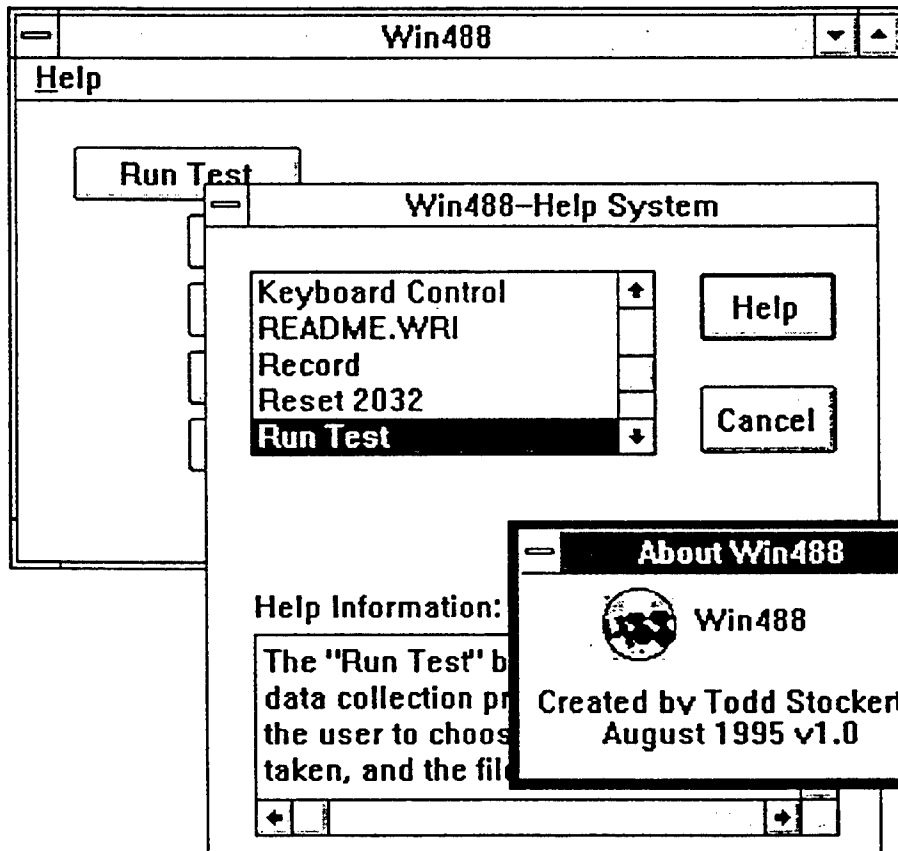
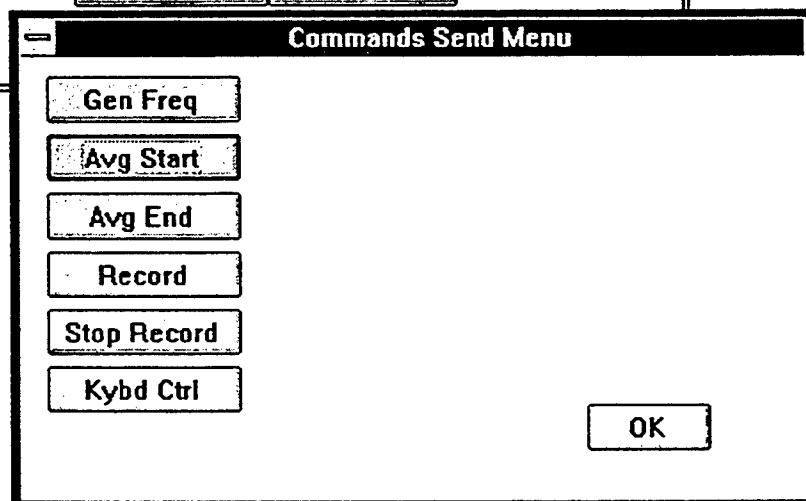
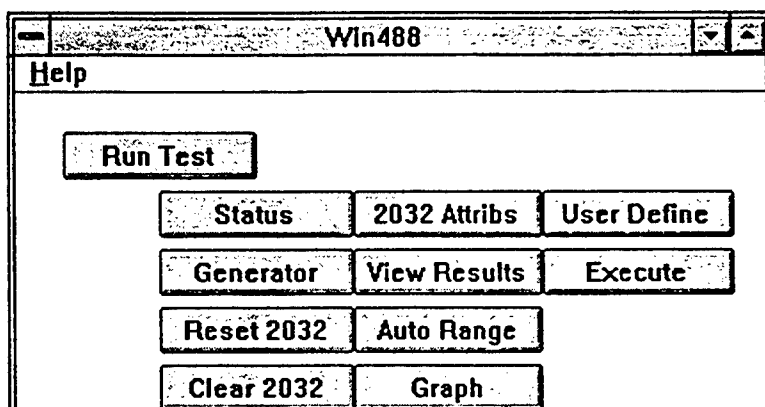


Table 1. Unit Programs Controlling HTDMS

UNIT NAME	FUNCTION OF UNIT
Bipfunc.Pas	Unit for bipolar functions; controls the measurements, collector voltage/current as well as oven temp. base emitter voltage/base current
Fetfunc.Pas	Allows for the entering of different values i.e.: diode start/stop voltage, number of voltage steps, min./max. vertical display, and more
Genfunc.Pas	Unit gives seven menu options allowing user to choose the function for operation; also controls setting the oven temp. and set point temp.
Comfunc.Pas	This initializes the IEEE 488 bus, and translates a command from the keyboard to a format that is compatible with the bus
Gpfunc.Pas	The Gpfunc.Pas unit allows for the entering of a voltage that all of the channels on the oven can use.
Psfunc.Pas	This Psfunc.Pas unit creates a plot file for the data obtained from the measurements taken from the heat oven .
Crtfunc.Pas	Uses For statements to control oven; also uses If/Then statements which allows for variations in the operation of the oven.
Ocomfunc.Pas	Shows user where an interruption in a signal is detected; states all procedures needed to finish testing and gives the final END of the program.

The HTDMS consists of many separate units to run one program. The units contained in the HTMEAS.PAS program are as follows: BIPFUNC.PAS, FETFUNC.PAS, GENFUNC.PAS, COMFUNC.PAS, GPFUNC.PAS, PSFUNC.PAS, CRTFUNC.PAS, and OCOMFUNC.PAS. The units all use CRT and DOS. Some also use OCOM, GPFUNC, AUXINOUT, COMFUNC, CRTFUNC, PSFUNC, and GENFUNC. Each unit contributes its own vital information to the proper running of the HTDMS program. More time would have allowed full implementation of the HTDMS program into the architecture of the interface program. But because of the time constraints, we were not given the opportunity to work with the program fully.

Conclusions

Learning Turbo Pascal was quite a challenge. The book entitled Mastering Turbo Pascal 5.5 by Tom Swan was helpful in understanding how to operate the language correctly. Program writing can be time consuming if the person is just learning the language. Swan's book introduced the reader to the fundamentals of programming in Turbo Pascal. Gaining the background information needed, the reader is then given practice problems. After a week and a half of studying this book and its problems, the focus of my studies was somewhat shifted.

Schaum's Book of Basic Circuit Analysis became another text book. In this discussion of circuitry and electricity, the reader is taught the formulas, definitions, and structure of circuits needed to succeed. Problems were given at the end of each chapter. The answers were provided so that the reader could check his answer to the correct one. Discussion of volts, amperes, and ohms were also included so that the reader could properly figure out the problems. A problem arises for the reader however, if he has not taken calculus or physics. The best thing for that person to do is to attempt to accomplish the problems as best as possible considering his or her lack of knowledge on these two subjects. I know because I am one of these people.

Working with computer programs, the dual channel signal analyzer, and an accelerometer have opened up new opportunities. These things allow for many new discoveries and tests to be ran on signals and countless other things.

The project, being the challenge that it was, has become something I will not forget. Stretching the brain to learn new concepts became an everyday occurrence. Hopefully some of this knowledge I will retain for future reference and use.

A STUDY OF SUBSTITUTED GLUCOPYRANOSE USING SINGLE POINT
CALCULATIONS WITH AM1 GEOMETRIES

Alfredo J. Garcia

Carroll High School
4524 Linden Ave.
Dayton, OH 45432

Final Report for:
High School Apprentice Program
Wright Laboratory

Sponsored by:

Air Force Office of Scientific Research
Bolling Air Force Base, DC

and

Wright Laboratory

August 1995

A STUDY OF SUBSTITUTED GLUCOPYRANOSE USING SINGLE POINT CALCULATIONS WITH AM1 GEOMETRIES

Alfredo J Garcia
Carroll High School

Abstract

The use of toxic de-icers costs the government large sums of valuable revenue. In hopes of reducing costs both financially and environmentally, this study was created to research the development of nontoxic de-icers through the process involved with the substitution of basic compounds onto a specific sugar. Glucopyranose was the target skeleton sugar in this study. The key to this research is in the comparison of $\log P$ of the variable compounds to the $\log P$ of present de-icers. The Ampac Solvent Package (Amsol) was employed to determine the $\log P$ value of the substituted molecule. Single point calculation parameters and AM1 geometries were the established limits set for the tests. Simple organic compounds were the substituent variables located at differing locations on the molecule. Experimental results show that there are possible candidates for the replacement of present de-icers, yet before these compounds can be established as replacements, more investigation of these candidates is required.

Introduction

In recent years, computational chemistry has been used more frequently to answer questions in molecular research. This is due to the increased comprehensive information that the combination of theoretical and actual research presents to its user. The government has many purposes for the application of this type of research. It can be used to explore the possibility of creating new substances from chemical de-icers to pharmaceutical products.

Most computational studies are done in gas-phase conditions where the experimental models provide accurate solvation free energies of specific solutes in water. The free energies can be used to calculate essential characteristics of the theoretical compounds. Because an accurate prediction can be made on the same attributes of the target compound, computational chemistry removes the guess work on new substance research.

Discussion of Problem

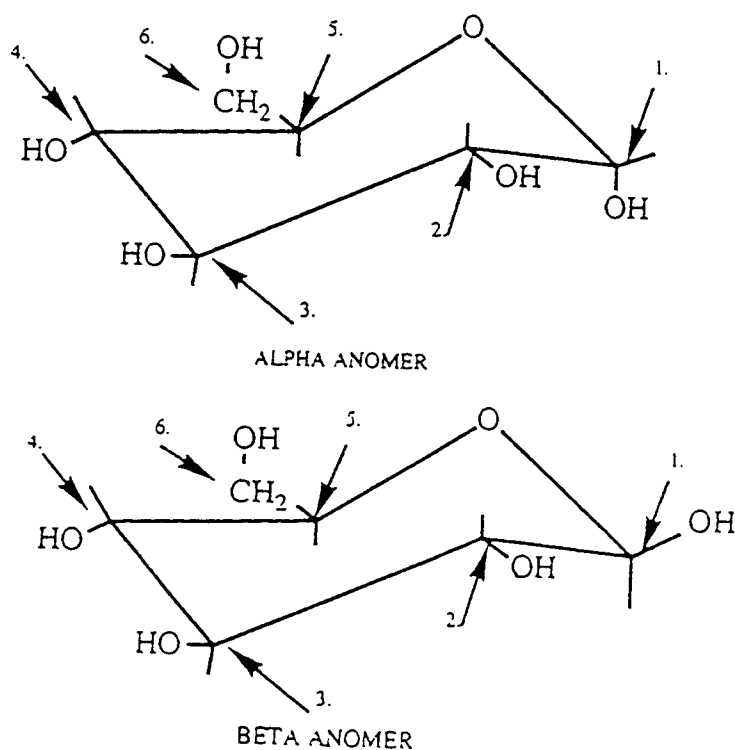
During winter months, fuel de-icers must be added to storage tanks to prevent the formation of ice in the fuel. Present de-icers are toxic and are extremely difficult to dispose of without the cost to the government and the environment. The feasible solution to this dilemma is the replacement of the current de-icers with nontoxic alternatives.

Methodology

Using the Amsol package, under single point and AM1 parameters, the experimentation

was run in solvents which were either polar or non-polar. Because extensive knowledge concerning hexadecane (hex) has been established by previous research, hex was used as the nonpolar solvent model in the experiment. Water was used as the polar solvent model. The tests had two water models the first abbreviated SRP and the later SRPnc (nc signifies the lack of C.O.G.s in this specific model). The alpha and beta anomers of glucopyranose were substituted at locations 1, 12, 13, 14, 16, 123, 124, 126, 134, 136, 146, 1234, 1236, 1246, and 1346. The substituents were either methyl, or phenyl.

Glucopyranose Models and Locations for Substitution



Results

After determining the log P value of each molecule, a comparison of the following log P values of present de-icing compounds was made. Those compounds were ethylene glycol monomethyl ether (egme) and propylene glycol monomethyl ether (pgme). The log P of egme was 1.264 and the log P of pgme was .945. To determine the log P, each Delta G of the hex models were divided by the corresponding Delta G of the SRP or SRPnc models.

Table 1. Methyl log P of the SRPnc Model

Location of Substitutions	Alpha Anomer	Beta Anomer
1	.53775	.43935
12	.63974	.58453
13	.67295	.59207
14	.63775	.68505
16	.67485	.54185
123	.94894	1.0308
124	.97207	1.0392
126	.79905	.76274
134	.88755	.76243
136	.80846	.69546
146	.63118	.77488
1234	1.4405	1.2480
1236	1.2986	1.1512
1346	1.3209	1.0692

Table 2. Methyl log P of the SRP Model

Location of Substitutions	Alpha Anomer	Beta Anomer
1	.59804	.50529
12	.74704	.70803
13	.83492	.70656
14	.78583	.69142
16	.77596	.65142
123	1.2503	1.1011
124	1.3047	1.1495
126	.95440	.93037
134	1.1685	.96949
136	.95692	.82281
146	.78148	.95743
1234	2.2386	1.8534
1236	1.8415	1.5373
1346	1.9520	1.4429

Table 3. Phenyl log P of the SRPnc Model

Location of Substitutions	Alpha Anomer	Beta Anomer
1	.676	.629
12	1.045	1.001
13	1.295	1.126
14	1.263	1.617
16	1.093	1.192
123	1.95	1.281
124	1.723	1.874
126	1.651	1.645
134	1.842	2.076
136	2.052	1.702
146	1.767	1.687
1234	2.392	3.143
1236	2.789	2.949
1246	2.413	2.416
1346	2.991	2.352

Table 4. Phenyl log P of the SRP Model

Location of Substitutions	Alpha Anomer	Beta Anomer
1	.756	.702
12	1.17	1.38
13	1.476	1.279
14	1.438	1.341
16	1.23	1.381
123	2.308	2.597
124	1.95	2.63
126	1.85	1.949
134	2.119	2.631
136	2.384	1.9602
146	2.064	2.002
1234	2.855	4.073
1236	3.271	3.763
1246	2.824	2.922
1346	3.609	2.86

Conclusions

In conclusion, the feasible replacement for present de-icers have higher log P values than those of present de-icing compounds. However, the log P values of the of these possible alternates must be greater than 1 or else the partition coefficient for the substance would not be high enough to act as suitable de-icer. Because the log P value is not a complete assessment of likely attributes for the potential alternates, it is essential that more testing on be run, specifically in determining the toxicity level of each theoretical compound

References

Giesen, David J.; Storer, Joey W.; Cramer Christopher J.; and Truhlar Donald G
J. Am Chem Soc. **1995**, *117*, 1057-1068

Krestov, G.A. *Thermodynamic of Solvation. Solution and Dissolution; Ions and Solvents Structure and Energetics*; Ellis Horwood: New York, NY, 1991

Still W.C.; Tempczyk A.; Hawley R.C. Hendrickson, T. *J. Am Chem Soc.* **1990**
112, 6127.

Lean Blow-Out Testing of Advanced Technology Combustors
for Aircraft Gas Turbine Engines Using a Variety of Liquid Fuels

Robert J. Glaser III

Carroll High School
4524 Linden Ave
Dayton, OH 45432

Final Report for:
High School Apprentice Program
Wright Laboratory

Sponsored by:
Air Force Office of Scientific Research
Bolling Air Force Base, DC

and

Wright Laboratory

August 1995

ABSTRACT

Lean blow-out experiments were conducted on an advanced research combustion system utilizing a variety of liquid fuels. An existing single nozzle research combustor representing the major features of the primary zone of an annular gas turbine combustor was operated at atmospheric pressures simulating engine high power level conditions. Airflow was delivered to the dome of the combustor and a separate controlled air delivery system supplied air to primary zone combustion jets located at 1/2 hydraulic diameter downstream of the combustor dome through 0.500-in diameter orifices. The airflow to the combustor dome was varied from 2.5 to 5.0 percent pressure drop. The airflow delivered to the side jets was kept at 30 percent of the airflow to the dome region. The fuel injector used was an advanced airblast atomizer using actual gas turbine engine hardware. Inlet air temperatures to the combustor were maintained at 500 deg F over a variety of airflows. Two liquid fuel types were used to study the evaporation effects of the fuel on combustion instability. The vaporization characteristics of the two fuel types along with the airflows through the combustor permitted a wide range of atomization characteristics to be studied. The data illustrates that improved atomization and evaporation does not always improve combustor stability.

INTRODUCTION

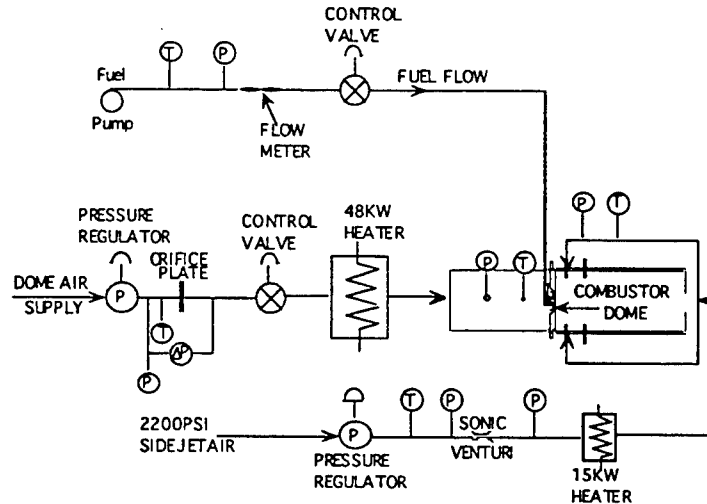
During development of combustors for industrial and aircraft gas turbine engines, the issue of adequate stability, or specifically lean blowout (LBO), margin is an important aspect in the design process. It is becoming increasingly more difficult to ensure that combustor designs have adequate stability margins concurrently with low emissions and high temperature rise. Achievement of flame stability over wide ranges of engine operating conditions is a function of the primary zone of the combustor; the flame structures established in the primary zone will also control the exhaust emissions. Many combustors use transverse air jets introduced through the liners to provide a nominal termination of the primary zone. The air jets supply some part of the total air necessary for complete combustion of the fuel. When aerodynamic preparation of a liquid fuel (airblast atomization) is used, extremely close coupling can exist between these transverse combustion air jets and the fuel/air jets (possibly swirling) issuing axially into the combustor from the fuel injectors. A detailed understanding of this jet-coupling is essential for a successful design that delivers low emissions while retaining adequate LBO margins. Extensive work looking at the LBO process using gaseous fuels has provided in depth insight of stability^{1,2,3}.

In 1987 the U.S. Air Force Wright Laboratory, Aero Propulsion and Power Directorate (WL/PO) Wright-Patterson Air Force Base, Ohio, established the Combustor Design Model Evaluation (CDME) program. This effort is a comprehensive joint Government, Industry and University research program aimed at improving the design and analysis capabilities for the combustors of aircraft gas turbine engines. Continuations of this program have one objective that is to establish the technology base needed to design and develop high heat-load gas turbine combustors that operate with high temperature rise. Since it can be argued that the technologies necessary to achieve high temperature rise (good fuel/air mixing and rapid chemical reaction rates) and low emissions are similar, complimentary investigations for these two design goals are possible. This does not imply that high temperature rise and broad low emissions capabilities can be achieved simultaneously, however. Investigations conducted by Shouse et al⁴ are sorting out the parameters that control the generation of emissions in the primary zone of current combustion systems.

RIG DESCRIPTION

The rig is mounted horizontally in a test cell of Wright Laboratories, Wright Patterson Air Force Base, Dayton Ohio. It supplies flow, metering and control of air and fuel for the rig, as well as air temperature to the combustor. A schematic of the various flows to the combustor is given in Figure 1. Compressor air is supplied to the dome region of the combustor passing through a pressure regulator then through an orifice plate for flow measurement. The dome air is then passed through a 48KW electric heater that utilizes a cascade control system to control the delivered air temperature to the rig at a constant 500 deg F. A separate air supply and control system is incorporated to deliver air to the primary combustion jets (side jets). The air is supplied by a 2200 psi trailer with the flow controlled by pressure and sonic venturis for flow measurement. The air is then passed through a 15KW electric heater before the air line is split to deliver air to the top and bottom primary combustion jet bosses. A thermocouple located in the liner jet boss provides temperature feedback to the heater controller. Pressure transducers connected to static pressure taps located in the dome and liner jet plenum provide a measure of the pressure drops across the dome and liners.

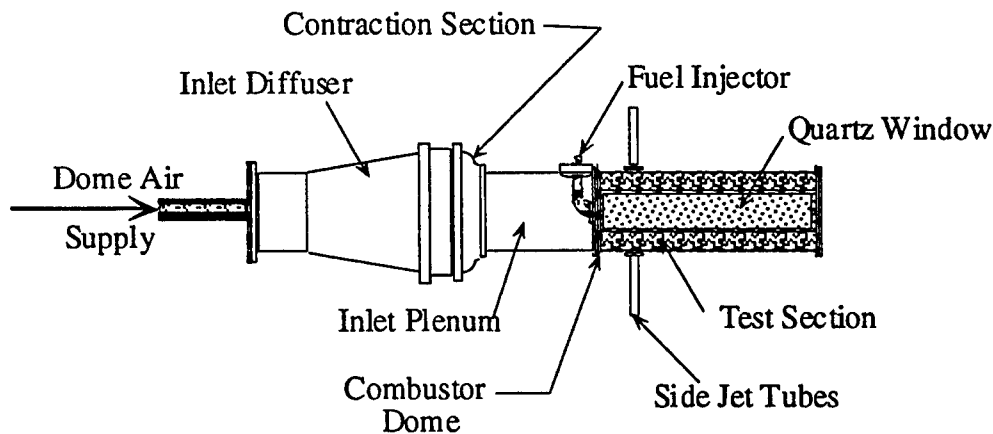
The liquid fuel is supplied to the test rig by a five gallon stainless steel vessel. The liquid fuel is metered via turbine flow meters with the flow controlled by Fisher controllers and Badger Research valves. The fuel is filtered before being delivered to the rig. The rig is ignited by a propane torch through a port located in the side wall of the combustor in the near dome region.



Facility Schematic
Figure 1

COMBUSTOR DESCRIPTION

The combustion chamber, shown in Figure 2, has been designed to be nearly axisymmetric and incorporate quartz windows to allow optical diagnostics (primarily laser-based optical measurements) to be made. Optical access also allows for visual observations of the flame behavior. The combustor test section is square with generously filleted corners to minimize secondary flow development. The hydraulic diameter is 150 mm. This box-section combustor with corner fillets allows reasonable optical access while providing a cross section that approximates a two-dimensional axisymmetric cross section. The bluff body provides a recirculation region which can stabilize the flame. Optical windows of fused quartz are provided on the four flat sides for a downstream length of 490 mm. The combustor overall length to hydraulic diameter ratio is 4.9. This combustor configuration has two air additions through the dome and through two 1/2 inch side jets located on the top and bottom of the combustor as shown in Figure 2. The combustor is mounted on a 240 mm length spool piece containing a mounting pad for the fuel injector flange. The combustor and spool piece are situated on an inlet air conditioning section, also shown in Figure 2. Reactants are supplied at ambient temperature and pressure. Ignition is by means of a removable torch-igniter. This combustion chamber allows the combustion characteristics of a practical injector to be investigated in a simple geometry where various diagnostic measurements can be made.



Research Combustor Figure 2

METHODOLOGY

The advanced technology combustor to be tested was installed into a custom dome plate, designed on an Intergraph Computer Aided Design system, as shown in figure 3. The dome plate was then installed into the existing test facility (Fig. 1). An initial test run was conducted on the combustor to ensure that the rig was operating properly. Once it was demonstrated that the combustor was working well, and operated over a range of airflow and fuel flows the testing could begin.

The combustor was lit and the torch was removed. The airflow to the dome as well as the side jets was kept constant during each test. The air inlet temperature was held constant at 500 deg. F on both the side jet air and the main air flow. The ratio of side jet air mass flow to main air mass flow was held constant at 0.30. The pressure drop across the dome was varied between tests from 2.5% to 5% at increments of 1/2%. The tests were each performed with both ethyl alcohol (ethanol) and JP-8. Once the test rig was warmed to a surface wall temperature of 800 deg F the fuel flow was then reduced in a series of progressively smaller steps, with the airflow kept constant, with allowance for thermal stabilization at each decrement in fuel flow. This process continued until the flame blew out because the mixture was too lean to sustain the flame. At this point a lean blow-out was achieved and a computer scan of the data was then collected at that point.

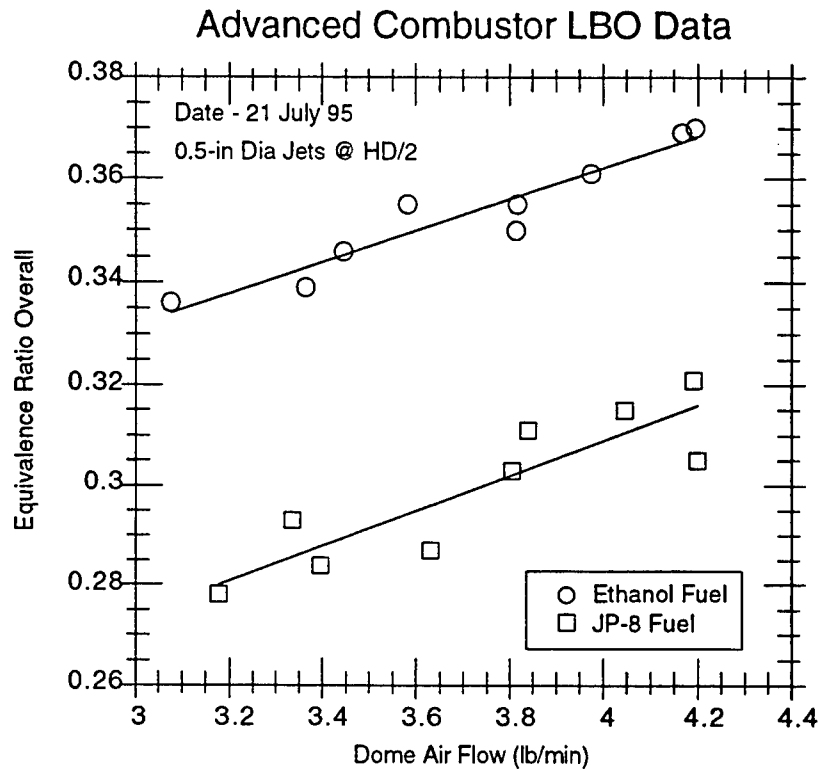


Figure 3

RESULTS AND CONCLUSION

As can be seen in Figure 3, The JP-8 liquid fuel used in the research combustor results in significantly lower stability limits than that for the ethanol over all conditions tested. On the average, the difference in the stability characteristics for the two fuels, the JP-8 provided an average of 18 percent lower stability limits than that for ethanol. The lower stability limits for the JP-8 fuel as compared to the ethanol can be addressed in several ways and is probably a combination of several.

The heating values of the two fuels are very different, for JP-8 is 22,000 btu/lb, with ethanol coming in at 11,000 btu/lb. This difference will effect the local equivalence ratio and flame temperature for a given air flow. The evaporation effects for the two fuels are very different in that the ethanol will behave very much like a gaseous fuel due to the heated inlet air temperatures.

The evaporation time for the ethanol fuel droplets are very short compared to that for the JP-8 fuel. The ethanol due to its short evaporation time will mix with the dome air much better than the JP-8 will. The ethanol will result in a more uniform and overall lean mixture which will act more like a premixed system. The JP-8 however, will not vaporize as quickly and will produce a richer mixture locally and this will sustain the flame as the overall fuel flow is reduced. According to Lefebvre⁵ the flammability limits for ethanol is three times higher than that for kerosene fuels like JP-8.

Acknowledgments

This research was made possible with the assistance of Harold Day, Dr. Mel Roquemore and Steve Pennington.

References

1. Sturgess, G.J., Sloan, D.G., Roquemore, W.M., Reddy, V.K., Shouse, D.T., Lesmerises, A.L., Ballal, D.R., Heneghan, S.P., Vangsness, M.D., and Hedman, P.O. 1991 "Flame Stability and Lean Blowout - A Research Program Progress Report" Proc. 10th International Symposium on Air Breathing Engines, Ed. F.S. Billig, ISABE, Nottingham, England, Sept 1-6, Vol. 1, pp. 372-384.
2. Sturgess, G.J., and Shouse, D.T. 1993 "Lean Blowout in a Generic Gas Turbine Combustor with High Optical Access," ASME Paper 93-GT-332, presented at the International Gas Turbine and Aeroengine Congress and Exposition, Cincinnati, Ohio, May 24-27: accepted for publication in the Transactions of the ASME.
3. Hedman, P.O., Sturgess, G.J., Warren, D.L., Goss, L.P., and Shouse, D.T., 1994 "Observations of Flame Behavior from a Practical Fuel Injector Using Gaseous Fuel in a Technology Combustor," ASME paper No. 94-GT-389, Presented at the International Gas Turbine and Aeroengine Congress and Exposition, The Hague, Netherlands, June 13-16, Winner of Best Technical Paper for 1994 and accepted for publication in the Transactions of the ASME.
4. Shouse, D.T., Frayne, C., Stutrud, J., Gogineni, S., Sturgess, G.J., 1996 "The Role of Transverse Air Jets in the Formation of Gas Turbine Emissions," Presented at the 34th Aerospace Sciences Meeting and Exhibit, Reno, Nevada, January 15-18.
5. Lefebvre, A.H., "Gas Turbine Combustion" in Hemisphere Publication 1983., pp. 35-37.

SIMULATION OF THE AIRFLOW OVER AIRFOILS BY DISCRETIZING PARTIAL DIFFERENTIAL
EQUATIONS

Ajay Goel

Centerville High School
500 E. Franklin Street
Centerville, Ohio 45459

Final Report for:
High School Apprentice Program
Wright Laboratory

Sponsored by:
Air Force Office of Scientific Research
Bolling Air Force Base, DC

and

Wright Laboratory

August 1995

SIMULATION OF THE AIRFLOW OVER AIRFOILS BY DISCRETIZING PARTIAL DIFFERENTIAL EQUATIONS

Ajay Goel
Centerville High School

Abstract

The airflow over various airfoils were studied. Results previously obtained by performing experiments in wind tunnels at NASA (formerly NACA) were compared with results obtained by discretizing partial differential equations. Several aspects of each airfoil were studied: the coefficient of lift vs. the angle of attack, mach contours of the airfoil, pressure contours of the airfoil, and stream contours of the airfoil. After this was done, several self-designed airfoils were tested, but without experimental wind tunnel results to compare them too. In the self-designed airfoils, suction and blowing mechanisms were introduced into the airfoil to study its affects on the overall airfoil. Suction was shown to bring air contours closer to the airfoil, thereby generating higher coefficients of lift.

SIMULATION OF THE AIRFLOW OVER AIRFOILS BY DISCRETIZING PARTIAL DIFFERENTIAL EQUATIONS

Ajay Goel

Introduction

During the 1940's and 1950's NACA (now NASA) did a series of experiments on their own airfoils. Experiments were conducted in wind tunnels to determine such factors as an airfoil's optimum coefficient of lift, the airfoil's mach contours, its pressure contours, and its stream contours. Recently, however, the Flight Dynamics Lab at the Wright Patterson Air Force Base in Dayton, Ohio has developed a mathematical method to simulate this airflow by discretizing partial differential equations related to the airflow. This allows experimentation with not yet created models of wings and other parts of airplanes. Testing the airflow over objects using mathematical numerical analysis is cheaper and doesn't sacrifice a great deal of accuracy. The ultimate goal in airflow simulation is to create the ideal wing for any particular plane. This would involve maximizing the lift that the wing creates while minimizing the drag that it creates. Unfortunately, these two have an inverse relationship. Lift is created by the air accelerating faster on top of the wing than on the bottom. This creates a low pressure region on top and a high pressure region on bottom. The higher pressure region, in an attempt to equilibrate with the low pressure region, then pushes up, creating lift.

Methodology

The discretization of partial differential equations involves highly advanced calculus, but generally consists of converting partial differential equations to linear algebraic form by expanding differential terms with the use of Taylor series expansions. As a preliminary step to grasp the concept of discretization, the 1-D and 2-D heat equations were discretized. Once the discretization had taken place, a Fortran program was written to calculate the heat distribution over a wire (1-D) and a mesh (2-D), given initial boundary conditions. In any computational fluid dynamics problem, the preliminary step is creating a grid, sometimes called a mesh. In the case of the 1-D wire, the mesh was simply 100 points on the simulated wire. In analyzing the heat distribution over an entire square surface, a 100x100 point grid was created, thereby giving 10,000 points of solution. In the case of an airfoil, a

mesh must be constructed around the boundary of the airfoil. The discretized differential equations will then be solved at each point on the mesh. Because most of the important airflow activity takes place at the very edge of the airfoil, the grid tends to be constructed so that the highest concentration of points occurs closest to the airfoil. A previously written program was used in constructing the various grids. The program allows the user to specify the dimensions of the grid and the x and y spacing between the points of the grid. Different spacings could be specified at different regions in the grid in order to capture the most accuracy near the edge of the airfoil. Once the grid was constructed, it was viewed by a commercial plotting program known as TecPlot. Next, a previously written program known as the "beam warming code" was used to actually compute the necessary data of the airfoil. The data was then once again plotted using TecPlot. All computer work was done on Silicon Graphics Unix workstations.

Discussion of Results

The first set of experiments involved the discretized forms of the 1-D and the 2-D heat equations. The following is the Fortran program used to calculate the relative temperature of the wire and the mesh after varying amounts of time. The first is the program used to solve the 1-D heat equation. The second is the program used to calculate the solution to the 2-D heat equation using Laplacian Analysis. With the 2-D equation, the Laplacian solution was compared to the ordinary numerical method solution. Laplacian Analysis is used only when the time factor goes to infinity, thereby setting the heat distribution on the mesh at equilibrium. Therefore, in the numerical method solution, although an infinite number of time steps could not be computed, the number was significantly large enough.

Fortran Program for Solving 1-D Heat Equation

```

program ajay1
parameter (imax=2,kmax=101)
dimension u(imax,kmax)
dimension uz(imax,kmax)
open(unit=1,file='heat.dat',form='formatted')
1000 format (e15.9,1x,e15.9)
dx=1.0/(11-1)
dxe=0.01
u(1,1)=0.0
u(1,11)=0.0
t=0.0
dt = .01
pi=4.*atan(1.0)

```

```

do i=2,(11-1)
u(1,i)=sin((i-1)*dx*pi)
end do
alpha=dt/(dx*dx)
do kt=2,6
do i=2,(11-1)
uz(1,i)=u(1,i)+alpha*(u(1,i+1)-2.0*u(1,i)+u(1,i-1))
end do
t = t + dt
do n=2,(11-1)
u(1,n)=uz(1,n)
end do
end do
do i=1,(11)
write(1,1000) (i-1)*dx,u(1,i)
end do
do i=1,101
x=(i-1)*dxe
u(2,i)=exp(-(pi*pi)*t)*sin(pi*x)
write(1,1000) x,u(2,i)
end do
write(1,*) dx
write(1,*) pi
write(1,*) t
write(1,*) x
write(1,*) exp(-pi*pi*t)
write(1,*) sin(pi*x)
stop
end

```

Fortran Program for Solving 2-D Heat Equation by Laplacian Analysis

```

program ajay2
parameter (imax=101,jmax=101,kmax=200)
dimension u(imax,jmax)
dimension uz(imax,jmax)
dimension uzx(imax,jmax,kmax)
open(unit=1,file='2Dheat2.dat',form='formatted')
open(unit=2,file='2Dheat3.dat',form='formatted')
open(unit=3,file='2Dheat5.dat',form='formatted')
1000 format (e15.9,1x,e15.9,1x,e15.9)
dh=0.01
t=0.0
do i=1,101
uzx(i,1,kmax)=100
uzx(i,101,kmax)=300
end do
do j=1,101
uzx(1,j,kmax)=400
uzx(101,j,kmax)=200
end do
c   do i=2,(imax-1)
c   do j=2,(jmax-1)

```

```

c    u(i,j)=50
c    end do
c    end do
      pi=4.0*atan(1.0)
do n=1,kmax
  print *, n
  do i=2,(imax-1)
    do j=2,(jmax-1)
      x=((i-1)*dh)
      y=((j-1)*dh)
      uzx(i,j,n)=((200*(-cos(n*pi)+1))/(n*pi*sinh(n*pi))*
/      sinh((n*pi*(1-y))/(1))+
/      (600*(-cos(n*pi)+1))/(n*pi*sinh(n*pi))*
/      sinh(n*pi*y/1))*sin(n*pi*x/1)+
/      ((800*(-cos(n*pi)+1))/(n*pi*sinh(n*pi))*
/      sinh((n*pi*(1-x))/(1))+
/      (400*(-cos(n*pi)+1))/(n*pi*sinh(n*pi))*
/      sinh(n*pi*x/1))*sin(n*pi*y/1)
    end do
  end do
end do
do i=2,imax-1
do j=2,jmax-1
do n=2,kmax
uzx(i,j,n)=uzx(i,j,n)+uzx(i,j,n-1)
end do
end do
end do
do i=1,imax
do j=1,jmax
u(i,j)=uzx(i,j,kmax)
write(3,1000) (i-1)*dh,(j-1)*dh,u(i,j)
end do
end do
c    dt=0.00001
c    pi=4.0*atan(1.0)
c    alpha=(dt/(dh*dh))
c    do kt=1,60000
c    print *, kt
c    do i=2,(imax-1)
c    do j=2,(jmax-1)
c    uz(i,j)=u(i,j)+alpha*(u(i+1,j)-2*u(i,j)+u(i-1,j)
c    /    +u(i,j+1)-2*u(i,j)+u(i,j-1))
c    end do
c    end do
c    t=t+dt
c    do k=2,(imax-1)
c    do l=2,(imax-1)
c    u(k,l)=uz(k,l)
c    end do
c    end do
c    if (kt.eq.50000) then

```

```

c      do i=1,(imax)
c      do j=1,(jmax)
c      write(1,1000) ((i-1)*dh),((j-1)*dh),u(i,j)
c      end do
c      end do
c      endif
c      end do
c      do i=1,(imax)
c      do j=1,(jmax)
c      write(2,1000) ((i-1)*dh),((j-1)*dh),u(i,j)
c      end do
c      end do
      stop
      end

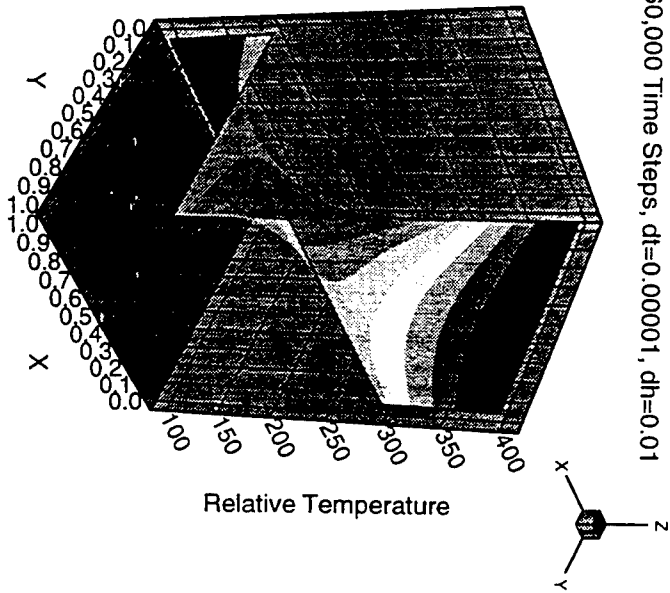
```

Next, the results are shown of the 1-D heat equation and the two methods used to solve the 2-D heat equation. In the case of the 1-D equation, a sine function heat distribution was initially set and then compared to the solution obtained from the numerical solution method, or the discretized 1-D heat equation. These equations can be found in the program. The results show that the smaller the time step, the closer the numerical analysis curve is to the exact sine curve initially set at the beginning. In the case of the 2-D heat equation, a 100x100 mesh was used and the boundary conditions were set so that one side would be initially set at 100 degrees, the next at 200 degrees, the third at 300 degrees, and the fourth at 400 degrees. Two different numerical analysis methods were used to determine the temperature at any point of the mesh after equilibrium was reached. Unfortunately, due to the complexity of the 2-D equation, the equation could not be converted to algebraic form, thereby making it impossible to compare it to any exact solution. The solutions must be quite accurate since two almost exact solution were obtained from two completely different numerical methods.

Comparison of Solutions to 2D Heat Equation Using the Numerical Analysis and Fourier Series Methods

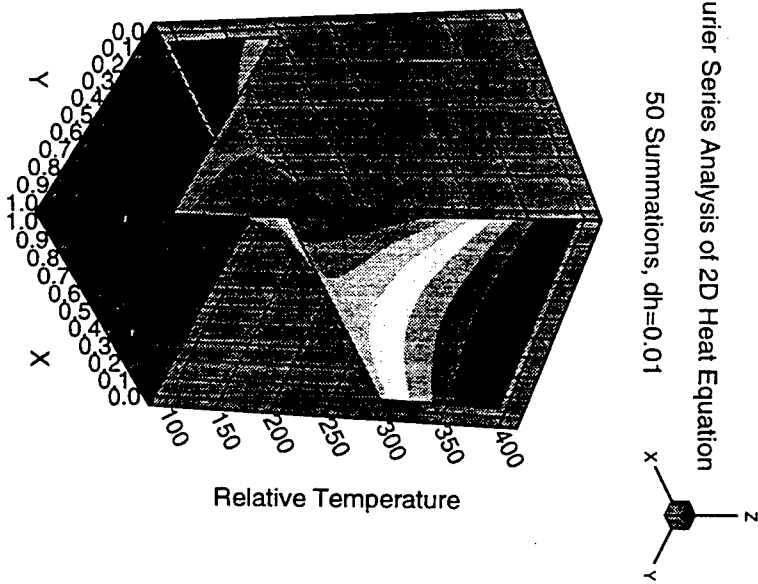
(3D) II Print II 8 Aug 1995 II 2Dheat3.plt II Heat Eqn 2D Case

Numerical Analysis of 2D Heat Equation at Equilibrium
60,000 Time Steps, $dt=0.00001$, $dh=0.01$

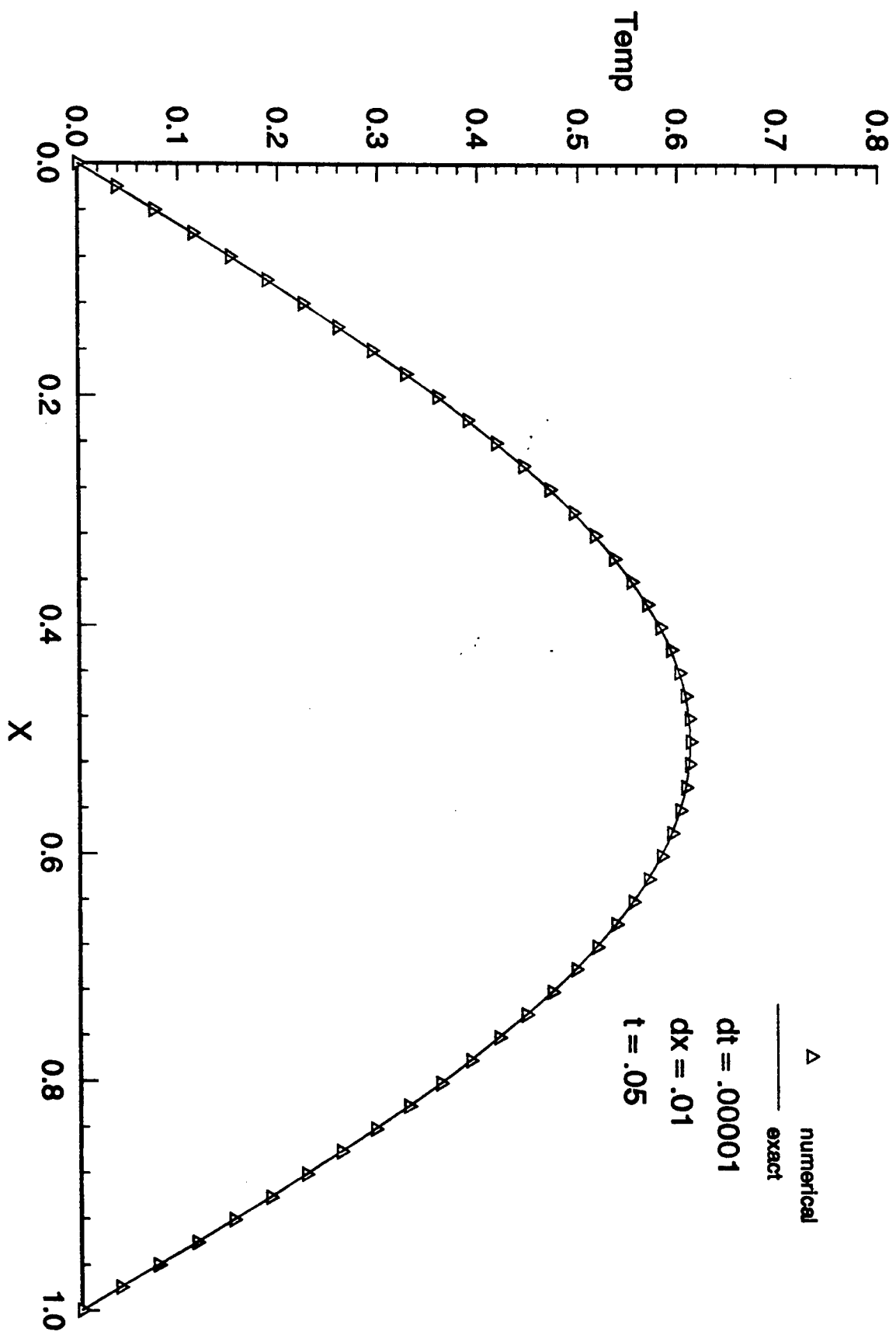


(3D) II Print II 8 Aug 1995 II 2Dheat4.plt II Heat Eqn 2D Case

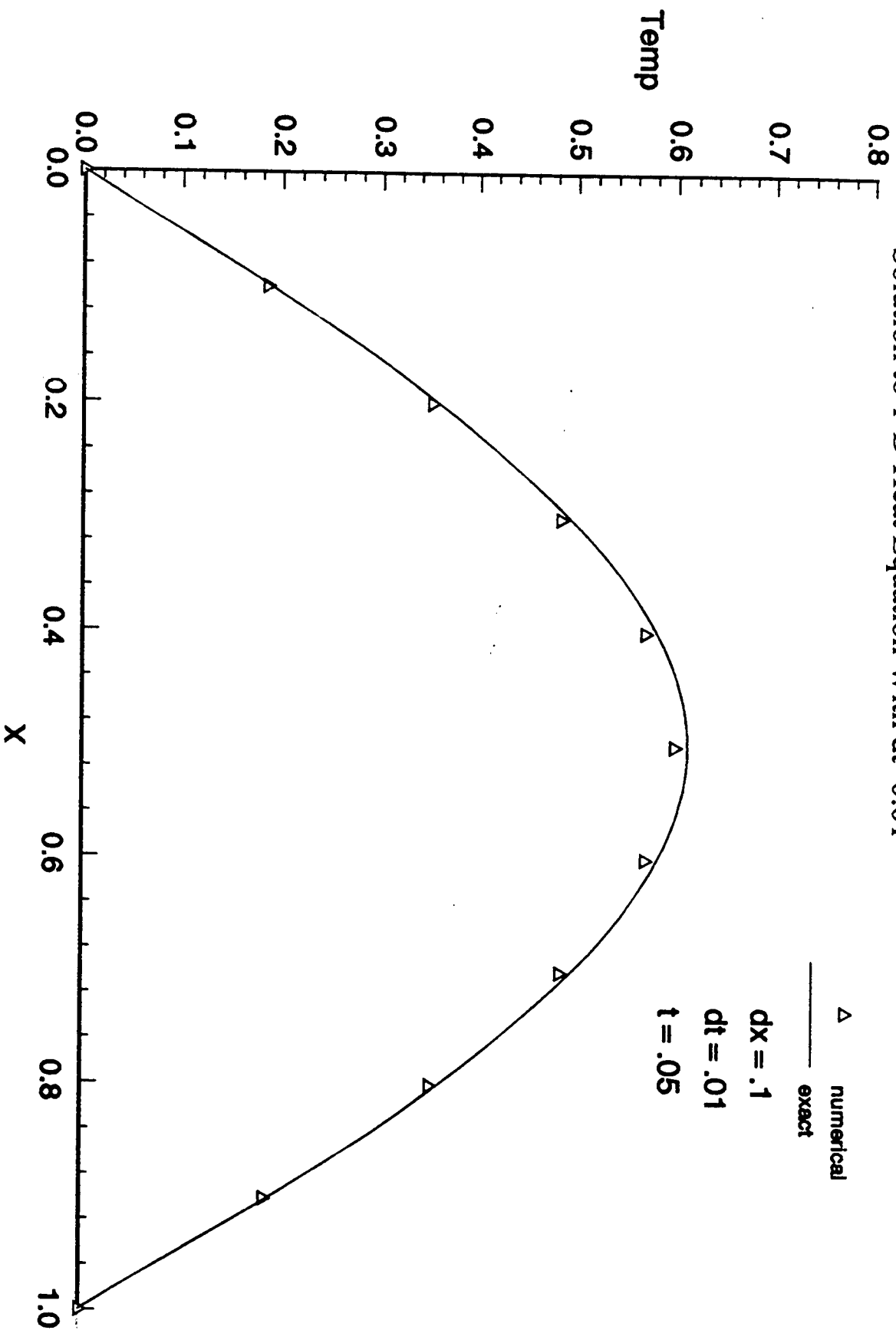
Fourier Series Analysis of 2D Heat Equation
50 Summations, $dh=0.01$



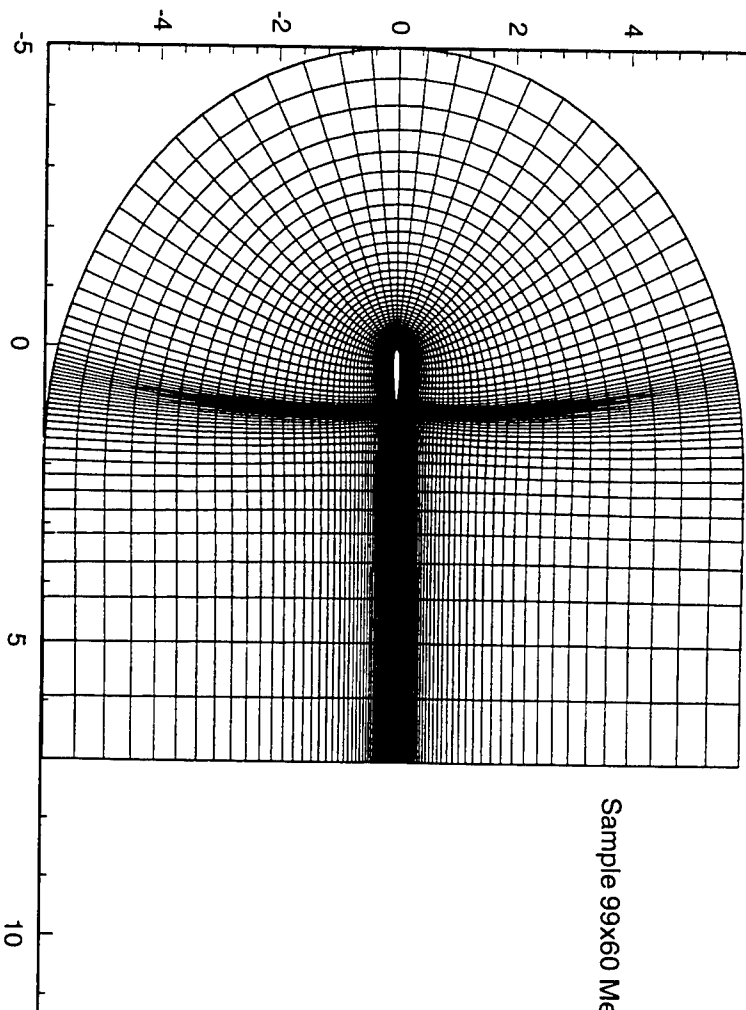
Solution to 1-D Heat Equation With $dt=0.00001$

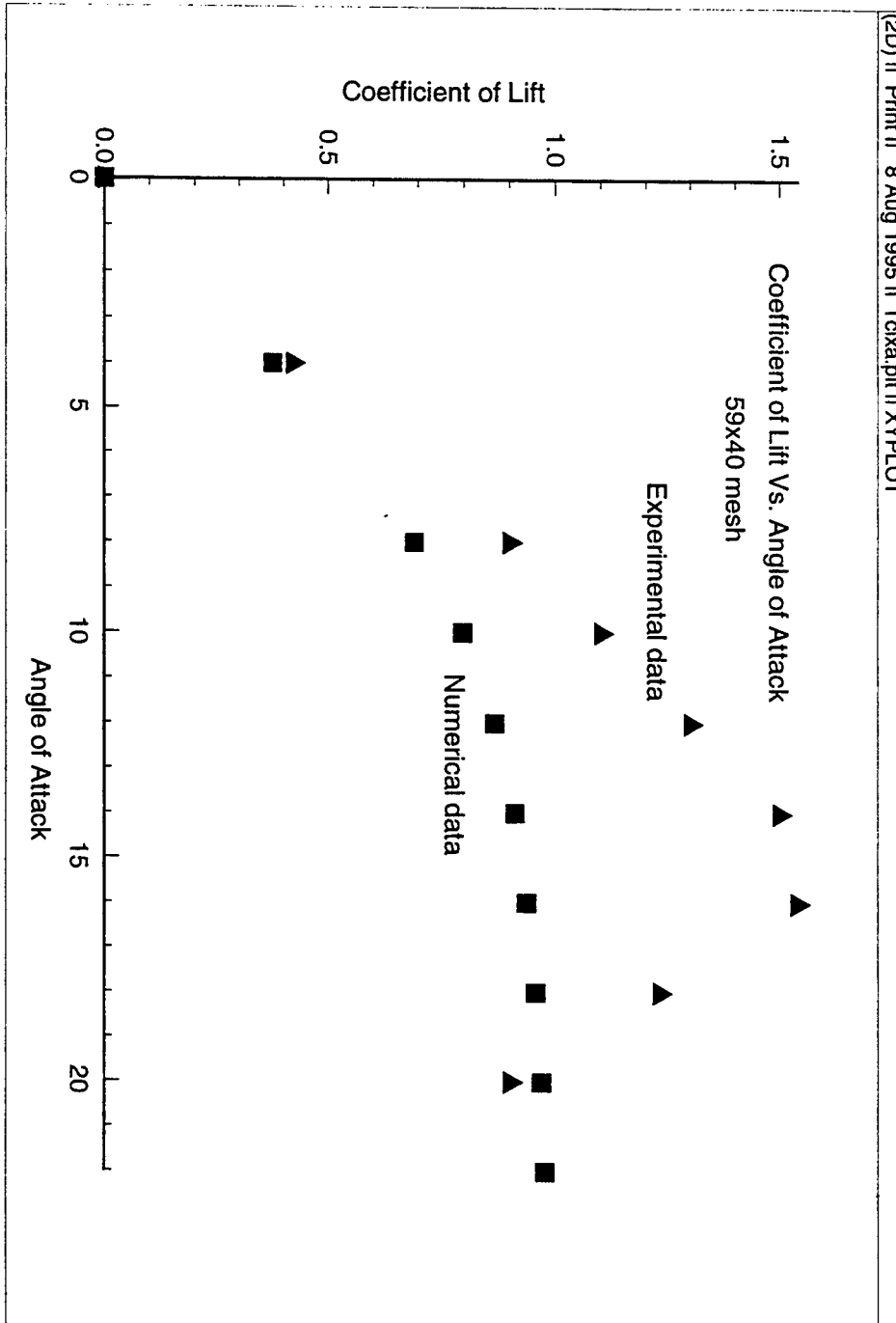


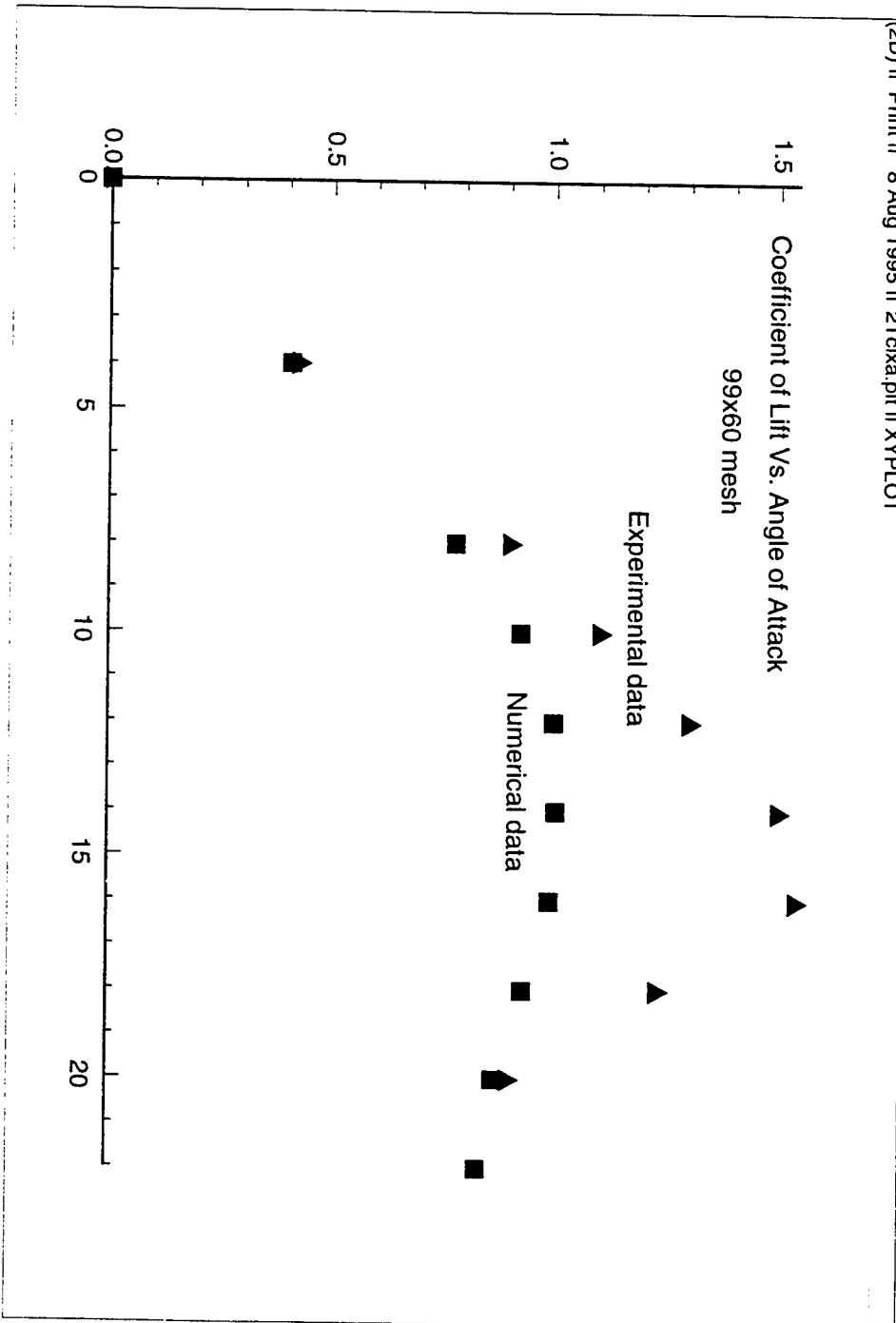
Solution to 1-D Heat Equation With $dt=0.01$

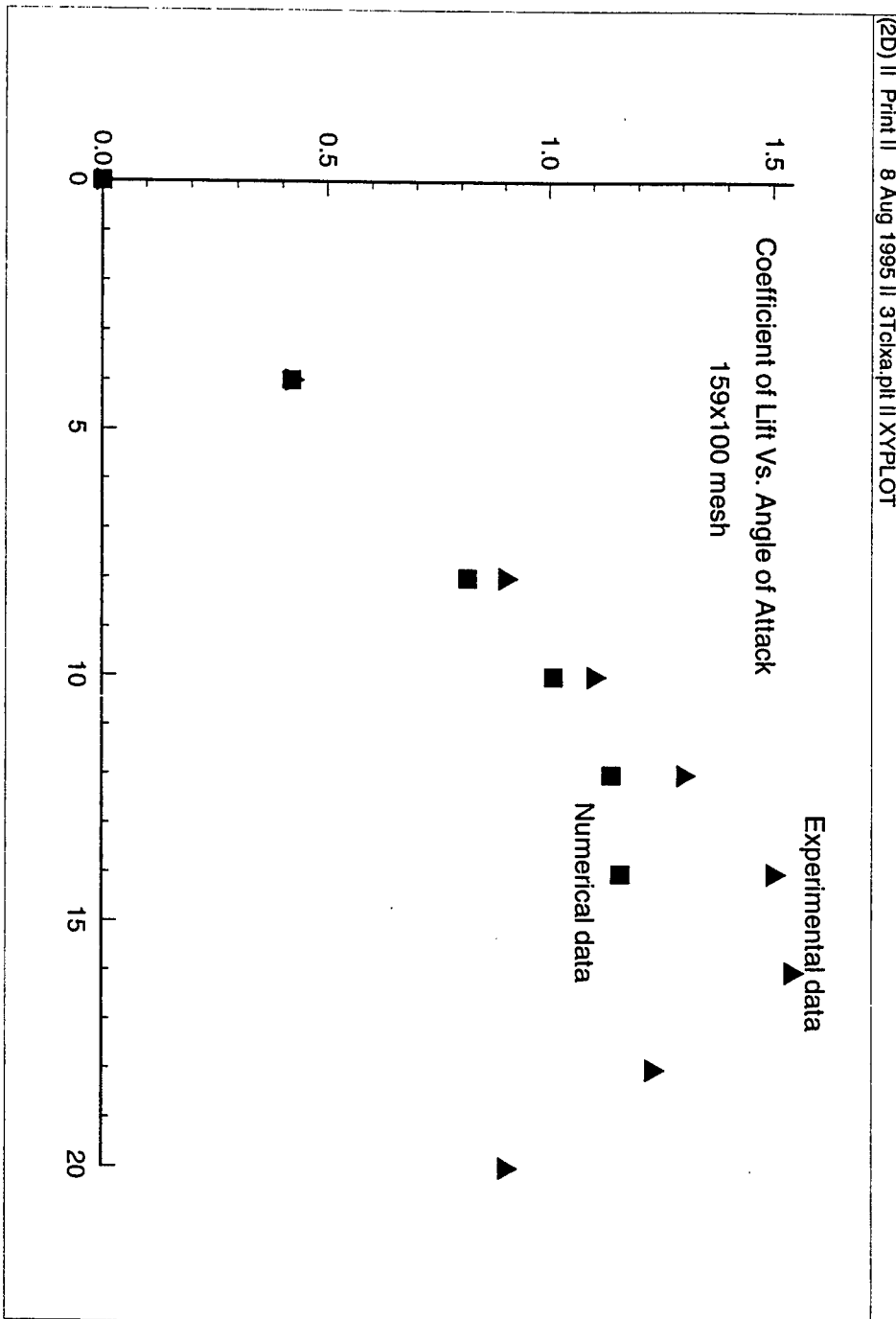


The tests on the heat equations were performed simply to gain an understanding of the discretization of partial differential equations. The bulk of the computational fluid dynamics experiment was concerned with testing the airflow over airfoils. The first set of experiments were run to primarily test the accuracy of the beam warming code by comparing its results with the actual results obtained from NASA windtunnels in the 1940's and 1950's. The results of these sets of experiments also showed that the finer the mesh was, the closer the computed results were to the actual windtunnel results. The picture on the following page is an example of a 99x60 mesh around the NACA 12 airfoil. The first experiment used the NACA 12 airfoil. The following three graphs show the coefficient of lift vs. angle of attack curves obtained through numerical analysis on three different grids and through the windtunnels. The numerical method curve slowly approaches the exact, windtunnel curve as the mesh becomes finer and finer.





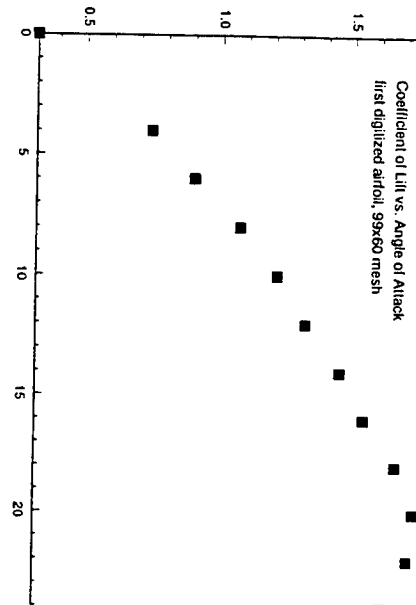




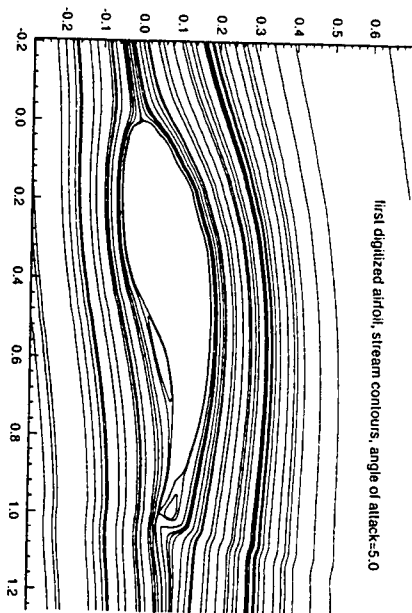
After experiments were done examining existing airfoils, several self-designed airfoils were experimented with. The airfoils were graphed with the use of a digitizer after I created them by hand with pencil and paper. The graphs on the next page show the coefficient of lift vs. angle of attack curves for both digitized airfoils and the stream contour plots that show the specific shape of the airfoils. The optimum coefficients of lift are higher on these two because of the camber. The NACA 12 airfoil had 0 camber. The digitized airfoils have camber and are slightly broader. As a result, they generate more lift. As a consequence, however, they generate more drag at the same time. The ideal airfoil would minimize drag yet optimize lift. After experiments testing the airflow around these digitized airfoils were run, the beam warming code was modified to take into account suction on the airfoils. The first digitized airfoil generates a slightly higher coefficient of lift than the second simply because of its much broader leading edge. As a consequence of this, much more drag (not shown here) is also generated. In looking at the stream contour plots, the airflow tends to break up on the underside of the first digitized airfoil. This is because of the large inward dip that the shape of the airfoil takes. The second digitized airfoil has a much smoother under surface, therefore making it easier for air molecules to flow right along the lower edge of the airfoil. In both airfoils, the airflow experiences break up around the trailing edge. This is because as the air comes over the top surface of the airfoil, there is nothing to bring it back down, as the slope begins to decrease. It tends to keep going in the same direction. As a result, the space underneath is filled with spiraling vortex breakdown patterns. Once this experiment was performed, a sucking mechanism was employed in the first airfoil to examine the affects of the airflow breakdown on the under surface and to examine any change in the coefficient of lift. The following page shows graphs of the converging coefficient of lift curve at an angle of attack of 5.0 degrees and the stream contour plot of the first digitized airfoil with the sucking mechanism. First, there is a much higher coefficient of lift. Without the sucking mechanism, at angle of attack of 5.0 degrees, the approximate coefficient of lift is about 0.8. With the sucking mechanism, however, the coefficient of lift jumps to 1.03. This is because the airflow is now closer to the airfoil and not breaking apart and forming vortex breakdown patterns. The stream contour plot shows this. On the underside of the airfoil, the airflow lines are no longer separated from the edge of the airfoil, as they were in the plot without the sucking mechanism. Furthermore, even at the trailing edge of the airflow, there is very little breakdown. 30% suction refers to a suction force equal to 30% of the speed of the plane.

In this case the speed of the plane is mach 0.250. The test runs fine for a simulated model, however if such a suction mechanism was to be employed in a real airplane, an alternate source of power would have to be provided for the suction so as to not deprive the main engines of their thrust capability. Further tests were run on 100% suction models. This often increased the coefficient of lift by two to three times the original amount. However, such a powerful mechanism is not yet feasible due to the enormous amount of energy this would require.

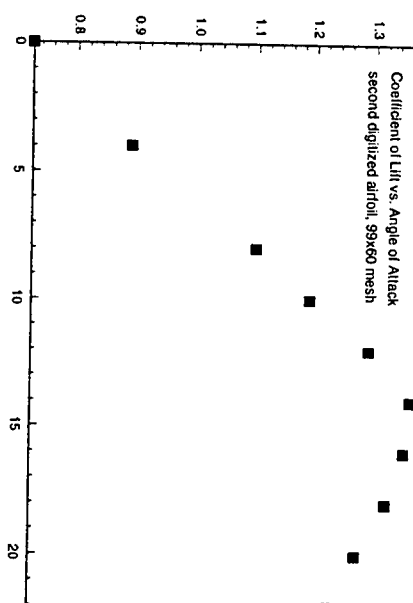
(2D) II Point II 8 Aug 1995 II cma.pl II XYPL OT



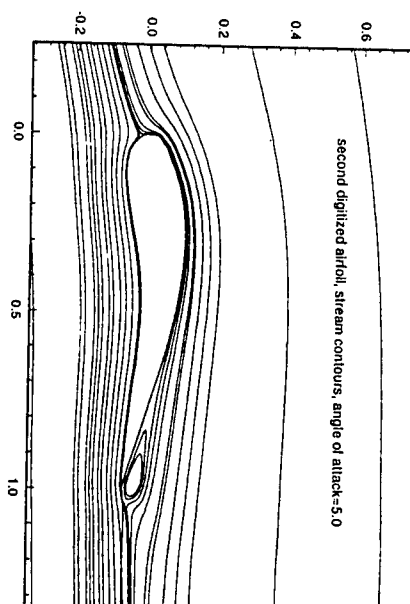
(2D) II Point II 8 Aug 1995 II Strakeops.pl II Airfoil Mach No. Data

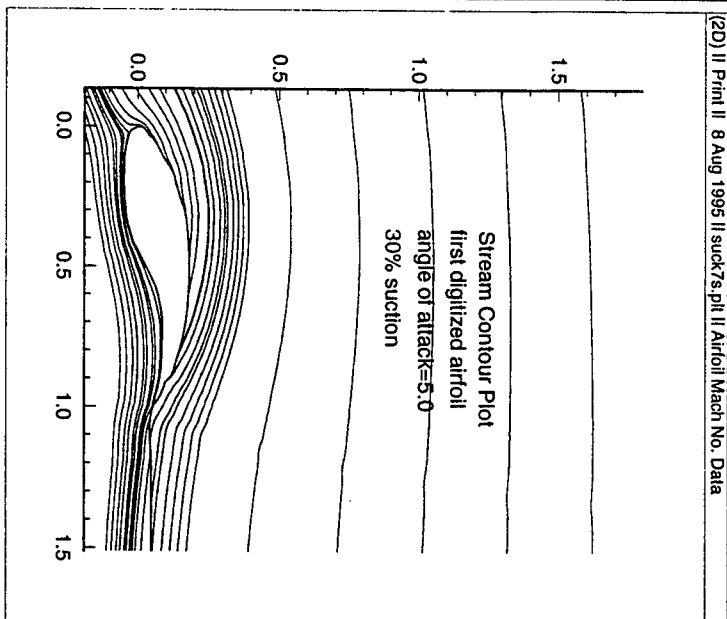
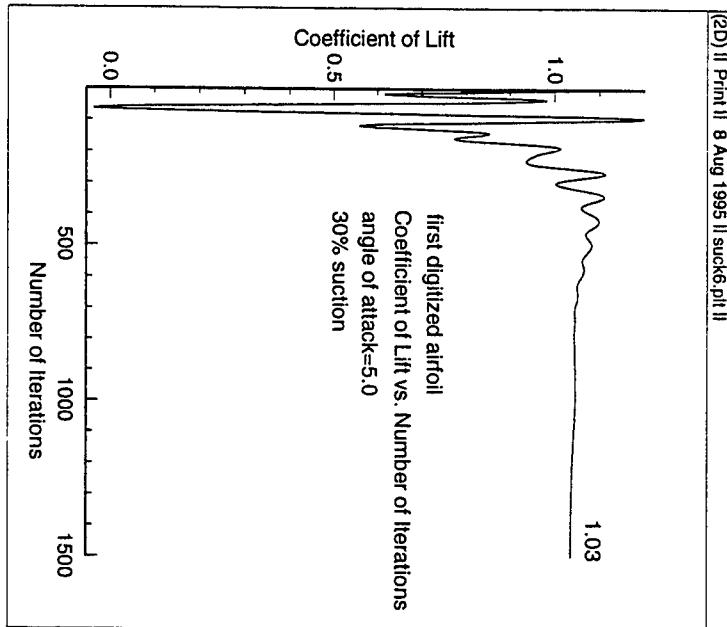


(2D) II Point II 8 Aug 1995 II Strakeops.pl II XYPL OT



(2D) II Point II 8 Aug 1995 II Strakeops.pl II Airfoil Mach No. Data





Conclusion

Several conclusions can be drawn from the above experiments. First, and most important, the discretization of partial differential equations (actual process not shown) can lead to highly accurate simulations of computational fluid dynamics problems, including the heat equations and the airflow over an airfoil. These numerical methods are proven to be accurate since two different numerical analysis methods produced the same results in regard to the 2-D heat equation. In general, the broader the leading edge of the airfoil is, the higher the lift generated will be and the more drag it will create. Large, upward dips in the underside of the airfoil usually allow the airflow to breakdown in that region. Suction, although usually not feasible due to the enormous energy requirement, often brings the airflow closer to the edge of the airfoil, for a tighter “fit.” This tighter “fit” generates much more lift.

Acknowledgments

I would like to thank Captain Mark Lutton and all the other scientists at the Flight Dynamics Lab at the Wright Patterson Air Force Base who helped me out during my eight week tour.

AN INVESTIGATION OF NEURAL NETWORK PROGRAMMING
AND USE FOR FINDING RELATIONSHIPS
AMONG SPIRAL INDUCTOR DATA

Stephen M. Govenar

Beavercreek High School
2660 Dayton-Xenia Road
Beavercreek, OH 45434

Final Report for:
High School Apprenticeship Program
Wright Laboratory

Sponsored by:
Air Force Office of Scientific Research
Bolling Air Force Base, Washington DC

and

Wright Laboratory

August 1995

AN INVESTIGATION OF NEURAL NETWORK PROGRAMMING
AND USE FOR FINDING RELATIONSHIPS
AMONG SPIRAL INDUCTOR DATA

Stephen M. Govenar
Beavercreek High School

Abstract

In this investigation, a neural network simulation program written in the Pascal programming language was converted to the C programming language. Later, an existing C program was modified to include sensitivity, correlation, and error calculations, and user interface changes were made. Rectangular spiral inductor physical characteristics, equivalent circuit parameters, and S-parameters were used to train and test the neural network.

AN INVESTIGATION OF NEURAL NETWORK PROGRAMMING AND USE FOR FINDING RELATIONSHIPS AMONG SPIRAL INDUCTOR DATA

Stephen M. Govenar

Introduction

Neural networks can be used to find the relationships among sets of data, and make predictions from other inputs using these relationships. A neural network consists of an input layer, any number of hidden layers, and an output layer of neurons. Weights connect each neuron of one layer to each neuron of the next layer. All of the inputs to a neuron are multiplied by the connecting weights, summed, and put through an activation function, the value of which is the output of the neuron. In this case, a two-layer feed-forward network was used, with the error backpropagation training algorithm using the delta learning rule. The activation function used was

$$f(\text{net}) = \frac{2}{1 + e^{-\lambda_{\text{net}}}} - 1 \quad (1)$$

The first part of this investigation was the conversion of a computer neural network simulation program written by Aleksander Malinowski in Pascal into the C language. In the next part, a C program written by Greg Creech called NNW was modified to include calculations of correlations and sensitivities of the data, and various error computations of the predicted versus desired outputs, and some of the user interface was changed.

Pascal To C Conversion

To convert the Pascal program into C, the same data structures were used, but converted into the C language syntax. The same general program flow was maintained, but small changes were made. The neural network library procedures and functions in `am_bplib.p` were put in `nnlib.c`. A header file, `nn.h`, was made to contain type definitions and function prototypes. The procedures for saving data to files readable by Maple and for pruning unimportant weights were omitted.

The apr.p program was converted to apr.c. Code was added to call the Correlation function and print the resulting correlation matrices. This function calculates the correlations between inputs/outputs and inputs/inputs using the formula

$$r_{ki} = \frac{\sum_{p=1}^N (X_{pi} - \bar{X}_i)(Y_{pk} - \bar{Y}_k)}{\sqrt{\sum_{p=1}^N (X_{pi} - \bar{X}_i)^2} \sqrt{\sum_{p=1}^N (Y_{pk} - \bar{Y}_k)^2}} \quad (2)$$

N is the number of patterns, X is the input vector, Y is the output vector. Element [k,i] of the input/output correlation matrix shows how variations in the i'th input affect the k'th output. A value of 1 means they vary in the same way and are exactly correlated, and a value of -1 means they vary in exactly reverse ways. A value of 0 means they are not correlated at all.

Various aesthetic changes were made to the apr program and it was debugged. However, it was decided that a better approach would be to modify an already existing C program.

C Program Modification

Many modifications were made to the nnw.c program. First the existing code was reformatted and converted to ANSI C. It was split into nnw.c and nnw.h, a header file containing the type definitions and function prototypes. The Randomize function, which performed pseudo-randomization of the weights by not seeding the random number generator with the current time, was removed (another function, TRandomize, which did set the seed this way, was kept). The program was made to automatically randomize the weights at the beginning of the program. Next, a function to shuffle the training patterns was added. A menu was added that allows the user to change the network parameters during training by pressing CTRL-C. The menu also appears when the network has trained for *cyclemax* cycles or the cumulative error goes below *emaxcum*, to let the user choose to continue training or stop. A *cyclemod* variable was added to control the frequency of display of the current network error. In addition to displaying the

cumulative squared error, a root mean square normalized error [1] calculation was added to the training function. The formula for this error is

$$\text{rmsn error} = \frac{1}{P \times K} \sqrt{\sum_{p=1}^P \sum_{k=1}^K (d_{pk} - o_{pk})^2} \quad (3)$$

P is the number of patterns, K is the number of output neurons, d is the desired output vector, and o is the predicted output vector.

The network testing option of the program was modified to allow testing with different input/output patterns, loaded from files. The interrupt signal handling was modified so that the training would not be interrupted in the middle of a cycle. This was done by having the signal handler only set a global variable, which is checked in the neural_net training function. Functions to calculate and print input/output correlations and input/input correlations were added. These were taken from the nnlib.c library and are described in the previous section.

Functions to calculate and print input sensitivities were added, from nnlib.c. The sensitivities show how important each input is in controlling each output, in a trained neural network. The formula used to calculate the sensitivity [2] of an output o_k with respect to an input x_j is

$$S_{ki} = \frac{\partial o_k}{\partial x_i} = o_k' \sum_{j=1}^{J-1} w_{kj} y_j' v_{ji} \quad (4)$$

y_j is the output of the j-th neuron of the hidden layer, o_k' is the value of the derivative of the activation function at the k-th output neuron, and y_j' is the value of the derivative of the activation function at the j-th hidden neuron.

Three overall sensitivity matrices are calculated over all N training patterns. The mean square average sensitivities [2] are found as

$$S_{ki, \text{avg}} = \sqrt{\frac{\sum_{n=1}^N (S_{ki}^{(n)})^2}{N}} \quad (5)$$

The absolute value average sensitivities [2] are computed as

$$S_{ki,abs} = \sqrt{\frac{\sum_{n=1}^N |S_{ki}^{(n)}|}{N}} \quad (6)$$

The maximum sensitivities [2] are calculated as

$$S_{ki,max} = \max_{n=1..N} \{S_{ki}^{(n)}\} \quad (7)$$

Checks were added for nonexistent files and out of memory situations. Four types of error calculations were added, that are performed after testing the neural network. The first is percent error, calculated using the equation

$$\text{percent error}_{pk} = \left| \frac{d_{pk} - o_{pk}}{d_{pk}} \right| \times 100\% \quad (8)$$

The second, root mean square error [2], is calculated by first finding the squared error,

$$SE_{pk} = (d_{pk} - o_{pk})^2 \quad (9)$$

for each output of each pattern, and using these in the formula

$$\text{rmse}_k = \sqrt{\frac{\sum_{p=1}^N (d_{pk} - o_{pk})^2}{N}} \quad (10)$$

The third error calculated is r [3], or the correlation between the desired and predicted outputs. Equation (2) is used for this, and it is expressed as a percentage here.

The fourth error found is R-squared [3], or percentage variation of the outputs, which is calculated by

$$R^2 = \frac{\sum_{i=1}^N (\hat{Y}_i - \bar{Y})^2}{\sum_{i=1}^N (Y_i - \bar{Y})^2} \quad (11)$$

and then multiplied by 100 to give a percentage. N is the number of patterns, Y is the desired output, \hat{Y} is the calculated output, and \bar{Y} is the mean of the desired outputs.

A User's Guide was written for this program and is included in Appendix A.

Testing The Neural Network

The neural network simulated by the nnw program was first tested using physical characteristics as inputs and equivalent circuit parameters as outputs. The physical properties used were width, spacing, length, and number of turns. The equivalent circuit parameters used were capacitance 1 & 2, resistance, and inductance. Sixteen patterns were used to train the network, and best results were obtained with an eta of 0.01 and lambda of 0.2, with 16 hidden layer neurons. After 124,907 cycles of training, the network was tested with the same patterns it trained on. The average percent errors for C1, C2, R, and L were 3.13%, 2.42%, 6.49%, and 0.58%, respectively. Plots were made of the desired versus predicted outputs. See scatter plots 1, 2, 3, and 4 in Appendix B.

The tests were then run in reverse, with the equivalent circuit parameters as inputs and the physical characteristics as outputs. Best results were obtained with 16 hidden layer neurons, an eta of 0.3, and lambda of 0.2. After 200,000 training cycles, the average percent errors for width, spacing, length, and number of turns were 2.84%, 10.38%, 1.84%, and 0.05%, respectively.

The next set of training data consisted of the physical characteristics described before as well as frequency as inputs, and eight S parameters as outputs. Eighty training patterns were used, and the best network had 14 hidden neurons, eta equal to 0.1 and lambda equal to 0.2. After 101,000 cycles, the average percent errors for MS11, AS11, MS12, AS12, MS21, AS21, MS22, and AS22 were 7.62%, 0.33%, 0.23%, 6.35%, 0.23%, 6.35%, 7.60%, and 0.20%, respectively.

Conclusion

In most tests of the neural network, it performed very well. The network did not train as well in the reverse direction as it did in the forward direction. A good training technique found was to give *eta* a large value, such as 0.1 or 1.0, to begin with, and then decrease *eta* to a smaller number, such as 0.01, when a relatively small error was reached. The neural network seemed to perform better than statistical methods in predicting outputs.

References

- [1] J.M. Zurada, *Introduction to Artificial Neural Systems*, West Publishing Company, St. Paul, Minn., 1992.
- [2] J.M. Zurada, A. Malinowski, I. Cloete, "Sensitivity Analysis for Minimization of Input Data Dimension for Feedforward Neural Network", *Intelligent Engineering Systems through Artificial Neural Networks*, vol. 3, ASME Press, 1993
- [3] N.R.Draper, H.Smith, *Applied Regression Analysis*, John Wiley & Sons, New York, 1981.

Appendix A

NNW User's Guide

=====

NNW is a program written in C that simulates a two-layer feed-forward neural network. It consists of the files nnw.c, nnw.h, and Makefile, and reads its data from various files, usually including a network parameter file, network info file, input vector file, and output vector file. They may have any filenames, but the following convention has been used so far: if the data being tested was from inductors, a prefix like 'ind' would be chosen, and the four files mentioned above would be named indnet.dat, indinfo.dat, indin.dat, and indout.dat.

Compiling

=====

To compile NNW, edit the Makefile if necessary and type 'make'. No changes to the Makefile should be needed, except to change the name of the C compiler. gcc is used by default, but any ANSI C compiler should work. The compiled binary is named 'nnw'.

Data Files

=====

Network Parameter File

The network parameter file contains constants used in the neural network (except for the number of inputs). It should look like:

```
eta 0.01
lambda 0.2
emaxcum 0.01
cyclemax 200000
J 16
K 4
tc 5
```

The values must be given in that order. The definition of each network parameter is:

eta - learning constant used in delta weight calculations

lambda - steepness factor in the network's activation function

emaxcum - desired cumulative error of the network; training

will stop when the error drops below this value

cyclemax - maximum number of cycles to train

When emaxcum or cyclemax is reached, a menu appears allowing the user to alter parameters and continue or stop training.

J - number of neurons in the hidden layer

K - number of neurons in the output layer

tc - number of patterns (input/output pairs) that are to be used

for training; the network will train on all except the last tc patterns

Network Information File

The network information file describes the number of neurons in the input layer, and the number of patterns. The first two entries in this file are the number of lines in the file (number of patterns + 1) and the number of words in the file. The rest of the file is ignored. The number of inputs, or I, is calculated by second_number/first_number. The UNIX command wc can be used to create this file, as in "wc -lw indin.dat > indinfo.dat". If indin.dat contained 16 patterns with 4 (68/17) inputs, the resulting file would look like this:

17 68 indinput.dat

Input Vector (Data) File

The input vector file consists of one header line describing the inputs, and then all of the inputs for the network separated by tabs, one pattern per line. An example would be

*Width	Spacing	Length	Turns
10	10	200	1.5
1e+1	1e+1	2e+2	2.5e+0
....etc....			

The words in the header are not used by the program, but must exist, and there should be one word per input.

Output Vector (Data) File

The output vector file contains the desired outputs for the network, and uses the same format as the input vector file (including the one line header).

Running the Program

=====

To begin program execution, one must type 'nnw' at the shell prompt. nnw takes no command line arguments. The appropriate options are then selected from different menus. The function each menu option performs is described below.

Main Menu

=====

When the program is started, the weights are randomized to random values between -0.125 and 0.125, and the main menu of NNW appears, and looks like this:

1. Load training patterns
2. Weight operations
3. Shuffle patterns
4. Edit network parameters
5. Train the neural network
6. Test the neural network
7. Calculate sensitivities
8. Calculate correlations
9. Quit the program

Each option is described below.

Load Training Patterns

=====

This prompts the user for the network parameter, network info, input vector, and output vector files. The network parameters are set, and their values are displayed. The input and output vectors are read in, and the inputs and outputs are normalized, or scaled down, to values between -0.9 and 0.9. The normalized vectors are written to the files normalin.dat and normalout.dat (for checking purposes; these files are not used again by the program).

Weight Operations

=====

This allows the user to randomize the network weights, store the current weights in a file, and read in weights from a file.

Shuffle Patterns

=====

This shuffles the input/output patterns, which should be done for the best training. The shuffled patterns are written to the files shuffin.dat and shuffout.dat (again, for checking purposes; they are not used again by the program).

Edit Network Parameters

=====

This displays a menu with options to read a new network parameter file, save the parameters to a file, and alter the parameters.

Train the Neural Network

=====

This starts training the neural net. Interrupting the program, usually by pressing CTRL-C or sending the SIGINT signal to the program, displays a menu that allows you to change the values of eta, lambda, emaxcum, cyclemax, and the display frequency (the variable cyclemod), and either continue or stop training. The current cycle number, cumulative network error, and root mean square normalized error are displayed every cyclemod cycles, which defaults to 500. If the error drops below emaxcum, or the cycle

number reaches cyclemax, training is stopped and this menu appears. If you want to continue training, emaxcum and/or cyclemax need to be changed. You may stop training temporarily to return to the main menu and save the weights, test the network, etc., and continue training where it left off.

Test the Neural Network

=====

This displays the following menu.

1. Test network using test vectors only
2. Test network using training vectors only
3. Test network using all vectors
4. Test network using different test vector files
5. Quit to main menu

The first option tests the network using only the last tc patterns. The second options tests the net using all the patterns up to the last tc patterns, i.e. the patterns the network was trained with. The third pattern tests the net using all (training + test) patterns. The fourth option tests the net using patterns loaded in from another set of input/output vector files. The user is prompted for a network info file. If a network parameter file has not been read, lambda and J (number of hidden neurons) are prompted for. Then the input vector and output vector files are prompted for and read. After this, for all testing options, filenames for the results and errors to be written to are prompted for. The neural network is then tested by putting the test inputs into the network, using the current weights and writing the desired and actual outputs to the result file, separated by tabs, one pattern per line (as D1 O1 D2 O2 etc.). Errors for the network's actual versus desired outputs are written to the error file in the following format (all numbers on a line are separated by tabs). First, the percent error for each output of each pattern, one pattern per line. Then, the average percent error for each output, on one line. Next, a blank line, and then the squared error for each output of each pattern, one pattern per line. Then, the mean square error for each output, on one line. Another blank line follows, and the next line contains the value of r (output correlation) as a percentage for each output. Another blank line, and then on one line, the value of R squared as a percentage for each output.

Calculate Sensitivities

=====

This prompts for a result filename, calculates the sensitivities (or importances) of the inputs to outputs, and writes them to the result file. The mean square average, absolute, and maximum sensitivities are written to the file in that order, each using the following format. First, a table of sensitivities, outputs horizontal from left to right, and inputs vertical, top to bottom. Then, the sorted average input sensitivities, along with the gap between successive values. Next, for each output, a sorted list of input sensitivities, with their gaps.

Calculate Correlations

=====

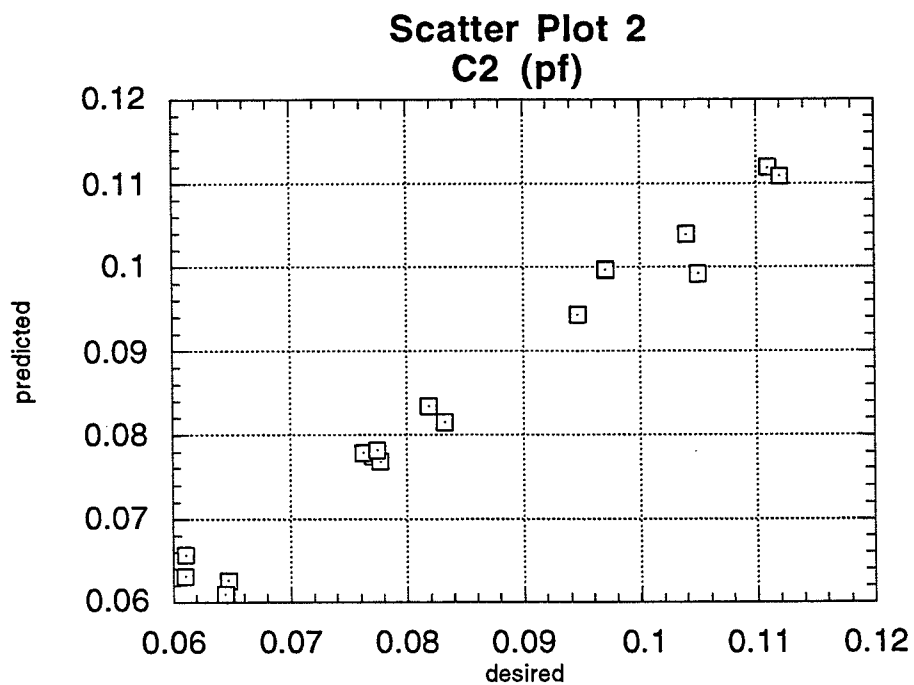
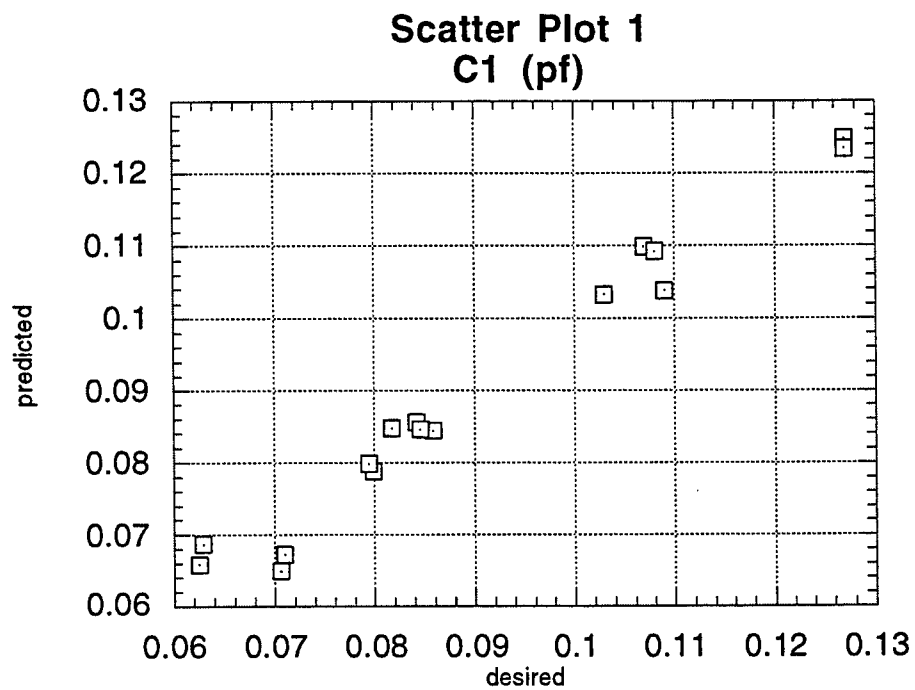
This prompts for a result filename and calculates the input/output correlations, and the input/input correlations. The correlations measure how each output varies as each input varies. A value of 1 means they vary in the same way and are exactly correlated, and a value of -1 means they vary in exactly reverse ways. A value of 0 means they are not correlated at all. The result file will contain the input/output correlation matrix in a table, outputs horizontal from left to right, and inputs vertical, top to bottom. Then a blank line, and the input/input correlation matrix.

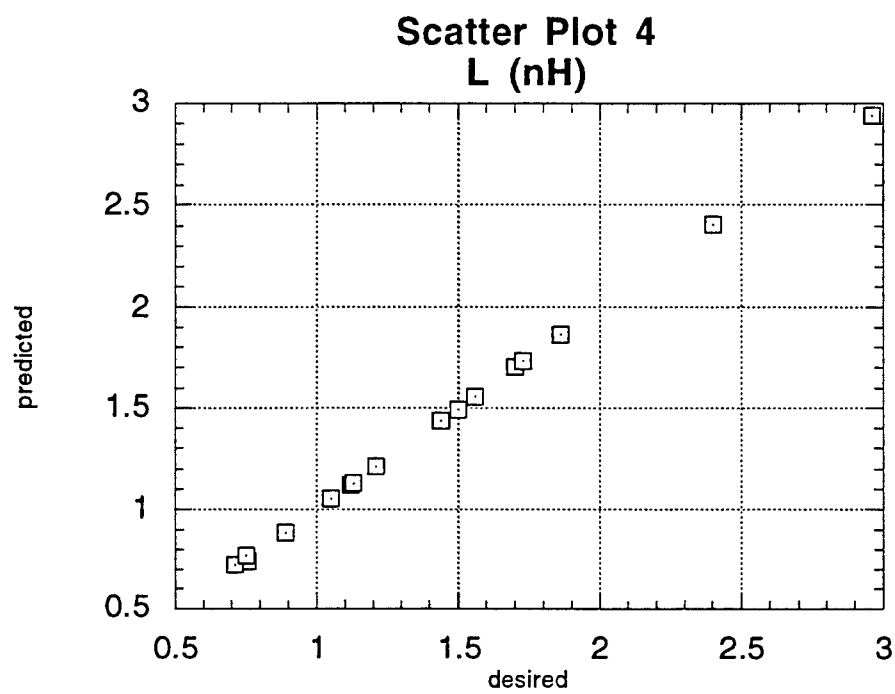
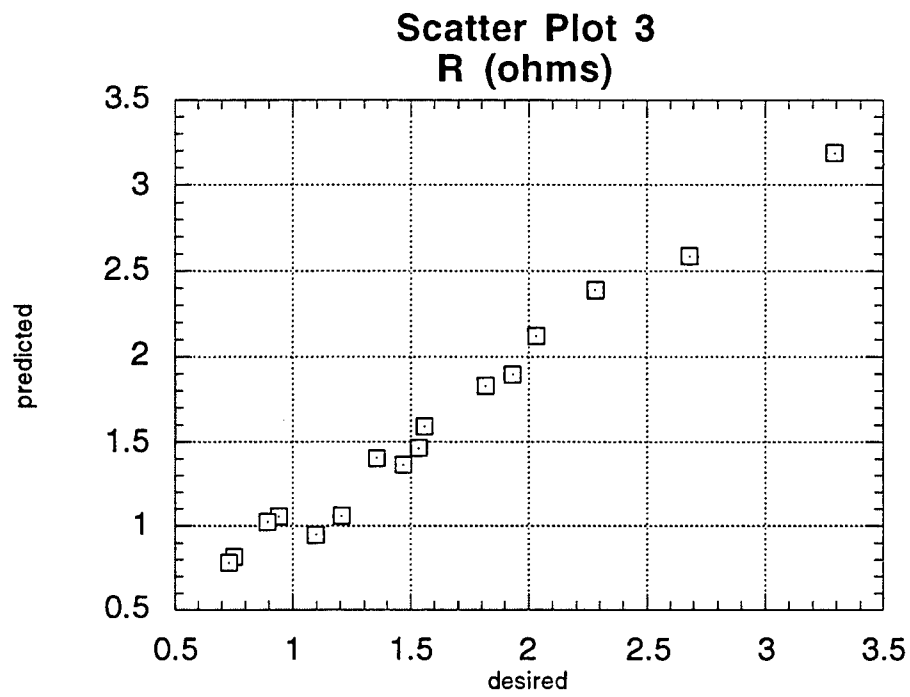
Recommended Use

=====

In normal use, the user should load the training patterns, shuffle the patterns, and begin training. The weights should be saved either periodically or whenever the error seems small. The network could be tested each time the weights are saved, or after all the training has finished, loading in the saved weight files for each test. The sensitivities could be used to determine which inputs are not very important in affecting the output, and could possibly be omitted to speed up network training.

Appendix B





HIGH PRESSURE FREQUENCY RESPONSE

Neil P. Griffy

Brookville High School
106 Hill Street
Brookville, OH 45309

Final Report for:
High School Apprentice Program
Wright Laboratory

Sponsored by:
Air Force Office of Scientific Research
Bolling Air Force Base, DC

and

Wright Laboratory

August 1995

HIGH PRESSURE FREQUENCY RESPONSE

Neil P. Griffy
Brookville High School

Abstract

A numerical analysis was conducted to determine the effects of tube diameter and tube length on the frequency response of the General Electric Swept Fan Assessment Rig (GESFAR) high-response pressure measurements. This measurement system, located over the second-stage rotor, must have a high frequency response to measure pressures on the casing wall. A computer program was used to perform the numerical analysis. The program tested the proposed transducer installation and its capability to measure transient pressure fluctuations over a frequency range of 0-50,000 hertz. The phase shift and amplitude ratios were evaluated as a function of frequency. The original 4.25 inch tube with a .062 inch diameter was tested, and the results were found to be unacceptable. Other tubes of different lengths and diameters were tested but most could not tolerate the high frequency response required for the kulite block. After all cases were investigated, it was concluded that a .030 inch tube with a .093 inch diameter had an acceptable frequency response, producing minimal phase shift and amplitude distortion. The GESFAR compressor hardware is now being modified to incorporate this new configuration

HIGH PRESSURE FREQUENCY RESPONSE

Neil P Griffy

This analysis was conducted to determine the effects of tube diameter and tube length on the frequency response of the GESFAR second-stage over-the-rotor high response pressure measurements. This measurement system must have a high frequency response to measure the pressure on the case between the rotating blades. The compressor operates at 13,288 revolutions per minute, or approximately 221 revolutions per second. Since there are 16 blades on the compressor, the blades will pass any given point on the compressor approximately 3,543 times per second. The frequency response of the measurement must be able to accommodate a frequency of at least 10 times the blade passage frequency or approximately 35,000 hertz.

The purpose of this analysis was to find a suitable tube length able to keep a transducer far enough away from the rotor, to prevent damage, while holding a frequency response of at least 35,000 hertz. When a tube is placed between a transducer and the pressure signal coming from the compressor, a change occurs in the signal. This change can either cause the pressure signal to be amplified or dampened, causing the sensed pressure signal to be different from the actual pressure. This change is defined as a phase shift.

Amplitude ratio is equal to the ratio of the amplitude of the actual wave, compared to the measured wave. Phase shift is the difference in the phase angle of the measured wave compared to the phase angle of the actual wave as it enters the tube. When a wave

enters the tube it has a certain phase angle. As the wave travels down the tube it becomes distorted. This distortion can alter the wave's phase angle causing it to lead or lag behind the original wave. When this wave reaches the transducer, it may measure a different value than the actual value, causing a difference in results. Phase shift and amplitude ratio measurements are important to the analysis because they must be as close to the actual value as possible.

The analysis was conducted on the VAX computer system using the program name TUBE.EXE. First, the tube length, diameter, pressure ratio, temperature ratio, transducer volume, starting frequency and ending frequency, were all inputted into the program. The program then evaluated the proposed transducer installation and its capability to measure transient pressure fluctuations over a frequency of 0-50,000 hertz. After the results were reduced, the phase shift and amplitude ratios were plotted as a function of frequency on a PC using Excel.

First, the existing case was tested which consisted of a transducer located in a tube that was 4.25 inches long and .062 inches in diameter. The test evaluation was performed with a pressure ratio of 4.3 and a temperature ratio of 1.69 which are the expected values over the second stage rotor at the compressor design conditions. The present testing temperature is equal to the standard atmospheric temperature multiplied by the temperature ratio. Likewise, the testing pressure is equal to the standard atmospheric pressure multiplied by the pressure ratio. When the results were analyzed, it was discovered that the tube could only reach a frequency of 300 hertz, with minimal distortion. As shown in Figure 1, this tube length and diameter combination would

resonate at many frequencies throughout the range of interest. These resonances rendered this tube configuration unacceptable for the new over the rotor pressure measurements.

A new design was investigated to provide an amplitude ratio of 1 over the desired frequency range. It consisted of shorter tube lengths and different tube diameters.

After all the proposed cases were investigated, it was concluded that the .030 inch tube, with a diameter of .093 inches, had the greatest possible frequency response obtainable, with a minimal phase shift and amplitude effect. Its frequency response was equal to 41,600 hertz. Frequency response is the frequency in which the amplitude ratio equals 1.1.

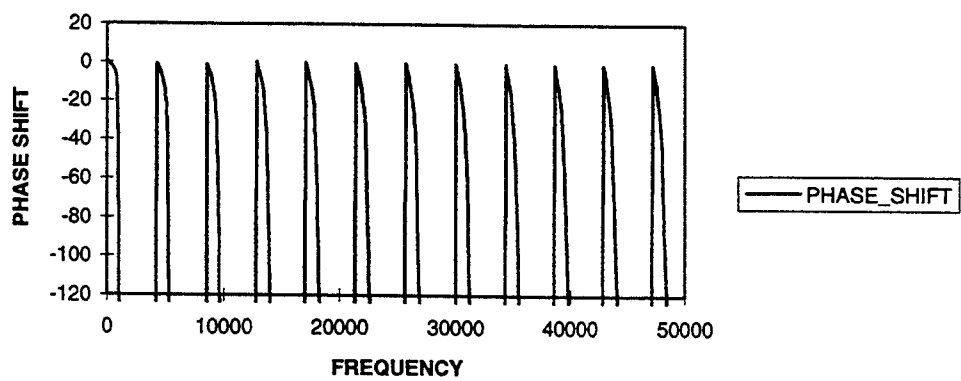
In an effort to improve the existing transducer configuration, various tube lengths and diameters were tested. As shown in Figure 1 and Figure 2, the difference in tube length changed the results dramatically. Figure 1 shows the 4.25 inch tube having an unfavorable amplitude effect because of the variance in the results. Figure 1 also shows the rather large phase shift depending on frequency inhibiting the ability to gather useful results, because of the potential of a large difference in the timing of adjacent pressure measurements. Figure 2 shows how the .030 inch tube with a .093 diameter reacted to the calculations. The amplitude ratio was constant at 1.1. The phase shift remained constant at 0 over the desired frequency range. Figure 3 shows the same tube with a .042 inch diameter. The results differed from the .093 diameter tube by only -200 hertz representing no real difference in amplitude effect. Table 1 shows the frequency response of the original case and the two alternatives that can provide acceptable frequency response.

After all possible cases were investigated, the conclusion was made that a tube with a .093 inch diameter could be used if its length was less than .030 inch. During the machining process of the case, some of the holes for the tubes chipped during drilling. The original design was to have .040 inch diameter holes. After the chipping occurred, if the .040 inch diameter were still used, it would affect the readings. This made the .093 inch diameter hole ideal because it would allow the hole to be drilled again.

Fig.1

4.25 inch tube

PRESSURE TUBE RESPONSE



PRESSURE TUBE RESPONSE

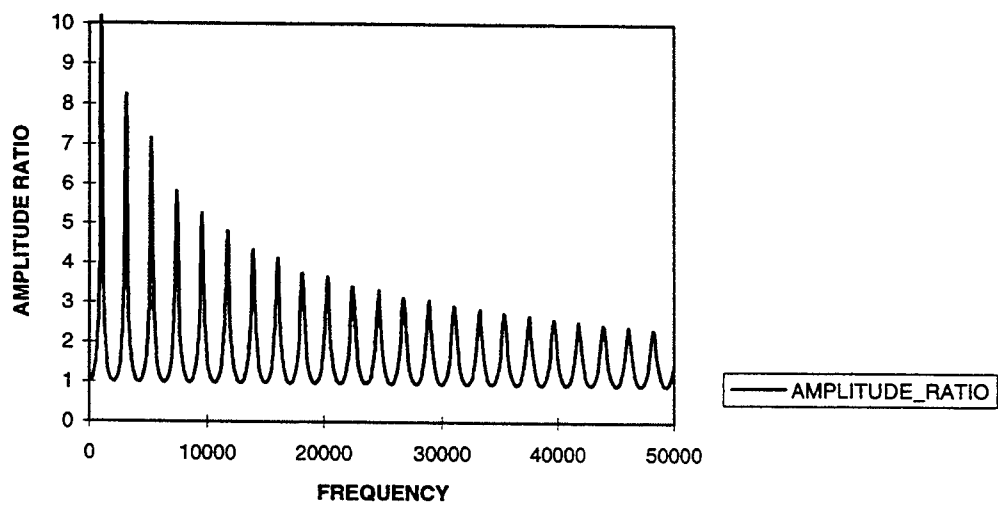


Fig.2

.030 inch tube

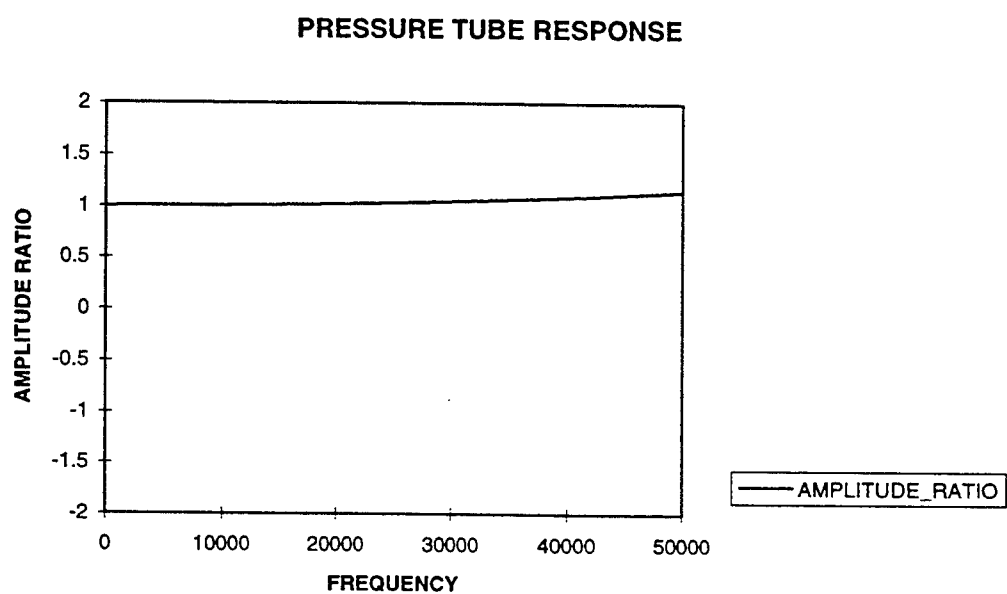
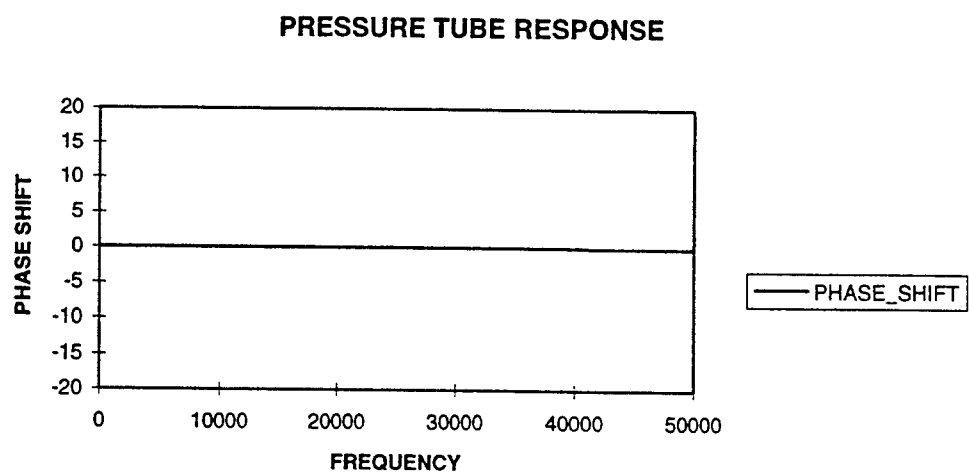


Fig. 3

.030 inch tube

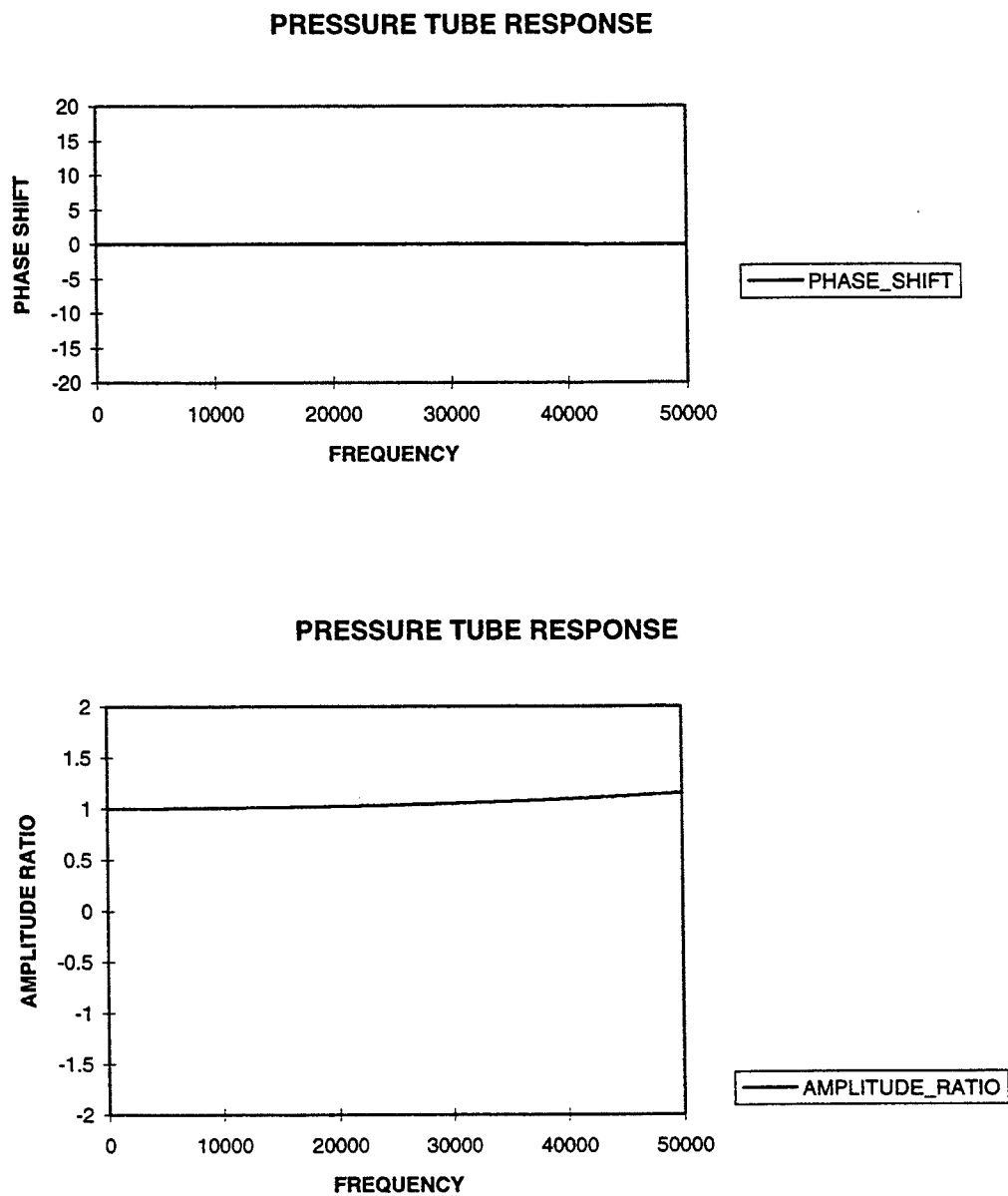


Table 1

Amplitude Ratio= 1.1

Length (in.)	Diameter (in.)	Frequency (hz.)
4.25	.062	300
.030	.042	41,400
.030	.093	41,600

The Preparation
and
Analysis of Carbon Fibers

Matthew T. Gudorf

Carroll High School
2309 Linden Ave.
Dayton, OH 45421

Final Report for:
High School Apprentice Program
Wright Laboratories

Sponsored by:
Air Force Office of Scientific Research
Bolling Air Force Base, DC

and

Wright Laboratories

July 1995

Abstract

The problem currently facing the Air Force is how to make a material light weight yet very strong. To use less material metals have been put through a series of processes to make them stronger and so less metal has been required but this is still too heavy for use in today's aircraft. The solution looks to be in the direction of using fibers imbedded in the material to greatly increase the strength but dropping the weight considerably. This process works very well but is still in the testing stages. The current tests being done are mainly on the fibers themselves which are tested in many ways. One such test was done on a set of fibers that were tested as received being the control group and another group were heat treated then they were tensile tested by adding increments of load until they failed. The fibers were then prepared and viewed to determine the reason for failure using a scanning electron microscope. The final step in the process was to analyze the data that was collected.

Fiber Testing

The fibers come from the manufacture on a spool and the fibers to be tested all come from the same spool. They are then cut into equal lengths and the group of fibers is divided into two. The one group will remain a control while the other group will be heat treated. The fibers to be heat treated were then subdivided into groups to be treated at different temperatures and for different durations ranging from 1000°C for 24 hours to 900°C for 100 hours. After the groups were removed from the furnace and allowed to cool they were tensile tested. This is a test which grips the fiber at each end and then adds increments of load until the fiber fails. Both the heat treated and control groups are tested in this manner.

During this test many different forms of data are collected. The stress at which the fiber failed is recorded or the U.T.S. in MPa 's. The Modulus is recorded in GPa 's and the failure site is recorded, the fiber failed in the grips, at the strain gage, or if the fiber shattered.

Fiber Preparation

After the fibers are removed from the grips they are saved by placing them onto a square sheet of glass making sure to keep them in order so that the data collected in the tensile test can be later matched up with the data to be collected when the fiber is viewed in the scanning electron microscope. A water soluble glue is used to keep the fibers in place. To mount the fibers such that their failure point is showing they must be mounted perpendicular. this is achieved by cutting a short solid cylinder made of Aluminum in half. The fiber can then be glued to one half of the cylinder using a conductive silver paint until about thirty fibers fit across the cylinder then the other half can be attached such that the

fibers are projecting straight up from the middle of the cylinder. (see fig 1)

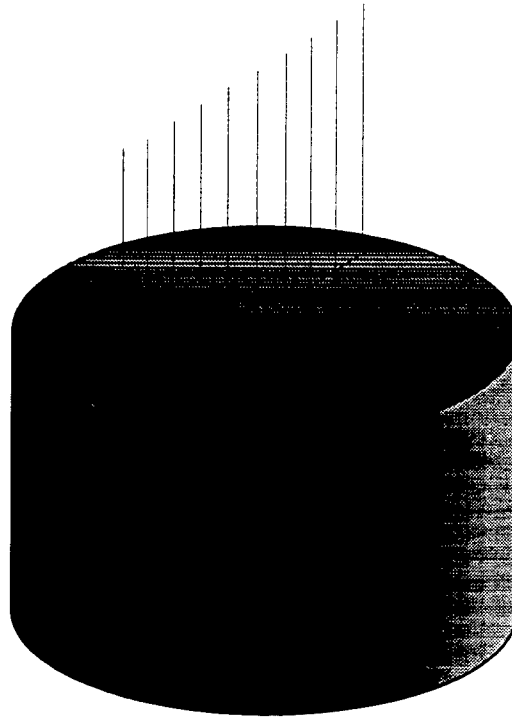


Fig. 1

Microscopic Analysis

The fibers are now viewed and the reason for the failure can be determined. Once the failure has been determined to be either internal or surface then this data can be recorded and used in the mathematical analysis called Weibull Analysis. The following pictures show the different flaws internal and surface.



Fig. 2

This is a surface flaw. It is very obvious by the reaction residue left on the top surface.

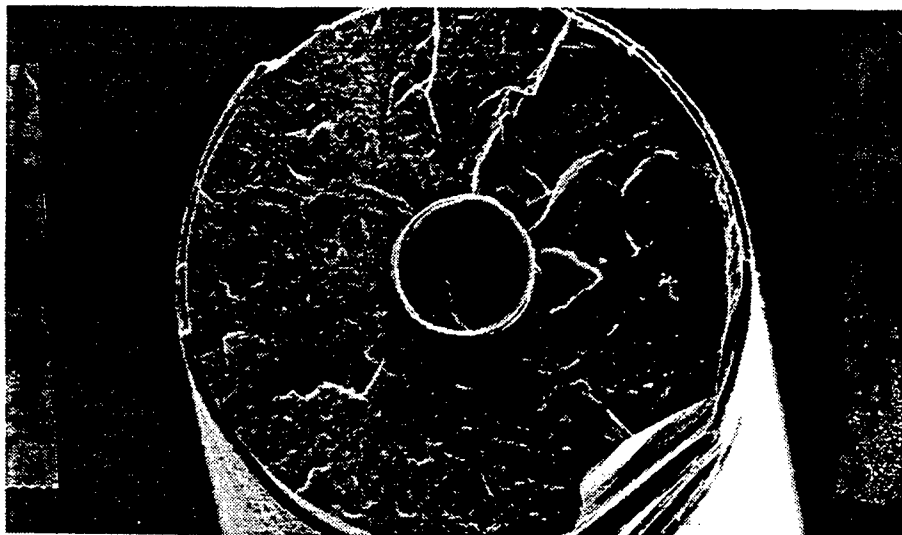


Fig. 3

This shows an internal flaw located in the bottom of the light stripe.

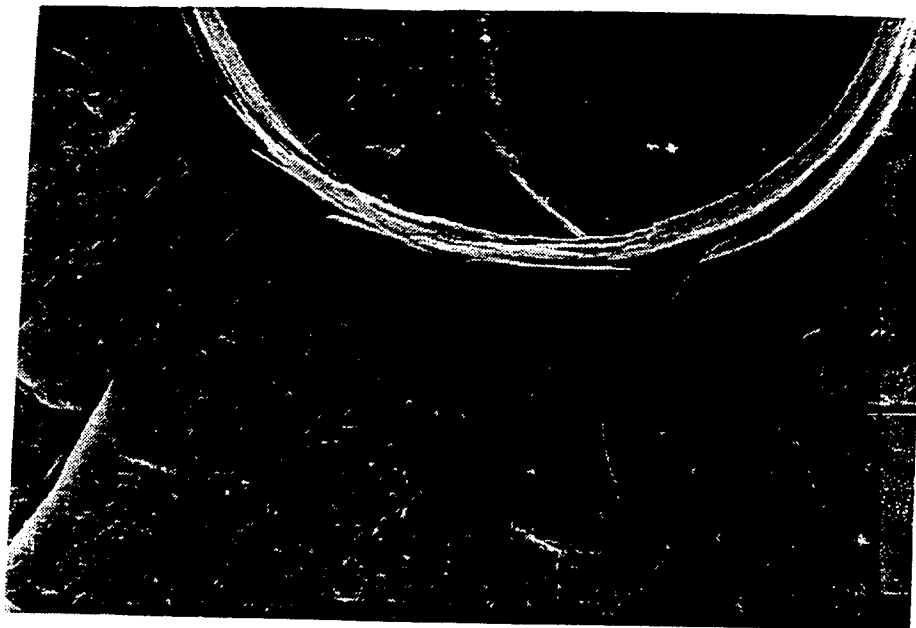


Fig 4

This is a high magnification photo of Fig. 3's internal flaw.

Analysis Of Data

The purpose of analyzing the data is to create a model that will predict the failure strength of fibers. The first step in analyzing the data is to sort the data such that all grip failures are removed from the data to be analyzed. The data is then sorted such that the U.T.S. stresses are in ascending order. From this you can calculate the probability of survival using this equation.

$$P_s = \exp \left[- \left(\frac{\sigma}{\sigma_o} \right)^m \right]$$

This equation however does not adequately represent the analysis done in a spreadsheet calculation the equations would break down like this:

Ps	1/Ps	LN(LN(1/Ps))	LN(Stress)	Stress/Stress σ
----	------	--------------	------------	------------------------

With the columns filled with a different value for each stress. When plotted to produce a graph the first graph plotted is the LN(LN(1/Ps)) vs. LN(Stress). If this line is a straight line and fitting a trendline to the data fits close to all of the data points then it may be hypothesized that only one type of flaw predominated in the fiber breaks. However if when the trendline is fit to the data it corresponds to only half the data then the fiber will appear to be bimodal. This is when there are to different types of flaws in the fiber a weak flaw, and a stronger flaw. If the fiber has the weak flaw it will be on one line of the data and if it has the other flaw it will be on the other line of data. This is best represented by a actual graph. (see Fig 5.)

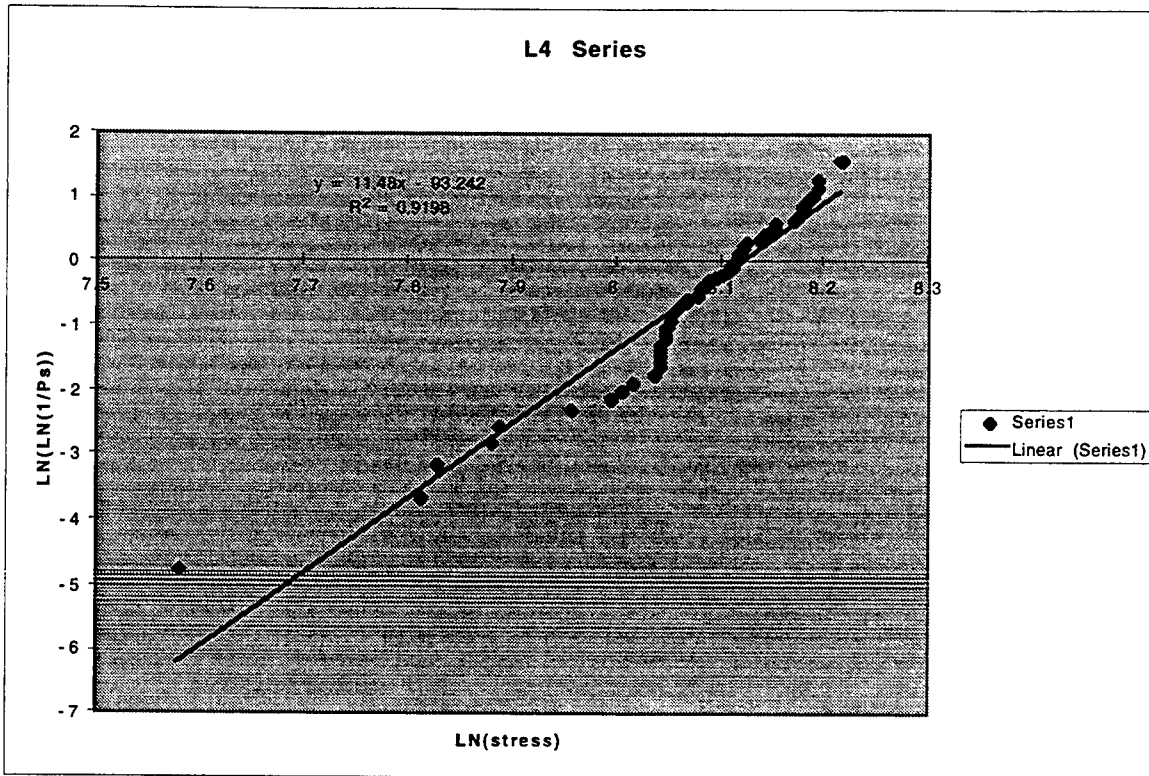


Fig 5

This graph shows two distinct groups of data, one fits to the line very well while the other is at a steep angle to the trendline. When Bimodal analysis is done using these equations:

$$1 - \exp \left[- \left(\frac{\sigma}{\sigma_{01}} \right)^{m_1} - \left(\frac{\sigma}{\sigma_{02}} \right)^{m_2} \right]$$

The above equation is the actual equation used but you must first solve for $M1$ and σ_{01} using separate equations. Once this is solved you can replot the data along with the bimodal line a overlapping or close fit denotes a true bimodal relationship. The graph below (Fig 6) shows a bimodal graph.

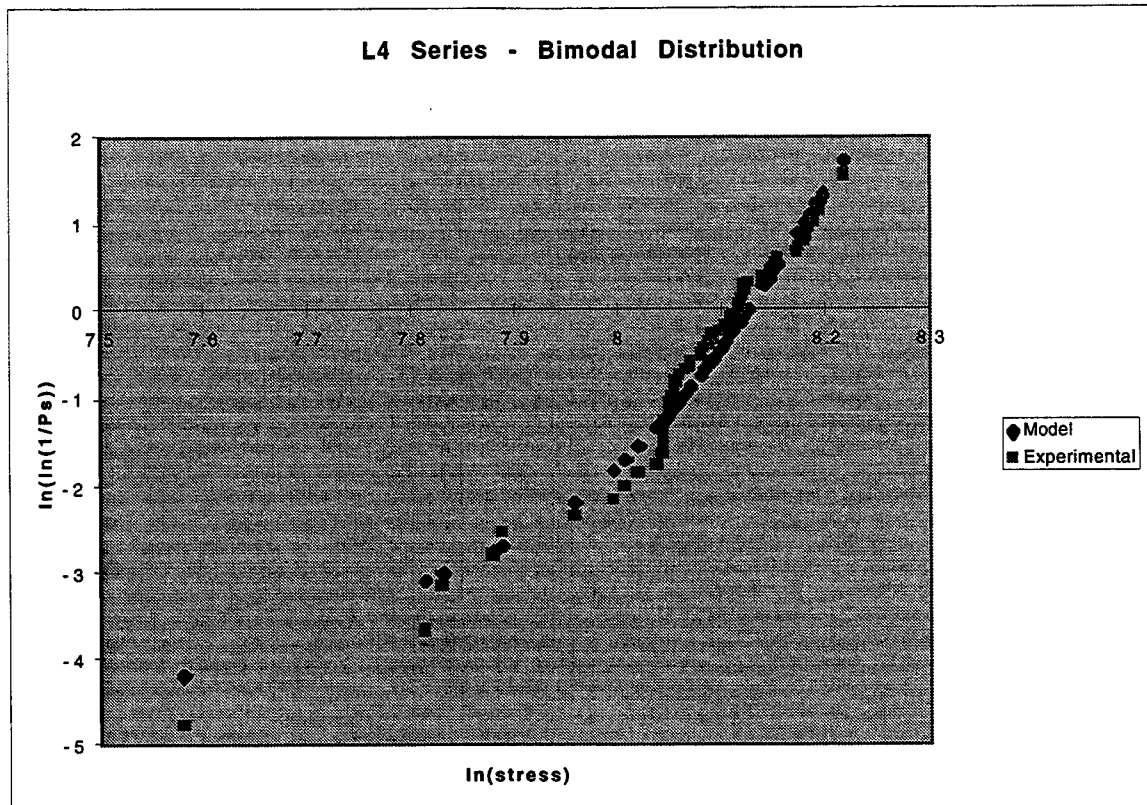


Fig 6

The final graph to be calculated is the graph of probability of survival vs. Stress/Stress σ .

This graph also creates a model that helps to show whether or not a fiber will fail at a given stress. (see Fig. 7)

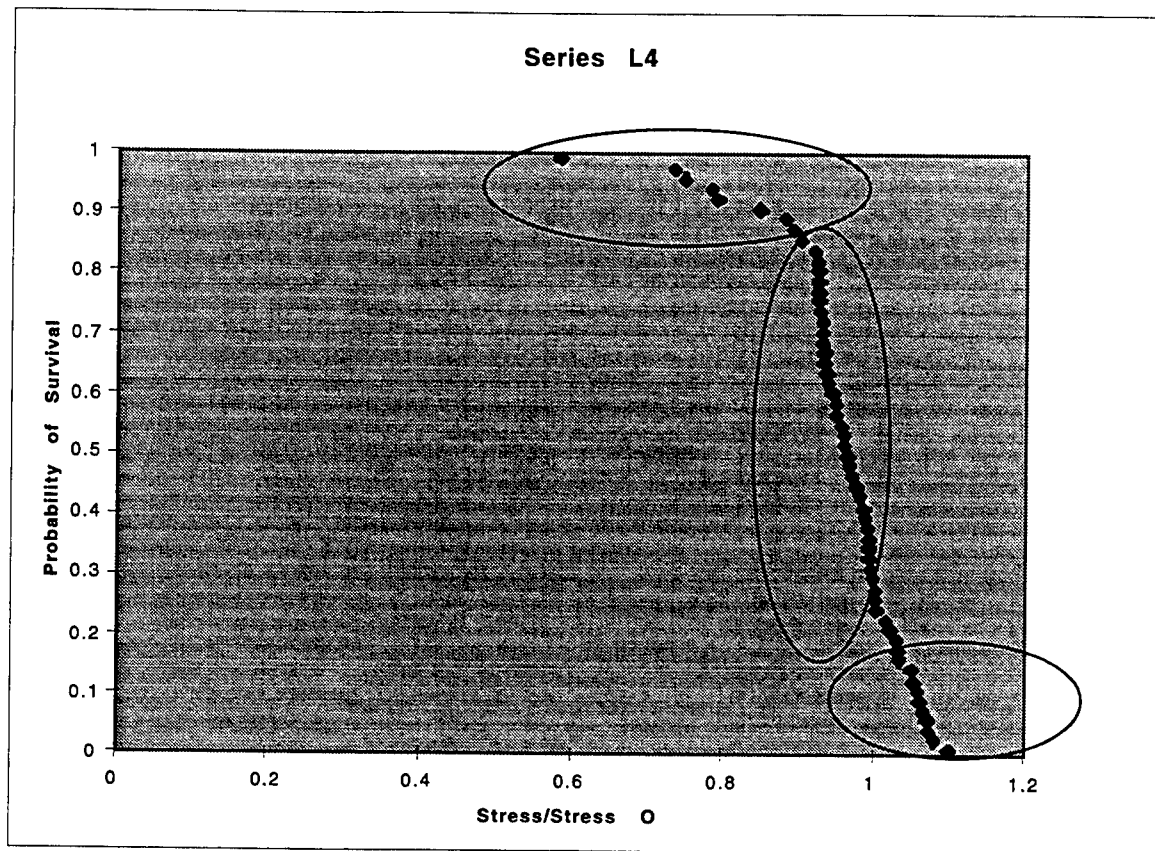


Fig 7

In the top circle the fiber has a high probability of not failing or it could be said this fiber in this area has a high probability of survival. The vertical ellipse shows the stress at which the fiber fails this line being very vertical depicts a definite stress at which the fiber fails. The third and lowest ellipse shown shows where the fiber has a high probability of failure and will probably not survive.

THERMAL EFFICIENCY OF A FLEXIBLE HEAT PIPE
SUBJECTED TO HEAT FLUX AND TRANSIENT
ACCELERATION ENVIRONMENTS

Shaun R. Guillermin

Chaminade-Julienne High School
505 S. Ludlow St.
Dayton, Ohio 45402

Final Report for:
High School Apprenticeship Program
Wright Laboratory

Sponsored by:
Air Force Office of Scientific Research
Bolling Air Force Base, DC

and

Wright Laboratory

August 1995

THERMAL EFFICIENCY OF A FLEXIBLE HEAT PIPE
SUBJECTED TO HEAT FLUX AND TRANSIENT
ACCELERATION ENVIRONMENTS

Shaun R. Guillermin
Chaminade-Julienne High School

Abstract

The effects of transient acceleration and heat input on a flexible heat pipe were studied. A flexible heat pipe was mounted on a centrifuge table to observe its response to combined variances in acceleration and heat in a simulated high performance aircraft environment. Heat input was transmitted via a heater in the evaporator section, while maneuvering was replicated by varying the frequencies of a sawtooth wave pattern in a low to high g setting. Dry out induced hysteresis can exist which produces two data sets for a given input. Thermal resistance was low for lesser heat values and/or higher frequencies. It was concluded that this particular heat pipe is more efficient at higher frequencies.

THERMAL EFFICIENCY OF A FLEXIBLE HEAT PIPE
SUBJECTED TO HEAT FLUX AND TRANSIENT
ACCELERATION ENVIRONMENTS

Shaun R. Guillermin

Introduction

1.1 History

As the use of technology to replace mechanical systems has rapidly increased in the last several decades, it has provided a wide new array of variables which must be taken into consideration in any operating system. One such problem is heat, both occurring as a function of the working environment and the processes taking place. A buildup of heat in an electronic component in an aircraft or satellite, for example, can cause malfunction or failure.

Even before the onset of the computer age researchers noted the need for ways to effectively transfer heat. In 1944 R.S. Gaugler made an attempt to solve this problem for General Motors by patenting a device to "...cause absorption of heat, or in other words, the evaporation of the liquid to a point above the place where the condensation or the giving off of heat takes place without expending upon the liquid any additional work to lift the liquid to an elevation above the point at which condensation takes place.'" Without realizing it, Gaugler had devised what would later be known as the heat pipe. However, other methods were used to solve the problem at hand and the concept was left undeveloped.

Later, in the 1960's, NASA researcher G.M. Grover independently invented a unit that utilized the same concept. This time, though, the promise of the heat pipe was realized. Soon, extensive research was being conducted worldwide. Major contributors included the Los Alamos National Laboratory and RCA in the U.S. and the Joint Nuclear Research Center in Italy. Over the years, a broad base of research was gathered and the heat pipe grew in its accessibility and applications (1).

1.2 Design and Operation

Scientists had reached a general consensus about the design of

the heat pipe as well, which has remained basically the same to this day (see figure 1). At one end is an evaporator containing the working fluid. The opposite end forms the condenser, and both are joined by a tube commonly known as the adiabatic region. Throughout the length of the heat pipe is a capillary wick structure formed by a thin wire mesh or gauze. When heat is applied to the working fluid at the evaporator end, it forms a vapor. The vapor flows through the tubing into the condenser, an area of lower temperature, where it cools down and condenses into its liquid form. That liquid is drawn back through the wick structure by means of capillary action. It rejoins the fluid in the evaporator to continue the ongoing cycle.

The heat pipe does however have its limitations, such as boiling, various pressure limits, drying out of the wick due to high temperatures and the effects of gravitational forces.

1.3 Contemporary Studies

Most recently, researchers are looking at wider applications for the heat pipe, including areas involving high g-loads. In the past, data was limited to forces of 1 g or less. With regard to today's high performance aircraft, though, greater analysis must be done concerning transient, not steady state, high acceleration loads. This is because of the effect that acceleration can have on the wicking height of the fluid within the heat pipe. Depending on the direction of the resulting gravitational pull, the returning liquid could be either pulled away from the evaporator or pushed towards it. If it was pulled away from the evaporator, the capillary limit would be greatly reduced, leading to poor heat transfer, less fluid in the region and even dry-out. On the other hand, a force acting in the opposite direction would force the liquid back to the evaporator and therefore increase the heat transfer of the unit. In a transient load situation, the effects could result in a combination of these factors due to the inertial properties of the fluid that become evident when acceleration is slowed and that fluid sloshes about the pipe.

In addition, as aircraft performance and maneuverability

increase, the limits of heat pipes will be under even greater scrutiny. Therefore, it is necessary to study areas where there is no data on heat pipe behavior and said behavior cannot be hypothetically modeled. One such area is that of acceleration and deceleration. A sudden change in speed resulting from an aircraft pulling out of a turn or a banking maneuver, for example, could possibly cause fluid to slosh around the unit as well as depriming the wick structure. Continued rapid patterns of deceleration may set up a wave-like condition in which the liquid sloshes back and forth, interfering with the efficiency of the heat pipe. In a worst case scenario, the pipe could fail altogether. Another possible phenomenon is the after-effects of dry out on performance. The chance exists that, when dry out occurs, a condition is created in which temperatures will return to a higher steady state than previously; i.e., when such heat measurements are recorded from the same experiment both before and after dry out, they would be drastically different. This would most likely be a result of the inability of the wick to completely re-wet itself in the presence of a continued heat input after dry out, therefore retaining some amount of heat. However, by starting the heat pipe "cold," there is no resistance to liquid/vapor transport and a different temperature would be recorded. By studying these behaviors now, it eliminates many unanswered questions and future problems.

2.1 Methodology

A flexible heat pipe was used for this investigation. The heat pipe itself utilizes three sections, the evaporator pad, heat pipe region and condenser pad. The evaporator is mounted to the evaporator pad. The condenser, with internal spiral grooves, mounts to the condenser pad. The flexible heat pipe region (adiabatic region) makes use of a braided copper cable to promote the return of liquid to the evaporator. This unit differs from the basic schematic in figure 1 in that it is flexible, and its shape matches the curvature of the edge of the centrifuge table. It is much longer, and has a larger condenser and evaporator area (see figures 2,3, and 4).

Experimental testing of the heat pipe was done on a 2.4m diameter centrifuge table, which produced the needed transient acceleration forces. A signal or wave form generator was used to control the angular velocity of the centrifuge. Monitoring of the time variant acceleration was done with a tri-axis accelerometer. It was necessary to mount the heat pipe in a way that would combine the radial and vertical acceleration forces, producing a transverse acceleration to the heat pipe axis (3).

The complete experimental test setup is shown in figures 5 and 6. Input instrument signals, coolant flow and electrical power were provided via slip rings and a rotating hydraulic joint. Data acquisition utilized a separate slip ring. Copper-Constantan thermocouples were used to monitor heat pipe temperatures. The milli-volt output signals from the thermocouples were converted into a 0-5 volt signal via a signal conditioner before leaving the centrifuge.

The maneuvering characteristics of a typical high performance aircraft must be simulated in this experiment. Therefore, the centrifuge is used as a tool to replicate the various acceleration forces induced by such conditions. The table serves two purposes: to take the place of an expensive, high maintenance jet airplane, and to provide a controlled environment as free of any extraneous factors as possible. In this case, testing involves a heat pipe that in theory would be located laterally in the wing of the aircraft, subject to axial and transverse acceleration forces induced by normal acceleration and rolling. This assumes that both of those forces, whether transient or steady state, could affect heat pipe performance (3).

The heat pipe requires a constant flow of an ethylene glycol/water coolant mixture across the condenser pad to aid in heat removal, and in order to properly determine the temperature of the condenser the coolant mass flow rate must be known. It is thus necessary to make flow calibrations based on the amount of coolant coming from the cool bath through the rotameter at a given setting and temperature (6). In this case, measurements were taken at cool

bath temperature setpoints of 0C, 20C and 36C, and at rotameter settings of 10, 20, 25, 30 and 40 for each temperature. The actual temperature of the coolant was also recorded for reference, due to the inability of the cool bath to cool within 1 to 3 degrees of the maximum and minimum setpoints of 0 and 36C. To facilitate measurements, a copper tube was installed on the outlet fitting of the rotameter and run back into the cool bath reservoir to create a closed system that the coolant could be drawn from. When the proper temperature setpoint had been reached, the flow setting was changed to 10. A container was placed under the return tube and a timer was immediately started. After approximately one minute the timer stopped as the container was removed. Then the container was weighed on an electronic top load balance and the mass recorded (data was corrected with respect to the weight of the container and any liquid residue that remained after being poured out). The process was repeated five times for each flow setting.

Later, the mass flow was calculated for every measurement by dividing mass by time. Using a regression analysis of each temperature, a general equation for mass flow could be derived. The original mass flow measurements were compared to a set of linear fit data based on those formulas. Percent error calculations were within +/- 4% in all cases except the 10 setting at 0 degrees C, which was within +/- 10% due to the small amount of fluid involved at that point. Figure 7 shows the mass flow plotted against the rotameter setting.

Then, that flow rate can be used to find the condenser heat flux using the formula

$$Q=MC_p(T_2-T_1) \quad (1.1)$$

where M denotes mass flow, C_p is the specific heat, and (T_2-T_1) represents the difference in temperature of the coolant entering and leaving the condenser pad.

The capillary wicking height of the fluid in the heat pipe is subject to two principal variables, its surface tension and the

force of gravity. This relationship can be expressed as

$$h = \frac{2\sigma}{R} \cdot \frac{1}{g(\rho' - \rho'')} \quad (1.2)$$

where h is the height of the fluid, or the wicking height, σ is the surface tension, g is the gravitational force, R represents the radius of curvature of the meniscus, and ρ' and ρ'' are the liquid and vapor densities, respectively. Wicking height varies directly with surface tension. As it increases (due to a decrease in temperature), so does the height. But, fluid levels are affected inversely with gravity. Therefore, by varying either or both factors experimentally, the wicking height can be controlled or altered.

As the centrifuge table spins, several acceleration induced forces play upon the performance of the heat pipe. Tangential and radial acceleration account for the majority of the behavior. Tangential forces are produced by the forward motion of the table, pushing the fluid towards the evaporator side. Radial forces, induced by the spinning of the centrifuge, pulls the fluid from the wick to the outside edge of the pipe. Combined, these forces can drain the liquid out of the wick and push it away from the condenser, adversely affecting performance. And, during transient acceleration, the slowing and speeding up of the table creates a fluid slosh that could also interfere in its behavior.

Experimental testing involved duplicating a pattern of acceleration and rapid deceleration with the centrifuge. This was done using a repeating sawtooth waveform with an amplitude from 1 to 10g. Frequencies were varied to 0.01, 0.05, 0.1, 0.15 and 0.2 Hz to control the rate of acceleration. Heat loading was done at 75, 100, 125 and 150 watts, and the coolant temperature was maintained at 35 degrees C. Temperature measurements were recorded from the outboard evaporator thermocouple.

To begin the experiment, the centrifuge was run at a constant slow speed at the specified heat input to achieve a steady state. The waveform generator specifications were tuned to 1.0v DC and

2.3v AC peak to peak to achieve the 1.0 g to 10.0 g peak to peak in radial acceleration. Frequencies began with 0.01 Hz and were increased after each period of steady state temperature. If dry out temperatures exceeded 100 degrees C, the function generator was set to the next highest frequency. This was repeated until a reasonable steady state could be reached. If temperatures continued to rise, the table was shut down and allowed to cool for a period of time. Then the experiment was restarted at the same frequency and allowed to reach steady state (6). As a result of dry out, certain experiments were re-run with the frequencies in the reverse order until dry out was again reached. Such a procedure was only required at 150W. Thus, two potential operating temperatures and thermal resistances can possibly exist for cases in which dry out occurs. (8).

3 Analytical

3.1 Waveform attenuation:

Graphs of the radial acceleration waveforms reveal a variance when compared to the waveform input signal (see figures 8 and 9). It is obvious that they are attenuated, and that the up-slope is "bowed" and the leg facing downward is at an angle. The "clipping off" of the bottom peak is the result of the dynamic limitations of the centrifuge table. The sawtooth wave is composed of many different waves, as given by the formula

$$\omega = \frac{1}{2} - \frac{1}{\pi} \sum \sin(2n\pi tf) \quad (3.1)$$

where frequency f is in Hz and ω is the angular velocity waveform (9). It propagates the series

$$\omega = \frac{1}{2} - \left(\frac{1}{\pi} \sin 2\pi tf + \frac{1}{\pi} \sin 4\pi tf + \frac{1}{\pi} \sin 6\pi tf \dots \right) \quad (3.2)$$

The motor which drives the table receives the sawtooth pattern and its speed is varied to mimic it. However, the mass and velocity of the table are so great that the motor cannot fully decelerate at

the end of each wave without losing momentum. In order to maintain the pattern, it must shorten each cycle, effectively "clipping" part of the formula in 3.2 and the waveform of the output acceleration signal (fig. 8). The attenuation occurs on the bottom of the wave because of its composition. As it is a composition of many waves, this particular area is one of high frequency, and when the ω series is clipped, it deletes a portion of the waves that constitute the lower peak area (6).

The "bow" and angle of the two legs is a function of the angular acceleration,

$$\alpha = \omega^2 r (3.3)$$

where r is the table radius and ω is the input signal (7). Squaring the sawtooth ω produces a curvature (much the same as in one side of a parabola) as well as offsetting the bottom intercept of the vertical component. As the input frequency increases, the wave is compressed and the vertical leg is now at a greater angle.

This attenuation results in the minimum acceleration peak being higher with each frequency increase. As a result the heat pipe is not experiencing the full exposure of 1 to 10 g at the higher test frequencies ($f \geq 0.05$ Hz) (6).

3.2 Surface tension/wicking height:

Increased temperatures inside the heat pipe cause the surface tension of the working fluid to decrease. With this comes a decrease in wicking height which also harms the performance of the heat pipe. As the g-load increases, the wicking height is decreased. Thus, the faster the acceleration cycle is completed, (from minimum to maximum back to minimum), the greater the working fluid "sloshes" due to the rapid increase and decrease in wicking height. Combined with high heat loads, performance can be seriously handicapped. Recall the formula

$$h = \frac{2\sigma}{R} \cdot \frac{1}{g(\rho' - \rho'')}$$

3.3 Dry out:

Dry out of the wick can come from a combination of heat input, acceleration, waveform and frequency, and coolant temperature. In this case the onset of dry out is denoted by a sharp temperature gradient between the outboard and inboard evaporator thermocouple locations. In most cases, temperatures will reach a steady state, but with high wattage, low frequency settings, dry out will continue up to or beyond 100 C, at which the frequency must be increased or the test shut down.

A hysteresis is noticeable as a characteristic of dry out. After dry out, temperatures will not return to the same levels when the function generator is reset to the frequency before that which resulted in the dry out. Thus, temperatures at the same frequency before and after dry out will, in most cases, not be the same (8).

4 Results:

Figure 9 shows the various waveforms at frequencies of 0.01, 0.05, 0.10, 0.15, and 0.20 Hz. Attenuation is noticeable starting from 0.05 Hz onward. Small spikes and the "rough" texture of the waves can be attributed to electrical noise and vibrations from the table picked up at a high sampling rate set to capture these waveforms.

The first data set, 75W, can be seen as figure 10. Temperatures remained generally at a steady level through all frequencies. The condenser section is subject to a temperature fluctuation on the order of about one degree, in a waveform the reverse of that which was input to the table. At 0.05 Hz, however, attenuation caused by the limits of the thermocouple response time prevents the phenomenon from being observed further. Adiabatic temperatures are midrange between the condenser and the evaporator, and all three follow the same trend, slight reductions in temperature as frequencies increase. The sharp drop off at the

tail of the graphs denotes the point where the heat input was shut off.

The next increment (fig. 11), 100W, shows relatively the same response as at 75W but with slightly higher temperatures (about 4 degrees). Again, attenuation and waveform are visible.

Figure 12 shows the onset of dry out conditions at 125W, beginning at 0.01 Hz and continuing through 0.10 Hz. The situation is resolved at 0.15 Hz and further cooling occurs at 0.20 Hz. Maximum temperature did not exceed 63 degrees C. Condenser and adiabatic temperatures remain essentially at steady state.

The experiment was run twice at 150W because of the dry out encountered. The first was in standard order (0 to 0.20 Hz) and the second was reversed (0.20 to 0.01 Hz). Standard order can be seen as figure 13a, the reverse as 13b. Evaporator temperatures began to rise sharply at 0.01 Hz and continued upwards. Frequency had to be adjusted to 0.10 Hz before a steady state could be reached. At 0.15 cool down began, continuing past 0.20 Hz. Maximum temperatures were above 100 degrees Celsius. Condenser and adiabatic temperatures remained steady. On the second run, observations of the temperatures were made for comparison to those of the first. Steady state temperatures were reached quickly at 0.20 and 0.15 Hz. Dry out occurred at 0.10 Hz and the experiment was shut down at 97 degrees C. Again, adiabatic and condenser temperatures were steady. Comparison of a and b temperatures reveals the presence of a definite dry out related hysteresis. A gradient of nearly 20 degrees exists at 0.20 Hz, while temperatures at 0 Hz were both 54.3 degrees.

Figure 14 is a graph of the thermal resistance plotted against frequency. As expected, 75W and 100 W were the most effective heat inputs followed by 125W. At 125W, the thermal resistance after 0.15 Hz closely matches that of the previous two. The final inputs, 150W, represent the two separate runs and the effects of the hysteresis. The plot of the increasing frequency shows degraded performance. However, the plot of the reverse order is somewhat better. At 0.10 Hz, thermal resistance is lower than the

increasing order, and the downtrend at 0.15 Hz is sharper. At 0.20, the graph has returned to almost the same position as those of 75, 100 and 125W.

5 Conclusions:

Based on the previous data, it is obvious that acceleration and heat input influence heat pipe performance. Figure 11 shows that low frequency application has an adverse effect on efficiency, all thermal resistance figures decrease as frequency increases. Combined with high temperatures, low frequencies create very poor heat transfer capabilities. At 0.10 Hz, a gradual reduction in thermal resistance occurs, most likely as a result of the higher frequency. Another downtrend, although not as great, is evident past 0.15 Hz, again a point at which frequency was increased. Sudden, transient acceleration loads in a saw tooth pattern are beneficial to heat pipe performance at all heat loads, while slower transient acceleration as appropriate at low to medium heat loads. This is may be a result of the fluid slosh that is produced by slower acceleration; the working fluid is slowly pushed towards the condenser and away from the evaporator where it is needed, and because of this speed that fluid is held at the condenser longer by the acceleration induced forces. Whereas, at higher frequencies (0.10 Hz upward) the fluid is sloshing at such a high rate that only a small portion is being kept from the evaporator at any given time. The fluid is "held" at the condenser for a much shorter period of time. Furthermore, recall the high frequency waveform attenuation. As this becomes more and more prominent, the acceleration range from peak to peak is decreased, which eliminates a portion of the low g exposure and therefore the harshness of the slosh.

Another phenomenon that stands out is the presence of the dry out induced hysteresis at 150W. The decreasing order of frequencies is much more efficient than the increasing order by almost 100 percent (at 0.15 Hz). However, in a real world application, one can never be certain that frequencies will progress from high to low in such a situation, thus preventing the

hysteresis and providing better thermal resistance. The two cases must always be taken into consideration together, especially in the case of a high performance aircraft where acceleration patterns are never set.

References

- (1) Dunn, p. and Reay, D.A. Heat Pipes. Oxford; Pergamon Press, 1982.
- (2) B & K Engineering, Inc. Heat Pipe Design Handbook, Volume 1. Towson, Md; National Technical Information Service, 1979.
- (3) Yerkes, Kirk L. and Beam, Jerry E. "Arterial Heat Pipe Performance in a Transient Heat Flux and Body Force Environment." Wright Laboratory, Wright Patterson Air Force Base, Ohio 45433, U.S.A.
- (4) Kestin, Joseph. A Course in Thermodynamics, Volume 1. U.S.A.; Hemisphere Publishing Co., 1979.
- (5) Dr. Kirk Yerkes, Personal Interviews, July-August, 1995.
- (6) Bueche, Frederick. Introduction to Physics for Scientists and Engineers. U.S.A.; McGraw-Hill, Inc., 1969.
- (7) Dr. Scott Thomas, Personal Interviews, July, 1995.
- (8) Selby, Samuel M. Standard Mathematical Tables. , Cleveland, Ohio; The Chemical Rubber Co., 1973.

figure 1: Principles of heat pipe operation.

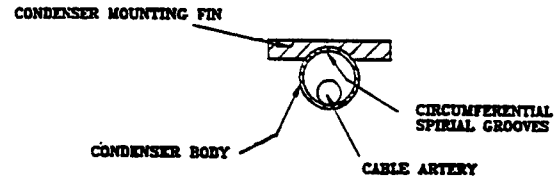
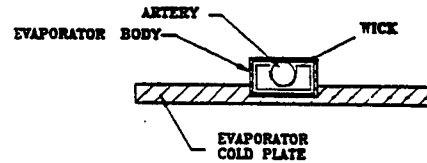
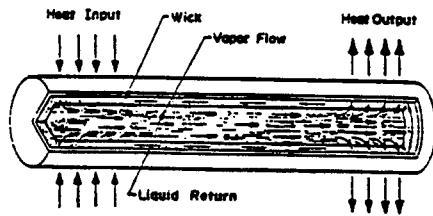


figure 4: Cross section of evaporator and condenser.

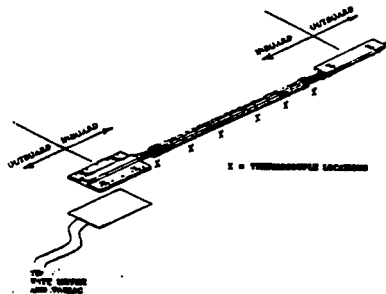
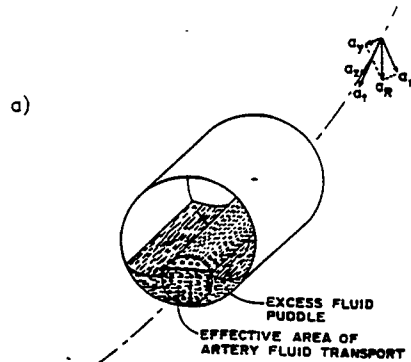
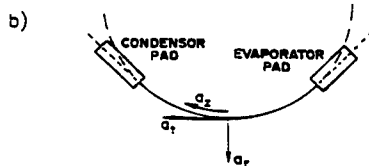


figure 2: Design of the heat pipe used in experimental investigation.

figure 3:



a) Puddle formation resulting from transverse acceleration;



b) heat pipe-to-table mounting schematic.

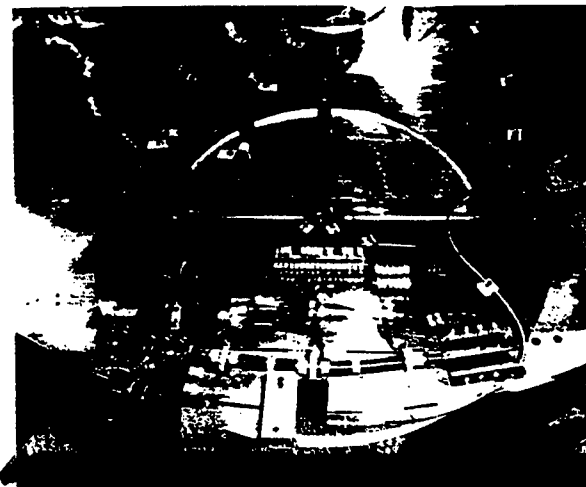


figure 5: Heat pipe mounted on centrifuge table.

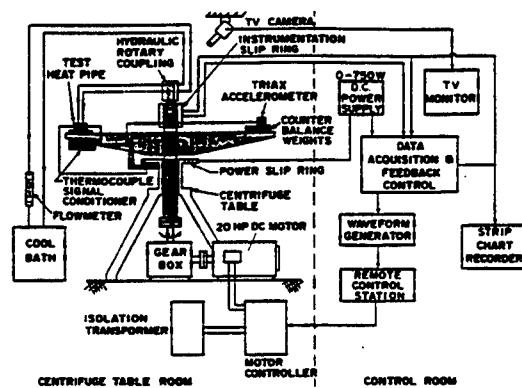


figure 6: Centrifuge schematic.

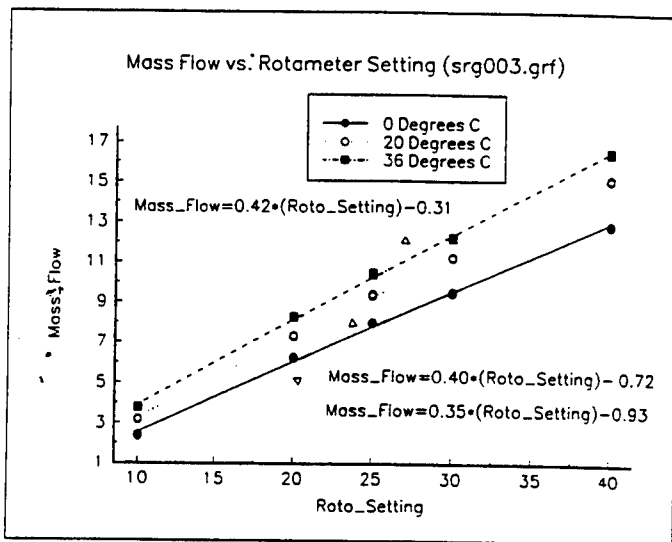


figure 7.

figure 9.

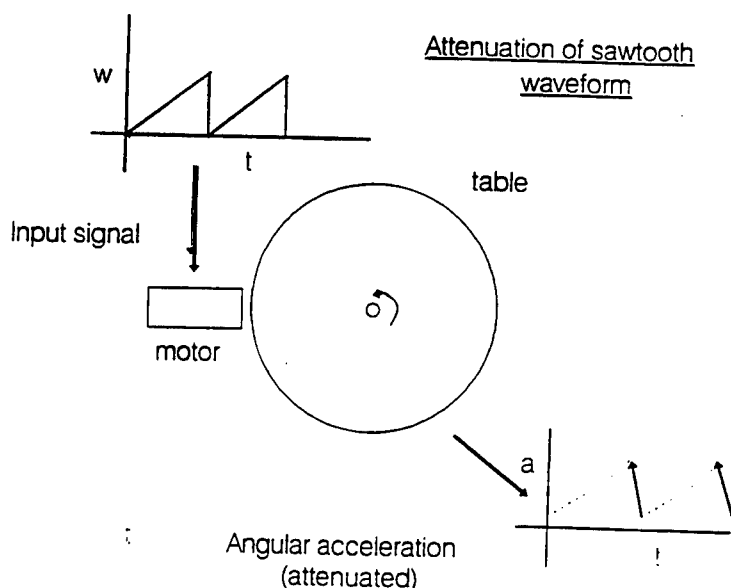
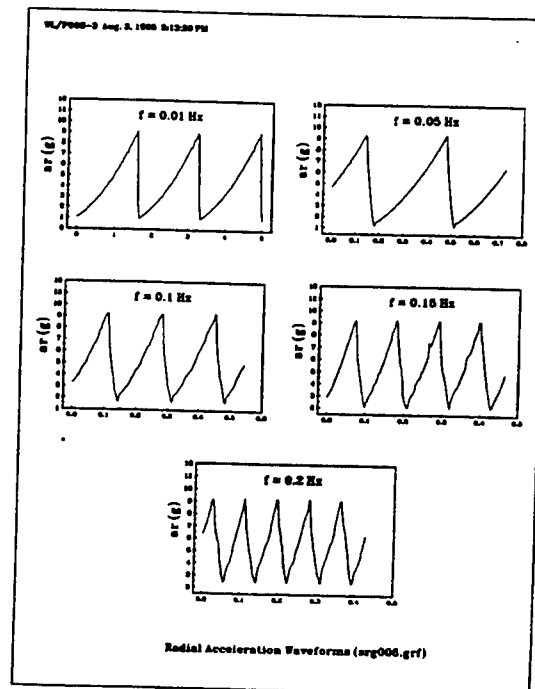


figure 8.

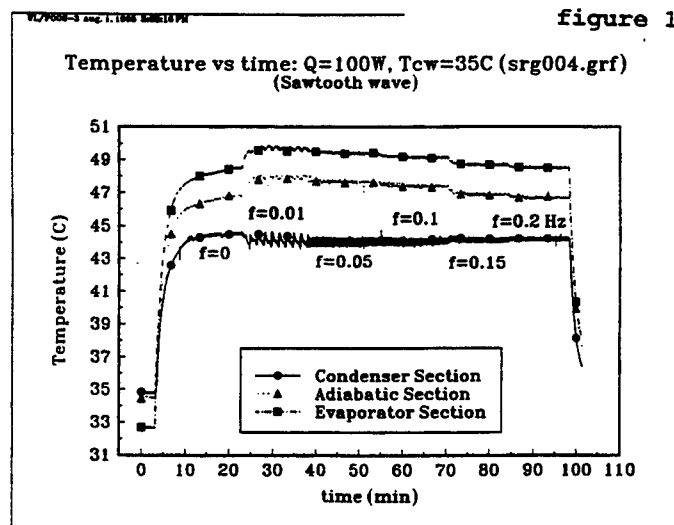
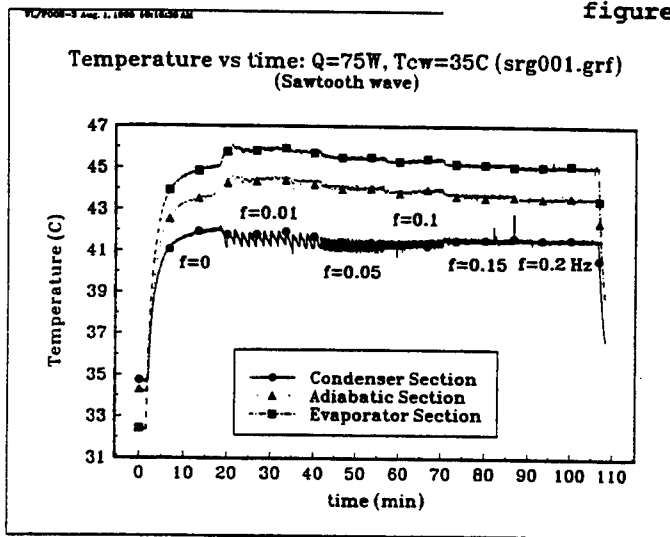
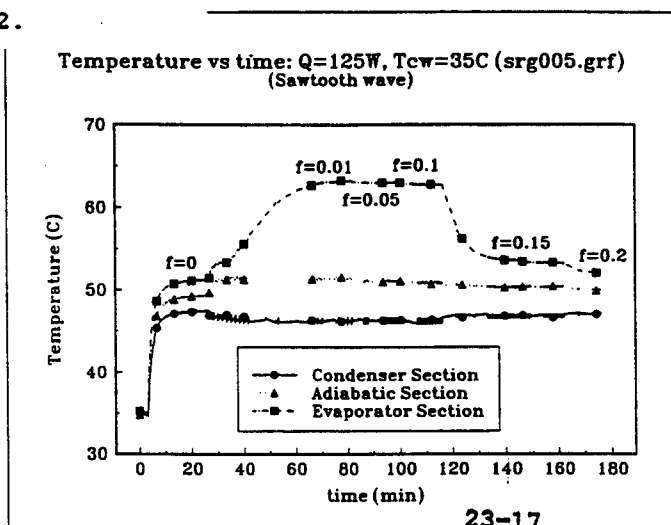


figure 12.



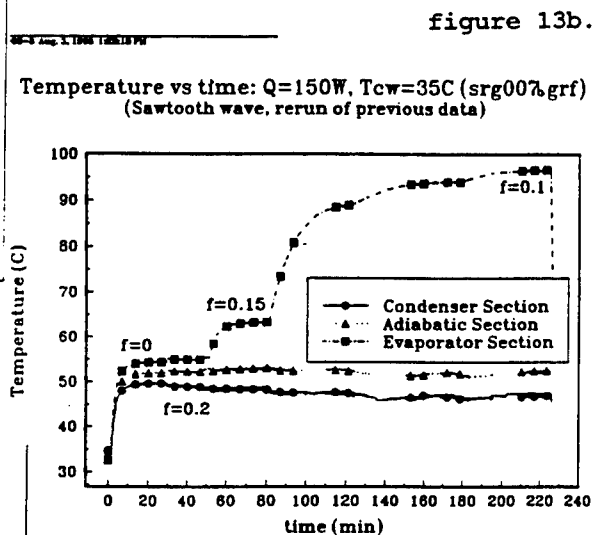
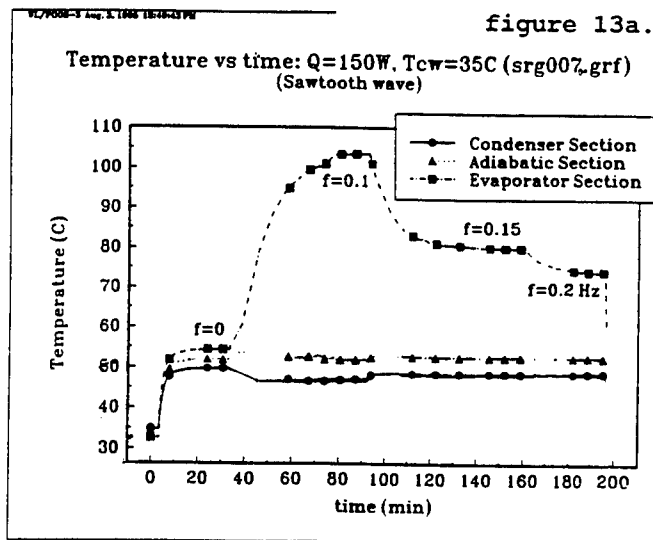
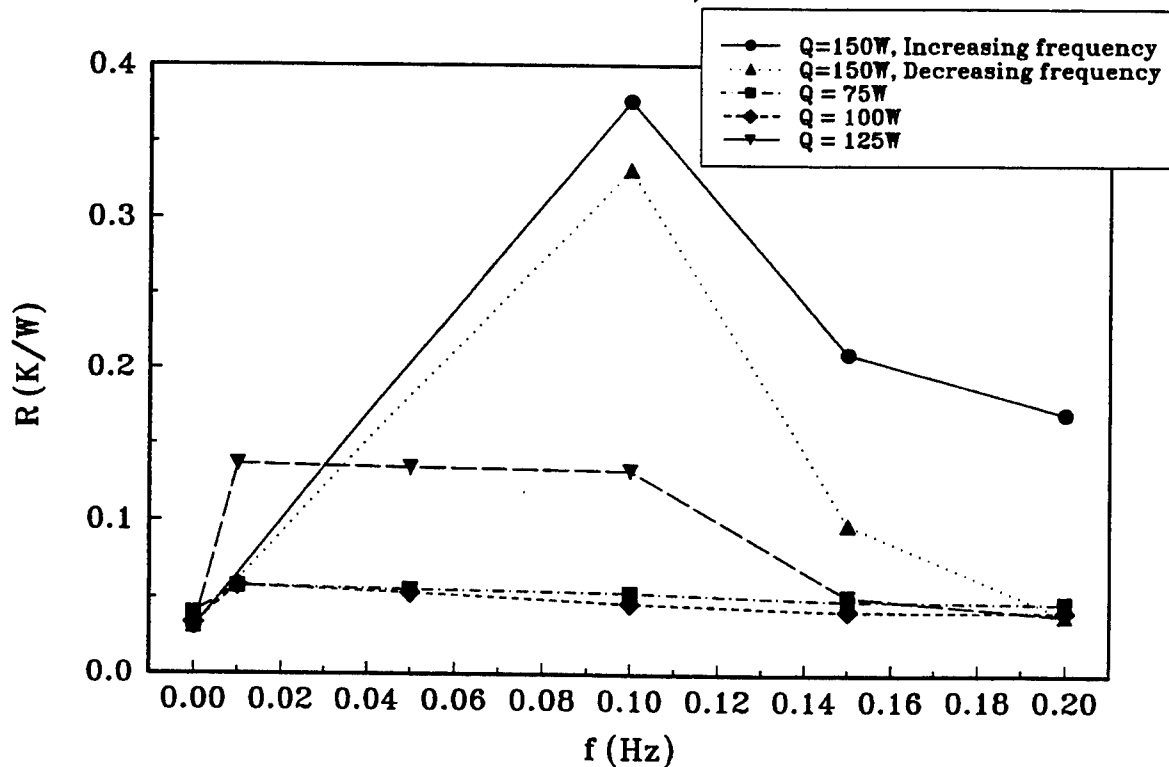


figure 14.

Thermal Resistance vs Frequency for $Q = 150\text{ W}$ (srg011.grf) (Sawtooth wave)



Precision Positioning Components for 3-D Holographic Reconstruction

David B. Hernandez

Freeport High School
Kylea Laird Dr.
Freeport, FL 32439

Final Report for:
High School Apprenticeship Program
Wright Laboratory

Sponsored by:
Air Force Office of Scientific Research
Bolling Air Force Base, DC

and

Wright Laboratory

August 1995

Precision Positioning Components for 3-D Holographic Reconstruction

David B. Hernandez
Freeport High School

Abstract

The Instrumentation Technology Branch (MNSI) of the Wright Laboratory Armament Directorate is involved in developing and evaluating new and better ways to accurately depict warhead/target interaction. One of these ways is by developing and making holograms of the warhead as it interacts with a target. Current methods are inadequate in providing reliable data on such things as the fragment mass, shape, orientation, and velocity. A new method that has been developed is a holographic technique to capture 3-dimensional images of the warhead/target interaction and the ensuing results of that interaction. The end product is a cylindrical 3-dimensional image that can be tilted, rotated, and digitally photographed to obtain the best possible image for analysis.

The aim of this project is to develop a computer program that automatically initializes, runs and controls all of the equipment used to reconstruct the holograms that provides and collects data of the debris field which results from warhead/target interaction. This project is required to provide a good, understandable interface for a user to control the equipment used in the holographic reconstruction process. Without this interface, valuable man hours are spent running numerous computer programs that independently run and control individual sections of the reconstruction process. The goal of this project is to eliminate the redundancy of so many computer programs and combine them into a single master program which runs everything.

Precision Positioning Components for 3-D Holographic Reconstruction

David B. Hernandez
Freeport High School

Introduction

This project dealt with computer software programming to control precision positioning components and systems for 3-D holographic reconstruction. An electronic camera is being used to digitize a series of 2-D images into a Sun Computer Workstation. These 2-D images are captured from a reconstructed hologram using the electronic camera. After a series of these 2-D images are taken of a single hologram they are then compiled in the Sun Computer Workstation to form a 3-D computed model of the hologram, which depicts a projectile as it penetrates an armor plate. The holograms that are taken clearly show the debris and exactly how the projectile interacts with the armor plate. The objective of this project was to write a program in LabVIEW that automatically initializes and controls all of the equipment used to reconstruct the holograms. Once this objective is accomplished the setup is to be used to reconstruct several holograms using the main program to control all of the equipment.

Discussion of Problem

The problem was that there was no main computer program that provided an efficient means to initialize and control the equipment that reconstructs the hologram. There were several different computer programs that had to be run in order to simply initialize the motion control boards. What needed to be done is all of those computer programs had to be combined into one main program that did everything, did it well, and provided an easy to use interface for the user. The stepper motor controller, which is what physically runs the equipment, also had to be modified using this program.

Currently the way each stepper motor controller works is it's current position during startup is it's home position (a numeric position number of 0). This is using an absolute scale. One can tell it to move to a position of 95 (i.e. 95 steps or degrees depending upon what virtual instrument (vi), or program, you are running) and it will move one direction until it reaches the target position, in this case 95. In order to reverse the direction the program must be told to move the stepper motor to a position less than the current position (i.e. current position is 95, tell the program to move the stepper motor to a position of 45, or back 50 steps). The stepper motor will not move beyond it's home position and that means negative numbers will not work. Thus far this was the only way to reverse the direction of the motion control, unless the stepper motor reaches it's maximum position (i.e. 360 degrees on a rotary table), in which case it will automatically reverse direction and start back to it's home position of 0. This is due to the stepper motors limit switch which limits the max steps able to be taken, or the max position attainable. This was another problem that needed to be solved.

Methodology

The first objective of my research project this summer was to learn LabVIEW. LabVIEW is a graphic user interface (gui) programming language designed primarily to initialize, setup and control the movement of lab equipment such as cameras, lasers and rotary tables. Toward this endeavor I was given a hands-on tutorial book on LabVIEW. It was filled with lesson after lesson with exercises designed to teach someone completely ignorant of LabVIEW how to program well with LabVIEW. For the next three weeks I worked my way through the lesson's in order to learn how to program with LabVIEW. Once I completed the tutorial book I was very proficient at programming with LabVIEW. After three weeks of learning LabVIEW I was moved to the Instrumentation Research Facility at Bay 10. It is at Bay 10 that the holograms are made and reconstructed.

The goal at this time was to write a virtual instrument (vi) program using LabVIEW. This program was to be written so that it automatically initialized the two motion control boards in order to control the movement of the camera and the rotation of the reconstructed hologram. The first motion control board, identified as slot #1, is used for the hologram rotary table which revolves around a single axis. This first motion control board has two axis, but only axis #1 is being used. The second motion control board, identified as slot #2, is used to control the cameras movement along the XY axis and the cameras rotation around the Z axis. The second motion control board is a three axis board where axis #1 is the X axis used to move the camera along the X axis, axis #2 is the Y axis used to move the camera along the Y axis, and axis #3 is used to rotate the camera around the Z axis.

The holograms at Bay 10 were made using a ruby pulse laser that has a wavelength of 694 nm. The film that is used to capture the image is first cut and placed in a cylinder 180 degrees around the cylinder. The cylinder is then placed in front of the projectile launcher so that when the projectile is fired it's flight path would take it straight through the center of the cylinder. A single pulse from the ruby pulse laser is then shot to record the image of the projectile as it penetrates the target, normally an armor plate.

As the laser light floods the area within the cylinder, the laser light reflects off of the projectile, the armor plate and all the debris generated from that interaction. The light reflected from the projectile and the debris is called the object beam and as it reflects back it interferes with the incoming laser light, called the reference beam. This interference is captured on the film and is what creates the hologram. A hologram is simply a 3-D representation of an object using light waves to reconstruct the image by the interference of an object beam and a reference beam. Once the hologram is developed and viewed the debris from the warhead/target interaction can be clearly seen and analyzed.

The following list is a list of equipment that was used for this project. The high power laser diode, with a wavelength of 688 nm, is used to illuminate the film in order to view the reconstructed hologram. The electric camera is used to take 2-D black and white pictures of the reconstructed hologram so the debris from the armor plate can be analyzed. The rotary turn table is used to rotate the hologram, and the XY stepper motion control is used to move the camera along the XY axis. The LabVIEW program was written on a 486 DX2/33 PC which is also the computer that contains the motion control boards that control all of the hologram reconstruction equipment. The Sun Computer Workstation is used to compile all of the 2-D pictures of a hologram into a 3-D computed model to view the placement of debris from the armor plate and collect other data.

Results

The results of this project are that the programming language LabVIEW was learned, the final computer program that was written in LabVIEW is able to control the equipment used to reconstruct the hologram. The setup that was designed and used works excellently. This setup has been used successfully to reconstruct several different holograms. The electronic camera was used to take 2-D pictures of the reconstructed hologram to view the debris field, and the Sun Computer Workstation can now be used more effectively to analyze and compile the data gathered from the reconstructed holograms.

Conclusion

The conclusion of this project is that the final LabVIEW program can be used as the control for all of the equipment used to reconstruct the hologram at Bay 10. This setup can now be used to take an already made hologram, reconstruct it, examine it, take 2-D pictures of the hologram and then store those to analyze the placement of debris. This setup is also capable of organizing and sorting vast amounts of data to be sent to warhead and target analysts so they can determine the effectiveness of the projectile, of the armor used, the lethality of the projectile and numerous other areas of research. This will greatly reduce the number of man hours spent preparing the setup to reconstruct and analyze holograms.

HOLOGRAPHIC RESEARCH AREA (BAY 10)

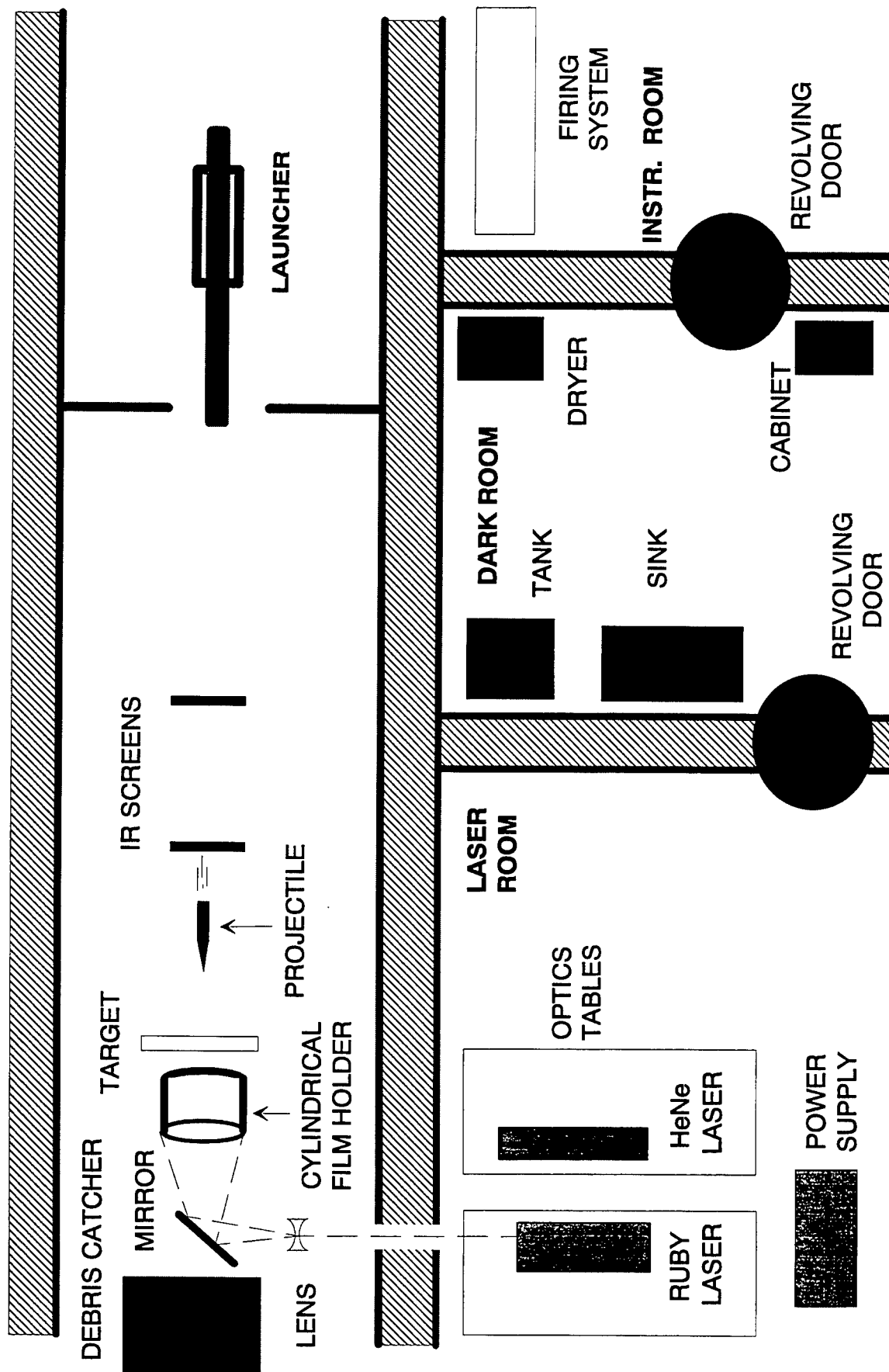


Figure 1. Holographic Research Area

HOLOGRAPHIC IMAGE RECONSTRUCTION MEASUREMENT SYSTEM (HIRAMS)

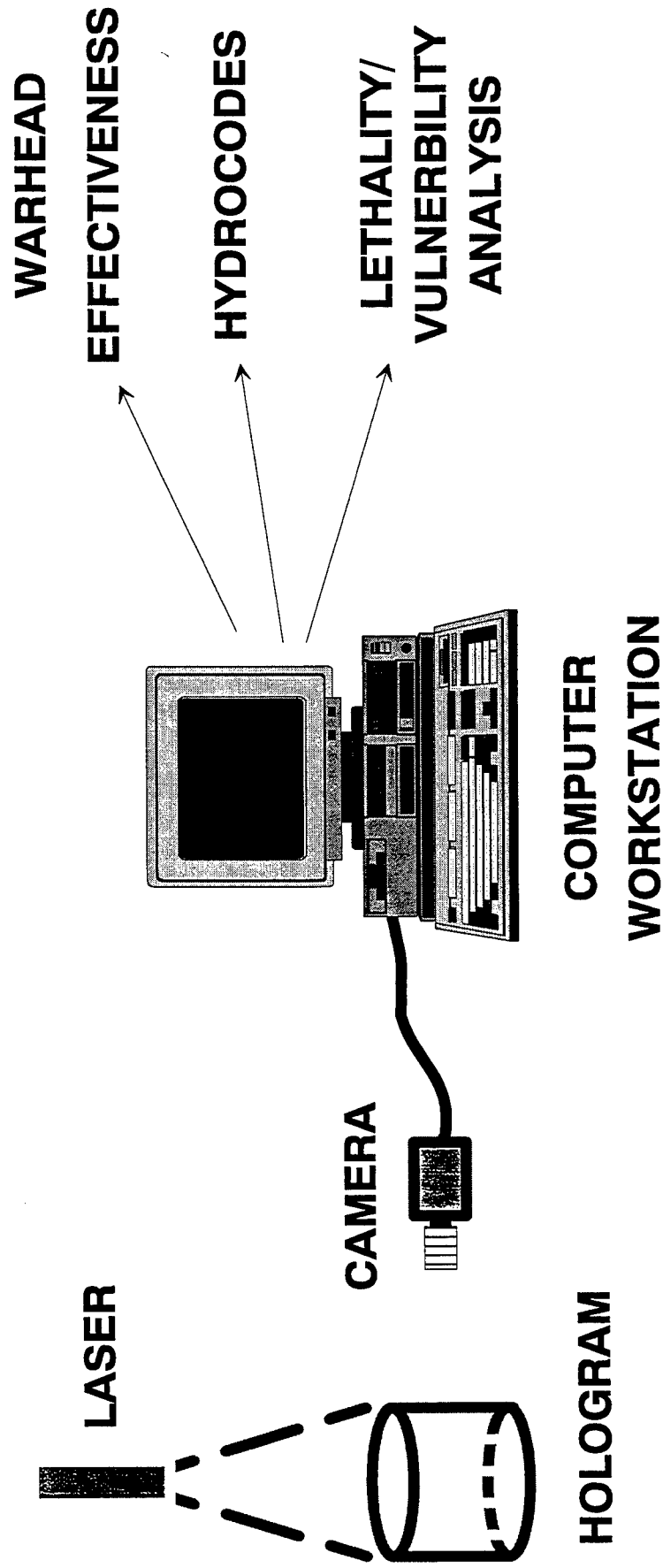


Figure 2. Data Reduction System

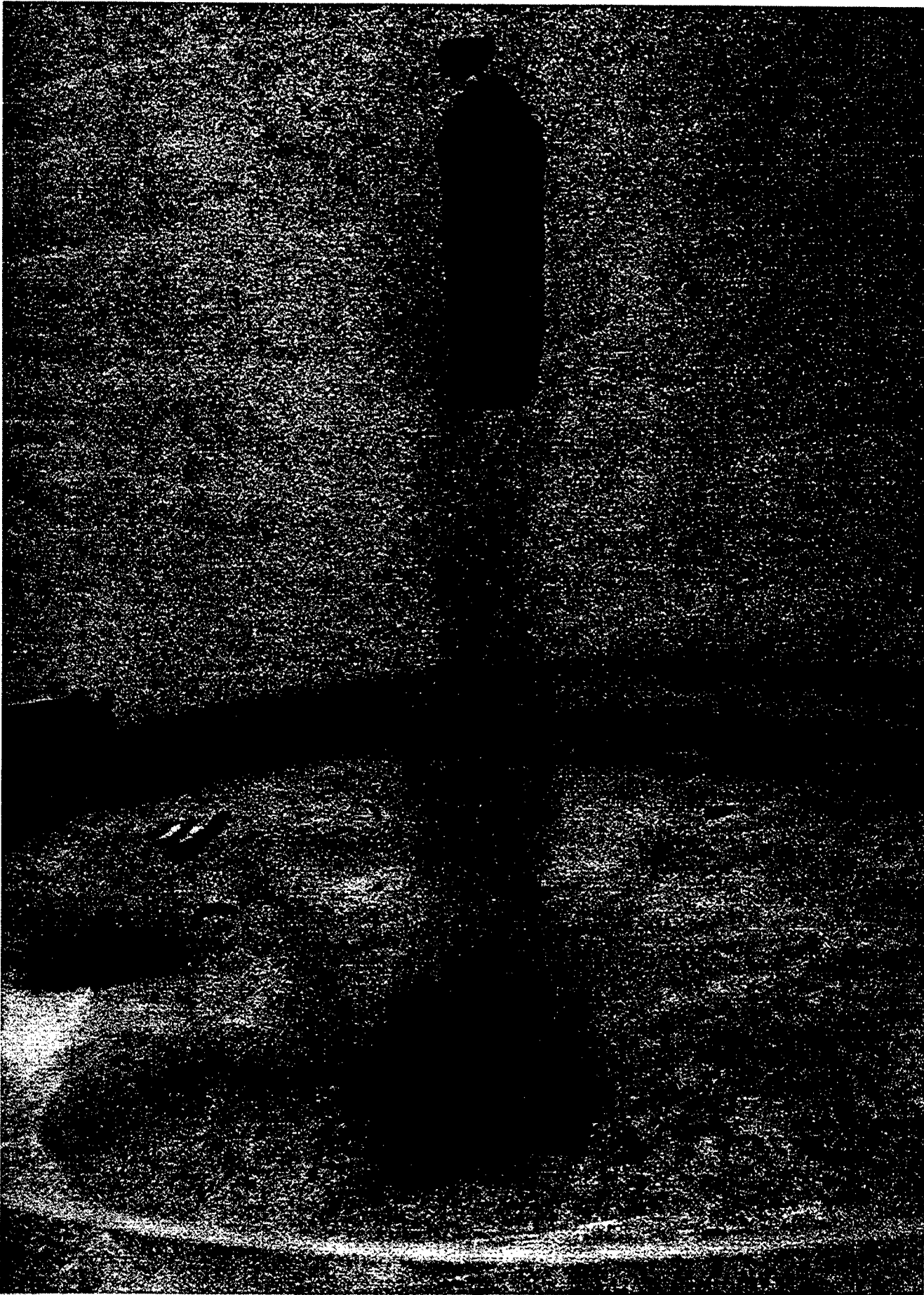


Figure 3. Cylindrical Hologram of 50 Cal. Projectile Perforating Armor

Acknowledgments

I wish to thank the following people for their help and support this summer: David Watts, my mentor who kept me focused and was always willing to explain anything to me; Joseph Gordon, who showed me the ropes and taught me all that I needed to know about holograms; Voncile Ashley, who showed me how to develop the holographic film and how things were done at Bay 10; Jim Marsh, who was always there to give me new insight into the world of physics; Dave Smith, who showed me how images were captured and reconstructed using a computer; Don Harrison and Mike Deiler, for running the HSAP Program and giving high school student's the opportunity to be involved in such a rewarding program; and everyone in MNSI for always being there to lend a helping hand.

DECOMPOSITION OF ENERGETIC MATERIALS
USING SODIUM HYDROXIDE

Venessa L. Hurst

Walton High School
555 Walton Road
DeFuniak Springs, FL 32433

Final Report for:
High School Apprenticeship Program
Wright Laboratory

Sponsored by:
Air Force of Scientific Research
Boillings Air Force Base, DC

and

Wright Laboratory

August 17, 1995

DECOMPOSITION OF ENERGETIC MATERIALS USING SODIUM HYDROXIDE

Venessa L. Hurst
Walton High School

Abstract

Base Hydrolysis was studied to determine what affects it would have on explosive decomposition. The base used was Sodium Hydroxide. Two explosives were chosen to be tested: Nitroguanidine (NQ) and 1,3,5-Trinitro-1,3,5 triazocyclohexane (RDX). NQ was used to duplicate the procedure used by Dr. Spontarelli at Los Alamos National Laboratory in New Mexico, and to become familiar with the test. The experiments with RDX were used to look mainly at the generated data and to improve the setup for future experiments.

DECOMPOSITION OF ENERGETIC MATERIALS USING SODIUM HYDROXIDE

Venessa L. Hurst

Introduction

The High Explosives Research and Development (HERD) facility, because of environmental concerns about open burning and open detonation of munitions, has been experimenting with new methods to demilitarize energetic materials. The process at the HERD starts with high pressure water washout to cut the explosive out of the munition's casing. Base hydrolysis is the second step of the process. It will be used to remove the small explosive chunks remaining on the sides of the munition's casing. Because base hydrolysis is an important part of the demilitarization process, it was necessary to determine whether the base used, sodium hydroxide, was effective in destroying energetic materials. It was also necessary to determine the effects of temperature on the reaction rate to determine an optimum temperature at which to run the base hydrolysis procedure.

Methodology

During this project several experiments were performed. Nitroguanidine was used for the first experiment because it is not a very sensitive explosive; therefore, it was safe to practice the procedure of the experiment. Base hydrolysis had also been done previously by Dr. Spontarelli at Los Alamos National Laboratory. A 1.5M solution of sodium hydroxide (NaOH) was used. Throughout the summer, the setup of the experiment was changed several times. Figure 1 (fig.1) shows the setup for NQ. The purging system, designed to replace the air in the reaction with helium, was connected to a vacuum pump and a helium gas line. After the system had been purged, the NaOH solution 1.5 molar was introduced to the flask containing NQ. The flask was heated to 100-106°C during the experiment. The experiment lasted for 52 minutes once the system had been heated to the desired temperature.

A differential scanning chromatograph (DSC) was used to characterize the thermal properties of the explosives used and any solid residues obtained from the experiments. A pure sample of NQ was analyzed by DSC and then compared to that from the solid residue obtained after the reaction solution was evaporated to dryness.

The next step was to subject RDX to base hydrolysis. In the first experiment, the setup was changed as depicted in (fig.4). It was decided to measure the amount of gas that was being produced. Two 50 ml burettes were added to the setup. After the system was evacuated to replace air with helium a pressure transducer was connected to determine when atmospheric pressure was reached. A separatory funnel was used to hold the 115 ml of NaOH solution to RDX contained in the reactor flask. After the system had been purged, with helium, 100 ml of the NaOH solution was added to the 10 g of RDX. The system was then heated to 100°C and the gas production measured and recorded. For safety reasons, the experiment was not monitored during a lightning advisory and, hence, a break in the data shown in (fig.5).

There were some changes in the setup of the second RDX experiment. The reactor flask was insulated to aid in temperature control and two more burettes were added to facilitate the gas collecting process..

In the last experiment (fig.12) the burettes were replaced with 100ml graduated cylinders. This was done because of the large amount of gas that was produced during the second experiment.

A DSC was taken of pure RDX and of the products of the RDX experiments. There were two samples taken from every experiment. A vacuum filtration was performed to separate the liquid from the solid particles remaining in solution. Both the liquid and the solid samples were dried and analyzed. The solids were labeled with a D, and the liquids were labeled with a W.

Results

In the Nitroguanidine experiment many problems arose. There were problems with the purging system, the temperature, and the data that was gathered. The problem with the purging system occurred after the vacuum had been pulled. Once the helium was pumped through the system, it was guess work to know when to open the stockcock so helium could flow through the tube and into the flask containing water. If opened too soon, water would backup into the system. The solution to this problem was to connect the vacuum and the helium to a pressure transducer so that it would be possible to know when the system was back to atmospheric pressure. The second problem was with the temperature.

It was taking too long to heat the system to 100°C. Tests were conducted to establish the exact setting on the heating mantle for it to reach 100°C.

A DSC was taken to compare the pure NQ (fig.2) and the product of the first experiment (fig.3). Pure NQ shows a peak at 248°C. In (fig.3) there was no peak at 248°C; therefore, NQ is not present in the solution.

In the first RDX experiment there was a large gap in the data on the graph (fig.5), because there was a lightning advisory. It was not possible to record data during that time. The experiment was terminated before it was finished since most of the data had been lost during the advisory. A DSC was run on a pure sample of RDX (fig.6) and two product samples. The two product samples were dried. The solid particles remaining on the filter were the dry sample (D) (fig.7) and the liquid sample was (W) (fig.8). The peak for pure RDX was at 239.58°C. The D sample matched the pure sample, and showed a peak at 239.58°C. It was concluded that some RDX was present in the sample, but that most was decomposed. The W sample showed no peak at 239.58°C; therefore, no RDX was left in the liquid portion.

In the second RDX experiment the insulation around the flask proved to be too effective. The temperature reached a high level at a very quick rate and it was not possible to bring it down (fig.9). This affected the rate that the reaction took place, and the amount of gas produced during the experiment. It took 1 hour and 45 minutes to complete the experiment. A DSC was run on the D sample (fig.10) and the W sample (fig.11). The results were similar to the first experiments.

In the last experiment the temperature was under control and 100 ml graduated cylinders were added to the setup. The recording of the amount of gas production was not as accurate, but there was less chances of losing gas. The graph in (fig.13) allows one to see that the experiment was finished by the way that it leveled off in the end. A DSC was also run on the D sample (fig.14) and on the W sample (fig.15). Results obtained in the third experiment were similar to the results obtained in the first and second experiments.

In the RDX experiments the dry samples were possibly RDX that had not been reacted with the NaOH solution. The liquid samples did show a peak at different areas but they were not studied to find out what the substance was.

Conclusion

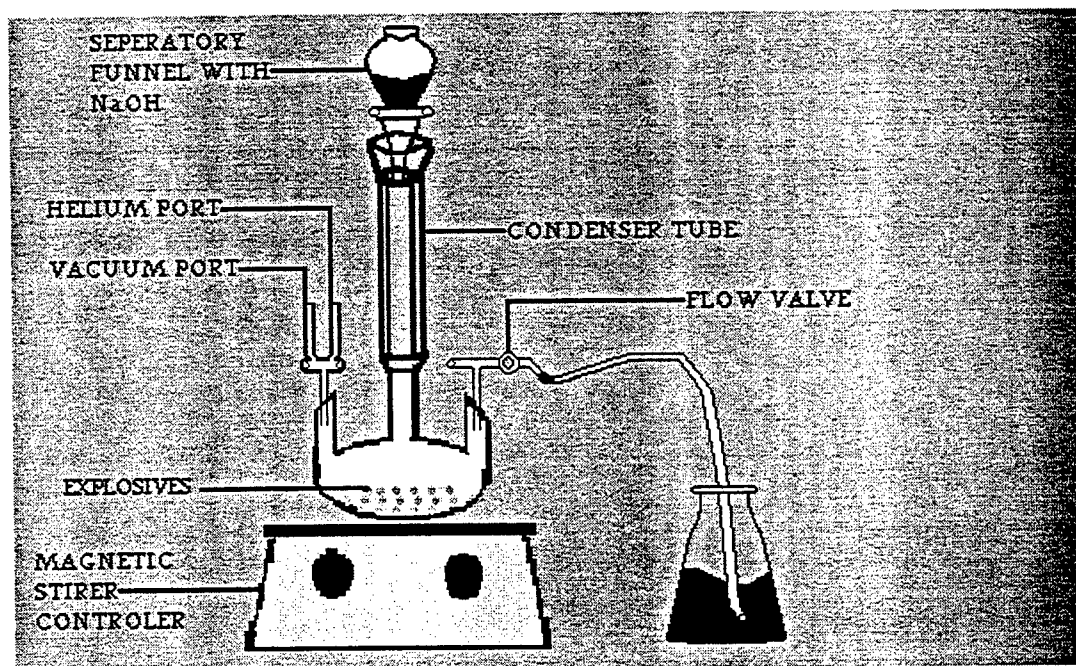
The 1.5M NaOH solution was effective at hydrolyzing NQ and RDX. This project also showed that temperature had a great impact on the rate of gas production in the experiments. If the temperature was increased, then the rate of reaction increased. Further experiments should be done using the methods developed here to quantify the extent of hydrolysis, and quantity of gas produced under various operating conditions.

References

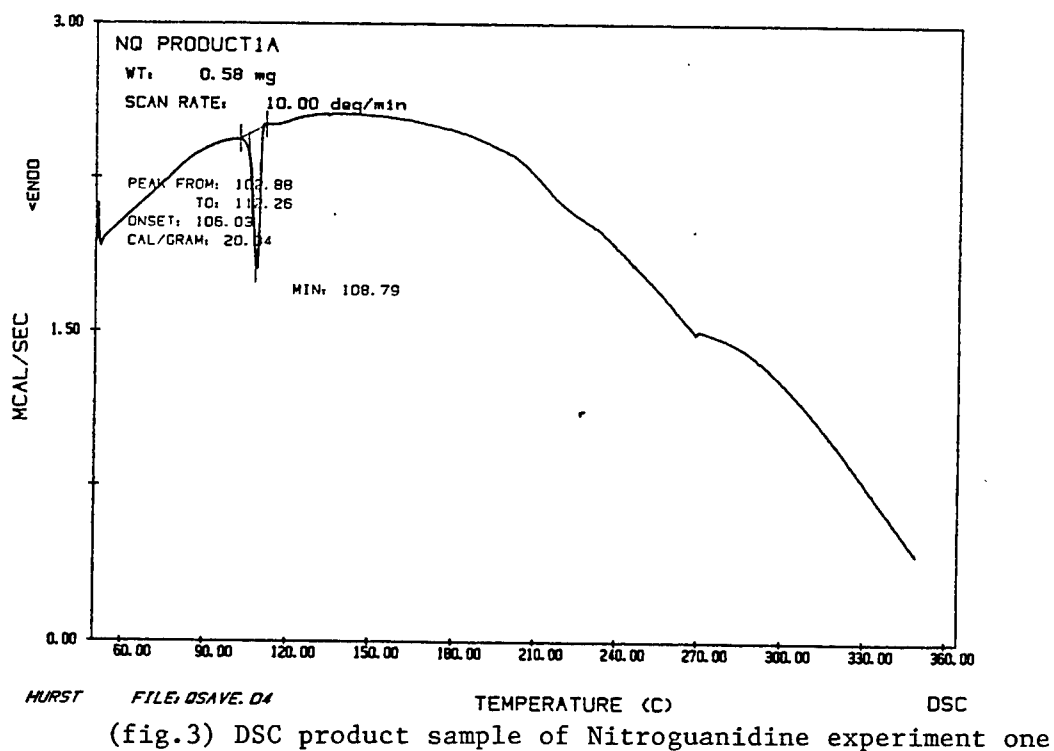
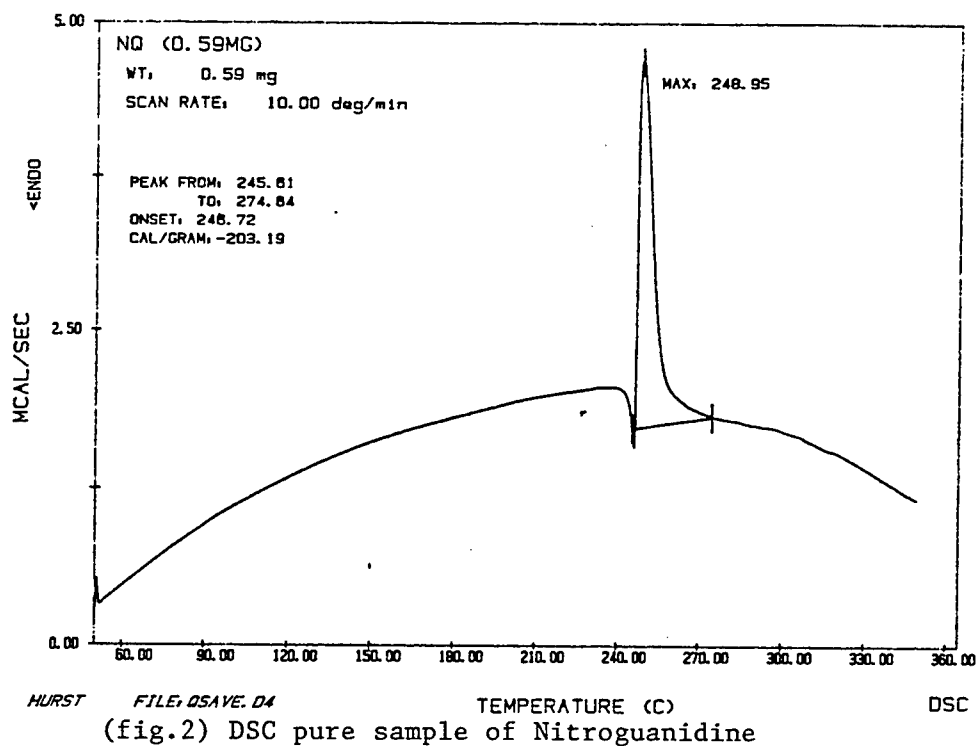
Benziger, T.M., Buntain, G.A., Sanchez, J.A., Spontarelli, T. "Destruction of Waste Energetic Material Using Base Hydrolysis" Incineration Conference, 1993.

Dell'Orco, Philip C., Flesher, Raymond L., Sanchez, John A. "Base Hydrolysis and Hydrothermal Processing of PBX-9404" American Chemical Society, 1994.

Attachments:



(fig.1) Setup of the Nitroguanidine experiement



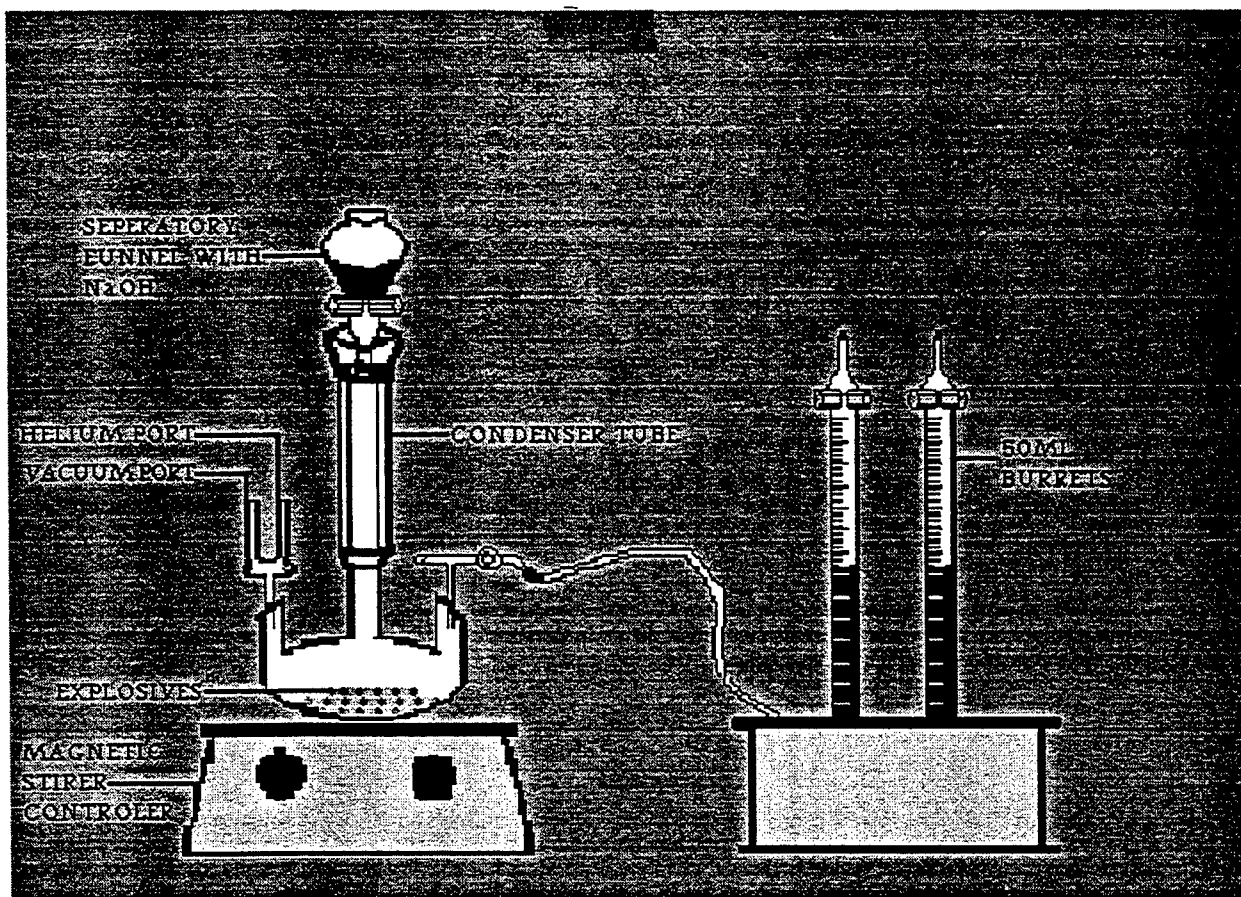


(fig.4) Setup of the RDX experiment one & two

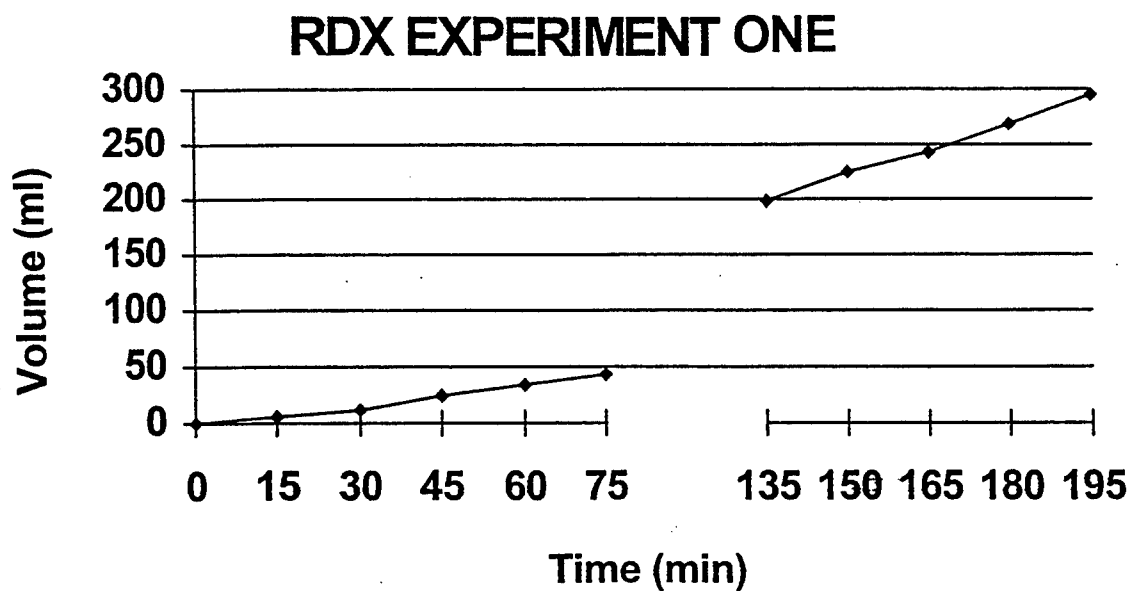


(fig.5) Gas Analysis graph of RDX experiment one

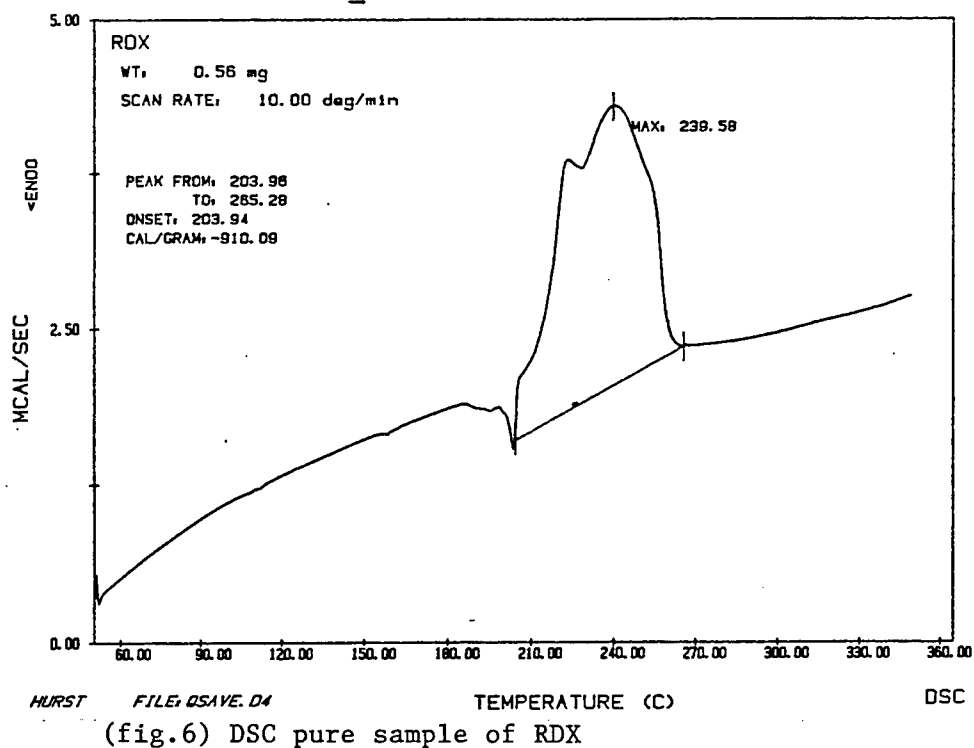


(fig.6) DSC pure sample of RDX

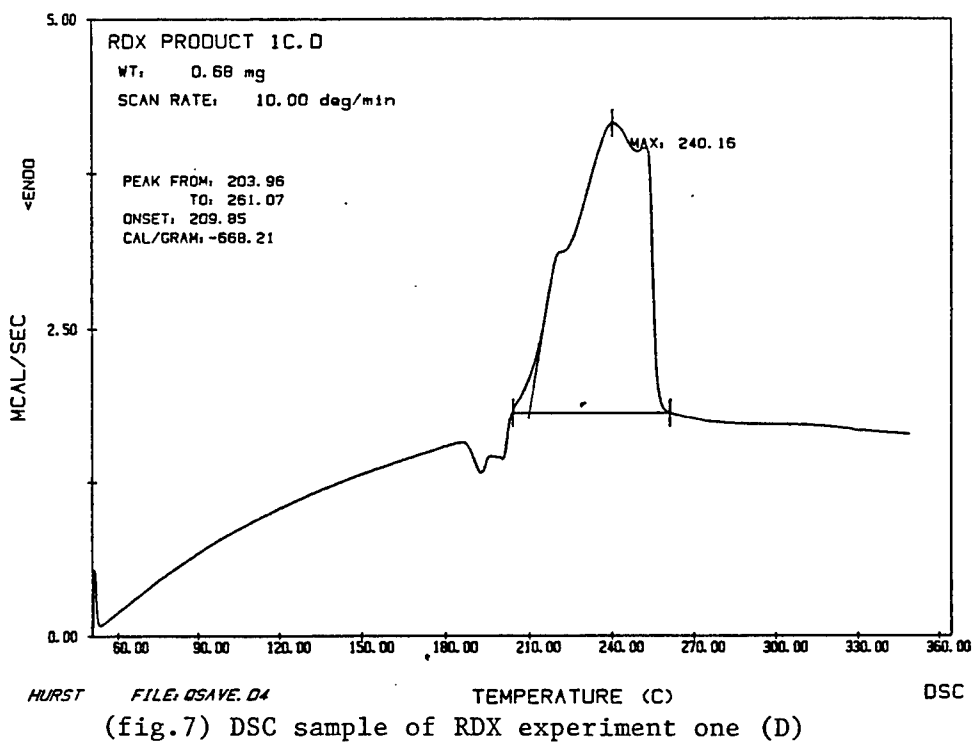


(fig.7) DSC sample of RDX experiment one (D)

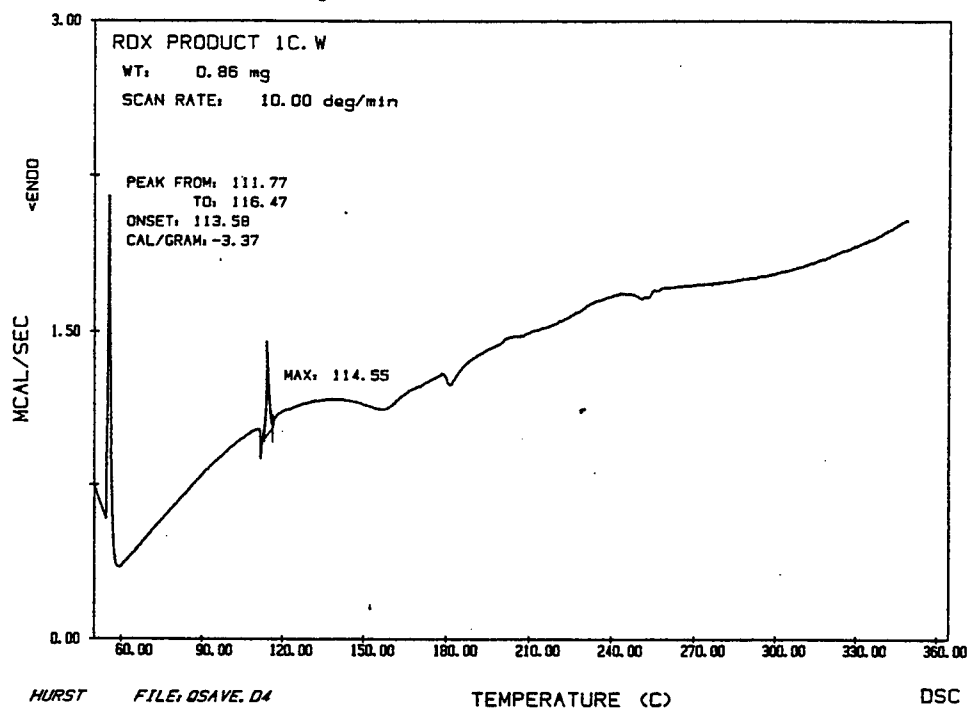


(fig.8) DSC sample of RDX experiment one (W)

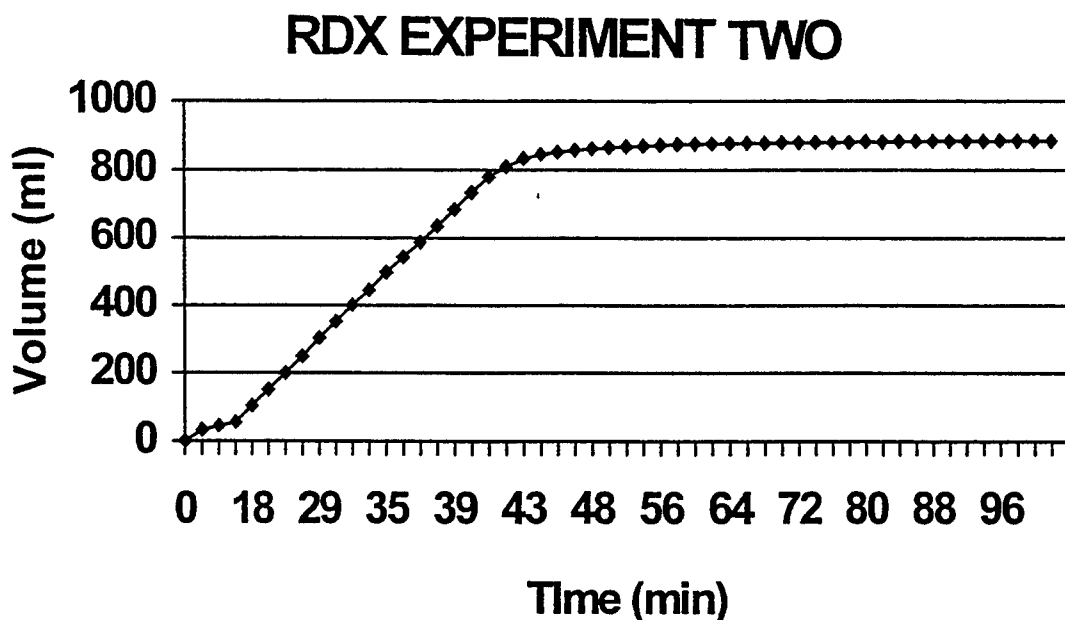


(fig.9) Gas Analysis graph of RDX experiment two

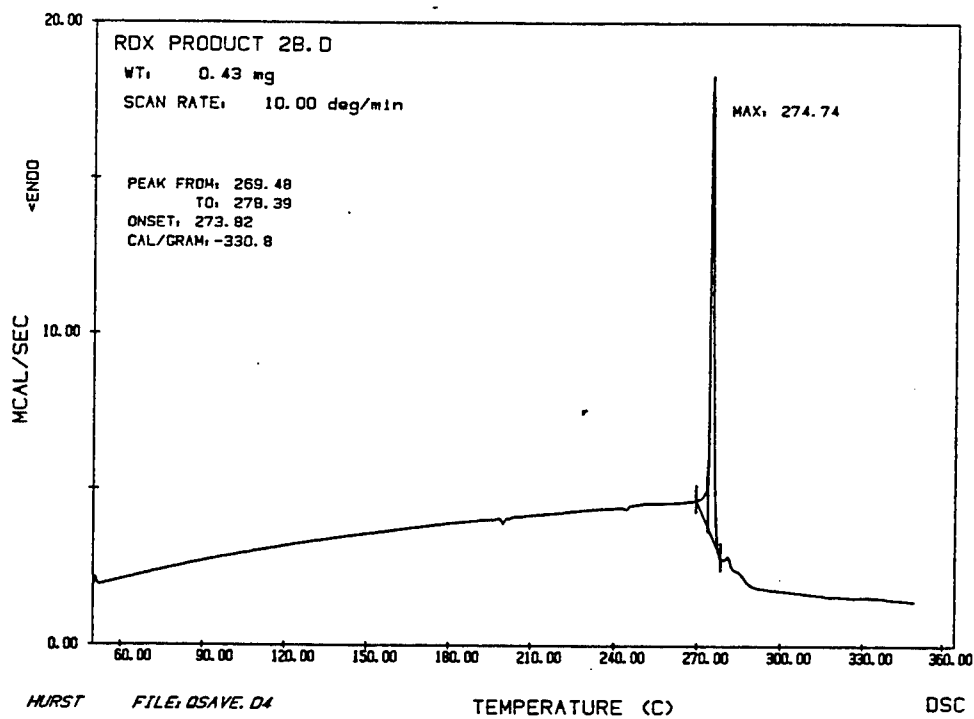


(fig.10) DSC sample of RDX experiment two (D)

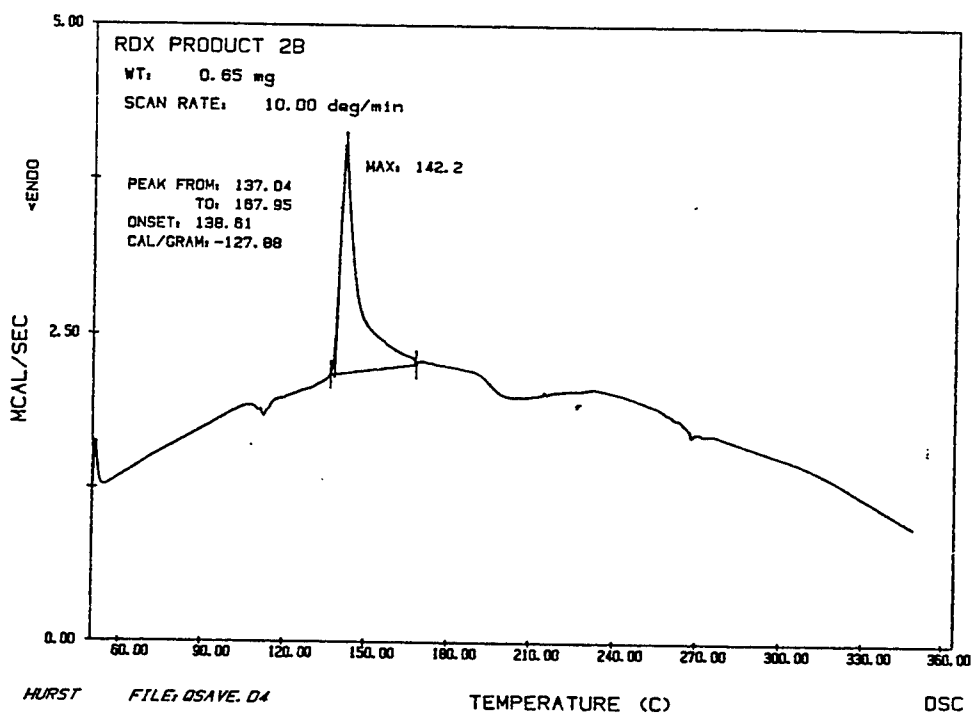


(fig.11) DSC sample of RDX experiment two (W)

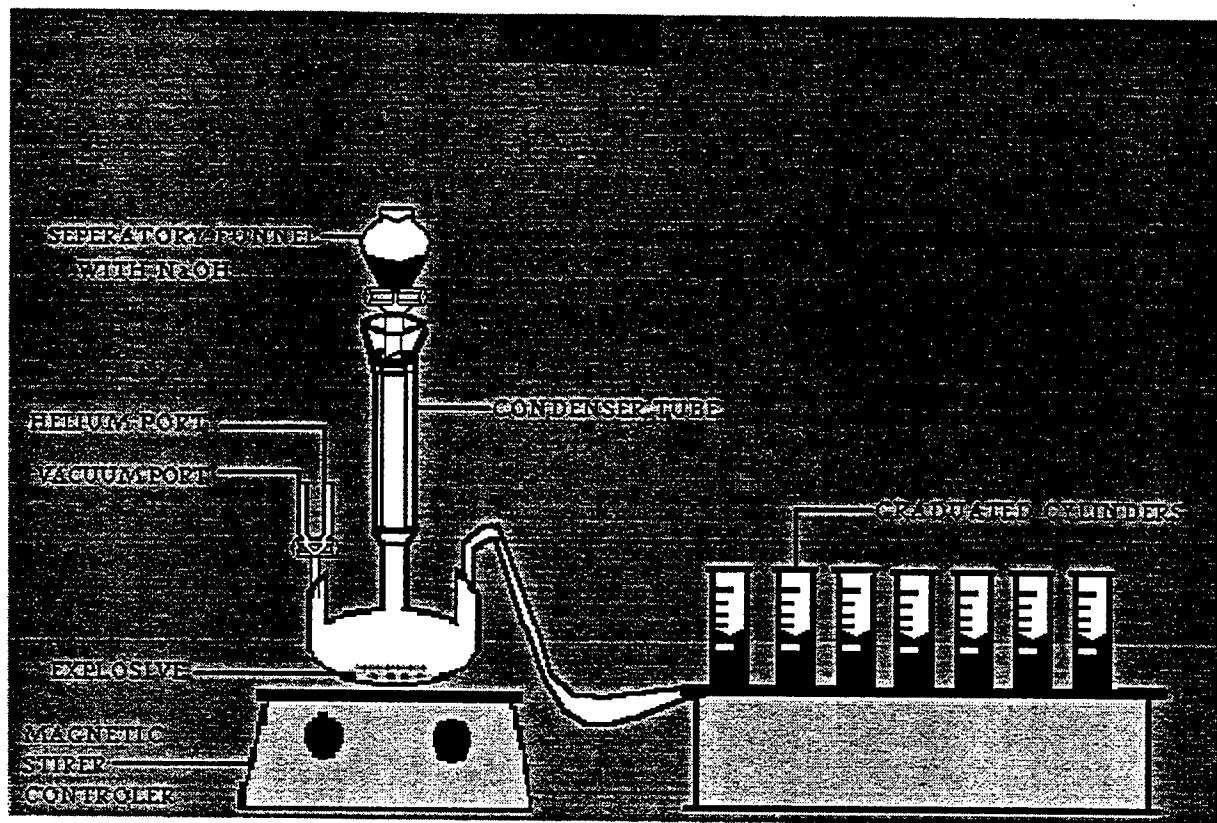


(fig.12) Setup of the RDX experiment three

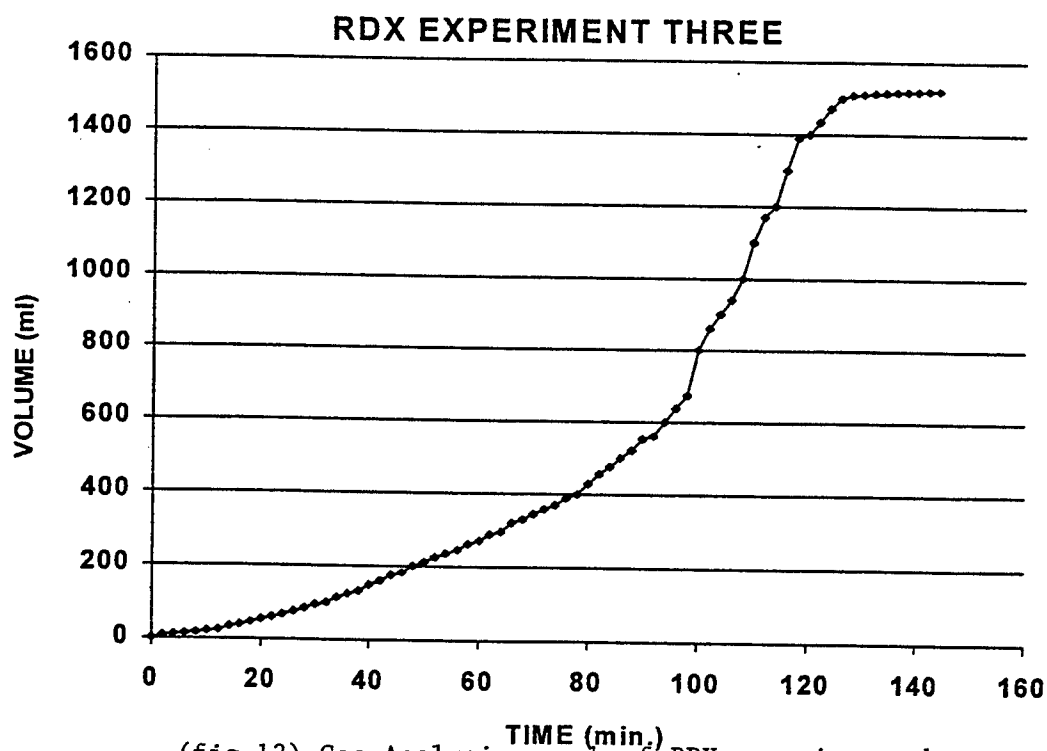


(fig.13) Gas Analysis graph of RDX experiment three

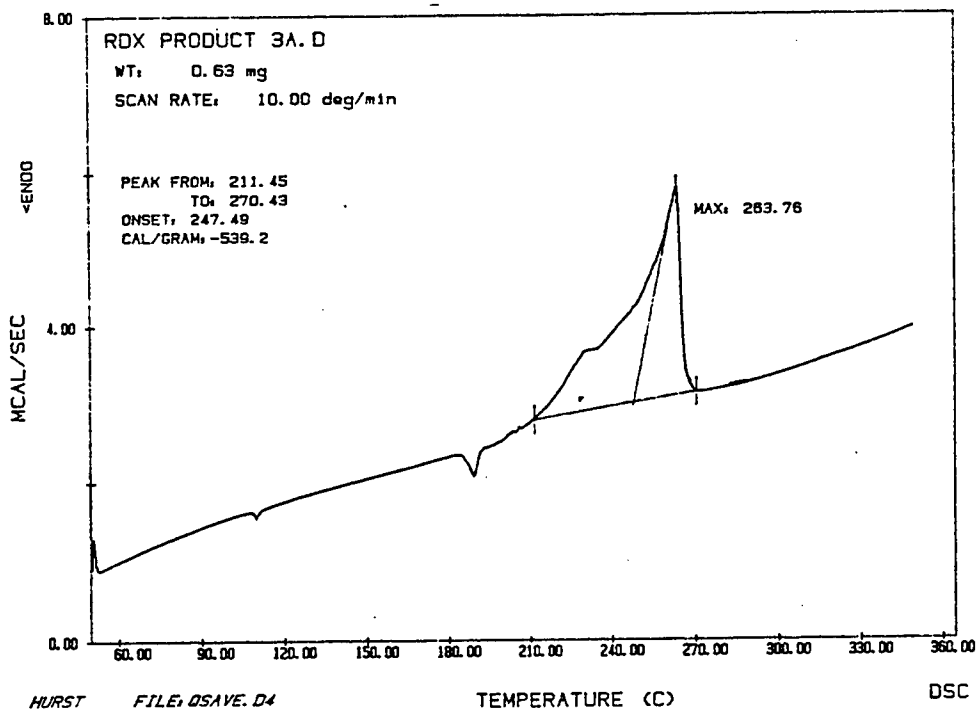


(fig.14) DSC sample of RDX experiment three (D)

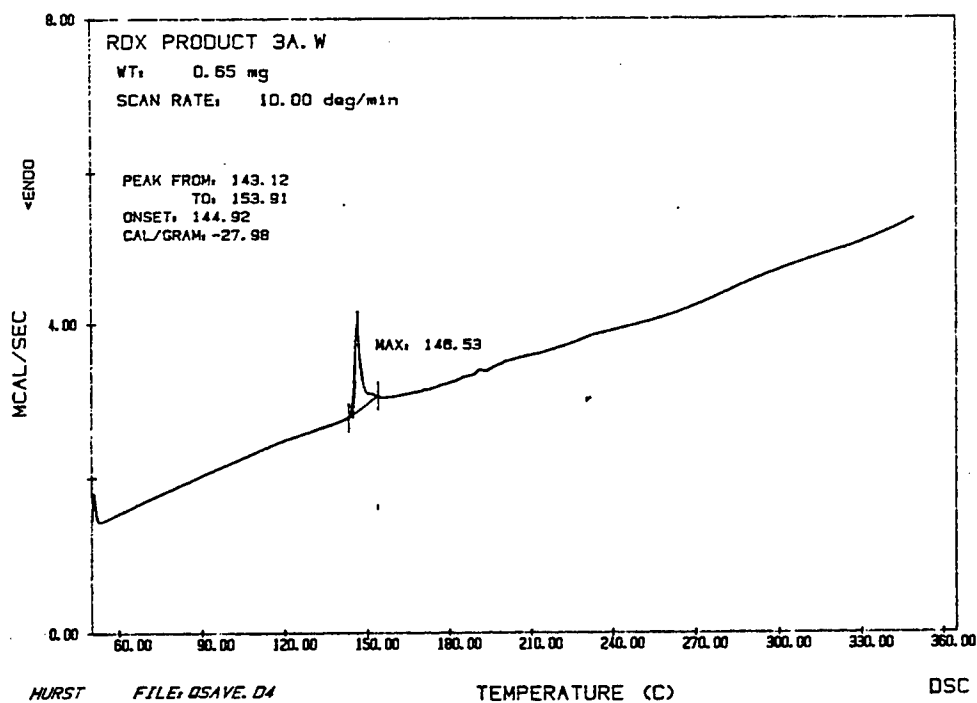


(fig.15) DSC sample of RDX experiment three (W)

A STUDY OF THE EFFECTS OF N-VINYLPYRROLIDONE
ON METHYLENE BLUE BASED
POLYMER DISPERSED LIQUID CRYSTAL SYRUPS

Jennifer M. Johnson

Carroll High School
4524 Linden Ave.
Dayton, OH 45432

Final Report for:
High School Apprentice Program
Wright Laboratory, Materials Directorate

Sponsored by:
Air Force Office of Scientific Research
Bolling Air Force Base, DC

and

Wright Laboratory

August 1995

A STUDY OF THE EFFECTS OF N-VINYLPYRROLIDONE
ON METHYLENE BLUE BASED
POLYMER DISPERSED LIQUID CRYSTAL SYRUPS

Jennifer M. Johnson
Carroll High School

Abstract

The results of varying the percentage composition by weight of N-vinylpyrrolidone (NVP) was studied. Syrups with NVP percentages from 0 to 20% at intervals of 5% were created and mixed. Samples from each syrup were exposed to a HeNe laser at 632.8nm for a period of 5 minutes and at an intensity of 3.2mW to 3.8mW so that a Bragg grating could be written. These samples were then characterized by finding their diffraction efficiencies in both s and p polarization. Results were that the optimal percentage for NVP was around 14.5%.

Introduction

Since the invention of the laser, the applications for the functions of coherent light have grown considerably. One of the uses for laser light is holography. A hologram is simply a recorded document of the interference pattern between two beams of light. Holograms may be applied to the technological world in such ways as head-up displays and in fiber optic switches. The simplest type of hologram, a grating, is a record of the interference between two coherent beams of light, producing alternating bands of high and low intensity. A Bragg grating was employed in the study of methylene blue based polymer dispersed liquid crystals (PDLC).

PDLCs are created when a mixture of liquid crystals and monomers are exposed to a coherent light source. A photoinitiator, in this experiment methylene blue, becomes excited when photons hit it, causing the dye to move up from ground state. The excited dye molecules react with N-phenylglycine (NPG), causing the NPG to have an excess electron and making it highly reactive. The NPG attacks the monomer, dipentaerythrol hydroxy penta acrylate (DPHPA), altering the chemical bonds and causing polymerization. The polymer is formed as a three dimensional web, and it is formed more rapidly in areas of high intensity in the interference pattern than in low intensity. Due to this phenomena, more monomer will flow into the areas of high intensity as the liquid crystals form droplets and move to the areas of low intensity in an effort to escape the polymerization. This process creates bands of polymer and liquid crystals, known as a grating.

Liquid crystals, specifically, E7, are substances that exist neither in the solid or the liquid phase, but rather in a phase between the two, possessing qualities of both phases. Liquid crystals are necessary in the formulation of the syrup because, due to their chemical structure and their mobility, the liquid crystals can easily form droplets and move to areas of low light intensity where the polymerization is not as rapid. Methylene blue is needed as the photoinitiator because it absorbs and can therefore be activated in the same wavelength as the HeNe laser produces light (632.8nm), enabling a grating to be written at a relatively low power (3.2mW-3.8mW). In the formulation used in this experiment, N-vinylpyrrolidone (NVP) is the cross-linking monomer. NVP functions to help strengthen the bonds in the polymer and thereby reinforce the grating.

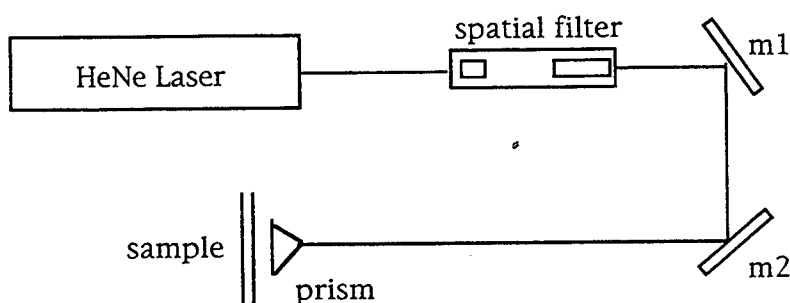
The reaction sequence of the components of the PDLC syrup has been understood and explained, for the most part. Yet, the most efficient ratio for the various chemicals is not totally known. The purpose of this experiment is to determine what the best percentage of the overall composition is for the chemical cross-linker N-vinylpyrrolidone.

Methodology

To run this experiment, the procedure was separated into three areas, creation of the syrup, writing of the grating, and characterization of the grating.

To create a syrup, NVP was added according to the planned percentage of the overall composition; varying from 0% to 20% in increments of 5%. The liquid crystal E7 was next added at a percentage of 30. Following this, 1% NPG and from 50% to 70% of the monomer, DPHPA, was added. The vial was then covered with aluminum foil and the room lights were turned off so that the methylene blue could be added without starting any chemical reactions as the dye is a photoinitiator and activated by light. The methylene blue was added at a one-half percent concentration. The syrup was then sonicated for 60 seconds to fully dissolve the chemicals and allowed to sit for 2-3 days as the syrups were found to perform better after a short length of time.

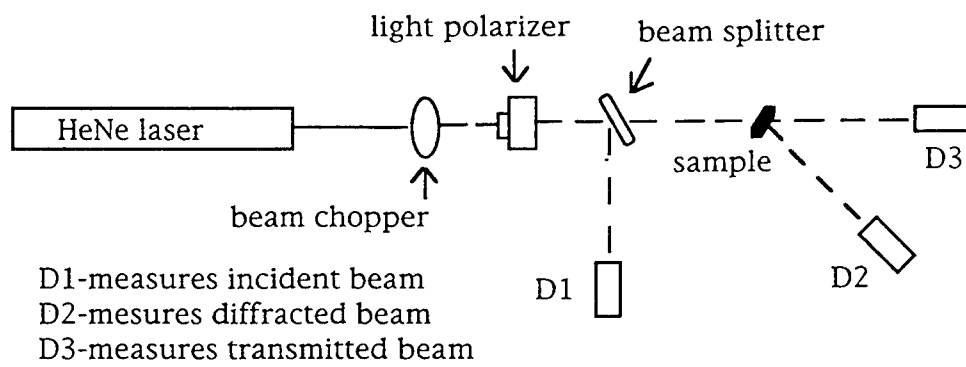
A sample was prepared on either glass or ITO plates using spacers of a 15 micron thickness and was exposed to the HeNe laser (wavelength 632.8nm) for a period of 5 minutes at an intensity ranging from 3.2mW to 3.8mW.



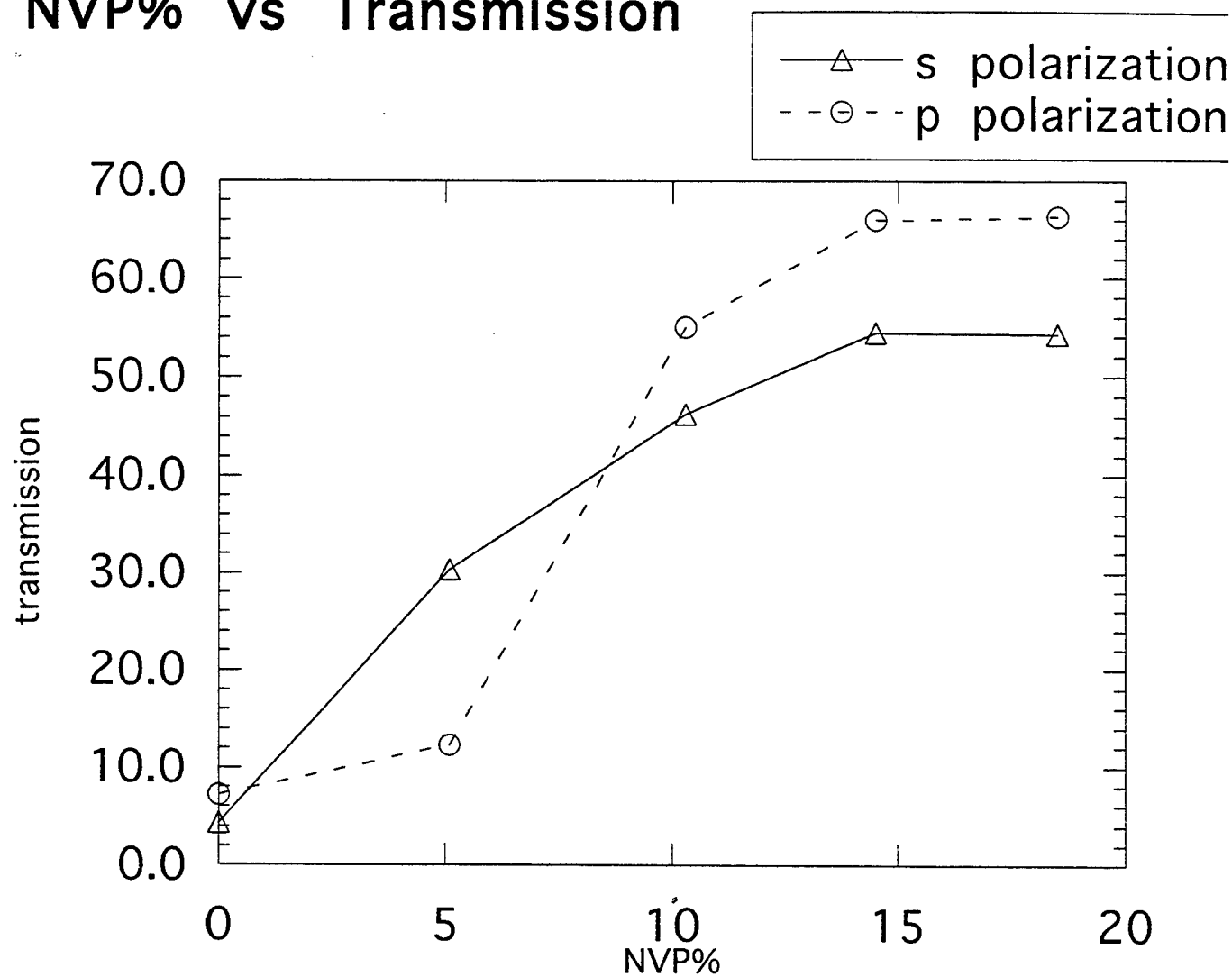
The sample was cured for 3-5 minutes under incandescent lamps to bleach any methylene blue that had not reacted during exposure and the samples were characterized by finding their diffraction efficiency in both s-polarization and p-polarization. This was done using the formula:

$$\frac{I}{t} * \frac{d}{I}$$

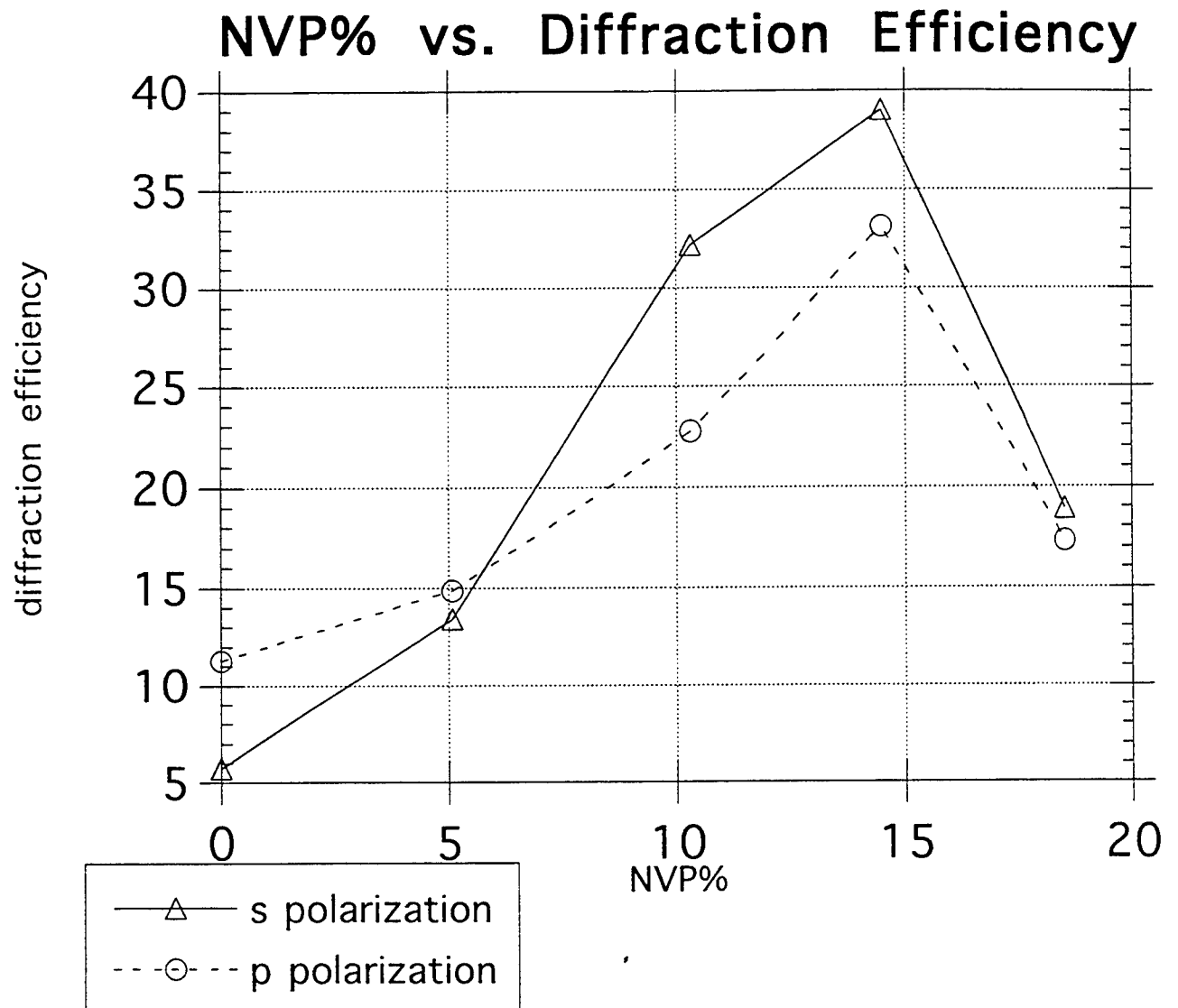
where I was the incident light intensity, d was the diffracted beam intensity, t was the light transmitted through normal glass.



NVP% vs Transmission



	NVP%	s polarization	p polarization
0	0.0000	4.3250	7.1500
1	5.0900	30.350	12.330
2	10.300	46.250	55.000
3	14.500	54.500	66.000
4	18.500	54.250	66.330



	NVP%	s polarization	p polarization
0	0.0000	5.7500	11.280
1	5.0900	13.410	14.850
2	10.300	32.170	22.770
3	14.500	39.000	33.130
4	18.500	18.900	17.290

Results and Conclusions

After collecting the data and finding the median values for each percentage value for NVP, it becomes apparant that a 15-20 percent composition is the optimal level for both the amount of light transmitted and the light diffracted. The data for diffraction efficiency values, in both the s and the p polarizations, clearly shows that a turning point occurs between ten and twenty percent, although further testing would be required to determine exactly where that point is. Another observatiom of interest is that NVP was not essential to the wrining of a grating. With 0% NVP in the solution, a grating with a 6% to 12% diffraction efficiency could be written.

The transmitted light, unlike the diffracted light, appears to level off at a maximum of about 55% in the s polarization and about 65% in p polarization. This may be explained in that the amount of phase separation, which scatters light and therefore reduces the amount of light transmitted, reaches a maximum. The sample cannot become any more clear and still have a grating in it. At 0% NVP, barely 5% of the light is transmitted. As more NVP is added, this value increases. Based on that trend, NVP probably helps reduce phase separation and clear the sample so that light may be transmitted.

After studying both the light transmitted and the light diffracted when varying the amounts of NVP, it is clear that NVP, although not necessary for a hologram to be created, is essential for a significant amount o flight to be transmitted and for the sample to be optically clear. However, further testing will be necessary to determine if 15-20% of NVP is also the optimal level when creating holograms that are switchable, or may be turned "on or off" by applying an electric field to them.

Acknowledgements

Jennifer M. Johnson thanks L. V. Natarajan, Vince Tondiglia, Bob Haaga, and Beth Funderburg for their help, guidance, and support.

References

1. Meloy, Thomas. "The Laser's Bright Magic," National Geographic. pp 858-881. December, 1996
2. Moller, K.D. Optics . University Science Books. Mill Valley, California. c1988
3. Siegman, Anthony E. Lasers. University Science Books. Mill Valley, California. c1986.
4. R.L.Sutherland, L.V.Natarajan, V.P.Tondiglia, T.J.Bunning, "Bragg Gratings in an Acrylate Polymer Consisting of Periodic Polymer-Dispersed Liquid Crystal Planes," *Chem. Matter* . 5, pp. 1533-1538 (1993)
5. R.L.Sutherland, L.V.Natarajan, V.P.Tondiglia, T.J.Bunning, W.W.Ad "Switchable Holograms in New Photopolymer-Liquid Crystal Composite Materials," *Proc.SPIE, Diffraction and Holographic Optics Technology II*, vol.2404, pp132-143, 1995

Associate did not participate in program.